

The role of NLRC5 in obesity

Dissertation to obtain the doctoral degree of
Natural Sciences (Dr. rer. nat.)

Faculty of Natural Sciences
University of Hohenheim

Institute of Clinical Nutrition

submitted by:

Sarah Katharina Bauer

from: Karlsruhe

2023

Dekan:	Prof. Dr. rer. nat. Jan Frank
1. berichtende Person:	Prof. Dr. rer. nat. Thomas A. Kufer
2. berichtende Person:	Prof. Dr. rer. nat. W. Florian Fricke
Mündliche Prüfung:	19.12.2023

Table of content

Abbreviations	IV
Abstract	VIII
Zusammenfassung	X
Introduction	1
Pattern recognition – a prerequisite for innate immunity	1
The NOD-like receptor family of pattern recognition receptors	1
NOD-like receptors as transcriptional regulators – NLRC5, the master regulator of MHC class I genes	3
Obesity and the innate immune system – an intimate relationship	7
NOD-like receptors in obesity and associated morbidities	8
NLRC5 – implications in metabolic traits.....	11
PPAR γ - The master regulator of adipogenesis.....	12
Aim of the study.....	14
Materials and Methods	16
Materials	16
Mice	16
Cell lines and bacteria	17
Chemicals and reagents	20
Kits	22
Plasmids	23
Oligonucleotides	24
siRNAs	27
Antibodies	27
Instruments.....	28
Software	29

Methods.....	30
Cell biological methods.....	30
Molecular methods.....	34
Biochemical methods.....	38
Bioinformatic methods	43
Results	46
Characterization of the effect of HFD on two <i>Nlrc5</i> deficient mouse lines	46
Female <i>Nlrc5</i> ^{ΔExon4-7} mice on HFD present with higher body weight gain and an increase in adipose tissue	46
Microbiome composition of <i>Nlrc5</i> ^{ΔExon4-7} animals.....	53
<i>Nlrc5</i> deficiency does not affect obesity in <i>Nlrc5</i> ^{ΔExon4} mice	56
Investigation of NLRC5's effect on adipocyte differentiation <i>in vitro</i>	60
The 3T3-L1 preadipocyte cell line is a suitable cell culture model for adipocyte differentiation	60
Characterization of 3T3-L1 <i>Nlrc5</i> knockout lines.....	63
Differentiation ability of <i>Nlrc5</i> modified 3T3-L1 cell pools does not differ from WT cells	66
NLRC5 interacts with PPAR γ , co-regulates PPAR γ target genes and modulates PPAR γ 's anti- inflammatory capacities.....	68
NLRC5 interacts with PPAR γ 1 via its NACHT domain.....	68
NLRC5 enhances transcription of PPAR γ target genes	71
Sin3A influences <i>FABP4</i> transcription by NLRC5	74
<i>NLRC5</i> deficiency in THP-1 macrophage like cells increases pro-inflammatory responses and reduces PPAR γ 's anti-inflammatory properties in LPS-induced inflammation	75
<i>NLRC5</i> deficiency in murine bone marrow-derived macrophages increases pro- inflammatory responses and reduces PPAR γ 's anti-inflammatory properties in LPS-induced inflammation	79
Investigation of the molecular mechanisms underlying PPAR γ target gene regulation by NLRC5.....	81
NLRC5 reduces PPAR γ 's transcriptional activity in luciferase reporter gene assays.....	81

Analysis of the NLRC5:DNA interaction at the <i>FABP4</i> promoter by CHIP	84
Influence of HFD and obesity on NLR expression in mouse and men.....	88
NLR expression in mouse adipose tissue and liver.....	88
Expression of <i>NLRC5</i> , <i>NOD1</i> and <i>NOD2</i> in obese human individuals.....	93
Discussion	95
The effect of <i>Nlrc5</i> deficiency on diet-induced obesity, microbiome composition and <i>in vitro</i> adipocyte differentiation	95
NLRC5 interacts with PPAR γ and synergistically regulates PPAR γ target genes involved in metabolism and inflammation.....	99
Other NLRs and their expression in relation to HFD	106
References	108
Supplement.....	132
Eidesstattliche Erklärung	135
Danksagung.....	136
Publications	138
Curriculum Vitae	139

Abbreviations

β2M	β-2-microglobulin
°C	Degree Celsius
15d-PGJ ₂	15-deoxy-Δ-12, 14-prostaglandin J ₂
AD	Acidic transactivation domain
AF	Activation function
ALT	Alanine aminotransferase
AP-1	Activating protein 1
APS	Ammoniumperoxidesulfate
ASC	Apoptosis-associated speck-like protein containing a CARD
ASV	Amplicon sequence variant
AT	Adipose tissue
ATM	Adipose tissue macrophage
ATP	Adenosine-triphosphate
BH	Benjamini-Hochberg
BIR	Baculovirus-inhibitor of apoptosis repeat
BMDM	bone marrow-derived macrophage
BMI	Body mass index
bp	Basepair
BSA	Bovine serum albumin
BTN	Butyrophilin
C-terminus	Carboxyl-terminus
C/EBPα	CCAAT/enhancer-binding protein α
cAMP	Cyclic adenosine monophosphate
CARD	Caspase-activation and recruitment domain
CD36	Cluster of differentiation 36
ChIP	Chromatin immunoprecipitation
CI	Confidence interval
CIITA	Class II Major Histocompatibility Complex Transactivator
CLR	C-type lectin receptor
CLS	Crown-like structure
cm	Centimetre
CREBP	cyclic AMP response element binding protein
CRISPR	Clustered Regularly Interspaced Short Palindromic Repeats
CS	Calf serum
Ctrl.	Control
DAMP	Danger-associated molecular pattern
DBD	DNA binding domain
DD	Death domain
DMEM	Dulbecco's modified Eagle's medium
DNA	Desoxyribonucleic acid
DR-1	Direct repeat-1
ds	Double-stranded
DSS	Dextran sodium sulfate
ELISA	Enzyme-linked immunosorbent assay
EMM	Estimated marginal mean

The role of NLRC5 in obesity - Abbreviations

ENA	European Nucleotide Archive
ER	Oestrogen receptor
ERK	Extracellular signalling-related kinase
EV	Empty vector
FABP4	Fatty acid binding protein 4
FAT	Fatty acid translocase
FATP	Fatty acid transport protein
FBS	Foetal bovine serum
FDR	False discovery rate
FL	Full-length
Flp-In	Flp-FRT recombination system
GAPDH	Glyceraldehyde-3-phosphate dehydrogenase
GLMM	Generalized Linear Mixed Models
gRNA	Guide RNA
GSDMS	Gasdermin D
GTT	Glucose tolerance test
h	Hour
H&E	Haematoxylin & Eosin
HDAC	Histone deacetylase
HDL	High-density lipoprotein
HEK293T	Human embryonic kidney 293T cells
HFD	High-fat diet
HLA	Human leukocyte antigen
HSL	Hormone-sensitive lipase
IAPP	Islet amyloid polypeptide
IBMX	3-Isobuthyl-1-methylxanthine
IF	Immunofluorescence
IFN	Interferon
IL	Interleukin
INDEL	Insertion or deletion
IP	Immunoprecipitation
IR	Insulin resistance
ISRE	Interferon stimulated response element
ITT	Insulin tolerance test
KD	Knockdown
kDa	Kilodalton
KO	Knockout
LB	Lysogeny Broth
LBD	Ligand-binding domain
LDL	Low-density lipoprotein
LMP	Low molecular mass peptide
LPL	Lipoprotein lipase
LPS	Lipopolysaccharide
LRR	Leucin-rich repeats
M	Molar
MAMP	Microbe-associated molecular pattern
MAPK	Mitogen-activate protein kinase
MEF	murine embryonic fibroblasts

The role of NLRC5 in obesity - Abbreviations

MetS	Metabolic Syndrome
mg	Milligram
MHC	Major histocompatibility complex
min	Minute
ml	Millilitre
mM	Millimolar
N-terminus	Amino-terminus
NACHT	Oligomerisation module, present in NAIP, CIITA, HET-E, TP-1
NaF	Sodium flouride
NAFLD	Non-alcoholic fatty liver disease
NCoR	Nuclear receptor co-repressor
NELF	Negative elongation factor
NF- κ B	Nuclear factor 'kappa-light-chain-enhancer' of activated B cells
NFY	Nuclear factor Y
ng	Nanogram
NHEJ	Non-homologous end joining
NK cell	Natural Killer cell
NLR	NOD-like receptor
NLRC5	Nucleotide-binding and oligomerization domain containing 5
NLS	nuclear localization sequence
nm	Nanometre
nM	Nanomolar
NOD	Nucleotide-binding and oligomerization domain
NR	Nuclear receptor
nRLU	Normalized relative luminescence unit
ONPG	Ortho-Nitrophenyl- β -galactoside
OR	Odds ratio
oxLDL	oxidatively modified low-density lipoprotein cholesterol
PAM	Protospacer adjacent motif
PCR	Polymerase chain reaction
PFA	Paraformaldehyde
PGN	Peptidoglycan
PLC	Peptide loading complex
PMA	phorbol 12-myristate 13-acetate
polyI:C	polyinosinic-polycytidylic acid
PPAR	peroxisome proliferator-activated receptor
PPRE	PPAR response element
PRR	Pattern recognition receptor
PYD	Pyrin domain
qRT-PCR	Quantitative real-time polymerase chain reaction
RFX	Regulatory factor X
RIPK2	Receptor-interacting serine/threonine-protein kinase 2
RLR	RIG-I-like receptor
RNA	Ribonucleic acid
RNA Pol II	RNA polymerase II
RNAi	RNA interference
ROS	Reactive oxygen species
Rpm	Rounds per minute

The role of NLRC5 in obesity - Abbreviations

RPMI 1640	Roswell Park Memorial Institute 1640 medium
RXR	Retinoid X receptor
S.D.	Standard deviation
SDS-PAGE	Sodium dodecyl sulfate polyacrylamide gel electrophoresis
sec	Second
siNT	non-targeting siRNA
siRNA	Small interfering RNA
SMRT	Silencing mediator of retinoid and thyroid hormonal receptors
SNP	Single nucleotide polymorphism
SPF	Specific pathogen free
T2DM	Type 2 diabetes mellitus
TAP	Transporter associated with antigen processing
TEMED	Tetramethylethylenediamine
TGF	Transforming growth factor
TH	Thyroid hormone
TLR	Toll-like receptor
TNF	Tumour necrosis factor
TSS	Transcriptional start site
U	Unit
uCARD	Untypical CARD
USP14	Ubiquitin-specific protease 14
WAT	White adipose tissue
WB	Western Blot
WCL	Whole cell lysate
WHO	World Health Organization
WRST	Wilcoxon rank-sum test
WT	Wildtype
Y2H	Yeast 2-hybrid
µg	Microgram
µl	Microlitre
µM	Micromolar

Abstract

Obesity and its associated morbidities are major global health problems. It has become evident in the last decades that the state of obesity is intimately linked with our immune system. Pattern recognition receptors (PRRs), the main sensor molecules of the innate immune system, were shown to play an essential role in the pathology of obesity and its associated morbidities. Among others, members of the nucleotide-binding and oligomerization domain (NOD)-like receptors (NLRs), a family of cytosolic PRRs, were associated with the obesity-accompanying low-grade inflammatory response contributing to obesity-associated morbidities. NLRC5 is a NLR protein functioning as key transcriptional regulator of major histocompatibility complex (MHC) class I genes responsible for antigen presentation. Recent observations now suggest novel roles of NLRC5 in metabolic trades, but so far, no confirmation of these singular observations is available, and the underlying mechanisms remain elusive.

The aim of this thesis was to characterize the role of the NLR protein NLRC5 in obesity. To this end, two *Nlrc5* deficient mouse lines (*Nlrc5*^{ΔExon4-7} and *Nlrc5*^{ΔExon4}) were subjected to high-fat diet (HFD) feeding and phenotypic, morphological, and biochemical analyses were performed. Female *Nlrc5*^{ΔExon4-7} mice presented with higher body and adipose tissue (AT) weight gain and larger adipocytes compared to wildtype (WT) animals. This phenotype, however, could not be recapitulated in the *Nlrc5*^{ΔExon4} mouse line. Microbiome analysis revealed subtle alterations of the faecal microbiome by diet:genotype interactions. To further characterize the effect of *NLRC5* deficiency on adipocyte differentiation, the CRISPR/Cas9 gene editing system was used to modify *Nlrc5* expression in the 3T3-L1 preadipocyte cell line. Using inducible HeLa cell lines with stable GFP-NLRC5 expression we showed NLRC5 to interact with the master regulator of adipogenesis peroxisome proliferator-activated receptor γ (PPAR γ) and to enhance the expression of PPAR γ target genes. In addition, a contribution of NLRC5 to PPAR γ 's anti-inflammatory actions was revealed using *NLRC5* deficient THP-1 macrophage-like cells and bone marrow-derived macrophages from *Nlrc5*^{ΔExon4-7} mice. To elucidate the mechanism behind the synergy between NLRC5 and PPAR γ , reporter gene and chromatin immunoprecipitation (ChIP) assays were performed. Lastly, the expression of multiple NLR family members was correlated with body mass index (BMI) in obese human patients and investigated in the adipose tissue and liver of HFD-fed mice, the latter revealing *Nlrp10* to be highly upregulated by HFD feeding.

The role of NLRC5 in obesity - Abstract

Taken together, this thesis provides a comprehensive characterization of *Nlrc5* deficient mice on HFD and reveals a function of NLRC5 as transcriptional co-regulator of PPAR γ targets and its anti-inflammatory properties. In addition, this work provides first insights into the potential mechanism behind the synergistic transcriptional regulation by NLRC5 and PPAR γ and extends the knowledge on the regulation of NLR expression by HFD feeding.

Zusammenfassung

Adipositas und die damit verbundenen Komorbiditäten sind ein großes globales Gesundheitsproblem. In den letzten Jahrzehnten wurde offensichtlich, dass der Zustand der Adipositas eng mit unserem Immunsystem zusammenhängt. Es wurde gezeigt, dass Mustererkennungsrezeptoren, die wichtigsten Sensormoleküle des angeborenen Immunsystems, eine wesentliche Rolle in der Pathologie der Adipositas und der damit verbundenen Morbiditäten spielen. Unter anderem wurden Mitglieder der Nucleotide-binding and oligomerization domain (NOD) -like Rezeptoren (NLRs), einer Familie zytosolischer Mustererkennungsrezeptoren, mit der mit Adipositas einhergehenden niedriggradigen Entzündungsreaktion assoziiert, die zu den mit Adipositas assoziierten Morbiditäten beiträgt. NLRC5 ist ein NLR Protein, das als Haupt-Transkriptionsregulator von Genen des Haupthistokompatibilitätskomplexes der Klasse I fungiert, welche für Antigenpräsentation verantwortlich sind. Neue Beobachtungen deuten darauf hin, dass NLRC5 eine bisher unbekannte Rolle im Stoffwechsel spielt, aber bisher gibt es keine Bestätigung dieser vereinzelt Beobachtungen, und die zugrundeliegenden Mechanismen sind noch unklar.

Ziel dieser Arbeit war es, die Rolle des NLR Proteins NLRC5 bei Adipositas zu charakterisieren. Zu diesem Zweck wurden zwei *Nlrc5* defiziente Mauslinien (*Nlrc5*^{ΔExon4-7} und *Nlrc5*^{ΔExon4}) mit einer fettreichen Diät gefüttert und phänotypische, morphologische und biochemische Analysen durchgeführt. Weibliche *Nlrc5*^{ΔExon4-7} Mäuse wiesen im Vergleich zu Wildtyp (WT) Tieren eine höhere Gewichtszunahme des Körpers und des Fettgewebes sowie größere Adipozyten auf. Dieser Phänotyp konnte jedoch in der *Nlrc5*^{ΔExon4} Mauslinie nicht rekapituliert werden. Mikrobiomanalysen zeigten leichte Veränderungen des fäkalen Mikrobioms durch Wechselwirkungen zwischen Ernährung und Genotyp. Um die Auswirkungen des Fehlens von *NLRC5* auf die Adipozytendifferenzierung näher zu charakterisieren, wurde das CRISPR/Cas9-Gen-Editing-System zur Modifikation der *Nlrc5* Expression in der 3T3-L1 Präadipozytenzelllinie angewendet. Unter Verwendung induzierbarer HeLa Zelllinien mit stabiler GFP-NLRC5 Expression konnten wir zeigen, dass NLRC5 mit dem Hauptregulator der Adipogenese peroxisome proliferator-activated receptor γ (PPAR γ) interagiert und die Expression von PPAR γ Zielgenen verstärkt. Darüber hinaus wurde ein Beitrag von NLRC5 zu der entzündungshemmenden Wirkung von PPAR γ mit Hilfe von *NLRC5* defizienten Makrophagen-ähnlichen THP-1 Zellen und Makrophagen aus dem Knochenmark

von *Nlrc5*^{ΔExon4-7} Mäusen nachgewiesen. Um den Mechanismus hinter der Synergie zwischen NLRC5 und PPAR γ aufzuklären, wurden Reporter- und Chromatin-Immunoprecipitationsversuche (ChIP) durchgeführt. Zuletzt wurde die Expression mehrerer Mitglieder der NLR Familie mit dem Body Mass Index (BMI) adipöser menschlichen Patienten korreliert und im Fettgewebe und in der Leber von mit fettreicher Diät gefütterten Mäusen untersucht, wobei sich bei Letzterem herausstellte, dass *Nlrp10* durch die Fütterung mit fettreicher Diät stark hochreguliert wird.

Zusammenfassend bietet diese Arbeit eine umfassende Charakterisierung des Einflusses einer fettreichen Diät auf *Nlrc5* defiziente Mäuse und zeigt eine Funktion von NLRC5 als transkriptionellem Co-Regulator von PPAR γ Zielgenen und seinen entzündungshemmenden Eigenschaften. Darüber hinaus liefert diese Arbeit erste Einblicke in den möglichen Mechanismus hinter der synergistischen Transkriptionsregulation durch NLRC5 und PPAR γ und erweitert das Wissen über die Regulation der NLR Expression durch fettreiche Ernährung.

Introduction

Pattern recognition – a prerequisite for innate immunity

The human body is confronted with a plethora of microorganisms co-existing in our everyday environment. The innate immune system provides the first line of defence against these daily microbial challenges. To successfully control these, the innate immune system must be able to recognize a broad range of microbial structures and precisely discriminate foreign, and thus potentially harmful, from endogenous molecules. This recognition and discrimination is mediated by germline-encoded pattern recognition receptors (PRRs) which sense highly conserved microbe-associated molecular patterns (MAMPs) (Janeway, 1989; Janeway & Medzhitov, 2002). Those include components of the bacterial cell wall, such as peptidoglycans (PGN) (Chamaillard et al., 2003; Girardin et al., 2003a; Girardin et al., 2003b) and lipopolysaccharide (LPS) (Poltorak et al., 1998), conserved structural proteins such as flagellin (Hayashi et al., 2001), or microbial DNA or RNA (Kawasaki, Kawai, & Akira, 2011). MAMP recognition by PRRs elicits a rapid pro-inflammatory response, aiming at microbial containment and, at best, elimination, which is followed by the induction of a highly antigen-specific, however slower, adaptive immune response.

As microbial challenges can arise at the cell surface as well as, for invasive bacteria and viruses, inside the cell, PRRs are either transmembrane proteins localized to the cell surface or of cytosolic localization. Membrane-bound PRRs most prominently include the Toll-like receptors (TLRs) (Fitzgerald & Kagan, 2020) and the C-type lectins (CLRs) (Brown, Willment, & Whitehead, 2018), examples for cytosolic PRRs are the RIG-I-like receptors (RLRs) (Rehwinkel & Gack, 2020) and the nucleotide-binding and oligomerization domain (NOD)-like receptors (NLRs) (Arnold et al., 2018).

Upon MAMP recognition, activation of a well-defined set of signalling cascades results in the transcriptional activation or modulation of pro-inflammatory cytokines and other pro-inflammatory genes. Thereby, the activated signalling pathways and downstream outcomes are specific to the type of activational trigger allowing for a tailored innate immune response.

The NOD-like receptor family of pattern recognition receptors

The mammalian NOD-like receptors (NLRs) are a group of cytosolic PRRs that share a common tripartite domain organization consisting of a central ATPase and oligomerization

domain (NACHT), mediating the oligomerization and thus activation of NLRs, a variable number of C-terminal leucine-rich repeats (LRRs), responsible for ligand recognition, and a variable N-terminal effector domain. So-called NLRAs possess an N-terminal caspase-activation and recruitment domain (CARD) associated with an acidic transactivation domain (AD), while NLRBs contain a baculovirus inhibitor of apoptosis protein repeat (BIR) domain (Arnold et al., 2018; Motta et al., 2015; Ting et al., 2008). NLRCs carry one or two CARD or CARD-like domains at the C-terminus, associated proteins for example are NOD1 (NLRC1), NOD2 (NLRC2) and NLRC5. The effector domain of the NLRPs consists of a pyrin domain (PYD), and the corresponding NLRs are designated NLRP1-14 (Arnold et al., 2018; Motta et al., 2015; Ting et al., 2008). Today we know that NLRs confer a plethora of important functions, also beyond acting as PRRs, according to which they can be grouped into the following functional classes: inflammatory NLRs, forming supramolecular signalling complexes mediating pro-inflammatory signalling, regulatory NLRs, modulating rather than initiating inflammatory signalling, and NLRs functioning as transcriptional regulators of molecules involved in antigen presentation.

Examples for 'classical' inflammatory NLRs, which sense MAMPs such as PGN, flagellin or viral RNA (Kim, Shin, & Nahm, 2016) or pathologically altered endogenous molecules, so-called danger-associated molecular patterns (DAMPs) (Matzinger, 2002), like extracellular ATP, crystallised cholesterol, or uric acid crystals (Arnold et al., 2018; Duewell et al., 2010; Motta et al., 2015), are NOD1, NOD2 and NLRP3. NOD1 and NOD2 upon activation oligomerize and recruit their adaptor molecule receptor-interacting serine/threonine-protein kinase 2 (RIPK2) to form the so-called NODosome and downstream activate the nuclear factor 'kappa-light-chain-enhancer' of activated B-cells (NF- κ B) (Arnold et al., 2018; Tattoli et al., 2007). NLRP3, as well as several other NLRP proteins, form so called 'inflammasomes', multiprotein complexes consisting of the corresponding NLR, apoptosis-associated speck-like protein containing a CARD (ASC) and pro-caspase-1. Activation of the inflammasome by a two-step process induces cleavage-mediated activation of caspase-1, ultimately resulting in the processing and thus activation of interleukin (IL) -1 β and IL-18 (Jo et al., 2016; Munoz-Planillo et al., 2013; Petrilli et al., 2007; Vladimer et al., 2013).

Examples for regulatory NLRs include NLRP11 and NLRP12. NLRP11 suppresses NLRP3 inflammasome activation (Kienes et al., 2021), while NLRP12 reduces NF- κ B signalling (Allen et al., 2012; Lich et al., 2007; Wang et al., 2002; Williams et al., 2005) and mitogen-activated

protein kinase (MAPK)/extracellular signalling-related kinase (ERK) activation (Zaki et al., 2011). Both NLRs have been shown to negatively regulate type I interferon (IFN) responses (Chen et al., 2019; Kienes et al., 2021).

The group of transcriptionally active NLRs to date only includes two members, nucleotide-binding and oligomerization domain containing 5 (NLRC5) and Class II Major Histocompatibility Complex Transactivator (CIITA). NLRC5 and CIITA function as master regulators for the transcription of the major histocompatibility complex (MHC) class I and class II genes, respectively, which code for molecules of the antigen presentation pathway, thus linking innate and adaptive immune responses (Meissner et al., 2010; Steimle et al., 1993).

NOD-like receptors as transcriptional regulators – NLRC5, the master regulator of MHC class I genes

NLRC5 generally shares the tripartite structure common to all NLR proteins, consisting of a central NACHT, C-terminal LRRs and an N-terminal effector domain. However, it presents with two rather unique structural features. Firstly, the C-terminal domain of NLRC5 consists of 27 LRRs, making NLRC5 the largest member of the NLR family with 1,866 amino acids in length and an estimated size of 204 kDa (Benko et al., 2010). And secondly, the N-terminal effector domain of NLRC5, which like the effector domains of all NLR proteins is predicted to adopt a death fold, shares homology with the N-terminal CARD domain of the NLRC subfamily, but presents with diverging structural features and is therefore termed untypical CARD (uCARD), in this work also referred to as NLRC5 death domain (NLRC5 DD) (Gutte et al., 2014; Motyan et al., 2013; Neerincx et al., 2010). NLRC5 is expressed by a broad variety of tissues, but high-level expression is found predominantly in immunological organs like spleen, lymph nodes, tonsils, and bone marrow, but also in the large intestine, lungs and prostate. On a cellular level, *NLRC5* is predominantly expressed in primary human immune cells, like CD4⁺ and CD8⁺ T cells, B cells and, to a lesser extent, CD14⁺ leukocytes. In addition, several cell lines present with high *NLRC5* expression, for example human THP-1 macrophage-like cells, human Jurkat T cells, as well as murine RAW264.7 macrophages (Benko et al., 2010; Cui et al., 2010; Kuenzel et al., 2010; Neerincx et al., 2010; Neerincx et al., 2012).

NLRC5 belongs to the sub-group of NLRs functioning as a transcriptional activator and was discovered as its second member after CIITA, which already in 1993 was identified as the master regulator of MHC class II genes mediating the presentation of extracellular antigens by

professional antigen-presenting cells to CD4⁺ T cells, thereby initiating an adaptive immune response against extracellular microbial challenges (Steimle et al., 1993). In correspondence with the high sequence homology with CIITA (Benko et al., 2010; Meissner et al., 2010), NLRC5 was shown to be the transcriptional master regulator of MHC class I molecules which are located on the surface of every nucleated body cell and mediate the presentation of cytoplasmic antigens to CD8⁺ T cells (Meissner et al., 2010). MHC class I molecules consist of an alpha chain (also referred to as heavy chain) and the non-covalently attached β -2-microglobulin (β 2M). Antigens presented on MHC class I molecules are derived from the degradation of cytoplasmic proteins via the so-called immunoproteasome. The resulting peptides are transported into the lumen of the endoplasmic reticulum via transporter associated with antigen processing (TAP) where they are loaded onto freshly synthesized MHC class I molecules by the peptide loading complex (PLC), consisting of TAP, the oxidoreductase ERp57 and the three chaperones tapasin, calnexin and calreticulin. Loaded MHC class I molecules are then released to the cell surface (Leone et al., 2013). Presentation of microbial or mutated endogenous peptides by MHC class I molecules leads to their recognition by CD8⁺ T cells culminating in lysis of the infected or mutated cell. Presentation of unmutated endogenous peptides serves as identification as endogenous and normally does not lead to CD8⁺ T cell activation (Leone et al., 2013). Missing MHC class I surface expression, often found on virus infected or tumour cells to escape immune recognition, leads to elimination of the cell by Natural Killer (NK) cells (Kumar & McNerney, 2005).

Transcriptional regulation of MHC class I genes is mediated by NLRC5. Ectopic expression or induction of NLRC5 in cell lines and primary cells leads to increased expression of MHC class I molecules (Biswas et al., 2012; Meissner et al., 2010; Neerinx et al., 2012; Staehli et al., 2012), whereas deficiency of *NLRC5* was shown to reduce MHC class I expression (Biswas et al., 2012; Neerinx et al., 2012; Robbins et al., 2012; Staehli et al., 2012; Yao et al., 2012). Furthermore, expression of human leukocyte antigen B (HLA-B), an MHC class I heavy chain paralogue, correlates with *NLRC5* expression in several human tissues, and human NLRC5 restores MHC class I expression in the MHC class I-deficient murine melanoma cell line B16F10 (Neerinx et al., 2012). NLRC5 additionally regulates genes related to MHC class I-dependent antigen presentation, including β 2M, TAP and the low molecular mass peptides (LMP) (Biswas et al., 2012; Ludigs et al., 2015; Meissner et al., 2010). Of interest, recent reports indicate NLRC5 as transcriptional regulator beyond MHC class I and related genes. *NLRC5*

deficiency led to reduced expression of peroxisome proliferator-activated receptor γ (PPAR γ) target genes, while ectopical NLRC5 was shown to increase PPAR response element (PPRE)-mediated luciferase reporter gene activity (Luan et al., 2019). In addition, NLRC5 recently has been shown to associate with the promoters and thus mediate the transcription of butyrophilin (BTN) genes, important mediators of $\gamma\delta$ T cell activation (Dang et al., 2021).

NLRC5 is shuttling between the nucleus and the cytoplasm. Nuclear translocation of NLRC5 is mediated by a bipartite N-terminal nuclear localization sequence (NLS) located between the uCARD and the NACHT domain (Meissner et al., 2010; Meissner et al., 2012a) and is dependent on a functional ATPase domain, as the ATPase deficient NLRC5 Walker A K234A mutant presents with exclusively cytoplasmic localization (Neerincx et al., 2012). Nuclear export of NLRC5 is Exportin 1-mediated (Benko et al., 2010; Meissner et al., 2010; Neerincx et al., 2012) and seems to be dependent on an intact LRR domain, as the naturally occurring Isoform 3 of NLRC5, devoid of most of the LRR domain, presents with predominantly nuclear localization, even in the absence of nuclear export inhibition (Neerincx et al., 2012). NLRC5 Walker A K234A, NLRC5 Isoform 3 and an NLRC5 construct lacking the N-terminal DD were shown to be deficient in MHC class I promoter activation. This effect, although less pronounced, was also seen for an NLRC5 construct with forced nuclear localization by introduction of two NLS motifs. Together, these data show that NLRC5 transcriptional activity depends on its nuclear localization and the presence of its LRR and DD domain, and potentially is modulated by cytoplasmic modifications preceding nuclear import (Neerincx et al., 2012). In fact, the N-terminal DD has been proven to mediate NLRC5 transcriptional activity (Neerincx et al., 2014).

Lacking a DNA binding domain (DBD), NLRC5, like CIITA, relies on the so-called MHC enhanceosome, a multiprotein DNA binding complex, to associate with conserved *cis*-regulatory S, X and Y box motifs in the regulatory regions within the MHC class I promoters (van den Elsen et al., 1998a; van den Elsen et al., 1998b). The MHC enhanceosome consists of the tripartite regulatory factor X (RFX) complex, cyclic AMP response element binding protein (CREBP) and the nuclear factor Y (NFY) complex, which associate with the X1, X2 and Y box, respectively (Downs et al., 2016; Ludigs et al., 2015; Meissner et al., 2012b; Neerincx et al., 2012). The transcription factor binding the S box to date remains unknown. Interestingly, the S box has been shown to be essential for both NLRC5 transcriptional activity and its specificity to MHC class I genes (Ludigs et al., 2015; Meissner et al., 2012b). In its own promoter, NLRC5

carries a predicted interferon stimulated response element (ISRE) and a potential NF- κ B consensus-binding site (Kobayashi & van den Elsen, 2012; Kuenzel et al., 2010), allowing for its induction by type I and II IFNs and viral infection (Benko et al., 2010; Kuenzel et al., 2010; Neerincx et al., 2010; Staehli et al., 2012), as well as by pro-inflammatory innate immune stimuli such as polyinosinic-polycytidylic acid (poly I:C) and LPS (Kuenzel et al., 2010; Neerincx et al., 2010; Staehli et al., 2012).

Beside its main function as transcriptional regulator, roles of NLRC5 in NF- κ B-mediated pro-inflammatory signalling (Benko et al., 2010; Cui et al., 2010; Kumar et al., 2011; Li et al., 2014; Robbins et al., 2012; Tong et al., 2012; Yao et al., 2012), IFN regulation (Cui et al., 2010; Kuenzel et al., 2010; Neerincx et al., 2010; Tong et al., 2012; Wu et al., 2017), malignant transformation (Chelbi & Guarda, 2016; Ma et al., 2016; Peng et al., 2016; Rodriguez et al., 2016; Shukla et al., 2021; Staehli et al., 2012) and inflammasome activation (Davis et al., 2011; Triantafilou et al., 2013; Yao et al., 2012) have been described, with NLRC5-mediated NF- κ B regulation being the best established, but controversially discussed function of NLRC5 away from transcriptional regulation. NLRC5 has been shown to inhibit NF- κ B signalling *in vitro* in a HEK293T cell-based reporter gene assay (Benko et al., 2010; Cui et al., 2010) and in RAW264.7 macrophages (Benko et al., 2010; Li et al., 2014), with ectopical NLRC5 expression resulting in reduced, and *NLRC5* silencing culminating in increased secretion of IL-6, tumour necrosis factor α (TNF- α) and IL-1 β and reduced levels of IL-10 (Benko et al., 2010; Li et al., 2014). *In vivo*, Tong et al. found enhanced IL-6 and IFN- β production in *Nlrc5* deficient murine embryonic fibroblasts (MEF), peritoneal macrophages and bone marrow-derived macrophages (BMDMs) in LPS or vesicular stomatitis virus-challenged *Nlrc5* knockout (KO) animals (Tong et al., 2012). In accordance, accelerated cardiac fibrosis and remodelling with increased NF- κ B activation and Tnf- α , transforming growth factor β (Tgf- β) and IL-6 production in *Nlrc5* KO mice on was reported upon high-fat diet (HFD) feeding (Ma & Xie, 2017) and cardiac pressure overload (Yu et al., 2023). In contrast, *Nlrc5* deficiency was reported to reduce diabetic kidney injury by suppression of NF- κ B and reduction of the TGF- β /Smad pathway compared to *Nlrc5* sufficient mice (Luan et al., 2018). For some *Nlrc5* KO mouse models, no differences in NF- κ B activation and downstream signalling were found (Kumar et al., 2011; Robbins et al., 2012; Yao et al., 2012). More recently, it was shown that NLRC5 undergoes ubiquitination after LPS treatment, disrupting its association with the NF- κ B inhibitor IKK- β , thereby allowing for IKK- β degradation and downstream NF- κ B activation.

Removal of these polyubiquitin chains from NLRC5 by ubiquitin-specific protease 14 (USP14), and thus stabilization of the NLRC5:IKK- β interaction, enhances NF- κ B inhibition by NLRC5. It was proposed that given the varying levels of USP14 in different cell types, this mechanism might explain the diverse NF- κ B inhibitory efficiencies of NLRC5 reported by independent groups using different experimental models (Meng et al., 2015).

Taken together, NLRC5 is the transcriptional master regulator of MHC class I genes with additional implications in innate immune signalling, best established the inhibition of NF- κ B-mediated inflammation.

Obesity and the innate immune system – an intimate relationship

The rates of obesity have increased alarmingly fast in the last decades, especially in countries with a Western industrialized lifestyle (Ng et al., 2014). According to data from the World Health Organization (WHO), its worldwide prevalence has nearly tripled from 1975 to 2016, with 13% of the world's adult population being obese in 2016. Obesity is defined by a body mass index (BMI) over 30 kg/m². Its main characteristics is the excess of adipose tissue (AT), whereby the presence of excessive visceral adipose tissue and the associated increased waist circumference in obese individuals is considered particularly unfavourable. Together with hypertension, hypertriglyceridemia, lowered high density lipoprotein (HDL) cholesterol and insulin resistance (IR), the disease pattern is called the metabolic syndrome (MetS), and is a risk factor for the development of type 2 diabetes mellitus (T2DM), atherosclerosis and non-alcoholic fatty liver disease (NAFLD) (Eckel, Grundy, & Zimmet, 2005).

Since the discovery that the AT produces TNF- α in a mouse model of HFD-induced obesity (Hotamisligil, Shargill, & Spiegelman, 1993), the intimate connection between our immune system, especially the innate immunity, and the state of obesity has become increasingly evident. To date, the AT is acknowledged to be not just a mere energy storage organ, but a tissue of high immunological relevance, especially in the state of obesity (reviewed in (Wellen & Hotamisligil, 2005)). One striking example for the close link of obesity and the immune system is the chronic state of sterile, low-grade inflammation, which is a pathological feature of obesity-associated IR, T2DM, atherosclerosis and NAFLD. Although clear evidence confirming these low-grade inflammatory responses as initial triggers of obesity-associated diseases is still lacking, a large body of evidence supports the contribution

of inflammatory signalling to the deterioration of adiposity-associated morbidities (Hotamisligil, 2006).

Initiation of this low-threshold inflammatory state has been proposed to be mediated by a condition termed metabolic endotoxemia, referring to the translocation of microbial and nutritional compounds from the gut into the circulation, the translocation being caused by an increase in gastrointestinal permeability upon HFD feeding (leaky gut syndrome) (Cani et al., 2007; Cani et al., 2008; Chan et al., 2017; Erridge et al., 2007; Luck et al., 2015). Increased pro-inflammatory signalling and cytokine release in the AT of obese humans and mice fed a HFD suggests a key role of adipocytes and AT-infiltrating and -resident immune cells, especially macrophages, as sensors for the metabolic endotoxemia and drivers of the subsequently induced low-grade inflammation (Olefsky & Glass, 2010; Shoelson, Lee, & Yuan, 2003; Weisberg et al., 2003). Adipocytes of obese individuals further contribute to this low-grade inflammation by dying from hypoxia, as oxygen supply, similar as in tumour tissue, does not accommodate to their extensive increase in size (Halberg et al., 2009). Dying adipocytes are rapidly surrounded and taken up by adipose tissue macrophages (ATMs), resulting in their pro-inflammatory activation (Lindhorst et al., 2021). Additionally, it has been shown that enlarged adipocytes stimulate collagen synthesis, thus leading to AT fibrosis which in turn is limiting the expansion and thus lipid storage capacity of adipocytes. This leads to a 'lipid-spillover', in turn leading to the production of lipotoxic, highly immunogenic molecules, for example ceramides. By that, AT fibrosis is contributing to AT inflammation, activation of stress pathways and additionally deposition of lipids outside the AT as ectopic fat, for example in the liver (Halberg et al., 2009; Khan et al., 2009; Sun et al., 2013).

All together, these AT-derived pro-inflammatory signals act in a paracrine and autocrine manner but are also distributed systemically and give rise to the state of chronic, low-threshold inflammation in obese individuals, that at least worsens, if not causes, obesity-associated morbidities.

NOD-like receptors in obesity and associated morbidities

As outlined above, the immune system plays an important role in the development and/or maintenance of obesity-associated morbidities. Most strikingly, knockout or knockdown (KD) of PRRs improves obesity-associated comorbidities and inflammation in mice

and human and murine cells. This has been first shown for TLR4, whose deficiency improved IR and AT inflammation in female mice on a 16-week HFD (Shi et al., 2006).

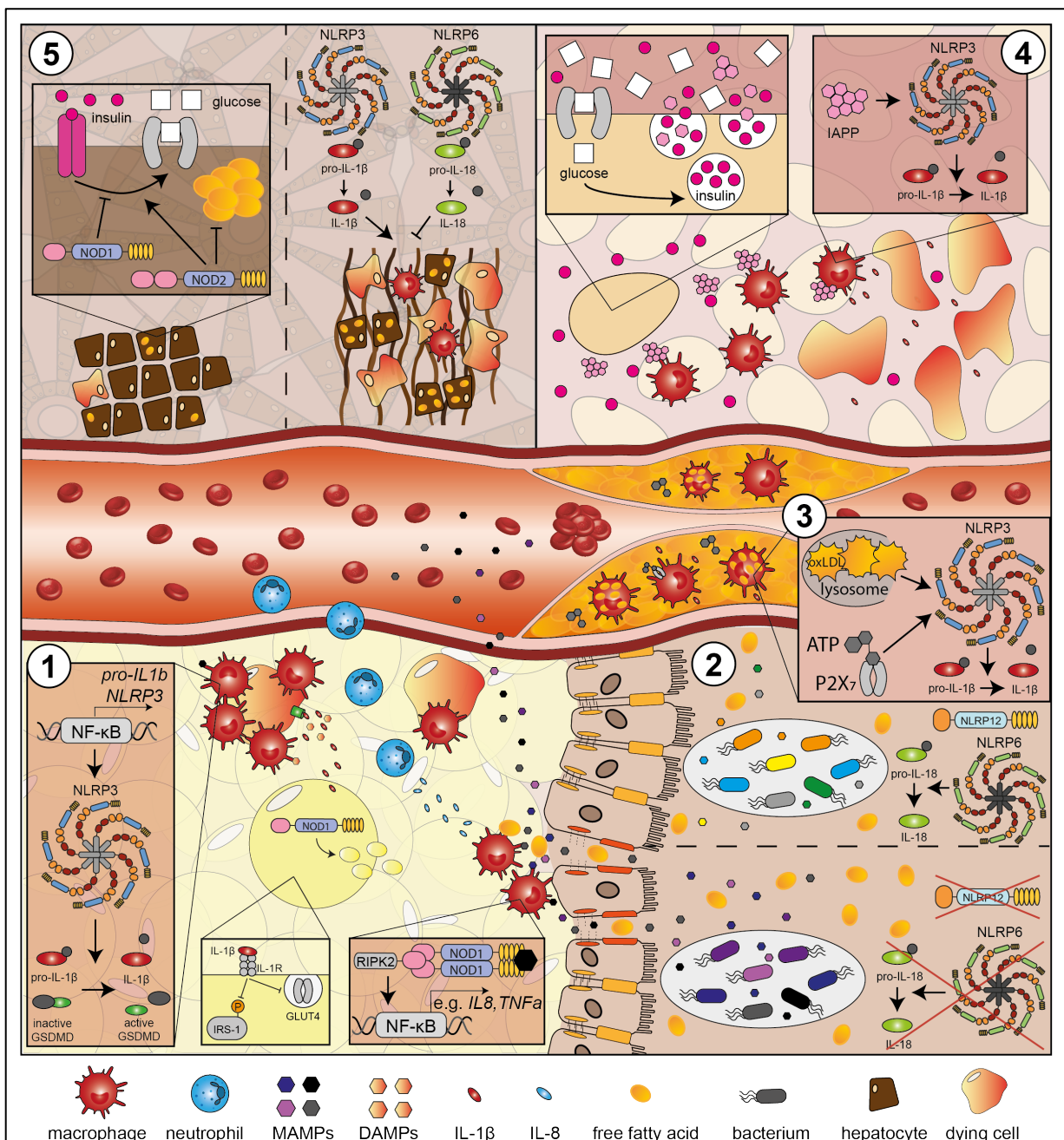
Also, the NLR family has been shown to be involved in the low-grade inflammatory status associated with obesity and its comorbidities. Genetic deficiency of the NLR protein NOD1 in mice reduced HFD-induced AT inflammation, weight gain and IR (Chan et al., 2017; Schertzer & Klip, 2011; Schertzer et al., 2011). NOD1 activation by PGN fragments, whose abundance is elevated in the circulation after HFD feeding, increases peripheral and hepatic IR and pro-inflammatory cytokine secretion (Chan et al., 2017; Schertzer et al., 2011; Sharma et al., 2022) (Figure 1, panel 1, 5). In humans, *NOD1* expression is increased in patients with T2DM (Shiny et al., 2013), gestational diabetes (Lappas, 2014) and MetS (Zhou et al., 2015). For the NLR protein NLRP3, similar effects have been reported, with *Nlrp3* KO in mice leading to reduced IR, AT infiltration of macrophages, and insulin and glucose levels in the serum and protection against HFD-induced, IL-1 β -mediated β -cell fibrosis (Figure 1, panel 1, 4) (Stienstra et al., 2011; Wen et al., 2011; Youm et al., 2011). In humans, NLRP3 and IL-1 β levels in the AT are positively correlated with the extent of obesity and IR (Bando et al., 2015; Esser et al., 2013; Serena et al., 2016; Yin et al., 2014). Furthermore, NLRP3 has been identified as the main driver of atherosclerosis-associated inflammation, being activated by cholesterol crystals (Düwell et al., 2010), and as contributing factor to HFD-induced liver steatosis and hepatic IR (Sokolova et al., 2019; Vandanmagsar et al., 2011; Wree et al., 2014) (Figure 1, panel 3, 5).

In contrast to NOD1 and NLRP3, the NLR proteins NOD2 and NLRP12 have been shown to confer protective roles in obesity and associated morbidities in mice. Although structurally and functionally closely related to NOD1, *Nod2* deficient mice present with increased weight gain and AT inflammation under both, normal and HFD feeding, while *Nod2* activation in obese animals led to reduced AT inflammation and IR (Carlos et al., 2020; Cavallari et al., 2017; Denou et al., 2015; Rodriguez-Nunez et al., 2017). Additionally, *Nod2* was shown to protect against HFD-induced liver steatosis and fibrosis and hepatic IR (Cavallari et al., 2017; Cavallari et al., 2020b) (Figure 1, Panel 5). Similarly, *Nlrp12* deficiency leads to increased body weight and AT inflammation and decreased insulin sensitivity in HFD-fed mice. Interestingly, co-housing studies revealed the effect of *Nlrp12* deficiency to be microbiome-mediated (Figure 1, Panel 2) (Truax et al., 2018). In fact, NLRP12 is not the only NLR protein known to positively influence the microbiome. Also NLRP6 has been shown to protect gut microbiome integrity, its deficiency altering microbiome composition and allowing for increased translocation of

The role of NLRC5 in obesity - Introduction

MAMPs into the circulation, thus contributing to metabolic endotoxemia (Henao-Mejia et al., 2012) (Figure 1, Panel 2).

So, the roles of NLR proteins in obesity are multifaceted. Some NLRs, like NOD1 and NLRP3, contribute to low-grade and AT inflammation and thus worsen obesity-associated morbidities via their 'classical' pro-inflammatory signalling. Others, like NOD2, NLRP12 and NLRP6, are rather conferring regulatory and protective effects in the obesity context, some mediated via alterations of the gut microbiome composition and gastrointestinal integrity. And yet for most of the NLR proteins known so far, their role in obesity has not yet been investigated or is just beginning to emerge. An example for the letter is NLRC5.



The role of NLRC5 in obesity - Introduction

Figure 1: **Effects and sites of action of NLR proteins in obesity and associated morbidities.** **(1)** In the adipose tissue (AT), metabolic endotoxemia is sensed by adipose tissue macrophages (ATMs) via NOD1. NOD1 activation leads to NF- κ B-mediated NLRP3 inflammasome priming, adipocyte lysis and the transcription of pro-inflammatory cytokines, which lead to the recruitment of neutrophils. Activation of the NLRP3 inflammasome induces IL-1 β - and Gasdermin D (GSDMD)-mediated AT inflammation, pyroptosis and insulin resistance (IR). **(2)** Deficiency in *NLRP6*, and subsequently IL-18, or *NLRP12* alters commensal gut microbiota composition, leading to increased translocation of microbe-associated molecular patterns (MAMPs) to the circulation (NLRP6) or the induction of obesity, IR and inflammation (NLRP12). **(3)** In atherosclerotic plaques, oxidatively modified low-density lipoprotein cholesterol (oxLDL) crystals lead to lysosomal rupture in macrophages; release of ATP leads to NLRP3 inflammasome activation and subsequent IL-1 β release. **(4)** Steadily elevated insulin secretion due to hyperglycaemia leads to high secretion and ultimately aggregation of islet amyloid polypeptide (IAPP). IAPP aggregates activate the NLRP3 inflammasome and IL-1 β production in pancreatic macrophages, leading to IL-1 β -mediated destruction of pancreatic β -cells. **(5)** In the liver, IL-18 production via the NLRP6 or NLRP3 inflammasomes leads to decreased liver steatosis and fibrosis, while IL-1 β leads to increased liver steatosis and fibrosis. NOD1 reduces while NOD2 increases hepatic insulin sensitivity in response to gut derived activators. Additionally, NOD2 reduces hepatic lipid accumulation.

NLRC5 – implications in metabolic traits

As stated above, the transcriptional regulation of MHC class I genes is the major function of NLRC5 known so far. Recent evidence now suggests a novel role for NLRC5 also in metabolic traits. Two independent epigenome-wide association studies identified the *NLRC5* locus to be differentially methylated in normal weight versus obese individuals, but with conflicting results. Meeks et al. identified the methylation of the *NLRC5* locus to be positively associated with BMI, obesity, and waist circumference in a Ghanaian cohort (Meeks et al., 2017). In contrast, Cao-Lei et al. found the *NLRC5* locus to be hypo-methylated in children with obesity compared to normal-weight children (Cao-Lei et al., 2019). Moreover, *NLRC5* was identified as a candidate gene to affect HDL cholesterol levels in humans (Charlesworth et al., 2009) and single nucleotide polymorphisms (SNP) in *NLRC5* and its promoters have been associated with altered triglyceride levels as well as dyslipidaemia (Hosseinzadeh et al., 2019; Lin et al., 2018). In mice, *Nlrc5* deficiency was shown to alleviate HFD-induced diabetic nephropathy (Luan et al., 2018) but to aggravate myocardial damage (Ma & Xie, 2017). Additionally, *Nlrc5* KO mice on HFD have been reported to gain more body weight (Ma & Xie, 2017).

Together, these studies support novel roles of NLRC5 in metabolism and body weight regulation, but the underlying mechanisms so far have not been studied.

PPAR γ - The master regulator of adipogenesis

PPAR γ is one of the three members of the PPAR family alongside PPAR α and PPAR β/δ . PPARs are nuclear receptors (NR) belonging to the steroid receptor superfamily and function as ligand-activated transcription factors, regulating the expression of genes involved in cell differentiation and metabolic control, most pronounced lipid and glucose metabolism (Grygiel-Gorniak, 2014). Concomitantly with its predominant expression in white adipose tissue (WAT) (Auboeuf et al., 1997), PPAR γ is designated the master regulator of adipogenesis, as it has been shown to be indispensable for adipocyte differentiation *in vitro* (Rosen et al., 1999; Tontonoz, Hu, & Spiegelman, 1994) and *in vivo* (Barak et al., 1999; He et al., 2003; Rosen et al., 1999; Wang et al., 2013). Heterozygous expression of a dominant negative version of PPAR γ as well as AT-specific *Pparg* KO in mice results in the development of lipodystrophy, IR, hyperlipidaemia, and hepatic steatosis (Freedman et al., 2005; He et al., 2003; Wang et al., 2013). In humans, dominant negative mutations of *PPARG* are known, their impacts ranging from modest increase in T2DM risk (Altshuler et al., 2000) to lipodystrophy, severe IR, T2DM, steatohepatitis and hypertension (Agarwal & Garg, 2002; Agostini et al., 2006; Barroso et al., 1999; Hegele et al., 2002; Savage et al., 2003). PPAR γ further is needed to keep adipocytes in a differentiated state, as inducible KO of *Pparg* in differentiated murine adipocytes is followed by adipocyte death (Imai et al., 2004). So far, no factor has been found, that is able to compensate for PPAR γ in adipogenesis, highlighting its importance in AT formation and maintenance.

PPAR γ is sharing the general structure of NRs, harbouring an activation function 1 (AF-1) motif in its C-terminal A and B domain, implicated in ligand-independent co-regulator binding, and a DBD in its central C domain (Kroger & Bruning, 2015). The DBD contains two highly conserved zinc finger proteins that bind to the DNA by docking to a consensus AGGTCA sequence repeated once and separated by one nucleotide in the promotor region of target genes, the so-called direct-repeat 1 (DR-1) or PPRE (A et al., 1997). Additionally, the DBD is also involved in dimerization with other NRs, thus containing a dimerization interface. The D domain of PPAR γ consists of a flexible hinge region and contains a NLS, while the N-terminal E domain harbours the ligand-binding domain (LBD) as well as an AF-2 motif and a second co-regulator binding site (Kroger & Bruning, 2015).

In the unbound state, PPAR γ is kept inactive by binding to a co-repressor, for example nuclear receptor co-repressor (NCoR) or silencing mediator of retinoid and thyroid hormonal

receptors (SMRT) (Yu et al., 2005). Upon ligand-binding, the LBD is stabilized, leading to a conformational change facilitating the binding of co-activators, which in turn increase chromatin accessibility, enabling gene transcription (Chandra et al., 2008; Helsen & Claessens, 2014; Johnson et al., 2000). For DNA binding, PPAR γ requires heterodimerization with the retinoid X receptor (RXR) (Miyata et al., 1994; Tontonoz et al., 1994), itself a NR serving as heterodimerization and DNA-binding partner for several NRs (Evans & Mangelsdorf, 2014).

The PPAR γ gene contains separate promoters, which together with alternative splicing is giving rise to three PPAR γ mRNAs. *PPAR γ 1* and *PPAR γ 3* are encoding for the same protein (referred to as PPAR γ 1), whereas *PPAR γ 2* encodes a longer version of PPAR γ with 28 and 30 additional N-terminal amino acids in human and mice, respectively (Beamer et al., 1997; Elbrecht et al., 1996; Fajas et al., 1997; Fajas, Fruchart, & Auwerx, 1998; Zhu et al., 1995). PPAR γ 1 is expressed in AT but also in relatively high levels in macrophages (Ricote et al., 1998), colon epithelium (Auboeuf et al., 1997; Mansen et al., 1996) and endothelia (Marx et al., 1999). The expression pattern of PPAR γ 2 is mainly restricted to the AT, and has been described to be induced by HFD in mice and elevated in obese individuals (Auboeuf et al., 1997; Vidal-Puig et al., 1996; Vidal-Puig et al., 1997).

Activation of PPAR γ in adipocytes initiates the expression of proteins involved in lipid metabolism and lipid accumulation, thereby leading to adipocyte differentiation. Examples are lipoprotein lipase (LPL), acyl CoA synthetase, fatty acid transport protein (FATP) and cluster of differentiation 36 (CD36) (also known as fatty acid translocase, FAT) (Grygiel-Gorniak, 2014; Nakachi et al., 2008). Another PPAR γ target is the fatty acid-binding protein 4 (FABP4). FABP4 maintains adipocyte homeostasis and regulates lipolysis and adipogenesis through interaction with the hormone-sensitive lipase (HSL) and PPAR γ , respectively (Jenkins-Kruchten et al., 2003; Schroeder et al., 2008). During lipolysis, FABP4 is believed to bind free fatty acids in the cytoplasm to guide them out of the cell (Hofer et al., 2015). As it is one of the most abundant proteins in fat cells (Matarese & Bernlohr, 1988), FABP4 is often used as marker for adipocytes and adipocyte differentiation.

Apart from its function as adipogenic master regulator, PPAR γ was also shown to confer anti-inflammatory properties, especially in monocytes and macrophages. PPAR γ activation in murine BMDMs and human monocytes contributes to their polarization to a homeostatic, alternatively activated phenotype (M2 phenotype) (Bouhlef et al., 2007; Odegaard et al., 2007). In line, stimulation of human monocytes with the PPAR γ agonist rosiglitazone led to a

reduction of TNF- α secretion upon phorbol 12-myristate 13-acetate (PMA) stimulation (Hong et al., 2003). The same has been shown for 15-deoxy- Δ -12, 14-prostaglandin J₂ (15d-PGJ₂) (Jiang, Ting, & Seed, 1998), which is a derivate of the prostaglandin J₂ series and has been identified as potent 'naturally occurring' PPAR γ ligand (Forman et al., 1995; Kliewer et al., 1995). Different mechanisms of PPAR γ 's inflammation-dampening properties have been proposed, most of them culminating in the suppression of NF- κ B signalling. PPAR γ , additionally to its function as transcriptional activator, functions as E3 ubiquitin ligase and was shown to ubiquitinate the p65 subunit of NF- κ B, leading to its degradation (Hou, Moreau, & Chadee, 2012). Furthermore, PPAR γ has been shown to directly bind to and thus potentially trap NF- κ B in LPS-stimulated macrophages (Chung et al., 2000). Another study proposed PPAR γ activation to lead to reduced p65 acetylation, thereby decreasing its nuclear translocation and reducing expression of pro-inflammatory genes (Zhang et al., 2016). Also, p38 MAPK phosphorylation and thus activation has been shown to be reduced by PPAR γ activation (Ji et al., 2010). However, how exactly PPAR γ is mediating its anti-inflammatory properties remains unknown.

PPAR γ has been reported to alleviate NLRP3-induced inflammation, for example in spinal cord neurons (Fu et al., 2021; Meng et al., 2019), but apart from these reports, only few studies link PPAR γ to the NLR protein family. Interestingly, it appears that especially the transcriptionally active NLRs are physically and functionally connected with PPAR γ . CIITA has been shown to be induced by and to interact with PPAR γ in human vascular smooth muscle cells and the context of collagen synthesis, respectively (Kong et al., 2009; Xu, Farmer, & Smith, 2007). Also NLRC5 recently was shown to interact with PPAR γ in human aortic smooth muscle cells in the context of vascular remodelling (Luan et al., 2019).

In summary, PPAR γ is the master regulator of adipogenesis, inducing and maintaining adipocyte differentiation and ensuring metabolic homeostasis, but also confers important functions in reducing and resolving inflammation.

Aim of the study

The intimate relationship between the innate immune system and the state of obesity has become increasingly clear over the last years, with the obesity-accompanying state of chronic, sterile, low-grade inflammation at least contributing to, if not causing, most of the obesity-associated morbidities. NLR proteins have been discovered as critical sensors shaping this low-grade inflammation, some aggravating, some protecting against obesity and its

morbidities. NLRC5, the master transcriptional regulator of MHC class I genes, recently has been implicated in metabolic trades, but the underlying mechanisms so far have not been studied.

To functionally assess the role of NLRC5 in obesity, the effect of *Nlrc5* deficiency in a mouse model of HFD-induced obesity was investigated using two different *Nlrc5* KO mouse lines. Mice were characterized by means of phenotypical, morphological, biochemical, and microbial analysis. The effect of NLRC5 on adipocyte differentiation was studied by modifying *Nlrc5* expression in the 3T3-L1 preadipocyte cell line using CRISPR/Cas9 technology. To elaborate on the mechanism of NLRC5's effect in obesity, *in vitro* studies using stable cell lines as well as primary cells were performed, investigating the influence of NLRC5 on the master regulator of adipogenesis, PPAR γ , and its targets in the context of obesity and inflammation. Lastly, the effect of obesity on the expression of a variety of NLRs was investigated in both mice and human to identify other NLR proteins potentially involved in the regulation of obesity and its associated morbidities.

Materials and Methods

Materials

Mice

Nlrc5^{ΔExon4-7} mice and HFD feeding protocol

Nlrc5 WT and *Nlrc5* deficient mice in C57BL/6N background were kindly provided by Philip Rosenstiel (University of Kiel). KO mice (B6.129Sv/Pas-*Nlrc5*tm1) were generated by GenOway. *Nlrc5* was targeted in 129SvPas embryonic stem cells that were injected into a blastocyst of a C57BL/6J mouse. A targeting vector was designed in which exons 4 – 7 were replaced by a loxP-flanked neomycin resistance cassette. Chimeric animals were mated to C57BL/6J mice. The *Nlrc5* KO, hereafter termed *Nlrc5*^{ΔExon4-7} mice were finally back crossed on C57BL/6N background (B6.129Sv/Pas-*Nlrc5*tm1geno). Genotyping was performed by Endpoint PCR using DNA isolated from tail tips. DNA was extracted using the DNeasy Blood & Tissue Kit (Qiagen) according to manufacturer's instructions. For Endpoint PCR, 2xKAPA2G Fast HotStart Genotyping Mix (KAPA Biosystems) and the corresponding oligos (Table 6) were used. Mice were imported by embryo transfer into the SPF (specific pathogen free) containment at the central animal facility of the University of Hohenheim and KO and WT littermates were outcrossed on a C57BL/6N background. Animals were started on experimental diet at the age of 8 weeks. For the experiment, mice were kept in the working area of the central animal facility of the University of Hohenheim. WT and *Nlrc5*^{ΔExon4-7} mice were not co-housed. All mice were fed a synthetic low-fat control diet (SSNIFF, E15000) (detailed diet composition see Suppl. Table 1) ad libitum for 1 week to adapt the mice to the diet. Afterwards, *Nlrc5* WT and KO mice were randomly distributed on the intervention groups (n=5), either receiving the low-fat control diet or a synthetic HFD containing 30% crude fat (SSNIFF, E15186) (for detailed diet composition see Suppl. Table 1). Mice were fed ad libitum for a total of 11 weeks and were weighed twice a week. Food uptake was determined once a week by back weighting the remaining food in each cage. Mice were kept in a 12 h light/dark cycle. Mice were dissected directly after sacrifice by CO₂ inhalation and blood collection by heart puncture, and epididymal and inguinal AT weights were determined. Tissues for RNA isolation were snap-frozen in liquid nitrogen and stored at -80°C until use. Tissues for histology were put in tissue embedding cassettes and maintained in 4% PFA at 4°C overnight before being dehydrated in an ascending ethanol series and paraffin-embedded using the Leica TP1020 automatic

benchtop tissue processor (Leica). The use of mice and all following treatments were performed according to FELASA and institutional guidelines and were approved by the local authorities of the state of Baden-Württemberg, in accordance with the animal protection law of Germany, under the license number V347/18 EM, 35-9185.81/0469 and are described in the NTP 00024601-1-4.

***Nlrc5*^{ΔExon4} mice and HFD feeding protocol**

Nlrc5^{ΔExon4} mice in C57BL/6N background were kindly provided by Dana Philpott (Department of Immunology, University of Toronto). Briefly, *Nlrc5* exon 4 was flanked by two loxP sites and mice were crossed with CMV-Cre mice, leading to deletion of the loxP-flanked region. Resulting *Nlrc5*^{ΔExon4} mice were then back crossed to allow for CMV-Cre elimination (Sun et al., 2019). C57BL/6N WT mice were used as controls. Genotyping was performed by Endpoint PCR using DNA isolated from liver. DNA was extracted using the DNeasy Blood & Tissue Kit (Qiagen) according to manufacturer's instructions. For Endpoint PCR, 2xKAPA2G Fast HotStart Genotyping Mix (KAPA Biosystems) and the corresponding oligos (Table 6) were used. Mice were housed in individually ventilated cages at maximum 4 animals per cage at the animal facility of the University of Sherbrooke under SPF conditions. Mice were started on a HFD containing 35% crude fat (Research Diets Inc., D12492; for detailed diet composition see Suppl. Table 2) at the age of 8 – 10 weeks and fed for 20 weeks. The experiment was started as and when the mice became available. Mice were weighted once a week. Mice were anesthetized with isoflurane, sacrificed by CO₂ inhalation and death was confirmed by cervical dislocation. Directly after sacrifice, mice were dissected and epididymal and inguinal AT as well as liver weight were determined. Tissues for RNA isolation were snap-frozen in liquid nitrogen and stored at -80°C until use. Tissues for histology were maintained in 4% PFA for 12 – 16 h before being embedded in paraffin. All experimental protocols on animals were carried out with the approval of the Université de Sherbrooke Animal Ethics Committee.

Cell lines and bacteria

All mammalian cell lines were maintained at 37°C and 5% CO₂ in 100% humidity in the indicated cell culture medium containing 10% heat-inactivated foetal bovine serum (FBS) (PAN Biotech) or 10% FBS Xtra (Capricorn Scientific) and 100 U/ml penicillin (Gibco) and 100 µg/ml

streptomycin (Gibco), if not stated otherwise. Cells were routinely monitored for the absence of mycoplasma infection by PCR.

Bacteria were grown at 37°C in Lysogeny Broth (LB), if not stated otherwise.

HEK293T

Human embryonic kidney 293T cells (HEK293T, ATCC, CRL-3216) were grown in Dulbecco's Modified Eagle Medium (DMEM) 4.5 g/L D-glucose (ThermoFisher Scientific).

Lenti-X™ 293T

Lenti-X™ 293T producer cells (originally purchased from Takara, Cat. No. 632180; kindly provided by Dr. Cathrin Hagenlocher, University of Stuttgart) were grown in DMEM 4.5 g/L D-glucose (ThermoFisher Scientific) supplemented with 10% heat inactivated FBS (Pan Biotech), 100 U/ml Penicillin (Gibco), 100 µg/ml Streptomycin (Gibco), 4 mM L-glutamine (Gibco) and 1 mM sodium pyruvate (Gibco).

HeLa Flp-In T-REx

Stable, inducible HeLa cell lines expressing GFP (Ellwanger et al., 2019), GFP-NLRC5, GFP-NLRC5 NLS I, GFP-NLRC5 2xNLS and GFP-NLRC5 Iso3 (Kienes, 2021) were previously generated in our lab. Briefly, HeLa Flp-In cell lines were generated by co-transfection of pOG44 and pcDNA5/FRT/TO-GFP, pcDNA5/FRT/TO-GFP-NLRC5, pcDNA5/FRT/TO-GFP-NLRC5 NLS I, pcDNA5/FRT/TO-GFP-NLRC5 2xNLS or pcDNA5/FRT/TO-GFP-NLRC5 Iso3 into HeLa Flp-In T-REx cells (kindly provided by the Hentze Lab, EMBL Heidelberg) using Lipofectamine™ 2000 (ThermoFisher Scientific). Transfectants were selected with 10 µg/ml blasticidin (InvivoGen) and 600 µg/ml hygromycin (InvivoGen). Single clones were selected and characterized for inducible and uniform expression. Target gene expression was induced by 1 µg/ml doxycycline for at least 20 h prior to further experiments. Stable cell lines were grown in DMEM 4.5 g/L D-glucose (ThermoFisher Scientific).

THP-1

The *NLRC5* deficient THP-1 cell line, generated using CRISP/Cas9 technology, and the corresponding WT cells were kindly provided by Veit Hornung (Ludwig-Maximilians-Universität, München). THP-1 cells were subcultured in Roswell Park Memorial Institute 1680

(RPMI1680) (ThermoFisher Scientific) supplemented with 2 mM L-glutamine (Gibco). To induce differentiation to macrophage-like cells, THP-1 cells were treated with 100 nM PMA (InvivoGen) over night. Then, cells were rested for 48 h in normal culture medium without PMA before performing the experiments. When indicated, differentiated THP-1 cells were activated with 0.4 or 1 µg/ml rosiglitazone (Sigma-Aldrich) and stimulated with 100 ng/ml LPS (InvivoGen) for the indicated time.

Bone marrow-derived macrophages

Bone marrow cells were isolated from the respective animal and cultured in DMEM 4.5 g/L D-glucose (ThermoFisher Scientific) supplemented with 5% heat-inactivated FBS (Pan Biotech), 100 U/ml penicillin (Gibco), 100 µg/ml streptomycin (Gibco), 1 mM sodium pyruvate (Gibco), 1% non-essential amino acids (Gibco), 50 µM β-mercaptoethanol (Carl Roth) and 30% L929 cell supernatant. Fresh L929 cell supernatant was added once (day 3) and BMDMs were harvested after 6 days. When indicated, cells were activated overnight with 0.4 µg/ml rosiglitazone (Sigma-Aldrich) and stimulated with 50 ng/ml LPS (InvivoGen) for 6 h the next day.

3T3-L1

3T3-L1 cells (kindly provided by the Graeve lab, University of Hohenheim, Stuttgart) were grown in DMEM 1 g/L D-glucose (ThermoFisher Scientific) supplemented with 10% heat inactivated calf serum (CS) (Gibco), 100 U/ml penicillin (Gibco) and 100 µg/ml streptomycin (Gibco). Cells were subcultured before reaching a confluency of 80%.

Chemically competent *Escherichia coli* DH5α

Escherichia coli DH5α (F⁻ Φ80*lacZ*ΔM15 Δ(*lacZYA-argF*)U169 *deoR recA1 endA1 bsdR17* (*r_k⁺, m_k⁺*) *phoA supE44 thi-1 gyrA96 relA1 λ⁻*), a non-pathogenic laboratory strain derived from *E. coli* K12, were used for plasmid amplification. Depending on the antibiotic resistance cassette included in the transformed plasmid, bacteria were cultured in LB containing 100 µg/ml ampicillin (Carl Roth) or 50 µg/ml kanamycin (Carl Roth).

NEB® Stable Competent *Escherichia coli*

NEB® Stable Competent *Escherichia coli* (F' *proA*⁺*B*⁺ *lacI*^q Δ (*lacZ*)M15 *zzf::Tn10* (Tet^R)/ Δ (*ara-leu*) 7697 *araD139 fhuA* Δ *lacX74 galK16 galE15 e14- Φ 80lacZ* Δ M15 *recA1 relA1 endA1 nupG rpsL* (Str^R) *rph spoT1* Δ (*mrr-hsdRMS-mcrBC*)) were used for amplification of lentiviral plasmids. For transformation with ligation reactions, bacteria were cultured in NEB 10-beta/Stable Outgrowth Medium (NEB). For overnight cultures, bacteria were cultured in LB containing 100 μ g/ml ampicillin (Carl Roth).

Chemicals and reagents

Table 1: Chemicals and reagents used in this study.

Chemical / Reagent	Supplier
3-Isobutyl-1-methylxanthine (IBMX)	Sigma-Aldrich
Acetic acid	Carl Roth
Adenosine-triphosphate (ATP)	Carl Roth
Agarose	Carl Roth
Ammoniumperoxidesulfate (APS)	Carl Roth
Anti-FLAG M2 affinity gel	Sigma-Aldrich
Beta-mercaptoethanol	Carl Roth
Bovine serum albumin (BSA)	Carl Roth
Bromphenolblue	Carl Roth
Clarity Western ECL Substrate	BioRad
cOmplete Mini Protease Inhibitor Cocktail	Roche
D-Luciferin	Sigma-Aldrich
Dako fluorescence mounting medium	Agilent
Dexamethasone	Sigma-Aldrich
Entellan®	Sigma-Aldrich
Eosin	Sigma-Aldrich / ThermoFisher Scientific
GFP-Trap Agarose resin	Chromotek
Glycerol Standard Solution	Sigma-Aldrich
Glycin	Carl Roth

The role of NLRC5 in obesity – Materials and Methods

Chemical / Reagent	Supplier
GW9662	Sigma-Aldrich
Haematoxylin	Sigma-Aldrich
HiPerFect transfection reagent	Qiagen
Hoechst 33342	ThermoFisher Scientific
Infinity™ Cholesterol Liquid Stable Reagent	ThermoFisher Scientific
Infinity™ Triglycerides Liquid Stable Reagent	ThermoFisher Scientific
Insulin	Sigma-Aldrich
Lipofectamine™ 2000	ThermoFisher Scientific
Lipopolysaccharide (LPS)	InvivoGen
Milk powder	Carl Roth
Sodium fluoride (NaF)	Sigma-Aldrich
NP-40	Sigma-Aldrich
Oil Red O	Sigma-Aldrich
Ortho-Nitrophenyl-β-galactoside (ONPG)	Carl Roth
PAP-Pen	Sigma-Aldrich
Paraformaldehyde (PFA)	Carl Roth
Permout mounting medium	ThermoFisher Scientific
Phorbol 12-myristate 13-acetate (PMA)	InvivoGen
Poly-L-Lysin	Sigma-Aldrich
Polybrene	Sigma-Aldrich
Polyethylene glycol p-(1,1,3,3-tetramethylbutyl)-phenyl ether (Triton-X100)	Carl Roth
Polyoxyethylene (20) sorbitan monolaurate (Tween-20)	Carl Roth
Ponceau S	Carl Roth
Protein G Dynabeads	ThermoFisher Scientific
Rosiglitazone	Sigma-Aldrich
ROTI® GelStain Red	Carl Roth
Roti®-Histol	Carl Roth

Chemical / Reagent	Supplier
Rotiphorese Gel 30: 30% acrylamide and bisacrylamide stock solution (ratio 37,5:1)	Carl Roth
Salmon sperm DNA	ThermoFisher Scientific
Sodium orthovanadate	Sigma-Aldrich
SuperSignal™ West Femto Maximum Sensitivity Substrate	ThermoFisher Scientific
Tetramethylethylenediamine (TEMED)	Carl Roth
X-tremeGENE™ 9 Transfection Reagent	Roche
Xylene	Sigma-Aldrich
β-Glycerophosphate	Fluka

Kits

Table 2: Commercial Kits used in this study.

Kit	Manufacturer
2xKAPA2G Fast HotStart Genotyping Mix	KAPA Biosystems
ChIP DNA Clean & Concentrator Kit	Zymo Research
DNeasy Blood & Tissue Kit	Qiagen
DuoSet ELISA (TNF-α)	R&D Systems
Fecal DNA Miniprep Kit	Zymo Research
GeneArt® Genomic Cleavage Detection Kit	ThermoFisher Scientific
Glucose Colorimetric Assay Kit	Cayman
GreenMasterMix	Genaxxon
iScript cDNA Synthesis Mix	BioRad
MiSeq Reagent Kit v3	Illumina
NucleoBond Xtra Midi Kit	Macherey-Nagel
NucleoSpin Gel and PCR Clean-up Kit	Macherey-Nagel
NucleoSpin Plasmid Mini Kit	Macherey-Nagel
Quick-16S NGS Library Prep Kit	Zymo Research
RNeasy plus Mini Kit	Qiagen
RNeasy Plus Universal Mini Kit	Qiagen
SYBR Green reaction Mix	BioRad

Plasmids

Table 3: Plasmids for ectopical expression in mammalian cells (expression plasmids) or lentiviral transduction (lentiviral plasmids) and reporter plasmids used in this study.

Plasmid	Insert	Tag	Backbone	Reference
Expression plasmids				
FLAG-CIITA	CIITA Isoform 3	FLAG	pCMV-Tag2B-FLAG	(Bauer et al., 2023a)
FLAG-NLRC5	NLRC5; aa 1 - 1866	FLAG	pCMV-Tag2B-FLAG	(Neerincx et al., 2010)
FLAG-NLRC5 DD	NLRC5; aa 1 - 133	FLAG	pCMV-Tag2B-FLAG	(Bauer et al., 2023a)
FLAG-NLRC5 Iso3	NLRC5 isoform 3; aa 1 - 720	FLAG	pCMV-Tag2B-FLAG	(Neerincx et al., 2010)
FLAG-NLRC5 LRR	NLRC5; aa 589 - 1866	FLAG	pCMV-Tag2B-FLAG	(Bauer et al., 2023a)
FLAG-NLRC5ΔDD	NLRC5; aa 134 - 1866	FLAG	pCMV-Tag2B-FLAG	(Bauer et al., 2023a)
FLAG-NOD1	NOD1	FLAG	pCMV-Tag2B-FLAG	(Kufer et al., 2008)
GFP-NLRC5	NLRC5; aa 1 - 1866	GFP	pCMV-Tag2B-pEGFP	(Neerincx et al., 2012)
HA-C/EBPα	C/EBP α	HA	pcDNA3	kind gift from AG Lausen, University of Stuttgart
myc-NLRC5	NLRC5 full length; aa 1 - 1866	myc	pcDNA3.1-3xmyc-B	(Neerincx et al., 2012)
pcDNA3.1	none	none	pcDNA3.1	Invitrogen
PPARγ1	PPAR γ 1	none	pcDNA3	(Tachibana et al., 2005; Tanaka et al., 2002)
PPARγ2	PPAR γ 2	none	pcDNA3	(Tachibana et al., 2005; Tanaka et al., 2002)
RXR	RXR2	none	pcDNA3	(Hoffart et al., 2012)

Plasmid	Insert	Tag	Backbone	Reference
β -galactosidase	β -galactosidase	none	pcDNA3.1	(Neerincx et al., 2012)
Lentiviral plasmids				
lentiCRISPRv2	Cas9 of <i>Streptococcus pyogenes</i>	none	lentiCRISPRv2	(Sanjana, Shalem, & Zhang, 2014), kindly provided by Cathrin Hagenlocher, University of Stuttgart
pCMV-VSV-G	none	none	pCMV-VSV-G	(Stewart et al., 2003), kindly provided by Cathrin Hagenlocher, University of Stuttgart
psPAX2	none	none	psPAX2	Didier Trono (Addgene plasmid #12260); kindly provided by Cathrin Hagenlocher, University of Stuttgart
Reporter plasmids				
mFabp4 PPRE	mFabp4 promoter fragment (bp 2300 – 4500)	none	pBV-Luc	this work
p4xACO-Luc	4x PPRE	none	pBV-Luc	(He et al., 1999)
PPRE 3x TK Luc	3x PPRE	none	ptkLuc	(Forman et al., 1995)

Oligonucleotides

All oligonucleotides used in this work were obtained from Eurofins Genomics.

Table 4: Oligonucleotides for qRT-PCR used in this study.

Target, Ref.	Primer fwd	Primer rev
Asc (Carty et al., 2019)	ACTGTGCTTAGAGACATGGGC	TGGTCCACAAAGTGCCTGTT
CD36 (Luan et al., 2019)	AGATGCAGCCTCATTCCAC	GCCTTGATGGAAGAACAAA
FABP4	AACCTTAGATGGGGGTGCC	GTGGAAGTGACGCCTTCAT

The role of NLRC5 in obesity – Materials and Methods

Target, Ref.	Primer fwd	Primer rev
(Luan et al., 2019)		
GAPDH	GGTATCGTGGAAGGACTCATGAC	ATGCCAGTGAGCTTCCCGTTCAG
H2K (Ludigs et al., 2015)	TTGAATGGGGAGGAGCTGAT	GCCATGTTGGAGACAGTGGA
HLA-A (Meissner et al., 2012b)	AAAAGGAGGGAGTTACACTCAGG	GCTGTGAGGGACACATCAGAG
Hprt (Almeida-Oliveira et al., 2017)	CCCTGGTTAAGCAGTACAGCCCC	AGTCTGGCCTGTATCCAACACTTCG
IL6	GATGGATGCTTCCAATCTGG	TGGCATTGTGGTTGGGTCA
NELFB	GGAGCCCAAGATGGAGGT	CTCCTGCAGAACTTAGTGAAG
Nlrc3 (Wang et al., 2022)	GTCAGCTGCTACAAGTCCGGGAC	GAGCCTCAGAGTGCTTCGGTATCC
NLRC5	CTCCTCACCTCCAGCTTCAC	GTTATTCCAGAGGCGGATGA
Nlrc5_1	TTGATGGGTTGGATGAGGCT	CAAAGCCCCACATGTGTACC
Nlrc5_2	TGGAGGAGGTCAGTTTGC	ATGCTCCTGATTGCTGTGTAG
Nlrp10	GGAGCTTGTAGACTACCTCA	AAAGTCTCCACATCGACAGG
Nlrp12 (Zaki et al., 2014)	CCTCTTTGAGCCAGACGAAG	GCCCAGTCCAACATCACTTT
Nlrp1b (Vilaysane et al., 2010)	GACTTTGTGGCTTGTTGAATGC	CATTTAGCTGCAGGTCTAGCTCTCT
Nlrp3 (Carty et al., 2019)	CCACATCTGATTGTGTTAATGGCT	GGGCTTAGGTCCACACAGAA
Nlrp6 (Gustin et al., 2015)	GGACGAGAGGAAGGCAGAG	GCACACGAAGGGCACAAG
Nlrx1 (Singh et al., 2018)	AACGGTGCTGGTGACACA	GCTCAGCTCATTGAAGTAGAGGT
Nod1	AGATGGAAGGCACCCCATTG	TCTTTCGGACCTTGTCAGGC
NOD1 (Tourneur et al., 2013)	AGGCCTCACGCATCTTAACTG	CCTCAGAGATTGATTTGCTGTTCTT

Target, Ref.	Primer fwd	Primer rev
Nod2	TTGTAGCCGACCACCAGAAC	TCCCTCGAAGCCAAACCTC
NOD2	GAAGTACATCCGCACCGAG	GACACCATCCATGAGAAGACAG
Ripk2 (Shimada et al., 2018)	CGTGTGGATCCTCTCTGCTC	AGTGGTGTGCCTTCAACGAA
Sin3A (El Maassarani et al., 2016)	CAGAATGACACCAAGGTCCTGAG	CATACGCAAGTGAGAGGTGTGG
Tgf-b	AGGAGACGGAATACAGGGCT	GGATCCACTTCCAACCCAGG
Tnf-a	AGAACTCCAGGCGGTGC	AGGGTCTGGGCCATAGAACT
TNF-a	ATGAGCACTGAAAGCATGATCC	GAGGGCTGATTAGAGAGAGGTC
ChIP qRT-PCR		
FABP4	TCCAGAGAGAGGGTATGTTTCC	CACTTTGCTCTCCTATGGACAG
GAPDH	GCTACTAGCGGTTTTACGGGCG	TGCGGCTGACTGTGCAACAGG
HLA-B	GGCGCAGCGTTGGGGATTC	GGCGACGCTGATTGGCTTCTC
HLA-DRA (Meissner et al., 2010)	ATTTTTCTGATTGGCCAAAGAGTAATT	AAAAGAAAAGAGAATGTGGGGTGTA

Table 5: Oligonucleotides for Cloning used in this study.

Primer	Sequence	Application
Fabp4promoter	AATTGCTAGCGTGTGTTGGCAGGGGGGTTA	Cloning of mFabp4 PPRE reporter construct
	AATTCGCGGGCCCTAACTTAGACATGTTCTCAAG	
mNlrc5 Exon 2	GTGTGCAGACAAACATCCTCAC	Amplification of DNA cleavage site targeted by mNlrc5 gRNA2
	GAAGGGATGAAACGGGGCTT	
mNlrc5 Exon 3	TGTCTCATACTTCTCTGCCTGG	Amplification of DNA cleavage site targeted by mNlrc5 gRNA3
	GGTCTGAGGTCACATCGGTT	
mNlrc5 gRNA2	CACCgCATGGTACAGCTGAGGTCCA	gRNA2 targeting exon2 of mNlrc5
	AAACTGGACCTCAGCTGTACCATGC	
mNlrc5 gRNA3	CACCgCTTCTTGCTGTTCTCCGAC	gRNA targeting exon 3 of mNlrc5
	AAACGTCGGAAGAAGCAAGAAGC	

The role of NLRC5 in obesity – Materials and Methods

Table 6: Oligonucleotides for Genotyping used in this study.

Primer	Sequence	Application	
Nlrc5 WT	GAGTCACTCACTCTCCAGGGACAGTGG	Genotyping of <i>Nlrc5</i>^{-/-} and corresponding WT mice	
	CTGTTGAGCTGACGGTGGATGACC		
Nlrc5^{-/-}	GCCAGACAGCATAGACCAGATAGTGG		
	CTACTTCCATTTGTCACGTCTGCACG		
Nlrc5^{Exon4}	CTGAGCCTTGATCAGACCC		Genotyping of <i>Nlrc5</i>^{ΔExon4} and corresponding WT mice
	CTACCTACCAACTTGGACCAC		
Nlrc5^{ΔExon4}	CTCGAGTTTAAACTAAGCGGCCG		
	CTACCTACCAACTTGGACCAC		

Table 7: Oligonucleotides for Sequencing used in this study.

Primer	Sequence	Application
hU6-F	GAGGGCCTATTTCCCATGAT	Verification of lentiCRISPRv2:gRNA constructs
pGLrev	CTTTATGTTTTTGGCGTCTTCC	Verification of mFabp4 promoter reporter construct
mNlrc5 Exon 2	GTGTGCAGACAAACATCCTCAC	Verification of DNA modifications by gCRISPR/Cas9:gRNA2 mediated cleavage
	GAAGGGATGAAACGGGGCTT	
mNlrc5 Exon 3	TGTCTCATACTTCTCTGCCTGG	Verification of DNA modifications by gCRISPR/Cas9:gRNA3 mediated cleavage
	GGTCTGAGGTCACATCGGTT	

siRNAs

Table 8: siRNAs used in this study.

siRNA	Target	Sequence	Manufacturer
Allstar Negative	Non-targeting	proprietary	Qiagen
siNELFB_7	NELFB	AAGGTACAAGAAGCTGGAAGA	Qiagen
siSin3A_5	Sin3A	GAGCGTGTAAGCAAGCGTCTA	Qiagen

Antibodies

Primary antibodies

Table 9: Primary antibodies used in this study. ChIP = chromatin immunoprecipitation, IF = (indirect) immunofluorescence, WB = Western Blot.

Target	Species	Application	Manufacturer/Reference	Identifier
CD68	rabbit	IF	Abcam	ab125212
FABP4	mouse	WB	Santa Cruz	sc-271529
FLAG	mouse	WB	Sigma-Aldrich	F3165

The role of NLRC5 in obesity – Materials and Methods

Target	Species	Application	Manufacturer/Reference	Identifier
GAPDH	rabbit	WB	Santa Cruz	sc-25778
GFP	mouse	WB, ChIP	Roche	#11814460001
HLA-B	mouse	WB	Santa Cruz	sc-55582
HLA-B/C	mouse	WB	Kind gift from Victor Steimle, University of Sherbrooke, Canada	
mouse IgG isotype control	mouse	ChIP	Millipore	#12-371
NLRC5	rat	WB	Sigma-Aldrich	MABF260
p38	rabbit	WB	Cell Signaling	#9212
phosphorylated p38	mouse	WB	Cell Signaling	#9216
PPARγ	rabbit	WB	Cell Signaling	#2443
rabbit IgG isotype control	rabbit	ChIP	Kind gift from AG Lausen, University of Stuttgart	
RNA polymerase II	rabbit	ChIP	Cell Signaling	#14958
β-2-microglubulin	rabbit	WB	Cell Signaling	#59035
β-actin	mouse	WB	Santa Cruz	sc-47778

Secondary antibodies

Table 10: secondary antibodies used in this study. IF = indirect immunofluorescence, WB = Western Blot.

Antibody	Application	Manufacturer	Identifier
Goat anti-mouse IgG HRP conjugate	WB	BioRad	#170-6516
Goat anti-mouse light chain specific HRP conjugate	WB	Jackson ImmunoResearch	#115-035-174
Goat anti-rabbit IgG Alexa Fluor™ 568	IF	ThermoFisher Scientific	A-11036
Goat anti-rabbit IgG HRP conjugate	WB	BioRad	#170-6515
IRDye® 800CW Goat anti-rabbit IgG	WB	LI-COR	#926-32211

Instruments

Table 11: Instruments used in this study.

Name	Manufacturer
Axioscope 2 Zeiss microscope	Carl Zeiss Microscopy GmbH

Name	Manufacturer
Axiovert 200M Zeiss microscope	Carl Zeiss Microscopy GmbH
Bioruptor Pico	Diagenode
CFX Connect™ Real-Time PCR Detection System	BioRad
DMI8	Leica
Eclipse TS100	Nikon
EnSpire Multimode Plate Reader	Perkin Elmer
FastPrep®-24 Tissue and Cell Homogenizer	MP Biomedical
Fusion FX Camera System	Vilber Lourmat
Hera Cell 150i Co2 Incubator	ThermoFisher Scientific
Illumina MiSeq	Illumina
Mini Protean Tetra System	BioRad
Nanophotometer p360	Implen
NanoZoomer Slide Scanner	Hamamatsu Photonics
PowerPac™ HC High-Current Power Supply	BioRad
Rotating wheel	Stuart
T100™ Thermal Cycler	BioRad
ThermoMixer F1.5	Eppendorf
TissueRuptor	Qiagen
Trans-Blot Turbo Transfer System	BioRad

Software

Table 12: Software and algorithms used in this study.

Software/algorithm	Supplier/Reference
Adipocyte U-NET	(Glastonbury et al., 2020)
Axiovision software	Carl Zeiss Microscopy GmbH
Fijii	NIH
GraphPad Prism 7.0	GraphPad
Image-Pro Plus Software	Media Cybernetics
Leica LasX software	Leica
Microsoft Excel	Microsoft

Software/algorithm	Supplier/Reference
NanoZoomer Digital Pathology software NDP.view2	Hamamatsu Photonics
QIIME2 v 2019.7	(Bolyen et al., 2019)
R (v3.6.1)	N/A

Methods

Cell biological methods

Differentiation 3T3-L1

Differentiation of 3T3-L1 preadipocytes into mature adipocytes was performed following a modified version of the protocol of Zebisch et al. (Zebisch et al., 2012). Briefly, 8×10^4 cells per well were seeded in a 6-well plate (Falcon™) and incubated for 48 h until reaching full confluency. Medium was renewed, and cells were incubated for another 72 h as confluent culture. To induce differentiation, medium was switched to differentiation medium I [DMEM 4.5 g/L D-glucose (ThermoFisher Scientific) + 10% heat inactivated FBS (Pan Biotech) + 100 U/ml Penicillin + 100 µg/ml Streptomycin (Gibco) + 0.25 µM dexamethasone (Sigma-Aldrich) + 1 µg/ml insulin (Sigma-Aldrich) + 0.5 mM 3-Isobutyl-1-methylxanthine (IBMX) + 1 mM sodium pyruvate (Gibco)]. After 48 h, medium was switched to differentiation medium II [DMEM 4.5 g/L D-glucose (ThermoFisher Scientific) + 10% heat inactivated FBS (Pan Biotech) + 100 U/ml Penicillin + 100 µg/ml Streptomycin (Gibco) + 1 µg/ml insulin (Sigma-Aldrich) + 1 mM sodium pyruvate (Gibco)] for five days. Afterwards, cells were maintained in adipocyte maintenance medium [DMEM 4.5 g/L D-glucose (ThermoFisher Scientific) + 10% heat inactivated FBS (Pan Biotech) + 100 U/ml Penicillin + 100 µg/ml Streptomycin (Gibco) + 1 mM sodium pyruvate (Gibco)] for the remaining time of differentiation, exchanging medium every two to three days.

Lentiviral production

3.8×10^6 Lenti-X™ 293T producer cells were seeded in 10 ml culture medium without antibiotics in a poly-L-lysine-coated 10 cm tissue culture dish (Greiner Bio-One). One day after seeding, Lenti-X™ 293T cells were transfected with 7.5 µg and 5 µg of the lentiviral packaging plasmids psPAX2 (Didier Trono, Addgene plasmid #12260) and pCMV-VSV-G (Stewart et al., 2003), respectively, and 10 µg of the lentiCRISPRv2:gRNA construct or the empty vector control

construct. Transfection was performed using Lipofectamine™ 2000 (Invivogen) according to the manufacturer's instructions. 18 h post transfection, medium was exchanged with fresh antibiotic-free medium (Gibco). 48 h post transfection, lentivirus-containing supernatant was harvested for the first time and replaced by 10 ml fresh culture medium without antibiotics. Lentiviral supernatant was cleared by centrifugation for 3 minutes at 1,200 rpm and stored at 4°C overnight. 72 h post transfection, lentiviral supernatant was harvested for the second time, cleared by centrifugation for 3 minutes at 1,200 rpm and pooled with virus harvested the day before. The virus was directly used to transduce 3T3-L1 cells or frozen at -80°C to be used at later timepoints.

Lentiviral transduction of 3T3-L1 cells

One day before transduction, 8×10^4 3T3-L1 cells per well were seeded in 3 ml culture medium in 6-well plates (Greiner Bio-One). For transduction, cells were incubated with 3 ml culture medium containing 400, 200 or 100 μ l viral supernatant. To increase transduction efficiency, 8 μ g/ml polybrene (Sigma-Aldrich) was added. 48 h after transduction, 3T3-L1 cell pools were either directly seeded for differentiation or splitted in a 1:10 ratio and re-seeded in 3 ml culture medium containing 3 μ g/ml puromycin (Invivogen) to allow for selection of successfully transduced cells. 3 μ g/ml puromycin was determined before as lowest concentration killing all non-transduced 3T3-L1 cells after seven days. Transduced 3T3-L1 cells were kept under selection for 21 days. When exceeding a confluency of 80%, 3T3-L1 cells were expanded to 10 cm tissue culture dishes (Greiner Bio-One) or T175 cm² tissue culture flasks (Greiner Bio-One). Transduced 3T3-L1 cell pools were tested for DNA modification at the potential cleavage using the GeneArt® Genomic Cleavage Detection Kit (ThermoFisher Scientific) according to the manufacturer's instructions. Cleavage of DNA was detected via agarose gel electrophoresis. gRNA efficiency (fraction cleaved) was calculated by dividing the sum of the band intensities of the fractions cleaved by the sum of the band intensities of the parental and the cleaved bands.

Generation of *Nlrc5* modified 3T3-L1 clones

3T3-L1 clones with CRISPR/Cas9-modified *Nlrc5* locus were generated by limited dilution in 96-well U-bottom plates (Greiner Bio-One). 0.5 – 0.8 cells/well were seeded in 3T3-L1 culture medium containing 3 μ g/ml puromycin. After 14 to 21 days, confluent wells

were expanded until being cultured on 10 cm tissue culture dishes. Clones were tested for DNA modifications at the potential cleavage site by Sanger Sequencing.

Reporter gene assay

3 x 10⁴ HEK293T cells/well were seeded in 96-well plates (Greiner Bio-One). Cells were transiently transfected using X-tremeGENE 9 transfection reagent (Roche) following the manufacturer's instructions with 8.6 ng of a β -galactosidase-encoding plasmid, either 50 ng of the PPRE 3x TK Luc or 100 ng of the mFabp4 PPRE reporter construct, if not indicated otherwise, and the indicated amounts of expression plasmids (Table 3). Total DNA amount was adjusted to 100 or 150 ng per well using pcDNA3.1 empty vector construct. 20 – 24 h post transfection, cells were lysed in 100 μ l lysis buffer [25 mM Tris pH 8.0; 8 mM MgCl₂; 1% Triton X-100; 15% glycerol in H₂O] for ten minutes at 600 rpm on an orbital shaker (Eppendorf). 50 μ l of the lysate were transferred to a non-transparent 96-well plate and luciferase activity was measured as relative light units (RLU) using a multiplate reader (PerkinElmer) with 2 seconds delay after automated dispersion of 100 μ l reading buffer per well [1.3 μ M ATP, 770 ng/ml D-luciferin in lysis buffer]. For readout of β -galactosidase activity, 100 μ l of 1 mg/ml Ortho-Nitrophenyl- β -galactoside (ONPG) in ONPG dilution buffer [60 mM Na₂HPO₄, 40 mM NaH₂PO₄, 10 mM KCl, 1 mM MgSO₄ in H₂O, pH 7.0] were added to the remaining 50 μ l lysate and the plate was incubated for 5 – 20 minutes at 37°C until a yellow colour developed. Absorbance was measured at 405 nm, using 620 nm as reference wavelength. RLU was normalized (nRLU) to β -galactosidase activity. Assays were performed in technical triplicates.

Transient transfection

For transient transfection, 3 x 10⁶ HEK293T cells per condition were seeded in a 10 cm tissue culture dish (Greiner Bio-One). Cells were transfected with 5 μ g of the indicated plasmid the next day with Lipofectamine™ 2000 (Invitrogen), following the manufacturer's instructions. Briefly, plasmid DNA and Lipofectamine™ 2000 were diluted in OptiMEM (Gibco) to obtain a final volume of 500 μ l each and a ratio of 1:2.5 (μ g DNA: μ l Lipofectamine™ 2000). DNA and Lipofectamine were combined and incubated for 20 minutes at RT to allow for complex formation. In the meantime, half of the medium of the cells seeded the day before was replaced with serum- and antibiotic-free medium (Gibco). The end mix was added to the

cells and dispersed by swirling the dish gently. Cells were incubated for at least 20 h to allow for gene expression before conducting further experiments.

siRNA-mediated gene silencing

HeLa Flp-In GFP and GFP-NLRC5 cells were transfected with 20 nM (siNT, siSin3A) or 10 nM (siCOBRA1) siRNA (Table 8) using HiPerFect transfection reagent (Qiagen) according to the manufacturer's conditions. Knockdown was performed for 48 h and efficiency was monitored by qRT-PCR.

Transformation of chemically competent *E. coli*

For amplification of mammalian expression plasmids (Table 3), 1 µl of a 100 – 2000 µg/ml plasmid solution was combined with 25 µl chemically competent *E. coli* DH5α. For ligations, 10 µl ligation reaction were combined with 50 µl chemically competent *E. coli* DH5α. Solution was gently mixed and incubated on ice for 30 minutes. Bacteria were heat-shocked for 30 seconds at 42°C and immediately afterwards placed on ice for 5 more minutes before 1 ml LB medium without antibiotics was added to the bacteria. When transformed with plasmids containing an ampicillin resistance cassette, 100 µl bacteria were directly spread on a LB agar plate containing 100 µg/ml ampicillin (Carl Roth). When transformed with plasmids carrying a kanamycin resistance cassette, bacteria were incubated for 1 h at 37°C and 180 rpm before 100 µl bacteria were spread on a LB agar plate containing 50 µg/ml kanamycin (Carl Roth). For ligations, bacteria were concentrated by precipitation at 6000 x g for 5 min and resuspension in 200 µl LB medium without antibiotics before spreading 100 µl on the LB agar plate. Selection plates were incubated overnight at 37°C.

Transformation of NEB® Stable Competent *E. coli*

For amplification of lentiviral plasmids, 1 µl low concentration lentiviral packaging plasmids or lentiCRISPRv2 vector or 4 ng ligated lentiRSPRv2:gRNA construct were transformed into NEB® Stable Competent *E. coli* (NEB), following a modified version of the manufacturer's protocol. Briefly, 50 µl NEB® Stable Competent *E. coli* were combined with the indicated DNA amount and incubated on ice for 30 minutes. The mixture was heat shocked at 42°C for 30 sec and then placed on ice for 5 minutes. 950 µl of NEB 10-beta/Stable Outgrowth Medium (NEB) were added to the cells and the mixture was incubated for 1 h at 30°C at 180 rpm. After

incubation the bacteria were pelleted for 5 minutes at 6000 rpm, resuspended in 100 μ l NEB 10-beta/Stable Outgrowth Medium and spread on selection plates containing 100 μ g/ml ampicillin (Carl Roth). Selection plates were incubated for 24 h at 30°C or overnight at 37°C in a shaker (Ecotron).

Molecular methods

Molecular Cloning

Ligation of guide RNAs into the lentiCRISPRv2 vector

Two guide RNAs (gRNAs) targeting exon 2 or 3 of murine *Nlrc5*, which encode for the uCARD domain of NLRC5 (Yao & Qian, 2013) were designed using the CCTop – CRISPR/Cas9 target online predictor of the University of Heidelberg (Stemmer et al., 2015). The gRNAs were flanked at the 3' end by the 3 bp *Streptococcus pyogenes* NGG protospacer adjacent motif (PAM) sequence. Only gRNAs with a calculated efficiency score above 0.56 (medium or high efficiency) were used. gRNAs were designed to have at least four mismatches to other DNA sequences to reduce potential off-target effects (Cho et al., 2014; Hsu et al., 2013). gRNA design was performed by Dr. Nora Mirza. gRNAs were phosphorylated and annealed following the protocol of the Zhang Lab (Sanjana, Shalem, & Zhang, 2014; Shalem et al., 2014). gRNAs were ligated into the lentiCRISPRv2 vector (Sanjana, Shalem, & Zhang, 2014) following a modified protocol of Bauer et al. (Bauer, Canver, & Orkin, 2015), using the Golden Gate assembly cloning strategy (Engler, Kandzia, & Marillonnet, 2008). Reaction composition and program are indicated in Table 13. One reaction only containing the empty vector, and no gRNA, was used as negative control. Samples were run in the thermal cycler (BioRad).

Table 13: Program and reaction composition for Golden Gate assembly.

Reagent	Volume	Temperature (°C)	Duration (min)	Cycle
Vector	50 ng	37	5	20
annealed oligos (1 μ M)	1 μ l	20	5	
BsmBI (ThermoFisher Scientific)	1.25 μ l	80	20	1
Tango buffer (10x)	2.5 μ l	Take out and let cool at room temperature.		
ATP (10 mM)	2.5 μ l			
BSA (20 mg/ml)	0.125 μ l			
T4 DNA ligase (NEB)	0.5 μ l			
H ₂ O	add to 25 μ l			

Restriction enzyme cloning of mFabp4 PPRE reporter construct

The desired part of the murine *Fabp4* promoter was amplified from genomic DNA isolated from 3T3-L1 cells by PCR according to the following protocol (Table 14). Oligonucleotides (Table 5) were designed with an overhang, containing the restriction site of NheI (fwd oligonucleotide) or SmaI (rev oligonucleotide) and four arbitrary nucleotides (AATT). The amplificate was visualized via agarose gel electrophoresis, cut out from the gel and DNA was purified using the NucleoSpin Gel and PCR Clean-up Kit (Macherey-Nagel) according to the manufacturer's instructions. DNA concentration was determined using a nanophotometer (Implen). Insert was digested in a double digest with NheI and SmaI (ThermoFisher Scientific) in 1 x Tango buffer for 1 h at 37°C. Restriction enzymes were heat-inactivated for 20 minutes at 65°C. 2 µg vector (p4xACO-Luc) were digested in a sequential digest with SmaI and NheI, according to the manufacturer's instructions. Ligation was performed using 1 µl T4 DNA ligase (ThermoFisher Scientific), 2 µl T4 ligation buffer (ThermoFisher Scientific) and vector and insert in a 1:7 molar ratio in a total volume of 20 µl for 1 h at room temperature. 10 µl of ligation reaction were transformed into chemically competent *E. coli*. Successful cloning was verified by Sanger Sequencing and control restriction digest, using NheI and SmaI in 1x Tango buffer for 1 h at 37°C.

Table 14: Composition of PCR reaction and PCR program for DNA amplification for cloning.

Reagent	Volume	Temperature (°C)	Duration	Cycle
2x Phusion Master Mix	10 µl	98	30 sec	1
fwd primer (10 pM)	1 µl	98	5 sec	30
rev primer (10 pM)	1 µl	58	20 sec	
genomic DNA	50 ng	72	2 min	
H ₂ O	add to 20 µl	72	5 min	1
		4	hold	1

Sanger Sequencing

Insert sequence of newly generated plasmids or DNA modifications by CRISPR/Cas9-mediated cleavage were verified by Sanger Sequencing which was performed by GATC, respectively Eurofins Genomics.

RNA isolation

For cell lines, RNA was isolated using the RNeasy Plus Mini kit (Qiagen) according to the manufacturer's instructions. For animal tissue, 100 mg adipose tissue or 30 mg liver were

homogenized in 900 µl Qiazol in Lysing Matrix D 2 ml tubes (MP Biomedicals) using the FastPrep®-24 Tissue and Cell Homogenizer (MP Biomedical) at 6.0 m/s for 40 sec. Homogenates were centrifuged for 10 minutes at 12,000 x g at 4°C and RNA was isolated from the resulting supernatants using the RNeasy Plus Universal kit (Qiagen) according to manufacturer’s instructions. Alternatively, tissue was homogenized for 30 sec in 600 µl buffer RLT (Qiagen) + 143 mM β-mercaptoethanol (Carl Roth) using the TissueRuptor (Qiagen). Homogenates were centrifuged for 3 minutes at maximum speed at room temperature and RNA was isolated using the RNeasy Mini kit (Qiagen) following the manufacturer’s instructions.

cDNA synthesis

Per reaction, 400 ng or 800 ng of total RNA was transcribed into cDNA using the iScript cDNA Synthesis kit (BioRad) according to the manufacturer’s instructions.

Quantitative real-time polymerase chain reaction

Quantitative real-time polymerase chain reaction (qRT-PCR) was performed using iQ SYBR Green Supermix (BioRad) or GreenMasterMix (Genaxxon) according to the manufacturer’s instructions on 2 µl cDNA per reaction obtained from isolated RNA of the indicated cell lines or animal tissues. Alternatively, 1 µl of cDNA obtained from full blood RNA of obese patients (kindly provided by the AG Bischoff, University of Hohenheim) per reaction was used. Reactions were run in the CFX Connect™ Real-Time System (BioRad) using the following program (Table 15) with a duration of the first step of 3 minutes for the iQ SYBR Green Supermix (BioRad) and 15 minutes for the GreenMasterMix (Genaxxon). Gene expression was normalized to *GAPDH* (human samples) or *Hprt* (murine samples) expression.

Table 15: Protocol used for qRT-PCR.

Temperature (°C)	Duration	Cycles
95	3 / 15 min	1
95	15 sec	45
59	45 sec	
55	5 sec	1
Temperature increment 0.5°C/5 sec from 55°C to 95°C		
95	5 sec	1

DNA Isolation

DNA isolation from animal tissue

Isolation of genomic DNA for genotyping was performed using the DNeasy Blood & Tissue Kit (Qiagen) according to manufacturer's instructions and either tail tips or 30 mg liver tissue.

Isolation of plasmid DNA from bacteria

Isolation of plasmid DNA from transformed *E. coli* DH5 α or NEB[®] Stable Competent *E. coli* (NEB) was performed using either the NucleoBond Xtra Midi Kit (Macherey-Nagel) or the NucleoSpin Plasmid Mini Kit (Macherey-Nagel), according to the manufacturer's instructions.

Genotyping

Genotyping was performed by endpoint PCR using the following protocol (Table 16) and the appropriate oligonucleotides (Table 6). Amplificates were analysed on a 2% agarose gel.

Table 16: Reaction composition and PCR program used for endpoint PCR.

Reagent	Volume	Temperature (°C)	Duration	Cycles
2xKAPA2G Fast HS Genotyping Mix	10 μ l	95	3 min	1
fwd primer (10 pM)	1 μ l	95	15 sec	40
rev oligonucleotide (10 pM)	1 μ l	60	15 sec	
genomic DNA	200 ng	72	45 sec	
H ₂ O	add to 20 μ l	72	3 min	1

Agarose gel electrophoresis

To separate DNA fragments, 1 or 2 g agarose (Carl Roth) were dissolved in 100 ml Tris-Acetic acid EDTA buffer (TAE) [40 mM Tris, 20 mM acetic acid, 1 mM EDTA in H₂O]. DNA solutions were mixed with DNA loading buffer [1.4 M saccharose, 3.73 mM bromphenolblue, 0.1 M EDTA in H₂O], either or not containing 0,05% GelRed (Carl Roth), in a 9:1 ratio (DNA solution:loading buffer). If no GelRed was contained in the loading dye, GelRed was added directly in the agarose gel at a concentration of 0,005%. Separation was performed at 80 V constantly for 30 – 50 minutes. DNA was visualized with UV light using the Fusion FX Camera System (Vilber Lourmat). Size of DNA fragments was estimated by running Gene Ruler 100 bp plus or GeneRuler 1 kb DNA ladder (ThermoFisher Scientific) as standards.

Biochemical methods

Indirect immunofluorescence microscopy (IF)

For indirect immunofluorescent staining of epididymal adipose tissue, paraffin sections were de-paraffinated at 50 – 60°C for 20 minutes. Sections were incubated in four baths of Xylene (Sigma-Aldrich) for 2 minutes each before being rehydrated in ethanol baths with decreasing concentrations (100 – 50%) for 2 minutes each and washed in double distilled H₂O for 5 minutes. Then, sections were incubated for 20 minutes in antigen retrieval solution [10 mM Tris-HCl, pH 8; 1 mM EDTA, pH 8; 0.05% Tween; in H₂O; pH adjusted to 9] heated to 90°C. Cool-down was performed at room temperature. Sections were washed for 10 minutes two times in double distilled H₂O and once in TBS-T [137 mM NaCl, 20 mM Tris, 25 mM EDTA, 1% Tween in H₂O; adjust pH to 7.6]. Then, hydrophobic circles were drawn around the tissue sections using a hydrophobic barrier pen (PAP-Pen, Sigma-Aldrich). Blocking was performed using 5% BSA (Carl Roth) in TBS-T for 1 – 2 h at room temperature in a humid chamber, before the primary antibody in the appropriate dilution in 5% BSA (Carl Roth) in TBS-T was applied overnight at 4°C in a humid chamber. Slides were washed three times for 10 minutes in TBS-T, followed by 1 – 2 h of incubation at 4°C with secondary antibody in the appropriate dilution in 5% BSA (Carl Roth) in TBS-T in a humid chamber. Slides were washed two times for 10 minutes in TBS-T and once for 10 minutes in TBS. For mounting, one drop of Dako Fluorescence mounting medium (Agilent) was applied to the sections before covering sections with a coverslip. Slides were dried overnight at room temperature before imaging. Imaging was performed using an Axioscope 2 Zeiss microscope (Carl Zeiss Microscopy GmbH). Images were taken at 10x magnification and processed using the Image Pro-Plus software (Media Cybernetics).

SDS-PAGE and immunoblot

For immunoblot, cells were lysed in Laemmli loading buffer containing β -mercaptoethanol and lysates were boiled for 5 – 10 minutes at 95°C. Proteins were separated by Laemmli sodium dodecyl sulfate polyacrylamide gel electrophoresis (SDS-PAGE) on a 10 or 12% Tris-buffered SDS-polyacrylamide gel in running buffer [25 mM Tris, 192 mM glycine, 3.467 mM SDS in H₂O], applying a voltage of 80 – 120 V. Proteins were then transferred to a nitrocellulose membrane (Amersham™ Protran®) by semi-dry blotting in transfer buffer [25 mM Tris, 192 mM glycine, 20% methanol in H₂O] using the Trans-Blot Turbo Transfer

System (BioRad). Blotting was controlled by Ponceau S staining [0.2% Ponceau S, 3% acetic acid in H₂O], followed by washing in PBS-T [137 mM NaCl, 2.7 mM KCl, 10 mM Na₂HPO₄, 2 mM KH₂PO₄, 0.05% Tween-20 in H₂O] and blocking for 1 – 2 h in 3% milk powder (Carl Roth) in PBS-T. Membranes were incubated overnight at 4°C with primary antibody (Table 9) diluted accordingly in 0.05% Roche Blocking solution (Roche) in PBS [137 mM NaCl, 2.7 mM KCl, 10 mM Na₂HPO₄, 2 mM KH₂PO₄ in H₂O]. Membrane was washed three times for 5 minutes with PBS-T and membrane was incubated for 1 – 2 h with secondary antibody (Table 10) in the appropriate dilution in 0.05% Roche Blocking solution (Roche) at room temperature. Detection of infrared signal or chemiluminescence was achieved by applying either ECL solution [Solution A: 0.25 mg/ml Luminol in 0.1 M Tris pH 8.8; Solution B: 1.1 mg/ml para-hydroxy coumaric acids in DMSO; ratio Solution A:Solution B 9:1], Clarity Western ECL Substrate (BioRad) or SuperSignal West Femto Maximum Sensitivity Substrate (ThermoFisher Scientific) according to the manufacturer's instructions. Signals were visualized using the Fusion FX Camera System (Vilber Lourmat). Immunoblot quantification was performed using Fiji.

Immunoprecipitation

Co-immunoprecipitation (co-IP) of GFP-NLRC5 from transiently transfected HEK293T cells or from HeLa Flp-In GFP and GFP-NLRC5 cell lines was performed with GFP-Trap Agarose resin (Chromotek). Co-immunoprecipitation of transiently transfected FLAG-tagged NLRC5 constructs, FLAG-tagged Sin3A or FLAG-tagged NELFB from HEK293T cells was performed with anti-FLAG M2 affinity gel (Sigma-Aldrich). Cells were lysed in NP-40 buffer for GFP pulldown [10 mM Tris/HCl pH 7.5 150 mM NaCl, 0.5 mM EDTA, 0.5% NP-40, 100 nM β-glycerophosphat, 100 nM sodium orthovanadate, 1 mM NaF and cOmplete Mini Protease inhibitor Cocktail (Roche)] and in Triton-X100 buffer for pulldown of FLAG-tagged NLRC5 constructs [10 mM Tris/HCl pH 7.5, 150 mM NaCl, 0.5 mM EDTA, 1% Triton-X100, 100 nM β-glycerophosphat, 100 nM sodium orthovanadate, 1 mM NaF and cOmplete Mini Protease inhibitor Cocktail (Roche)]. For pulldown of FLAG-tagged Sin3A or FLAG-tagged NELFB, cells were lysed in modified NP-40-HEPES buffer [10 mM HEPES, 50 mM NaCl, 0.1 mM EDTA, 0.1 mM EGTA, 0.1% NP-40 100 nM β-glycerophosphate, 100 nM sodium orthovanadate, 1 mM NaF and cOmplete Mini Protease Inhibitor Cocktail (Roche)]. Lysates were cleared by centrifugation (10 minutes, 4°C, 20,000 x g for GFP pulldown and 10 minutes, 4°C, 2,000 x g for FLAG pulldown) before the supernatants

were loaded onto the matrix. Precipitation was performed at 4°C for 3 h before matrix was washed with lysis buffer. Proteins were identified by immunoblot.

Chromatin immunoprecipitation

Chromatin immunoprecipitation (ChIP) of GFP-NLRC5 from HeLa Flp-In GFP-NLRC5 cells was performed using either antibody-coupled Protein G Dynabeads (ThermoFisher Scientific) or GFP-Trap Agarose resin (Chromotek). HeLa Flp-In cells, treated overnight with 1 µg/ml doxycycline and 0.4 µg/ml rosiglitazone if indicated, were cross-linked by adding paraformaldehyde (PFA) (Carl Roth) to the medium of cells to a final concentration of 1% for 10 minutes at room temperature. Cross-linking was stopped by adding glycine (Carl Roth) to a final concentration of 0.125 M and incubating for 5 minutes. Cells were washed two times with ice-cold PBS, harvested by scraping in 10 ml ice-cold PBS, pelleted by centrifugation at 1,200 rpm for 5 minutes at 4°C and then frozen at -80°C until lysis. Cells were lysed in 1 ml lysis buffer [10 mM Tris-HCl, pH 7.5; 150 mM NaCl; 1% NP-40; 1% sodiumdeoxycholate; 1 mM EDTA, pH 8.0; 0.2% SDS] supplemented with protease inhibitors per 1×10^7 cells. Lysates were incubated on ice for 30 minutes with extensive resuspending every ten minutes, before being divided on sonication tubes (Diagenode) in a volume of 200 µl per tube. Chromatin was sheared by applying ultrasound for 20 seconds, followed by a 30 second pause in 15 cycles in total using the Bioruptor® Pico (Diagenode). After sonication, lysates were cleared at 13,000 rpm for ten minutes at 4°C. Successful chromatin shearing was controlled by decrosslinking 50 µl of sonicated lysate by applying 2 µl RNase (20 mg/ml) overnight at 65°C, followed by incubation with 2 µl Proteinase K (10 mg/ml) for 1 h at 60°C. Chromatin was purified using the ChIP DNA Clean & Concentrator Kit (Zymo Research) following the manufacturer's instructions. DNA concentration was determined, and 600 ng DNA were loaded onto a 1% agarose gel to document DNA fragment size. 18 – 25 µg chromatin per reaction were diluted with lysis buffer not containing SDS [10 mM Tris-HCl, pH 7.5; 150 mM NaCl; 1% NP-40; 1% sodiumdeoxycholate; 1 mM EDTA, pH 8.0] to a final concentration of 0.1% SDS before being incubated with the corresponding beads. For pulldown with the GFP-Trap Agarose resin, 20 µl of equilibrated GFP-Trap or corresponding control agarose resin (Chromotek) were incubated with the sonicated chromatin overnight at 4°C on a rotating wheel. For pulldown with antibody-coupled Protein G Dynabeads (ThermoFisher Scientific), 25 µl equilibrated beads per reaction were blocked in a two-step process by incubating them first in 100 mg/ml salmon sperm DNA (ThermoFisher

Scientific) followed by incubation in 0.1 mg/ml BSA (Carl Roth) both diluted in lysis buffer with 0.1% SDS and applied for 30 minutes at 4°C on a rotating wheel. Blocked beads were then incubated with 2 µg of the corresponding antibody (Table 9) overnight at 4°C on a rotating wheel. The next day, sheared chromatin was added to the beads and pulldown was performed for 6 h at 4°C on a rotating wheel. After pulldown, agarose resin as well as antibody-coupled beads were washed with wash buffers A [0.1% SDS; 1% Triton X-100; 2 mM EDTA, pH 8; 150 mM NaCl, 20 mM Tris-HCl, pH 8 in H₂O] and B [0.1% SDS; 1% Triton X-100; 2 mM EDTA, pH 8; 500 mM NaCl, 20 mM Tris-HCl, pH 8 in H₂O] for five minutes at 4°C on a rotating wheel three times each. Then, 120 µl of elution buffer [100 mM NaHCO₃, 1% SDS in H₂O] were applied and samples incubated for 20 minutes at room temperature on a rotating wheel. 4.8 µl of a 5 M NaCl solution were added and samples were decrosslinked and purified as described above before qRT-PCR was performed.

ELISA

TNF- α release was measured in cell supernatants by ELISA (DY410, R&D Systems) according to the manufacturer's instructions.

Oil Red O

Oil Red O Staining was performed following a modified version of the protocol of Kraus et al. (Kraus et al., 2016). Briefly, cells were fixed in 4% PFA (Carl Roth) in PBS for 15 minutes before staining them with the Oil Red O Working Solution [0,2% Oil Red O (Sigma-Aldrich) in 40% isopropanol (Carl Roth)] for 30 minutes. After washing five times with distilled water, pictures of the stained cells were taken with the Axiovert 200M Zeiss microscope (Carl Zeiss Microscopy GmbH) and processed with the Axiovision software. 6 representative pictures per condition were taken at 20x magnification. During imaging, cells were covered with water to avoid drying of cells. Oil Red O was eluted from the cells on an orbital shaker (Eppendorf) at 600 rpm for 10 minutes, using 600 µl 100% isopropanol per well. The absorbance of the eluates was measured at 510 nm, 100% isopropanol serving as blank.

Serum lipids

Blood was obtained by heart puncture directly after sacrifice. Serum was obtained by incubating the blood for 3 – 4 h in Microtainer® SST™ tubes (BD Medical), followed by

centrifugation at 6,000 x g for 8 minutes. Serum cholesterol and triglyceride concentrations were determined using the Infinity™ Triglycerides Liquid Stable Reagent and the Infinity™ Cholesterol Liquid Stable Reagent (ThermoFisher Scientific). As standard, a 500 mg/dl cholesterol solution prepared according to Abele and Khayam-Bashi (Abele & Khayam-Bashi, 1979) for cholesterol measurements and a glycerol standard solution of 2.5 mg/ml equivalent triolein concentration (Sigma-Aldrich) for triglyceride measurements were used. Standards were prepared by 1:2 serial dilutions, the highest standard being 500 mg/dl. 2 µl of standard solution or mouse serum were incubated for 15 minutes at 37°C with 200 µl Infinity™ Triglycerides or Infinity™ Cholesterol Liquid Stable Reagent in a 96-well plate format. Standards and samples were run in duplicates. Absorbance was measured at 540 nm, with a reference wavelength of 660 nm. A standard curve was generated and the serum cholesterol and triglyceride concentrations of the individual samples were calculated.

Glucose and insulin tolerance test

Intraperitoneal insulin (ITT) and glucose (GTT) tolerance tests were performed in *Nlrc5^{ΔExon4}* mice in the last week of HFD feeding. Mice were injected with 1 U insulin and 2 g glucose per kg bodyweight, respectively, and blood was drawn before and at the indicated time points after injection. Blood glucose was measured in the serum using the Glucose Colorimetric Assay kit (Cayman Chemical) following the manufacturer's instructions.

Haematoxylin & Eosin Staining

Histological analysis was performed on 5 µm paraffin sections of mouse epididymal adipose tissue. For *Nlrc5^{ΔExon4-7}* and corresponding WT animals, paraffin sections were deparaffinated with Roti®-Histol (Carl Roth) and rehydrated in ethanol baths with decreasing concentrations (100 – 30%). After washing with ultrapure water, Haematoxylin (Sigma-Aldrich) was applied for 3 sec. Tissue was dehydrated by ethanol baths (75% and 85%) before Eosin (Sigma-Aldrich) was applied for 3 sec. Tissue was further dehydrated by short baths in ethanol (95% and 100%), then treated with Roti®-Histol and fixed with Entellan®. Stained sections were imaged using a Leica DMI8 microscope with a HC PL Fluotar L 20x/0.40 objective and processed using the Leica LasX software and Fiji 38. For determination of adipocyte diameter, Fiji with the PlugIn Adiposoft (Galarraga et al., 2012) was used. For determination of adipocyte area, the deep learning-based method Adipocyte U-Net (Glastonbury et al., 2020) was used as

published, except for setting the threshold for segmentation to 0.5. Determination of adipocyte area was performed by Lucy Hezinger and Felix Biber.

For *Nlrc5*^{ΔExon4} animals, paraffin sections were de-paraffinated by melting the paraffin at 50 – 60°C for 20 minutes before incubating them in four bathes of Xylene (Sigma-Aldrich) for 2 minutes each. Then sections were incubated in ethanol bathes with decreasing concentrations (100 – 50%) for 2 minutes each before being incubated for 5 minutes in tap water. Haematoxylin (Sigma-Aldrich) was then applied for 25 second for adipose tissue and one minute for liver sections. Excess staining was removed by 5 minutes incubation in tap water, followed by one minute incubation in glacial acid [1% in H₂O], 3 minutes in tap water, one minute in saturated LiCO₃ in H₂O, 5 minutes in tap water and 2 minutes in double distilled water. Then, sections were incubated in ethanol baths with decreasing concentrations (50 – 100%) for one minute each, before applying Eosin (ThermoFisher Scientific) for one minute or 45 seconds for adipose tissue and liver sections, respectively. Eosin staining was followed by two times 2 minutes incubation in 100% ethanol, before incubating the section for 2 minutes in two bathes of Xylene. For mounting, one to two drops of Permount mounting medium (ThermoFisher Scientific) were applied, the sections were covered with a coverslip and left to dry overnight before imaging. Slides were scanned using the NanoZoomer Slide Scanner (Hamamatsu Photonics, Japan) and analysed using the NanoZoomer Digital Pathology software NDPview2.0.

Bioinformatic methods

Taxonomic microbiota analysis

Mouse faeces of *Nlrc5*^{ΔExon4-7} and corresponding WT animals were collected on three consecutive days in week 1, weekly in week 3, 6 and 9, and on two days in week 11. Faecal samples were snap-frozen in liquid nitrogen immediately after collection and stored at -150°C.

Metagenomic DNA was extracted via mechanical lysis by bead beating in 700 μl lysis buffer (Zymo Research) for 40 seconds at 6 m/s in MP lysing matrix B tubes (0.1 mm silica spheres, MP Biomedicals). Subsequently, the DNA was purified and eluted in 100 μl RNase-free water using the ZR Fecal DNA Miniprep Kit (Zymo Research) according to the manufacturer's protocol.

The 16S rRNA gene region V3-V4 was amplified and prepared for sequencing with the Quick-16S NGS Library Prep Kit (Zymo Research) according to the manufacturer's recommendations.

The pooled and normalized library was sequenced on an Illumina MiSeq Instrument (MiSeq Reagent Kit v3, 600 cycles, Illumina) at the University of Hohenheim, Stuttgart, Germany.

The processing of raw sequences was carried out with QIIME2 v 2019.7 (Bolyen et al., 2019) comprising the denoising of data with the DADA2 plugin (Callahan et al., 2016), adapter trimming and chimera checking. Amplicon sequence variants (ASV) with less than 100 sequence reads were considered sequencing artifacts and excluded from subsequent analyses resulting in a total of 5.26 million reads. The sequencing depth was rarefied to 15,203 reads per sample and the taxonomic composition determined via mapping ASV sequences to the Silva Database (Quast et al., 2013). The sequence data has been deposited at the European Nucleotide Archive (ENA) at EMBL-EBI under accession number PRJEB57871 and is publicly available. Statistical analyses and data visualizations of the microbiome data were carried out using R (v3.6.1) and the packages *vegan*, *biomformat*, *phyloseq*, *moments*, *nortest*, *lmerTest*, *emmeans*, *sjPlot* and *ComplexHeatmap*. Anderson-Darling and Shapiro-Wilks tests were used to test for normal distribution of microbiota related parameters. As non-normal distribution was confirmed, non-parametric tests like the Wilcoxon rank-sum test (WRST) were used for group comparisons followed by Benjamini-Hochberg (BH) false discovery rate correction (FDR) when multiple testing was applied. Associations between the taxonomic microbiota composition with the dietary intervention or genotype were assessed via Generalized Linear Mixed Models (GLMMs). Only taxa with a relative abundance of > 0.001%, which were found in at least two samples, were included. A pseudocount of 1 was added to all samples to replace zero counts and the resulting relative abundances centered-log ratio-transformed. Associations of each relative taxon abundance with fixed effects including the dietary intervention (d), genotype (g), the interaction between both effects (d:g), and controls, i.e. the amplification plate batch effects, were assessed, while adjusting the model for repeated sampling within individuals and litter mates as random effects. Model fits were verified using diagnostic plots, estimated marginal means (EMMs) of subgroups compared by Tukey's Test and p-values adjusted using the BH procedure across all taxa. Significance thresholds were chosen as follows: $q \geq 0.05$ not significant, $q < 0.05$ *, $q < 0.01$ ** and $q < 0.001$ ***. Odds ratios (OR) with 95% likelihood-based confidence intervals (CI), as well as marginal and conditional R² were calculated and reported for all significant models.

Quantification and statistical analysis

Data were analysed by two-way ANOVA with Tukey's multiple comparisons test, unpaired t-test or Kruskal-Wallis test. (Adjusted) p-value ≤ 0.0332 (two-way ANOVA, Kruskal-Wallis test) or p-value ≤ 0.05 (unpaired t-test) was regarded as significant. Data was analysed in Microsoft Excel and plotted using GraphPad Prism version 7.00.

Results

Characterization of the effect of HFD on two *Nlrc5* deficient mouse lines

In order to investigate the effect of NLRC5 in HFD-induced obesity, two different *Nlrc5* deficient mouse lines were subjected to HFD feeding. Given its size, complete deletion of the *Nlrc5* locus is not feasible. Instead, specific exons coding for essential parts of the Nlrc5 protein were depleted. In the first *Nlrc5* deficient line, which was generated by the lab of Philip Rosenstiel (Christian-Albrechts University of Kiel, Germany), exons 4 – 7, coding for the NACHT domain (exon 4) and parts of the LRR domain (exon 5 – 7), were targeted for deletion. This mouse line therefore will be referred to as *Nlrc5*^{ΔExon4-7}. The second *Nlrc5* deficient mouse line was generated by the lab of Dana Philpott (University of Toronto, Canada). In these animals, only the NACHT domain was deleted by targeting of exon 4 (Sun et al., 2019). Accordingly, these animals will be referred to as *Nlrc5*^{ΔExon4}. Both mouse lines were generated on a C57BL/6N background. *Nlrc5*^{ΔExon4-7} mice were housed at the central animal facility of the University of Hohenheim while *Nlrc5*^{ΔExon4} mice were kept at the animal facility of the University of Sherbrooke. Both *Nlrc5* deficient mouse lines and corresponding WT controls were subjected to HFD feeding, but feeding protocols varied. While *Nlrc5*^{ΔExon4-7} mice were fed a HFD or corresponding low-fat control diet for 11 weeks, using female mice only, *Nlrc5*^{ΔExon4} mice were fed only HFD for 20 weeks, using both male and female animals. The effect of HFD feeding on both mouse lines is described below.

Female *Nlrc5*^{ΔExon4-7} mice on HFD present with higher body weight gain and an increase in adipose tissue

The following paragraph describes the effect of HFD feeding on female *Nlrc5*^{ΔExon4-7} mice, which for better legibility in this section will be referred to as *Nlrc5*^{-/-} mice.

To investigate the effect of NLRC5 in HFD-induced obesity, 8-week-old female *Nlrc5*^{-/-} mice and wildtype (WT) littermate controls were fed a HFD, containing 30% crude fat, or a control diet (ctrl.) matched in protein content, containing 4% crude fat, for 11 weeks (for detailed diet composition, see Suppl. Table 1). Genotype of mice was verified by endpoint PCR (Figure 2 A) and by determining the mRNA levels of *Nlrc5* and its target *H2K* in epididymal AT (Figure 2 B, D) and liver (Figure 2 C, E). As expected, *Nlrc5* was not to be detected and *H2K* levels were markedly reduced in *Nlrc5*^{-/-} animals in both tissues.

The role of NLRC5 in obesity – Results

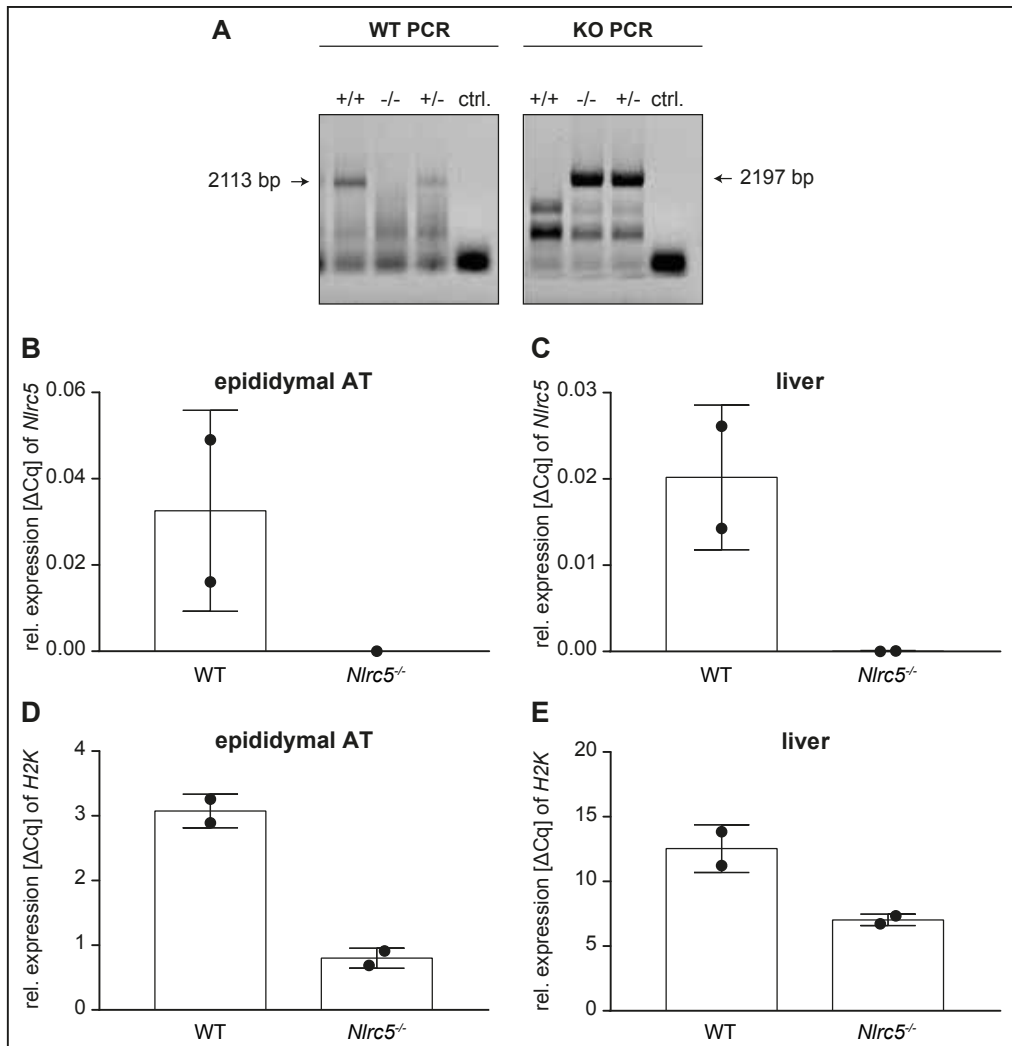
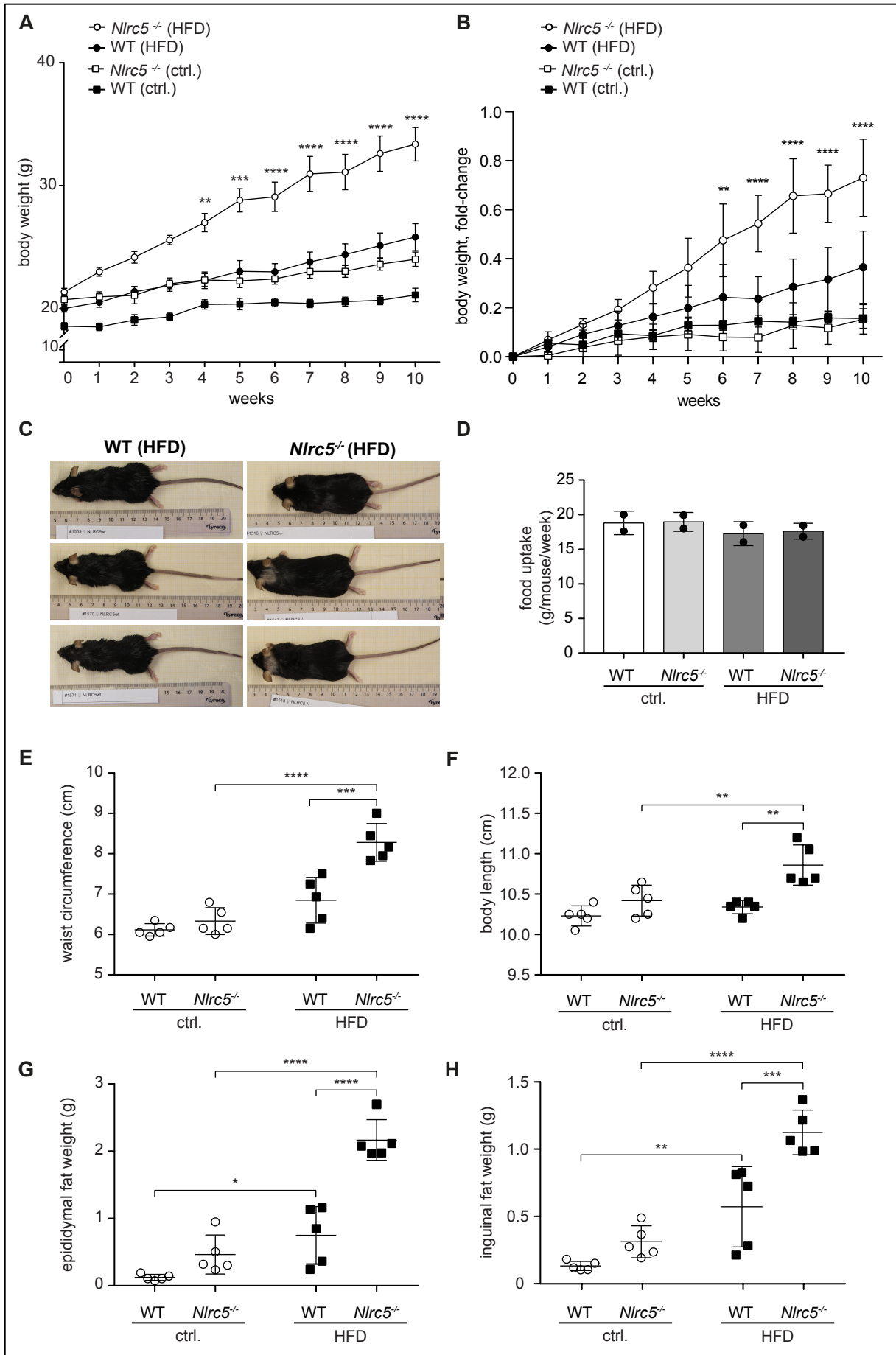


Figure 2: **Characterization of *Nlrc5*^{-/-} mice.** (A) Genotyping of *Nlrc5*^{-/-} and WT mice by PCR using genomic DNA from tail tips. (B-E) *Nlrc5* (B, C) and *H2K* (D, E) mRNA expression in epididymal adipose tissue (AT) and liver of *Nlrc5*^{-/-} and WT female mice after 11 weeks of HFD feeding (n = 2 per genotype). Data show mean \pm S.D.

All animals on HFD gained more weight compared to animals on control diet. Interestingly, *Nlrc5*^{-/-} mice on HFD gained significantly more weight compared to WT animals on HFD, the difference becoming significant from week 4 of feeding on (Figure 3 A). As *Nlrc5*^{-/-} animals presented with slightly higher baseline weight compared to WT mice, the body weight fold-change was calculated by normalizing on the starting weight. Still, *Nlrc5*^{-/-} animals on HFD gained more weight compared to HFD-fed WT animals, the difference starting to be significant in week 6 of feeding (Figure 3 B). The higher body weight gain for *Nlrc5*^{-/-} animals on HFD was also visible by eye (Figure 3 C) and was not due to hyperphagia, as *Nlrc5*^{-/-} and WT animals on both diets consumed similar amounts of food (Figure 3 D). Also, metabolizable energy intake was similar between both genotypes on control or HFD (WT[ctrl.] 0.28 MJ/mouse/week; *Nlrc5*^{-/-}[ctrl.] 0.28 MJ/mouse/week; WT[HFD] 0.36 MJ/mouse/week; *Nlrc5*^{-/-}[HFD] 0.37 MJ/mouse/week). HFD feeding increased the waist circumference for both genotypes, but

statistical significance was only reached for *Nlrc5*^{-/-} mice, which on top presented with significantly higher waist circumference compared to WT animals on HFD diet, again demonstrating more pronounced adiposity phenotype for *Nlrc5*^{-/-} compared to WT mice (Figure 3 E). Interestingly, also body length was significantly increased for *Nlrc5*^{-/-} animals on HFD compared to *Nlrc5*^{-/-} animals on control diet and compared to HFD fed WT animals (Figure 3 F). No significant difference in body length and waist circumference was observed for *Nlrc5*^{-/-} animals on control diet, although a slight increase was to be seen compared to WT animals (Figure 3 E, F). As the increased body length for *Nlrc5*^{-/-} animals might confound the significantly increased weight gain for those animals, final body weight was normalized to body length. The difference between the two genotypes was still significant (WT [HFD] 2.609 g/cm, S.E.M. 0.147; *Nlrc5*^{-/-} [HFD] 3.272 g/cm, S.E.M. 0.095; adjusted p value 0.0007 two-way ANOVA with Tukey's multiple comparisons test). HFD feeding led to a significant increase in body fat for both genotypes (Figure 3 G, H). Concomitantly with the higher body weight gain, the gain in body fat upon HFD feeding was more pronounced for *Nlrc5*^{-/-} mice, which at the end of the experiment presented with significantly larger epididymal (Figure 3 G) and inguinal (Figure 3 H) AT depots compared to WT animals on HFD. Interestingly, this effect was already evident, albeit not statistically significant, for the KO animals on control diet, and largely reinforced by HFD feeding.

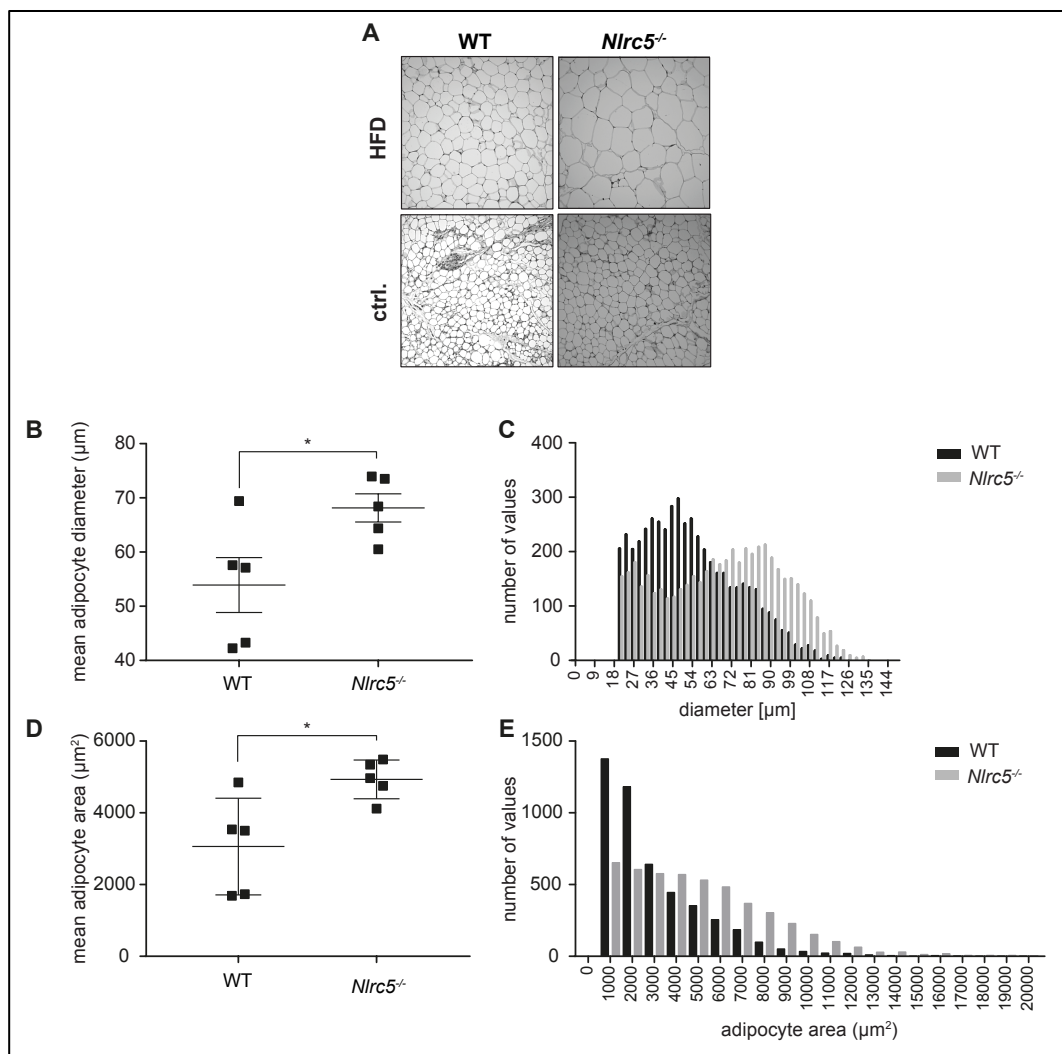
The role of NLRC5 in obesity – Results



The role of NLRC5 in obesity – Results

Figure 3: ***Nlrc5* deficiency aggravates HFD-induced obesity.** Female WT and *Nlrc5*^{-/-} mice (n=5) were fed a control (ctrl.) or high-fat diet (HFD) for 11 weeks. **(A)** Body weight of mice over course of feeding. Data show mean ± S.D. of 5 animals per condition for each of the indicated time points. **(B)** Body weight fold-change of mice over the course of feeding. Body weight was normalized to starting weight for every animal. Data show mean ± S.D. of 5 animals per condition for each of the indicated time points. **(C)** Representative pictures of WT and *Nlrc5*^{-/-} mice after 11 weeks of HFD feeding. **(D)** Average food uptake per mouse per week. Data show mean ± S.D. of two cages with two or three animals. **(E, F)** Mouse waist circumferences (E) and body lengths (F) after 11 weeks of feeding. Data show mean ± S.D. **(G, H)** Weights of epididymal (G) and inguinal (H) fat depots after 11 weeks of feeding. Data show mean ± S.D. *adjusted $p \leq 0.0332$, **adjusted $p \leq 0.0021$, ***adjusted $p \leq 0.0002$, and ****adjusted $p < 0.0001$ two-way ANOVA with Tukey's multiple comparisons test. Data were generated and analysed by Vanessa Aeißen.

Because of this very pronounced effect of *Nlrc5* KO on AT, we took a closer look into fixed epididymal AT sections of *Nlrc5*^{-/-} and control animals on HFD. *Nlrc5*^{-/-} mice presented with larger adipocytes (Figure 4 A) with increased mean adipocyte diameter and mean adipocyte area (Figure 4 B, D). In accordance, the size distribution by diameter or area of adipocytes in the epididymal AT shifted towards larger adipocytes in the *Nlrc5*^{-/-} compared to the WT animals (Figure 4 C, E).



The role of NLRC5 in obesity – Results

Figure 4: ***Nlrc5* deficiency increases epididymal adipocyte size.** Female WT and *Nlrc5*^{-/-} mice (n=5) were fed a control (ctrl.) or high-fat diet (HFD) for 11 weeks. **(A)** Representative pictures of PFA fixed epididymal adipose tissue sections from WT and *Nlrc5*^{-/-} mice on ctrl. or HFD. **(B – E)** Average adipocyte diameter (B, C) and area (D, E) in PFA fixed epididymal adipose tissue sections of WT and *Nlrc5*^{-/-} mice after 11 weeks of HFD feeding. (B, D) mean adipocyte diameter (B) or mean adipocyte area (D) per mouse, data show mean ± S.D. (C, E) histogram showing distribution of adipocytes by diameter (C) or by area (E), data show pooled results of 5 animals per condition. *p ≤ 0.0332, unpaired t-test. Data were generated and analysed by Vanessa Aeissen. Analysis of the adipocyte area was performed with help from Lucy Hezinger and Felix Biber.

Given the pronounced adiposity phenotype in female *Nlrc5*^{-/-} animals on HFD, mRNA levels of the pro-fibrogenic and pro-inflammatory cytokines *Tgf-β* and *Tnf-α* in epididymal AT (Figure 5 A, B) and liver (Figure 5 C, D) were determined. HFD non-significantly increased levels of *Tnf-α* and *Tgf-β* in the epididymal AT, but no difference between the genotypes was observed (Figure 5 A, B). In the liver, *Tnf-α* and *Tgf-β* levels remained stable independent of dietary intervention or genotype (Figure 5 C, D). Next, serum cholesterol and serum triglycerides were measured. In accordance with the body and adipose tissue weight gain, HFD feeding significantly increased serum cholesterol and serum triglyceride levels for both genotypes (Figure 5 E, F). Interestingly, in contrast to the more pronounced weight gain and AT formation, *Nlrc5*^{-/-} mice on HFD presented with a trend to reduced serum cholesterol (Figure 5 E) and significantly reduced serum triglyceride levels (Figure 5 F) compared to the WT HFD group. A trend to reduced triglyceride levels was also observed for *Nlrc5*^{-/-} animals on control diet (Figure 5 F).

Thus, *Nlrc5* deficiency in female mice on HFD led to an obesity-like phenotype with increased weight gain and waist circumference, more AT and larger adipocytes in the epididymal AT. However, despite the pronounced adiposity phenotype, lipid metabolism was not impaired, but rather improved, neither were inflammatory reactions affected by *Nlrc5* deficiency. Male mice were also included in the feeding study, however presented with a less robust and pronounced adiposity phenotype and therefore were not analysed further (data not shown).

The role of NLRC5 in obesity – Results

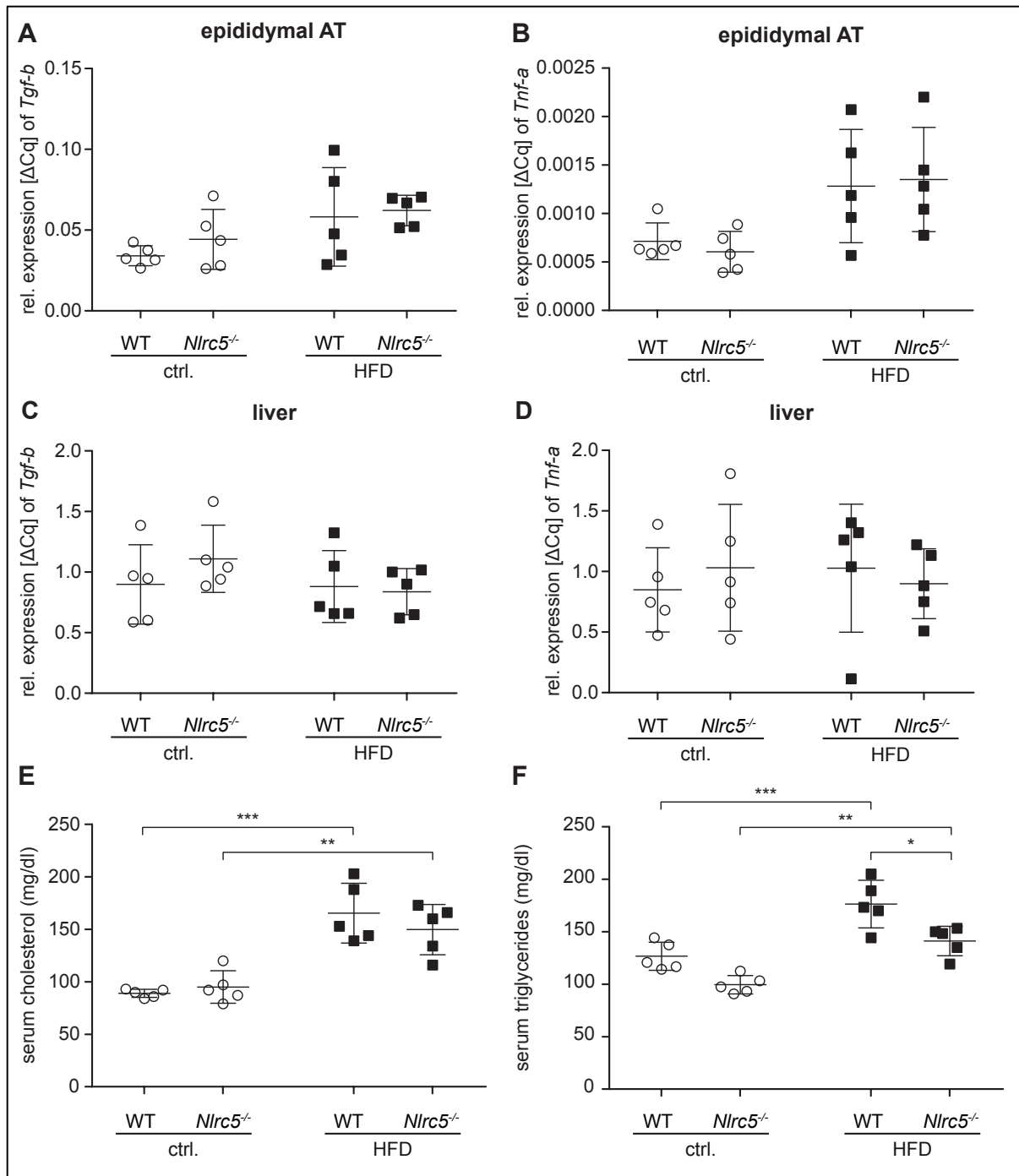


Figure 5: *Nlrc5*^{-/-} mice on HFD present with reduced serum triglyceride levels. Female WT and *Nlrc5*^{-/-} mice (n=5) were fed a control (ctrl.) or high-fat diet (HFD) for 11 weeks. (A – D) mRNA expression of *Tgf-b* and *Tnf-a* in epididymal AT (A, B) and liver (C, D) determined by qRT-PCR. (E, F) Serum cholesterol (E) and serum triglyceride (F) levels. Data show mean ± S.D. *adjusted p ≤ 0.0332, ** adjusted p ≤ 0.0021, *** adjusted p ≤ 0.0002 two-way ANOVA with Tukey’s multiple comparisons test. Data were generated and analysed by Vanessa Aeissen.

Microbiome composition of *Nlrc5*^{ΔExon4-7} animals

Certain NLRs, such as NLRP12, may modulate the organismal threshold to obesity by affecting gut microbial community composition (Truax et al., 2018). As the effect of NLRC5 on microbiota composition here thereto has not been reported and to investigate if the observed HFD-induced phenotype in the *Nlrc5* deficient animals could be related to microbial alterations in the gut, taxonomic profiling of faecal samples of *Nlrc5*^{ΔExon4-7} (here again referred to as *Nlrc5*^{-/-}) and WT animals via 16S rRNA gene amplicon sequencing was performed (Figure 6, Figure 7). Overall, *Nlrc5*^{-/-} mice showed a reduced microbiota alpha diversity compared to WT mice, which was significant for the HFD group (HFD[KO vs WT]: $q = 0.018$, control diet[KO vs WT]: $q = 0.36$, Shannon Index, WRST, Figure 6 A). The alpha diversity was influenced by batch effects (separate amplification runs: $p = 0.00025$, WRST, Figure 6 B), but an even distribution of samples across these two batches, as well as the inclusion of the batch as a fixed effect in subsequent statistical analyses, were used to control for plate effects on compositional microbial analyses. The differences in microbial diversity were accompanied by alterations of the taxonomic composition as determined by generalized linear mixed models (GLMM). In total, ten bacterial taxa were differentially associated with either diet (d) or genotype (g) alone or the interaction between diet and genotype (d:g) (Figure 6 C). Altered relative abundances due to *Nlrc5* KO or the HFD only were identified for two genera each. Comparing *Nlrc5* WT to KO mice revealed increased *Ruminococcaceae* UCG 004 ($q = 0.015$) and decreased *Lachnospiraceae* GCA 900066575 ($q = 0.012$) relative abundance, whereas in response to the HFD, the genera *Lactobacillus* ($q = 0.053$) and *Oscillibacter* ($q = 0.025$) were both increased (GLMMFDR, Figure 6 C). Two taxa were further significantly associated with diet and genotype concurrently. While the genus *Erysipelatoclostridium* was increased by HFD ($q = 0.031$) and *Nlrc5* KO ($q = 0.0027$) independently, the abundance of the family *Ruminococcaceae* was reduced by *Nlrc5* deficiency ($q = 0.0012$) and increased by HFD ($q = 0.03$). The four remaining taxa, *Ruminococcaceae* UCG 003 ($q = 0.013$) and *Clostridiales* Family XIII AD3011 group ($q = 0.006$), as well as the genera *Lachnospiraceae* NK4A136 group ($q = 0.006$) and *Marvinbryantia* ($q = 0.015$) were associated with the interaction of diet and genotype by the GLMM (Figure 6 C).

The role of NLRC5 in obesity – Results

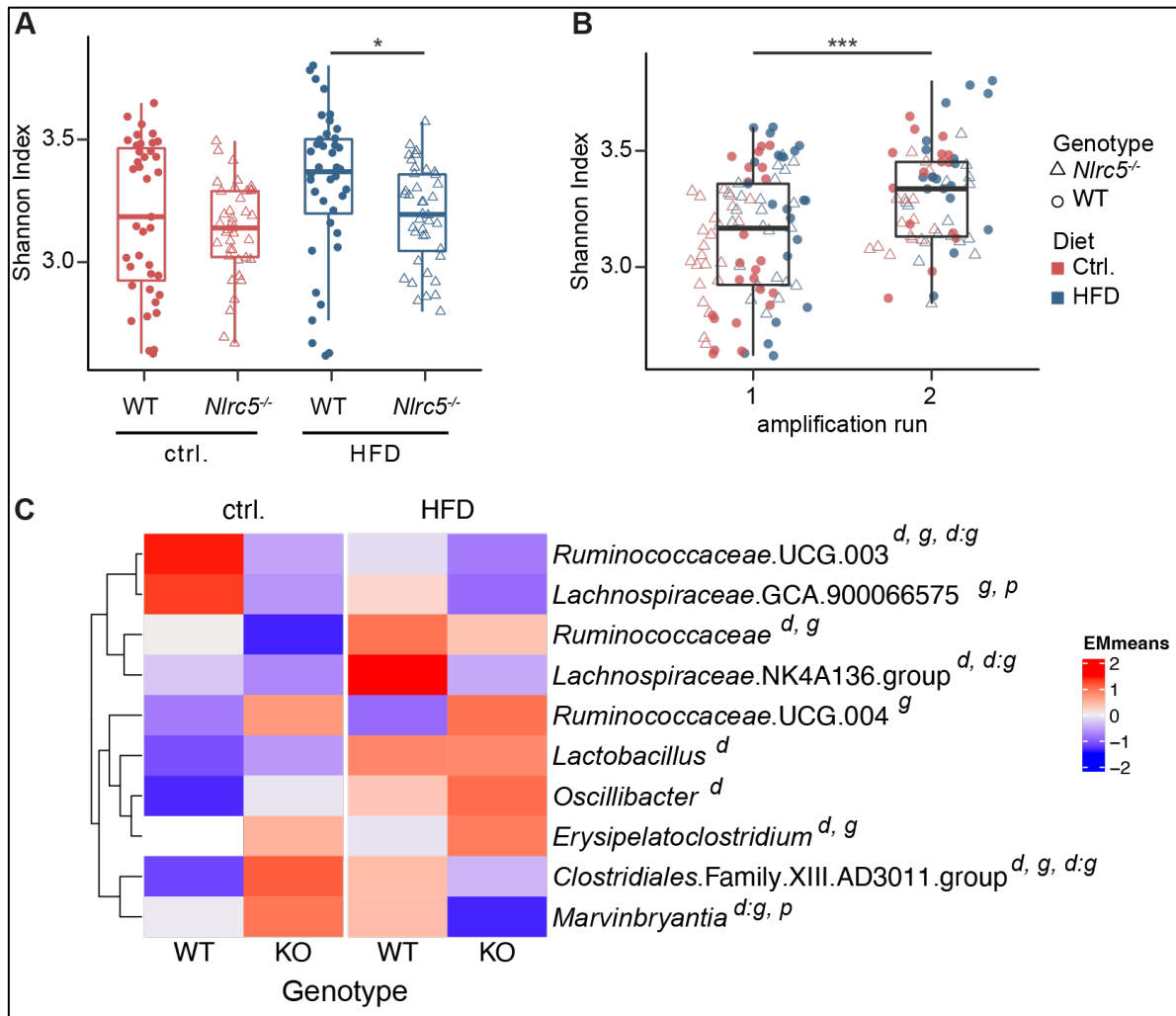


Figure 6: HFD and *Nlrc5* deficiency alter microbial diversity and composition. (A) Shannon Index of faecal samples from WT and *Nlrc5*^{-/-} mice on control (ctrl.) or high-fat diet (HFD). (B) Shannon Index of amplifications runs during library preparation. (A, B) Data show median with first and third quartiles and upper and lower Whiskers of in total 39 (ctrl.) or 40 (HFD) faecal samples collected from each of the 5 animals per condition at 8 different time points. WRST with BH-corrected p for multiple comparisons. ns p ≥ 0.05, *p < 0.05, **p < 0.01, ***p < 0.001. (C) GLMM analysis modelled with repeated measurements per mouse and littermates as random effects. Significant (q < 0.05) associations between relative abundance alterations of microbial groups and dietary intervention (d), gene knock out (g), both (d:g) and technical procedures (p) are shown. GLMM p values were BH-corrected with *q < 0.05, **q < 0.01, ***q < 0.001. Data were generated and analysed by Alena M. Bubeck and Mona Scheurenbrand.

However, post-hoc analysis of subgroups by Tukey's Test revealed statistical significance only for the *Lachnospiraceae* NK4A136 group. For this genus, HFD significantly increased the relative abundance in WT animals (q = 0.049), but not HFD-fed *Nlrc5*^{-/-} mice (q = 0.044, Figure 7 A). Similar trends were observed for the genus *Clostridiales* Family XIII AD3011 group, were *Nlrc5* deficiency (q = 0.077) and HFD (q = 0.144) were separately correlated to increased relative abundance, while a combination of both diminished the effect (q = 0.339, TukeyFDR, Figure 7 B). For *Marvinbryantia*, HFD alone did not change the relative abundance in WT animals (q = 0.574) but reduced it in KO animals (q = 0.0625, TukeyFDR, Figure 7 C). Although

The role of NLRC5 in obesity – Results

for this taxon associations with batch effects were identified (Figure 7 D), due to the even distribution of samples across both batches, no obvious clustering by diet or genotype was determined which could explain the observed interaction effect of diet and genotype. For *Ruminococcaceae* UCG 003, the diet:genotype interaction was primarily driven by genotype, as the taxon was only present in half of the WT animals and further reduced when mice received HFD (q = 0.044, TukeyFDR, Figure 7 E).

Taken together, HFD and *Nlrc5* deficiency alone as well as the interaction between diet and genotype influenced taxonomic gut microbiota composition. These microbiota alterations likely contribute to the adiposity phenotype observed for *Nlrc5*^{ΔExon4-7} mice.

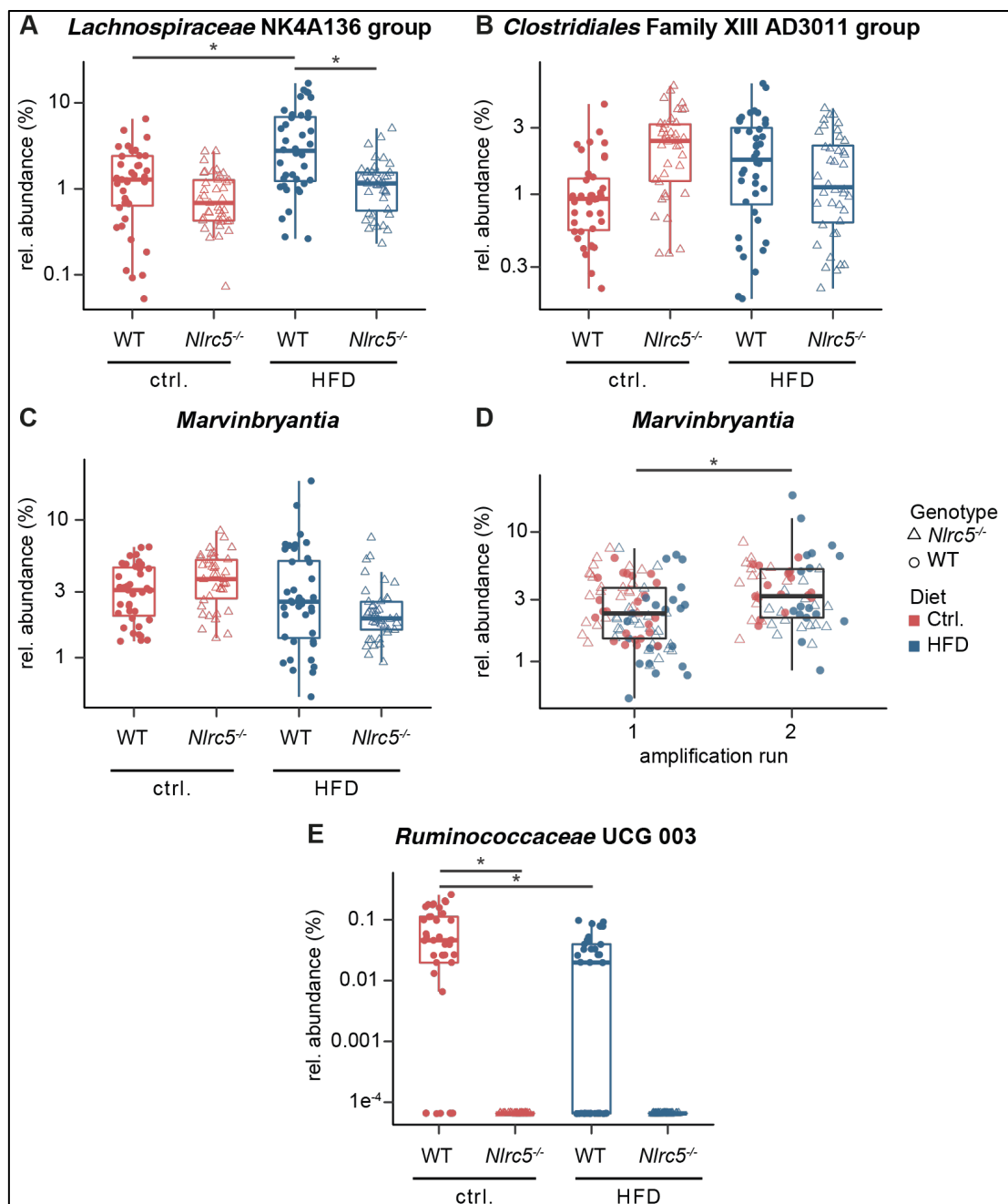


Figure 7: **Three bacterial species are altered in abundance by the interaction between HFD and *Nlrc5* deficiency.** (A – C) Relative abundance of (A) *Lachnospiraceae* NK4A136 group (B) *Clostridiales* Family XIII AD3011 group and (C) *Marvinbryantia* in WT and *Nlrc5*^{-/-} animals on control (ctrl.) or high-fat diet (HFD). (D) Relative abundance of *Marvinbryantia* in amplification runs. (E) Relative abundance of *Ruminococcaceae* UCG 003 in WT and *Nlrc5*^{-/-} animals on control (ctrl.) or high-fat diet (HFD). Data show median with first and third quartiles and upper and lower Whiskers of in total 39 (ctrl.) or 40 (HFD) faecal samples collected from each of the 5 animals per condition at 8 different time points. Relative abundances are displayed on a log-scale and statistics determined based on post-hoc comparisons of estimated marginal means via Tukey's Test with BH-corrected p for multiple comparisons. *q < 0.05, **q < 0.01, ***q < 0.001. Data were generated and analysed by Alena M. Bubeck and Mona Scheurenbrand.

***Nlrc5* deficiency does not affect obesity in *Nlrc5*^{ΔExon4} mice**

To further corroborate the adiposity phenotype observed for female *Nlrc5*^{ΔExon4-7} mice on HFD, the feeding study was repeated using a second *Nlrc5* deficient mouse line lacking exon 4 only (Sun et al., 2019), therefore termed *Nlrc5*^{ΔExon4} hereafter. Additionally, feeding duration was prolonged to 20 weeks. The feeding study was conducted in cooperation with the group of Sheela Ramanathan, University of Sherbrooke, Canada. For better feasibility, *Nlrc5*^{ΔExon4} and WT animals were fed HFD only.

The genotype of all animals was verified by endpoint PCR (Figure 8 A) and by determination of the mRNA levels of *Nlrc5* (Figure 8 B) and its target *H2K* (Figure 8 C) in liver tissue. For three animals, the genotype differed from the genotype stated from the animal facility. Mice 2.4 and 5.3 were genotyped as heterozygous, while mouse 3.1, which was stated to be WT, proved to be KO (Figure 8 A). These animals were excluded from further analysis. As seen for *Nlrc5*^{ΔExon4-7} mice (Figure 2 B – E), *Nlrc5* was not detectable and *H2K* levels were diminished in *Nlrc5*^{ΔExon4} mice (Figure 8 B, C).

The role of NLRC5 in obesity – Results

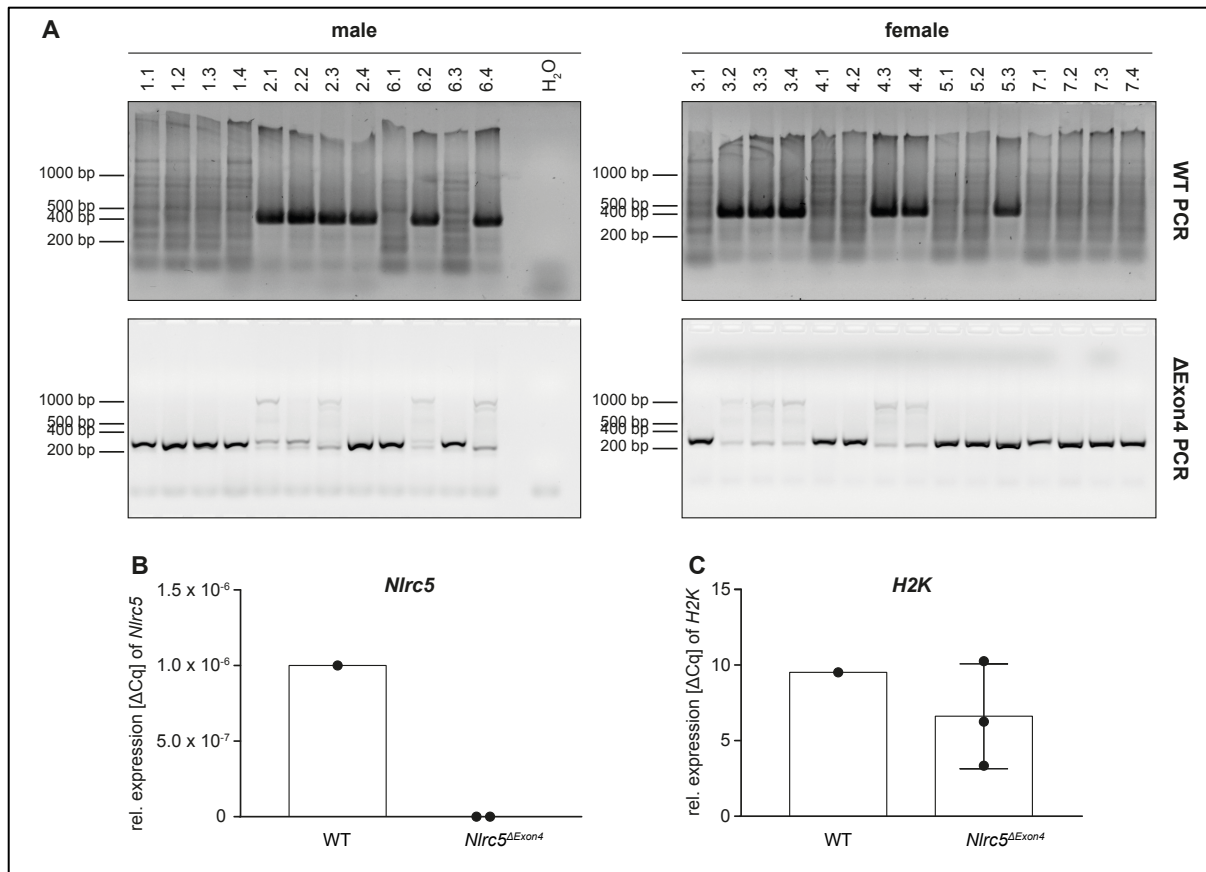
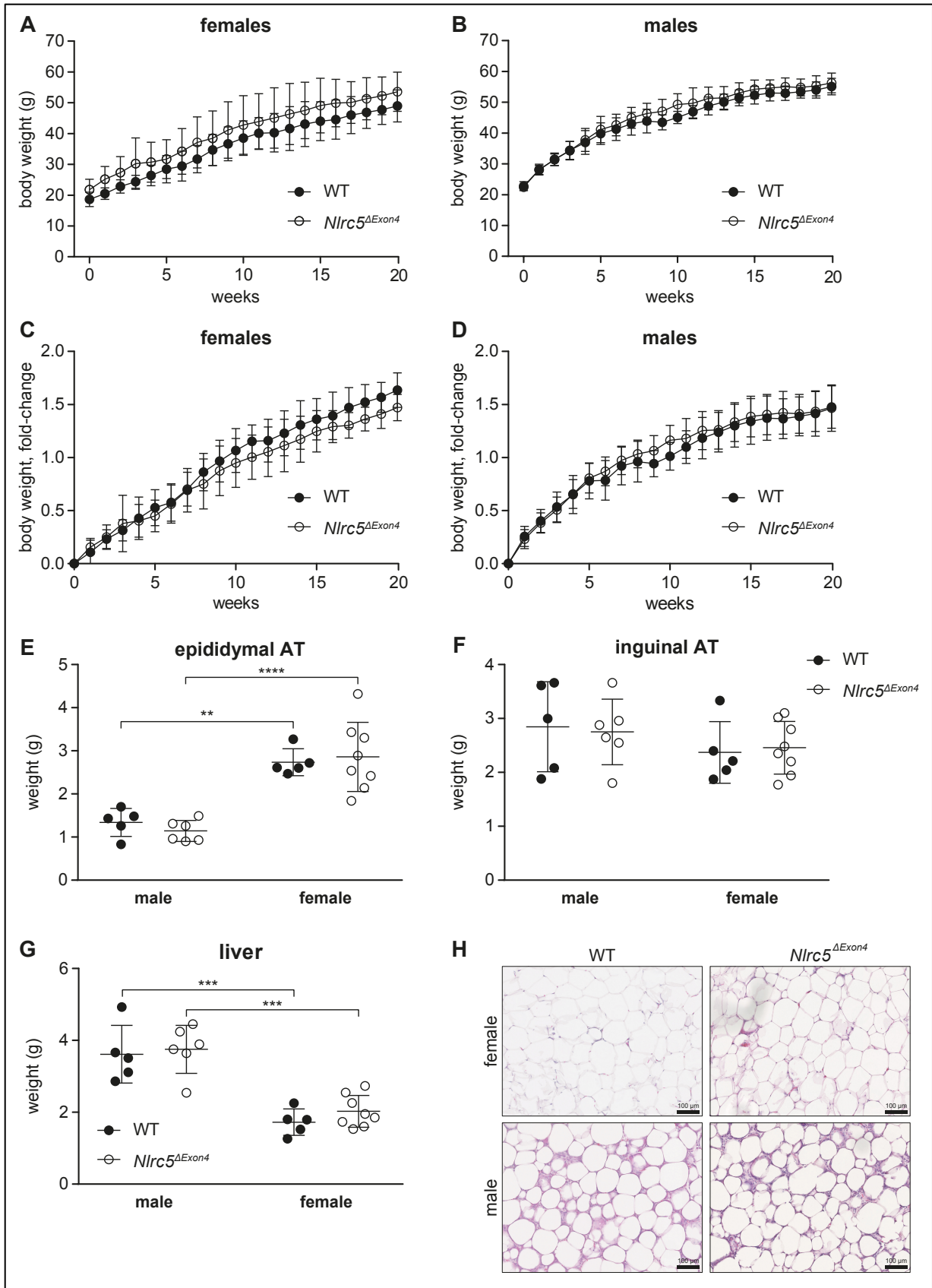


Figure 8: **Characterization of *Nlrc5*^{ΔExon4} mice.** (A) Genotyping of *Nlrc5*^{ΔExon4} mice by PCR using genomic liver DNA. (B, C) *Nlrc5* (B) and *H2K* (C) mRNA expression in liver of *Nlrc5*^{ΔExon4} and WT mice after 20 weeks of HFD feeding. WT n = 1, *Nlrc5*^{ΔExon4} n = 3. Data show mean ± S.D.

Other than expected body weights of *Nlrc5*^{ΔExon4} and WT animals did not differ after 20 weeks of HFD feeding, neither for female nor for male mice (Figure 9 A, B). As female *Nlrc5*^{ΔExon4}, like *Nlrc5*^{ΔExon4-7} mice, at baseline presented with slightly higher body weight compared to WT animals, the body weight fold-change was calculated by normalizing on the starting weight. Still, no difference was observed in weight gain between the two genotypes for both sexes (Figure 9 C, D). Consistent with the body weight, no difference in epididymal (Figure 9 E) and inguinal AT (Figure 9 F) nor liver weight (Figure 9 G) was observed between *Nlrc5*^{ΔExon4} and WT animals at the end of the experiment. Interestingly, female mice presented with significantly higher epididymal AT weight (Figure 9 E) whereas male mice were observed to have significantly higher liver weight (Figure 9 G). Also adipocyte size did not differ between *Nlrc5*^{ΔExon4} and WT animals in H&E stained epididymal AT sections (Figure 9 H).

The role of NLRC5 in obesity – Results



The role of NLRC5 in obesity – Results

Figure 9: ***Nlrc5* deficiency does not influence body weight in *Nlrc5*^{ΔExon4} mice.** Male and female *Nlrc5*^{ΔExon4} and WT animals were fed a high-fat diet (HFD) for 20 weeks. **(A, B)** Body weight of mice over the course of feeding. Data show mean ± S.D. of 5 (WT) or 8 (*Nlrc5*^{ΔExon4}) animals per condition for each of the indicated time points. **(C, D)** Body weight fold-change of mice over the course of feeding. Body weight was normalized to starting weight for every animal. Data show mean ± S.D. of 5 (WT) or 8 (*Nlrc5*^{ΔExon4}) animals per condition for each of the indicated time points. **(E – G)** Weights of epididymal (E) and inguinal (F) fat depots and liver (G) after 20 weeks of feeding. Data show mean ± S.D. **(H)** Representative pictures of PFA fixed and H&E stained epididymal adipose tissue sections from WT and *Nlrc5*^{ΔExon4} mice on HFD. Scale bar = 100 μm. *adjusted p ≤ 0.0332, **adjusted p ≤ 0.0021, ***adjusted p ≤ 0.0002, and ****adjusted p < 0.0001 two-way ANOVA with Tukey's multiple comparisons test.

To assess potential effects of *Nlrc5*^{Exon4} deficiency on pro-inflammatory processes in the AT, epididymal AT sections were stained for CD68 to investigate macrophage infiltration (Figure 10 A). Macrophages forming crown-like structures (CLS) surrounding adipocytes, typical features of obese AT (Cinti et al., 2005; Murano et al., 2008), were visible upon CD68 staining. In accordance with the literature (Medrikova et al., 2012; Pettersson et al., 2012), male mice presented with more macrophages and CLS compared to female mice, but no difference in macrophage infiltration was observed between the genotypes (Figure 10 A).

To investigate potential metabolic alterations caused by *Nlrc5*^{Exon4} deficiency, intraperitoneal glucose (GTT) (Figure 10 B) and insulin tolerance tests (ITT) (Figure 10 C) were performed on a subgroup of three to five animals per genotype at the last week of HFD feeding. As only female *Nlrc5*^{ΔExon4-7} mice presented with a pronounced adiposity phenotype on HFD (Figure 3, Figure 4), GTT and ITT were performed using female mice only. No difference in glucose tolerance was observed between *Nlrc5*^{ΔExon4} and WT animals for the timepoints investigated (Figure 10 B). Also insulin tolerance did not differ between the genotypes (Figure 10 C), although it has to be noted that due to the low amounts of serum available for conducting the test, the lower detection limit might have been undercut. Thus, these data must be interpreted with caution.

Taken together, the pronounced adiposity phenotype observed for female *Nlrc5*^{ΔExon4-7} animals on a 11-week HFD could not be reproduced in *Nlrc5*^{Exon4} mice on a 20-week HFD.

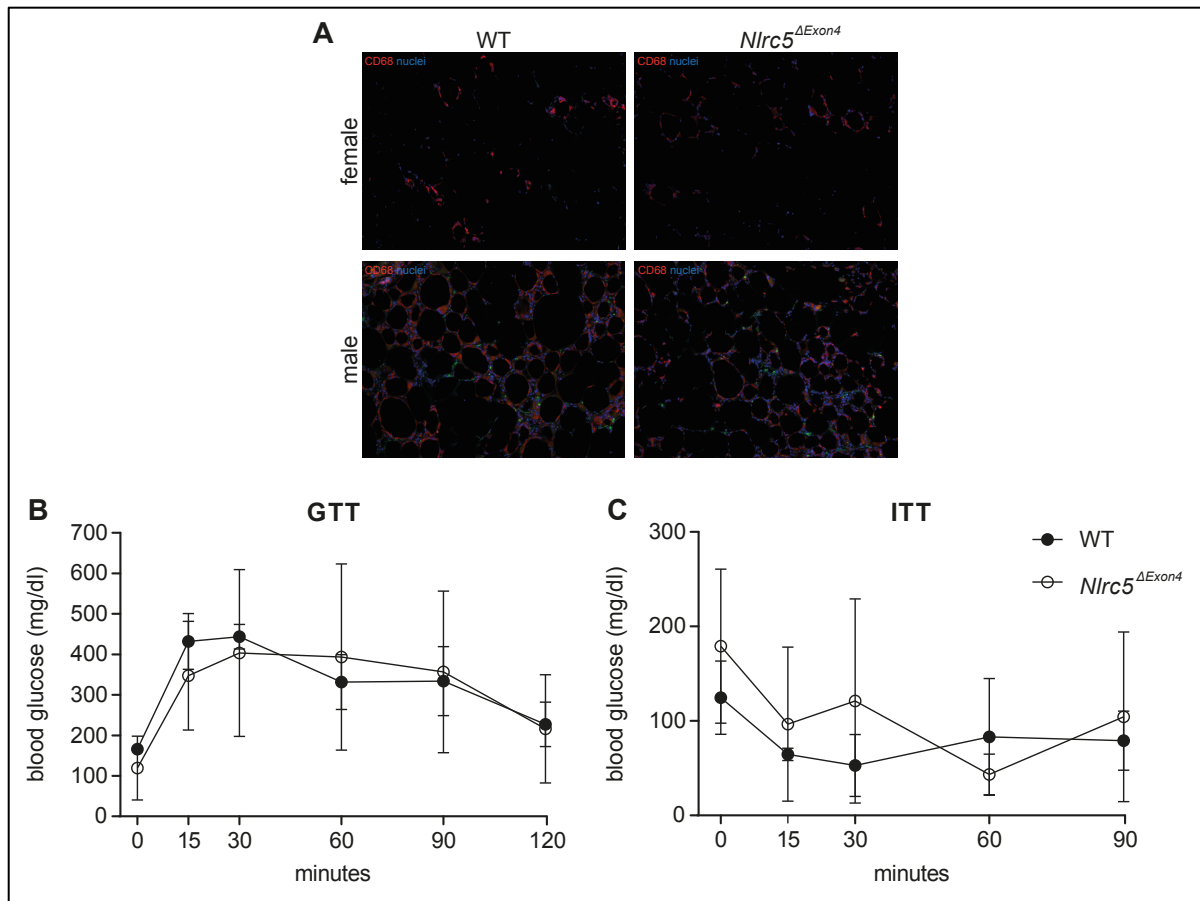


Figure 10: *Nlrc5* deficiency does not influence AT inflammation or glycaemia in *Nlrc5*^{ΔExon4} mice. (A) Representative pictures of indirect immunofluorescent micrographs of epididymal AT sections from WT and *Nlrc5*^{ΔExon4} mice on HFD. CD68 (red) staining is shown. Nuclei are stained with Hoechst (blue). (B, C) Intraperitoneal glucose tolerance test (GTT) (B) or insulin tolerance test (ITT) (C) was performed in female *Nlrc5*^{ΔExon4} and WT mice in week 20 of HFD feeding. Blood glucose levels were determined at the indicated timepoints. Data show mean ± S.D. of 3 - 5 animals per genotype.

Investigation of NLRC5's effect on adipocyte differentiation *in vitro*

The 3T3-L1 preadipocyte cell line is a suitable cell culture model for adipocyte differentiation

Given the strong effect of *Nlrc5* deficiency on AT weight and adipocyte size in *Nlrc5*^{ΔExon4-7} mice (Figure 3 G, H; Figure 4), a cell culture model for adipocyte differentiation was established (Figure 11) to allow for studying the effects of *Nlrc5* deficiency on adipocyte differentiation *in vitro* and to subsequently identify the factors involved. We opted for the best characterized and most frequently used preadipocyte cell line, the 3T3-L1 cells. These cells are easily available and can be propagated for a substantial number of passages (Ruiz-Ojeda et al., 2016). During their differentiation they recapitulate every step of adipocyte differentiation (Tang & Lane, 2012) and they have been shown to morphologically (Novikoff et al., 1980) and

biochemically (MacDougald & Lane, 1995) resemble adipocytes *in situ*. 3T3-L1 cells have been established from MEFs obtained from 17 to 19-day-old disaggregated Swiss 3T3 mouse embryo cells (Green & Meuth, 1974). Under the influence of a hormonal cocktail consisting of insulin, dexamethasone and 3-Isobutyl-1-methylxanthin (IBMX), a cyclic adenosine monophosphate (cAMP)-elevating substance, 3T3-L1 cells differentiate to mature adipocytes within 14 days (Zebisch et al., 2012).

3T3-L1 cells were differentiated following a modified version of the protocol of Zebisch et al. (Zebisch et al., 2012) (Figure 11 A). Briefly, cells were seeded five days prior to the induction of differentiation in a cell number that resulted in a confluent culture after two days as which cells were incubated for three more days. Differentiation was induced by a cocktail of insulin, dexamethasone and IBMX (differentiation medium I) for two days, before cells were cultured in medium containing insulin only for five more days. For the remaining seven days of differentiation, cells were kept in normal culture medium. All media were supplemented with sodium pyruvate. At days 0, 4, 7, 10 and 14 of differentiation, 3T3-L1 cells were stained using Oil Red O (Figure 11 B, C) and lysed for subsequent immunoblot analysis (Figure 11 D). Oil Red O Staining is a well-established method to stain intracellular neutral lipids and triglycerides. Thus, it is frequently applied to quantify lipid accumulation, often used as a surrogate for differentiation efficiency, during adipocyte differentiation *in vitro* (Kraus et al., 2016). Applying the differentiation protocol described above resulted in 3T3-L1 cells accumulating lipid droplets, their frequency and size increasing over the course of differentiation, indicating successful induction of adipocyte differentiation (Figure 11 B). Quantification of lipid accumulation and thus differentiation efficiency was performed by elution of the Oil Red O from the cells and quantifying the eluant's absorbance. Absorbance increased over the course of differentiation, peaked at day 10 and then slightly subsided, highlighting day 10 as timepoint of maximal differentiation (Figure 11 C). As a second readout for differentiation efficiency, the protein levels of Pparg and Fabp4 were determined. Them being the master regulator of adipogenesis and the most abundant protein in fat cells (Matarese & Bernlohr, 1988), respectively, they are often used as markers for adipocyte differentiation. Pparg1 was detectable from day 4 on, peaking at day 10 and then decreasing slightly towards the end of differentiation, mirroring the Oil Red O data. Pparg2, 2 kDa bigger in size, was detected at robust levels only at days 10 and 14 of differentiation (Figure 11 D).

Fabp4, like Ppar γ , was not detectable in undifferentiated cells. Its levels peaked directly at day 4 of differentiation, followed by gradual decrease over the remaining time (Figure 11 D).

Taken together, the 3T3-L1 preadipocyte cell line was successfully established as adipocyte cell culture model.

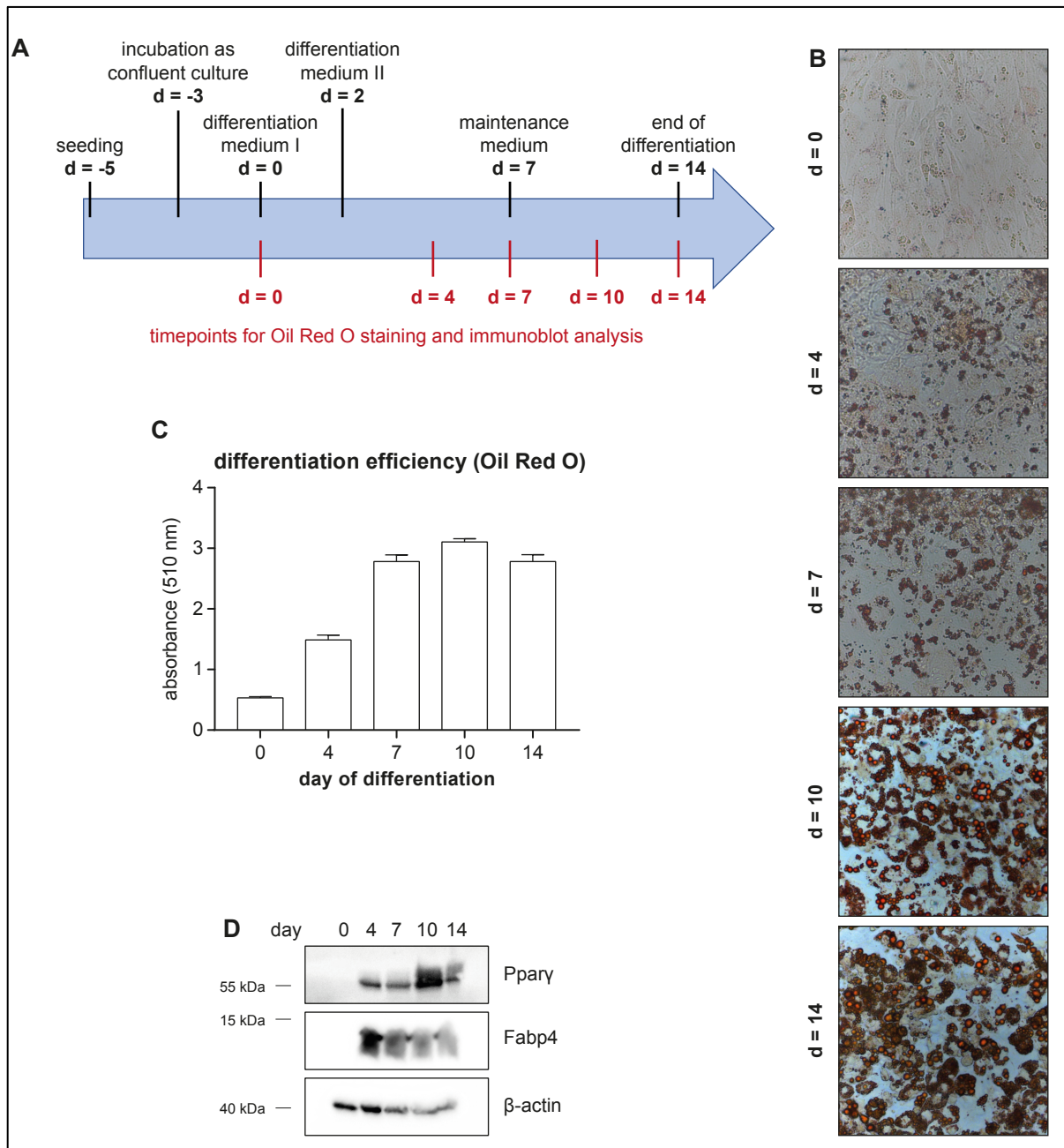
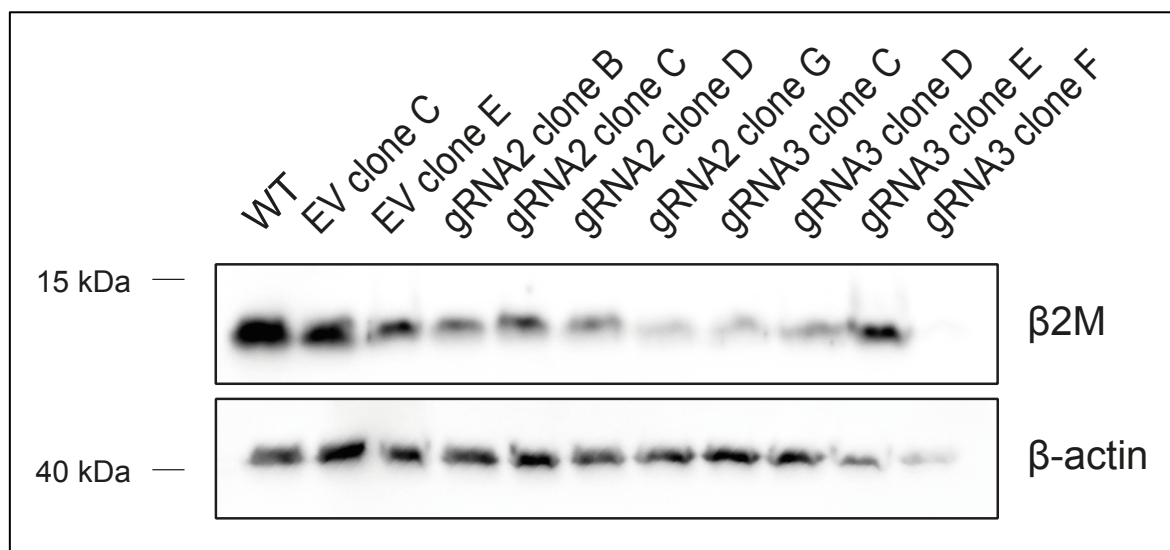


Figure 11: **The 3T3-L1 preadipocyte cell line is a suitable cell culture model for adipocyte differentiation.** (A) Schematic overview over the 3T3-L1 differentiation protocol adapted from (Zebisch et al., 2012). (B) Representative pictures of Oil Red O stained 3T3-L1 cells at the indicated time point of differentiation. d = day of differentiation. (C) Absorbance of Oil Red O eluates of the cells from (B) at the indicated time point of differentiation. (D) Immunoblot of 3T3-L1 protein lysates at the indicated time point of differentiation. Blot was probed for Ppar γ , Fabp4 and β -actin as loading control.

Characterization of 3T3-L1 *Nlrc5* knockout lines

We next aimed at investigating the effects of *Nlrc5* deficiency on 3T3-L1 differentiation. To this end, *Nlrc5* was modified by CRISPR/Cas9 technology, targeting either exon 2 (guide RNA 2, gRNA2) or exon 3 (gRNA3) of *Nlrc5* which code for the transcriptionally active CARD domain (Neerincx et al., 2014; Yao & Qian, 2013). Lentiviral transduction of 3T3-L1 cells with an expression plasmid encoding only the Cas9 endonuclease but no target sequence was used as empty vector (EV) control. Successfully transduced cells were submitted to limited dilution to generate single cell clones. As no reliably working antibody detecting mouse *Nlrc5* is available, the levels of β 2M, a direct NLRC5 target (Ludigs et al., 2015; Meissner et al., 2010), were determined as a surrogate for *Nlrc5* levels and functionality. EV clones C and E presented with similar β 2M levels compared to 3T3-L1 WT cells, indicating no modification of *Nlrc5* by the EV construct (Figure 12). However, as these EV clones in pilot experiments presented with defects in differentiation and cell adhesion, respectively (data not shown), EV clone D was used for further experiments. gRNA2 and gRNA3 clones presented with reduced β 2M levels to varying degrees (Figure 12). Three clones, gRNA2 clone G and gRNA3 clones C and D presented with particularly low β 2M levels, indicative of impaired *Nlrc5* levels and/or functionality in these clones. As gRNA2 clone G presented with defects in proliferation, gRNA3 clones C and D were chosen for further experiments. Modification of *Nlrc5* at the Cas9 cleavage site in these clones was verified by Sanger Sequencing. gRNA3 clone C proved to be highly modified with sequence alterations up- and downstream of the Cas9 cleavage site. gRNA3 clone D turned out to be polyclonal, presenting with various indels (data not shown).



The role of NLRC5 in obesity – Results

Figure 12: **Characterization of 3T3-L1 clones with CRISPR/Cas9 modified *Nlrc5*.** *Nlrc5* in 3T3-L1 cells was modified by CRISPR/Cas9 technology using guide RNAs (gRNA) targeting exon 2 (gRNA2) or exon 3 (gRNA3) of the *Nlrc5* gene or an empty vector (EV) as control. Single clones were generated by limited dilution. Immunoblot of 3T3-L1 cell clones with CRISPR/Cas9 modified *Nlrc5* or WT cells is shown. Blot was probed for β -2-microglobulin (β 2M) and β -actin as loading control.

Upon induction, cells in all conditions differentiated, their lipid accumulation increasing over the course of differentiation (Figure 13 A, B). Compared to WT cells, gRNA3 clones C and D presented with markedly reduced lipid accumulation, an effect more pronounced for gRNA3 clone D cells which barely doubled their lipid content during differentiation (Figure 13 A, B). However, also EV clone D presented with a reduction in lipid accumulation comparable to gRNA3 clone C (Figure 13 A, B). Notably, lipid accumulation was not generally lowered, but most of the gRNA3 clones C and D and EV clone D cells did not differentiate at all, while some cells differentiated normally (Figure 13 A). In WT cells, the two adipocyte differentiation markers *Ppar γ* and *Fabp4* were only detectable in differentiating cells, their levels peaking at day 4 and 7, respectively. In comparison, CRISPR/Cas9 modified clones all showed reduced or not detectable levels of both proteins, again suggesting reduced differentiation ability (Figure 13 C). Notably, especially *Ppar γ 2* was reduced by CRISPR/Cas9 intervention, as it was either not or only detected at very low amounts (Figure 13 C). As observed before (Figure 12), β 2M levels of gRNA3 clone C and especially clone D were reduced compared to WT cells, reflecting the data on reduced differentiation ability of these clones. Unexpectedly, also EV clone D presented with reduced β 2M expression comparable to levels observed in gRNA3 clone C cells (Figure 13 C), paralleling its differentiation behaviour.

Taken together, 3T3-L1 cells with targeted modification of the *Nlrc5* locus present with reduced differentiation ability compared to WT cells. However, the corresponding EV control cells also presented with reduced differentiation comparable to gRNA3 clone C cells. Thus, the question arises, whether *Nlrc5* modification in 3T3-L1 cells truly results in reduced adipocyte differentiation, which notably would contrast the more pronounced adiposity phenotype of *Nlrc5* ^{Δ Exon4-7} animals (Figure 3, Figure 4), or if this observation is just an artefact of lentiviral CRISPR/Cas9 intervention or bottlenecking during (single cell) selection.

The role of NLRC5 in obesity – Results

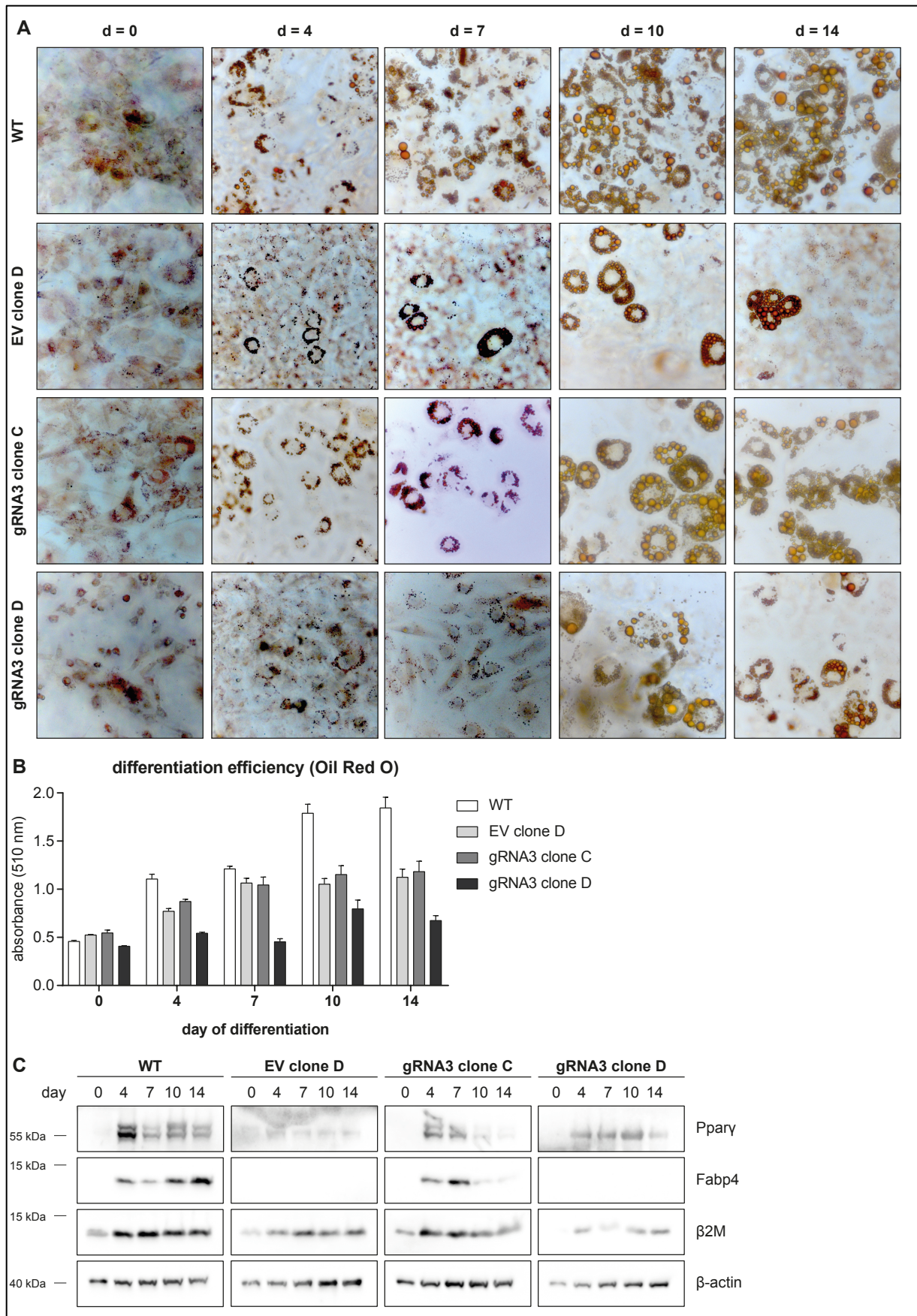


Figure 13: **Characterization of 3T3-L1 *Nlrc5* KO lines.** *Nlrc5* in 3T3-L1 cells was modified by CRISPR/Cas9 technology using a guide RNA (gRNA) targeting Exon 3 of the *Nlrc5* gene (gRNA3) or an empty vector (EV) as control. Single clones were generated by limited dilution. **(A)** Representative pictures of Oil Red O stained 3T3-L1 WT, EV clone D, gRNA3 clone C and gRNA3 clone D cells at the indicated time point of differentiation. d = day of differentiation. **(B)** Absorbance of Oil Red O eluates of the cells from (A) at the indicated time point of differentiation. **(C)** Immunoblot of protein lysates of cells from (A) at the indicated time point of differentiation. Blot was probed for Ppar γ , Fabp4, β -2-microglobulin (β 2M) and β -actin as loading control.

Differentiation ability of *Nlrc5* modified 3T3-L1 cell pools does not differ from WT cells

One of the drawbacks of using 3T3-L1 cells as cell culture model for adipocyte differentiation is their loss of differentiation ability upon heavy passaging (Wolins et al., 2006). Given the nature of generating single cell clones, including selection of successfully transduced cells, followed by limited dilution and expansion of clones, the 3T3-L1 clones used in the previous experiment (Figure 13) had been passaged 13 to 22 times before being seeded for differentiation, while 3T3-L1 WT cells were seeded at considerably lower passage number. To control if the reduced differentiation ability observed for all CRISPR/Cas9 clones (Figure 13) was due to senescence, new CRISPR/Cas9 modified cell pools were generated from one batch of 3T3-L1 cells. 48 h after lentiviral transduction with an expression plasmid for the Cas9 endonuclease and a target sequence for either *Nlrc5* exon 2 (gRNA2), exon 3 (gRNA3) or no target sequence (EV), cells were seeded for differentiation. No selection of successfully transduced cells was performed to avoid bottlenecking and to maintain cells at the same passage number. 3T3-L1 WT cells were treated according to the same protocol and alongside the other cell pools, with the only difference of no lentiviral transduction. DNA modification at the Cas9 cleavage site for gRNA2 and gRNA3 cell pools was verified by T7 endonuclease assay, which proved approximately 50% of the gRNA2 cell pool to have a modified *Nlrc5* locus. For gRNA3 pool cells, cleavage efficiency was lower compared to the gRNA2 cell pool, but an exact number could not be calculated due to difficulties in visualization of the fragments cleaved by the T7 endonuclease (data not shown).

3T3-L1 WT, EV and gRNA2 and gRNA3 cell pools all presented with comparable lipid accumulation over the course of differentiation (Figure 14 A, B). Protein levels of Ppar γ and Fabp4 were slightly reduced for gRNA2 and gRNA3 but also EV pool compared to WT cells. Also, β 2M levels were altered in transduced cells, with EV and gRNA3 pools presenting with lower, while gRNA2 pool cells presented with higher levels compared to WT cells (Figure 14 C).

The role of NLRC5 in obesity – Results

Thus, modification of *Nlrc5* in 50% of a passage-matched 3T3-L1 cell pool does not alter differentiation behaviour as measured by lipid accumulation, indicating the pronounced reduction in differentiation ability of 3T3-L1 gRNA3 clones in comparison to WT cells (Figure 13) to be caused by senescence due to heavy passaging.

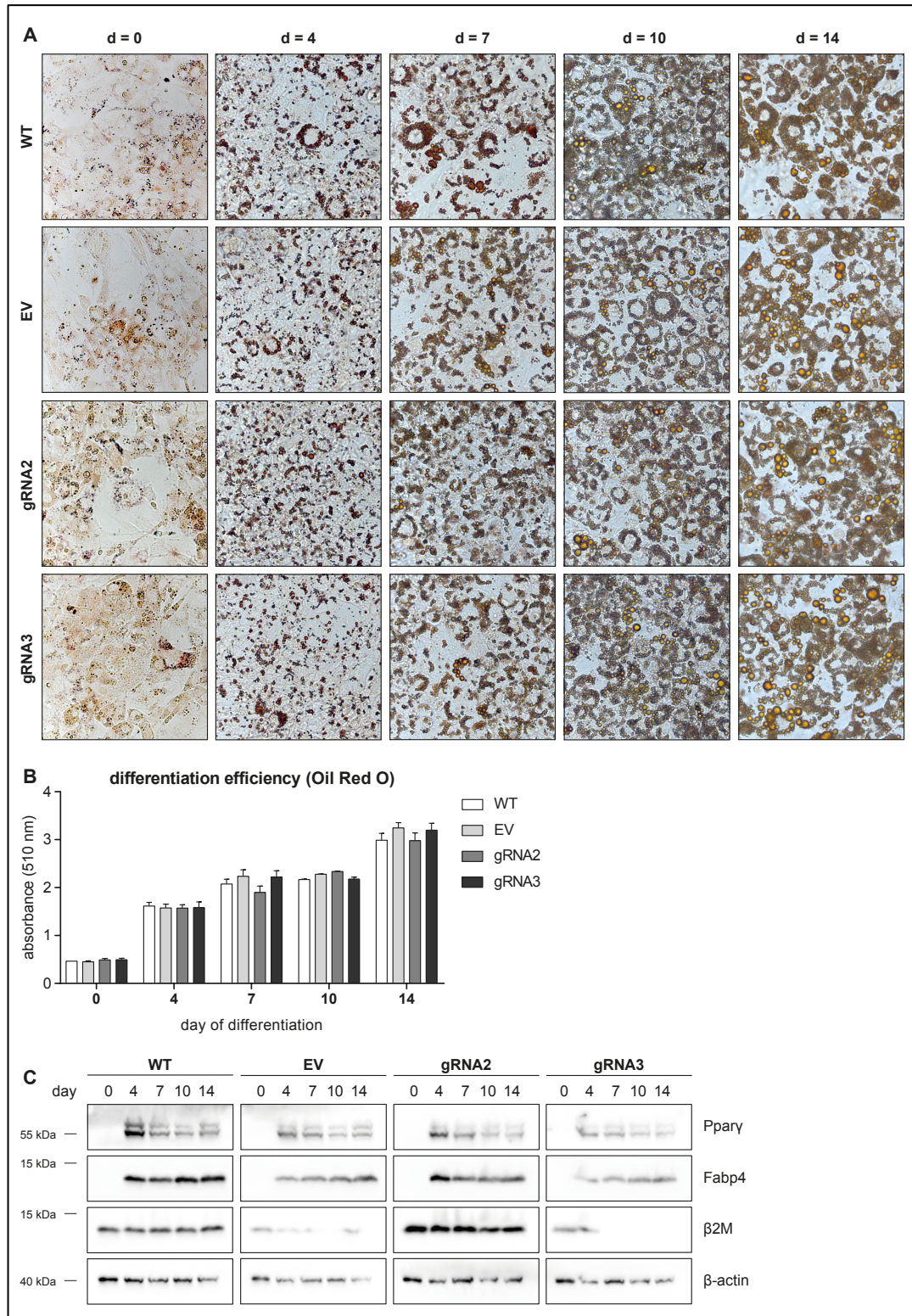


Figure 14: **Differentiation ability of *Nlrc5* modified 3T3-L1 cell pools does not differ from WT cells.** *Nlrc5* in 3T3-L1 cells was modified by CRISPR/Cas9 technology using two guide RNAs (gRNA) targeting exon 2 (gRNA2) or exon 3 (gRNA3) of the *Nlrc5* gene or an empty vector (EV) as control. Cell pools were used for differentiation 48 h after transduction. **(A)** Representative pictures of Oil Red O stained 3T3-L1 WT, EV, gRNA2 and gRNA3 cell pools at the indicated time point of differentiation. d = day of differentiation. **(B)** Absorbance of Oil Red O eluates of the cells from (A) at the indicated time point of differentiation. **(C)** Immunoblot of protein lysates of cells from (A) at the indicated time point of differentiation. Blot was probed for Ppar γ , Fabp4, β -2-microglobulin (β 2M) and β -actin as loading control.

NLRC5 interacts with PPAR γ , co-regulates PPAR γ target genes and modulates PPAR γ 's anti-inflammatory capacities

NLRC5 interacts with PPAR γ 1 via its NACHT domain

PPAR γ is the master regulator of adipocyte differentiation (Barak et al., 1999; Rosen et al., 1999; Tontonoz, Hu, & Spiegelman, 1994). As we observed pronounced changes in adipocyte size in the *Nlrc5* ^{Δ Exon4-7} animals on HFD, although this could not be reproduced in the *Nlrc5* ^{Δ Exon4} animals, we wanted to test, whether NLRC5 affects PPAR γ . To this end, we first tested for protein-protein interactions and used co-expression of either PPAR γ isoform 1 or PPAR γ isoform 2 with GFP-tagged NLRC5 in HEK293T cells. GFP-NLRC5 specifically co-precipitated with PPAR γ 1, but not PPAR γ 2, and activation of PPAR γ by treatment with its specific agonist rosiglitazone slightly reduced binding of PPAR γ 1 to GFP-NLRC5 (Figure 15 A). Taking advantage of stable HeLa cell lines with doxycycline-inducible expression of GFP-NLRC5 (HeLa GFP-NLRC5) or GFP (HeLa GFP) as control, the binding of endogenous PPAR γ 1, but again not PPAR γ 2, to NLRC5 was confirmed (Figure 15 B). This is in line with data showing that NLRC5 interacts with PPAR γ in endothelial cell types (Luan et al., 2019), albeit the isoform specificity was not addressed by these authors. To map the domain of NLRC5 responsible for interaction, PPAR γ 1 was expressed together with different FLAG-tagged NLRC5 deletion constructs (Figure 15 C) in HEK293T cells and co-immunoprecipitation (co-IP) against FLAG was performed. Co-purification of PPAR γ 1 was observed for full-length FLAG-NLRC5 (FLAG-NLRC5 FL), for the NLRC5 construct lacking the N-terminal uCARD domain, here termed death domain (DD) (FLAG-NLRC5 Δ DD) and, to a smaller extent, for NLRC5 isoform 3 (FLAG-NLRC5 Iso3), a naturally occurring NLRC5 isoform lacking most of the LRRs (Neerinx et al., 2010) (Figure 15 D). Co-immunoprecipitation was neither observed for the N-terminal DD nor for the C-terminal LRRs (Figure 15 D). This binding pattern shows that the NACHT domain of NLRC5 is necessary for interaction with PPAR γ 1.

As the NACHT domain is a common structural feature of all NLR proteins, FLAG-tagged NOD1 and CIITA, two other NLR family members that are phylogenetically closely related to NLRC5 (Benko et al., 2010), were tested for interaction with PPAR γ 1. CIITA, like NLRC5, functions as transcriptional regulator and is known as the master regulator of MHC class II genes (Steimle et al., 1993). NOD1 in contrast functions as classical PRR, recognizing intracellular PGN and initiating pro-inflammatory responses (Caruso et al., 2014). PPAR γ 1 co-immunoprecipitated with FLAG-CIITA to a similar extent as NLRC5 FL. In contrast, no binding over background level of PPAR γ 1 to FLAG-NOD1 was detected (Figure 15 D). Thus, binding of PPAR γ 1 to the NACHT domain of NLRC5 seems to occur with high specificity, but not exclusivity, as PPAR γ 1 also co-immunoprecipitated with NLRC5's closest phylogenetic relative, CIITA, but not with NOD1.

In summary, our data show that PPAR γ isoform 1, but not isoform 2, interacts with NLRC5 via its central NACHT domain, proposing a role of NLRC5 in the regulation of PPAR γ activity.

The role of NLRC5 in obesity – Results

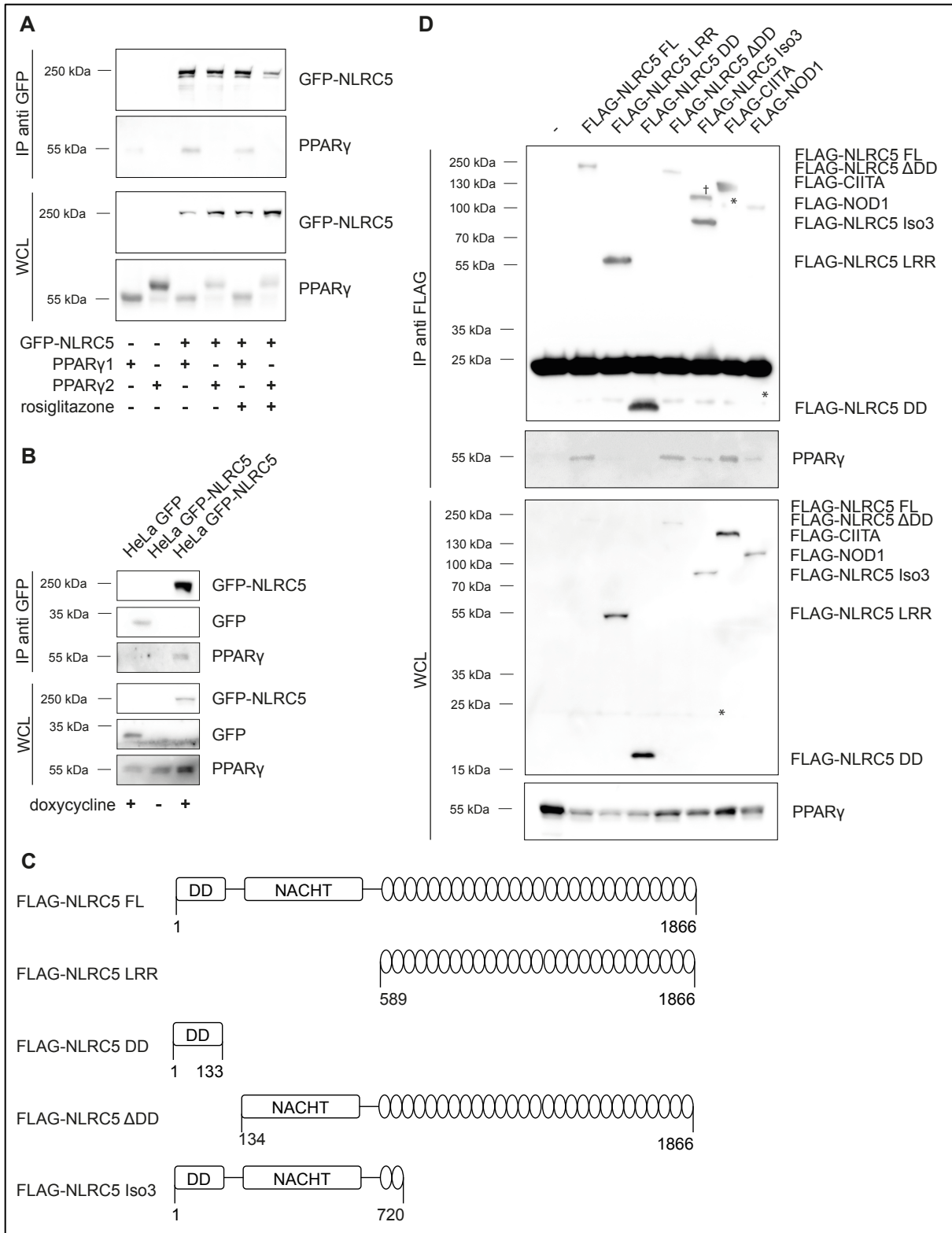


Figure 15: NLRC5 interacts with PPAR γ isoform 1 by its NACHT domain. (A) Immunoblots from anti-GFP immunoprecipitations (IP) of HEK293T cells transfected with GFP-NLRC5, PPAR γ isoform 1 or PPAR γ isoform 2 and stimulated overnight with 0.4 μ g/ml rosiglitazone where indicated. IPs and whole cell lysates (WCL) were probed for GFP and PPAR γ . **(B)** Immunoblots from anti-GFP IPs of HeLa GFP and HeLa GFP-NLRC5 cells induced overnight with 1 μ g/ml doxycycline. Blots were probed for GFP and PPAR γ . **(C)** Domain organization of the NLRC5 constructs used in (D). **(D)** Immunoblots from anti-FLAG IPs from HEK293T cells transfected with PPAR γ isoform 1 and the indicated FLAG-NLRC5 construct. Blots were probed for FLAG and PPAR γ . Representative blots of 1 (B) or 2 (A, D) experiment is shown. †, SDS-stable dimer; *, unspecific bands.

NLRC5 enhances transcription of PPAR γ target genes

Having demonstrated interaction between NLRC5 and PPAR γ 1, in a next step we investigated the effects of NLRC5 on PPAR γ -mediated transcriptional regulation. To this end, HeLa GFP and HeLa GFP-NLRC5 cells were used which predominantly express PPAR γ isoform 1 (Figure 16 A). Functionality of the cell lines was verified on protein and mRNA level by immunoblot and qRT-PCR, respectively (Figure 16 A – C). GFP and GFP-NLRC5 were only detected upon doxycycline induction (Figure 16 A, B). As expected, expression of HLA-A or -B, two MHC class I molecules, was detectable on protein and mRNA level only in HeLa GFP-NLRC5 cells (Figure 16 B, C). HLA-A/B was detected in both, induced and uninduced HeLa GFP-NLRC5 cells, to a similar extend (Figure 16 B, C) due to a very low basal GFP-NLRC5 expression in uninduced cells (Figure 16 C). Thus, minor amounts of NLRC5 are sufficient to boost a full-blown MHC class I response, highlighting the potency of NLRC5 as transcriptional regulator. To analyse the influence of NLRC5 on PPAR γ transcriptional activity, we measured the expression of *CD36* and *FABP4*, two known PPAR γ targets. Successful induction of *NLRC5* expression was verified on mRNA level (Figure 16 D). To activate PPAR γ , cells were treated with rosiglitazone. As expected (Seimandi et al., 2005; Vara et al., 2013), rosiglitazone treatment led to increased expression of both PPAR γ targets in HeLa GFP and HeLa GFP-NLRC5 cells (Figure 16 D). Expression of NLRC5 by doxycycline treatment alone was sufficient to increase *FABP4* transcription to approximately the levels observed in rosiglitazone stimulated HeLa GFP cells (Figure 16 D). As seen for MHC class I genes, even the very low expression of NLRC5 in uninduced HeLa GFP-NLRC5 cells was sufficient to drive *FABP4* transcription (Figure 16 D). Simultaneous rosiglitazone treatment and expression of GFP-NLRC5, both, basal and induced, led to a strong synergistic activation of *FABP4* transcription compared to rosiglitazone-treated HeLa GFP cells. As seen for the cells without rosiglitazone treatment, only a slight further increase was observed when inducing the expression of GFP-NLRC5 by doxycycline treatment (Figure 16 D). For *CD36*, similar observations were obtained, although the effect was less pronounced compared to *FABP4* (Figure 16 D).

To further investigate the positive synergistic effect of NLRC5 on PPAR γ -mediated transcription of target genes, the expression of *FABP4* in HeLa GFP and HeLa GFP-NLRC5 cells treated with increasing concentrations of rosiglitazone was analysed (Figure 16 E). As shown above, *FABP4* expression was not detectable in untreated HeLa GFP cells but increased upon rosiglitazone treatment, expression peaking at a concentration of 0.2 μ g/ml (Figure 16 E, white

bars). In HeLa GFP-NLRC5 cells, *FABP4* expression was readily detectable without rosiglitazone treatment and treatment of these cells with rosiglitazone potentiated the expression of *FABP4* compared to HeLa GFP cells, validating a synergy in transcriptional activation between NLRC5 and PPAR γ . Minor amounts of NLRC5 were sufficient to mediate this synergistic transcriptional activation of *FABP4*, as the leaky expression of NLRC5 in HeLa GFP-NLRC5 cells was sufficient to drive this synergistic effect (Figure 16 E, grey bars, middle panel) and induction of NLRC5 expression by doxycycline treatment only slightly further enhanced this effect for the lower concentrations of rosiglitazone (Figure 16 E, grey bars, right panel). Inhibition of PPAR γ by the specific antagonist GW9662 led to complete abrogation of the rosiglitazone-induced increase in *FABP4* transcription in both HeLa GFP and HeLa GFP-NLRC5 cells. GW9662 also abolished the synergistic effect of NLRC5 expression on *FABP4* transcriptional upregulation in HeLa GFP-NLRC5 cells but did not affect NLRC5-induced *FABP4* expression (Figure 16 F). These data conclusively support that PPAR γ and NLRC5 synergistically drive the transcription of PPAR γ target genes.

While PPAR γ as a nuclear receptor is localized to the nucleus (Akiyama et al., 2002; Umemoto & Fujiki, 2012), NLRC5 is predominantly present in the cytoplasm but able to translocate into the nucleus (Benko et al., 2010; Meissner et al., 2010; Meissner et al., 2012a; Neerinx et al., 2012). The nuclear shuttling is mediated by a NLS localized between the CARD and NACHT domains of NLRC5 (Meissner et al., 2010). In a next step, we sought to investigate which NLRC5 localization is needed to mediate its synergistic effect with PPAR γ on *FABP4* transcription. For this, we used stable HeLa cell lines with doxycycline inducible expression of three different NLRC5 variants which we recently characterized (Neerinx et al., 2012): NLRC5 NLS I harbours a mutation in the NLS rendering it incapable of translocating to the nucleus, NLRC5 2xNLS possesses two SV40 NLS and therefore is predominantly localized to nucleus, and NLRC5 isoform 3, lacking most of the LRR domain, presents with impaired nuclear export and thus is localized predominantly to the nucleus compared to WT NLRC5 (Neerinx et al., 2012). As seen before, GFP-NLRC5 expression in combination with rosiglitazone treatment led to a strong increase in *FABP4* expression compared to a GFP expressing control cell line (Figure 16 G). In contrast, expression of GFP-NLRC5 NLS I did not upregulate *FABP4* and activation of PPAR γ in these cells led to a less pronounced increase in *FABP4* transcription compared to HeLa GFP-NLRC5 cells (Figure 16 G). As seen in previous work for MHC class I genes (Neerinx et al., 2012), expression of GFP-NLRC5 Isoform 3 did not induce *FABP4* transcription over the levels

The role of NLRC5 in obesity – Results

observed in HeLa GFP cells. Expression of GFP-NLRC5 2xNLS failed to induce *FABP4* expression and simultaneous activation of PPAR γ in these cells led to a somewhat lower increase in *FABP4* transcription compared to GFP-NLRC5 WT cells (Figure 16 G). Thus, nuclear localization, the NLRC5 C-terminal LRR domain and, to a lesser extent, nuclear shuttling are important for PPAR γ target gene activation by NLRC5, confirming a model in which direct interaction in the nucleus is necessary for the observed biological effects.

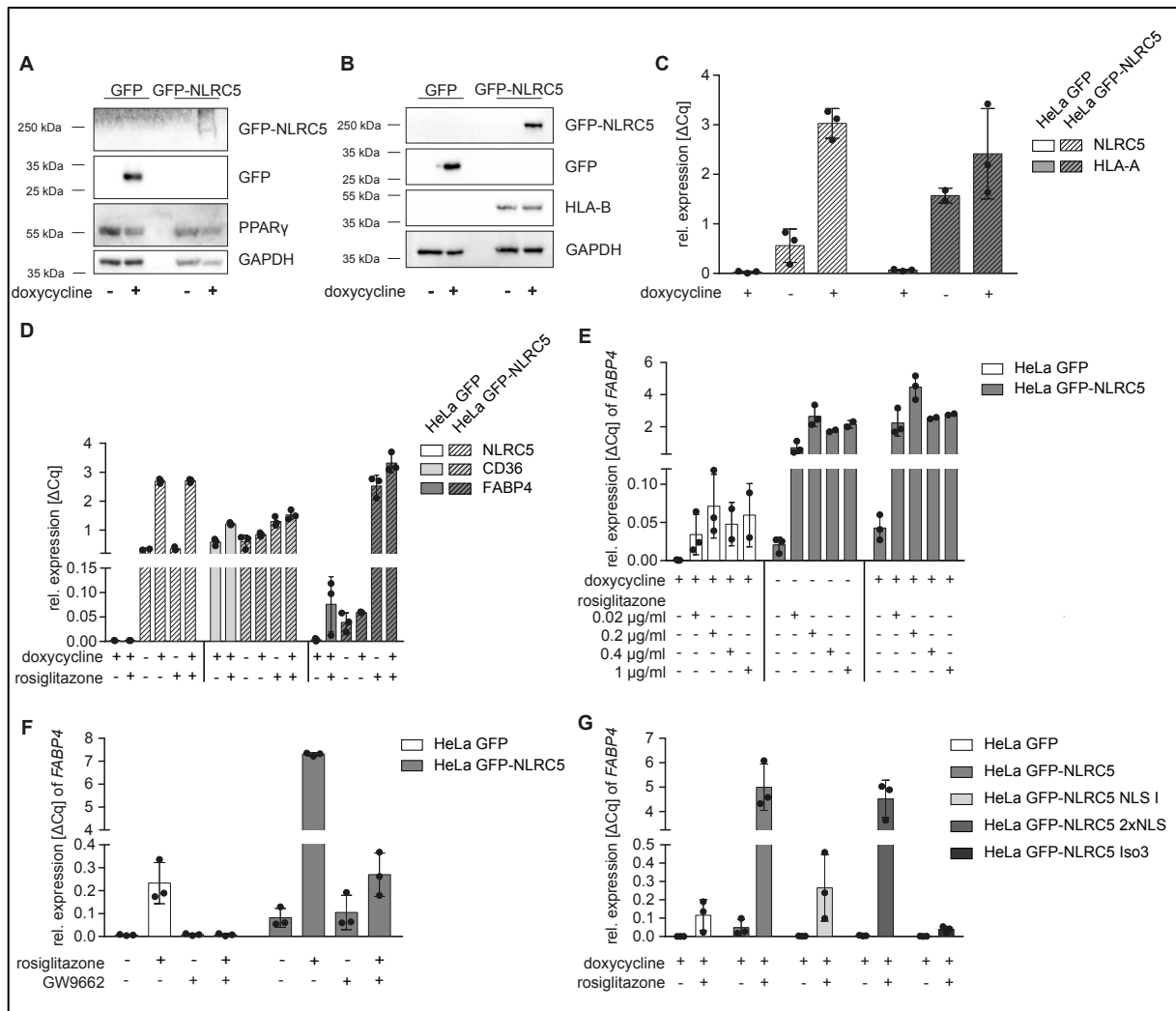


Figure 16: NLRC5 enhances *FABP4* transcription. (A, B) Immunoblot of protein lysates from HeLa GFP and HeLa GFP-NLRC5 cells, induced overnight with doxycycline where indicated. Probing for GFP, PPAR γ , HLA-B and GAPDH as loading control is shown. (C - G) Expression of *NLRC5* (C, D), *HLA-A* (C), *CD36* (D) and *FABP4* (D - G) in HeLa cell lines expressing GFP, GFP-NLRC5 (C - G) or GFP-tagged NLRC5 mutants (G). (C) HeLa GFP and HeLa GFP-NLRC5 cells were treated with 1 μ g/ml doxycycline and 0.1 μ g/ml rosiglitazone for 20 - 24 h. (D) HeLa GFP and HeLa GFP-NLRC5 cells were treated with 0.2 μ g/ml doxycycline and 0.02 μ g/ml rosiglitazone 20 - 24 h. (E) HeLa GFP and HeLa GFP-NLRC5 cells were treated with 1 μ g/ml doxycycline and the indicated concentrations of rosiglitazone for 20 - 24 h. (F) HeLa GFP and HeLa GFP-NLRC5 cells were treated with 1 μ g/ml doxycycline, 0.1 μ g/ml rosiglitazone and 10 μ M GW9662 for 20 - 24 h. (G) HeLa GFP, HeLa GFP-NLRC5 WT or HeLa cells stably expressing GFP-tagged NLRC5 mutants were treated with 1 μ g/ml doxycycline and 0.2 μ g/ml rosiglitazone for 20 - 24 h. (C - G) Gene expression was determined by qRT-PCR. Data show mean \pm S.D. of at least two independent experiments conducted in technical replicates.

Sin3A influences *FABP4* transcription by NLRC5

Recently, our group identified Sin3A and negative elongation factor (NELF) B as novel interaction partners of the NLRC5 N-terminal DD using yeast 2-hybrid (Y2H) screening and co-immunoprecipitations assays (Kienes, 2021). Sin3A is an essential scaffold for the histone deacetylase (HDAC) complex, interacting with eight core proteins, and controls transcription both positively and negatively (Silverstein & Ekwall, 2005). NELFB is part of the NELF complex that binds and stalls the RNA polymerase II complex at the promoter region downstream of the transcriptional start site (TSS) (Li et al., 2013; Nechaev et al., 2010). Thus, as both novel NLRC5 interaction partners function as transcriptional regulators, we investigated the influence of Sin3A and NELFB on the NLRC5-mediated PPAR γ target gene expression. To this end, siRNA-mediated KD of either *Sin3A* or *NELFB* was performed in HeLa GFP and HeLa GFP-NLRC5 cells. PPAR γ was activated by rosiglitazone treatment after KD and *FABP4* levels were determined by qRT-PCR. As we showed above that the leaky expression of NLRC5 in combination with PPAR γ activation was sufficient to induce high levels of *FABP4* transcription, GFP-NLRC5 expression was not actively induced by doxycycline treatment. As shown above, PPAR γ activation highly increased transcription of *FABP4* in HeLa GFP-NLRC5 cells compared to HeLa GFP cells. Whereas KD of *NELFB* did not affect *FABP4* expression in both cell lines, reduced levels of *Sin3A* led to an increased expression of *FABP4* in HeLa GFP as well as HeLa GFP-NLRC5 cells compared to cells treated with a non-targeting control siRNA (siNT). This effect was more pronounced in HeLa GFP-NLRC5 than in HeLa GFP cells, as *Sin3A* KD in GFP-NLRC5 expressing cells led to more than a 120% increase in *FABP4* expression compared to a 92% increase in *FABP4* mRNA for HeLa GFP cells (Figure 17 A). This effect of *Sin3A* KD was specific for the PPAR γ target *FABP4* as *Sin3A* KD barely increased *HLA-A* mRNA levels compared to siNT control (Figure 17 B). KD of *Sin3A* and *NELFB* was verified by qRT-PCR, as no reliable antibody for Sin3A was available. KD led to a significant reduction of the corresponding mRNA level by more than 50% compared to non-targeting control siRNA (siNT) (Figure 17 C, D).

Taken together, Sin3A, one of the two transcriptional regulators identified as novel NLRC5 interaction partners, contributes to the synergistic transcriptional regulation of *FABP4* by NLRC5 and PPAR γ .

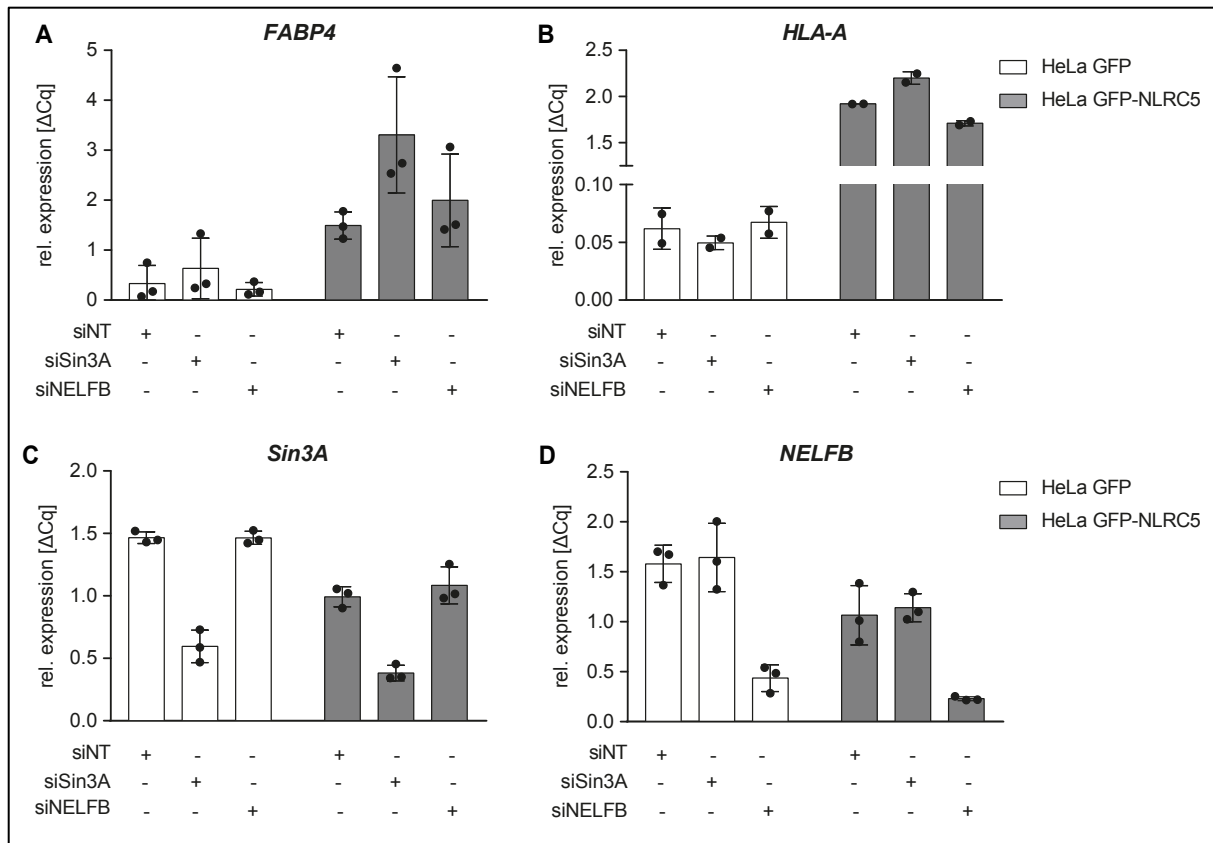


Figure 17: **Sin3A** influences **FABP4** induction by **NLRC5**. **FABP4** (A), **HLA-A** (B), **Sin3A** (C) and **NELFB** (D) expression in HeLa GFP and HeLa GFP-NLRC5 cells after siRNA-mediated **Sin3A** or **NELFB** knockdown. Cells were treated with 0.2 $\mu\text{g/ml}$ rosiglitazone for 22 h after 48 h of knockdown. Gene expression was determined by qRT-PCR. Data show mean \pm S.D. of two (**HLA-A**) or three (**FABP4**, **Sin3A**, **NELFB**) independent experiments.

NLRC5 deficiency in THP-1 macrophage like cells increases pro-inflammatory responses and reduces **PPAR γ** 's anti-inflammatory properties in LPS-induced inflammation

The state of obesity often is accompanied by a chronic state of sterile, low-grade inflammation. NLR proteins have been shown to play an essential role in this low-level inflammatory state (Bauer et al., 2023b). NLRC5 in specific has been shown to be involved in inflammatory signalling, although conflicting results have been reported, with some groups finding NLRC5 to reduce (Benko et al., 2010; Cui et al., 2010; Li et al., 2014; Tong et al., 2012) and some to have no effect (Kumar et al., 2011; Robbins et al., 2012; Yao et al., 2012) on inflammatory signalling. **PPAR γ** in turn has been proven to confer anti-inflammatory effects, especially in monocytes and macrophages, reducing pro-inflammatory cytokine secretion upon pro-inflammatory stimulation and promoting M2 macrophage polarization (Bouhleb et al., 2007; Hong et al., 2003; Jiang, Ting, & Seed, 1998; Odegaard et al., 2007). Given the

pronounced adiposity phenotype in *Nlrc5*^{ΔExon4-7} animals (Figure 3, Figure 4), the involvement in inflammatory signalling of PPAR γ and NLRC5, the interaction between both (Figure 15) and the regulation of PPAR γ targets by NLRC5 (Figure 16), we next sought to investigate if NLRC5 might also be implicated in the anti-inflammatory properties of PPAR γ . To this end, the monocytic cell line THP-1 was used in which *NLRC5* was depleted by CRISPR/Cas9 technology. KO of *NLRC5* was verified by immunoblot (Figure 18 A). To assess NLRC5's potential involvement in PPAR γ 's anti-inflammatory properties, PMA-differentiated THP-1 macrophage-like WT and *NLRC5*^{-/-} cells were treated with the indicated concentrations of LPS and rosiglitazone for 6 h and TNF- α secretion was determined (Figure 18 B). TNF- α secretion increased dose-dependently with increasing concentrations of LPS for WT and *NLRC5*^{-/-} cells. Interestingly, TNF- α secretion in general was slightly higher for *NLRC5*^{-/-} compared to WT THP-1 cells, arguing for an inflammation-reducing effect of NLRC5. In accordance with the literature (Hong et al., 2003), PPAR γ stimulation by rosiglitazone moderately, but dose-dependently decreased TNF- α secretion in THP-1 WT cells. In contrast, reduced TNF- α secretion in THP-1 *NLRC5*^{-/-} cells was only observed for the higher rosiglitazone concentration used. *NLRC5*^{-/-} cells treated with 0.4 μ g/ml rosiglitazone presented with comparable TNF- α secretion to cells not treated with rosiglitazone (Figure 18 B). Thus, NLRC5 seems to aid PPAR γ in conferring its anti-inflammatory function. However, as the effect of rosiglitazone treatment on TNF- α secretion was only moderate, we set out for a second approach to investigate the effects of *NLRC5* deficiency on PPAR γ activation in the context of LPS-induced inflammation. To this end, *TNF- α* and *IL6* mRNA levels were determined by qRT-PCR in THP-1 *NLRC5*^{-/-} and WT cells treated with rosiglitazone for 6 h and 100 ng/ml LPS for the indicated amount of time (Figure 18 C – F). 0.4 μ g/ml rosiglitazone were used, as this concentration was sufficient to reduce TNF- α secretion in THP-1 WT cells (Figure 18 B). For both, *NLRC5*^{-/-} and WT THP-1 cells, *TNF- α* and *IL6* levels increased until 90 minutes of LPS stimulation and then subsided (Figure 18 C, E). In contrast to what was observed for TNF- α secretion, *NLRC5*^{-/-} cells presented with less *TNF- α* (Figure 18 C) or similar *IL6* (Figure 18 E) mRNA levels as THP-1 WT cells in the first 30 minutes of LPS stimulation. However, upon prolonged LPS stimulation, *NLRC5*^{-/-} cells presented with higher *TNF- α* (90 minutes) and *IL6* (60 and 90 minutes) levels compared to WT cells (Figure 18 C, E). Rosiglitazone treatment reduced *TNF- α* and *IL6* levels in both cell lines for every timepoint investigated (Figure 18 C, E), but the effect size of PPAR γ activation differed between WT and *NLRC5*^{-/-} cells. Calculating the expression fold-change of *TNF- α* (Figure 18 D) and *IL6* (Figure

The role of NLRC5 in obesity – Results

18 F) by normalizing on cytokine expression without rosiglitazone treatment, proved *NLRC5*^{-/-} cells to respond less to rosiglitazone treatment, and thus to present with a lower reduction of pro-inflammatory cytokine mRNA compared to WT THP-1 cells at most timepoints investigated. These results further point towards NLRC5 aiding PPAR γ in its anti-inflammatory properties in LPS-induced inflammation.

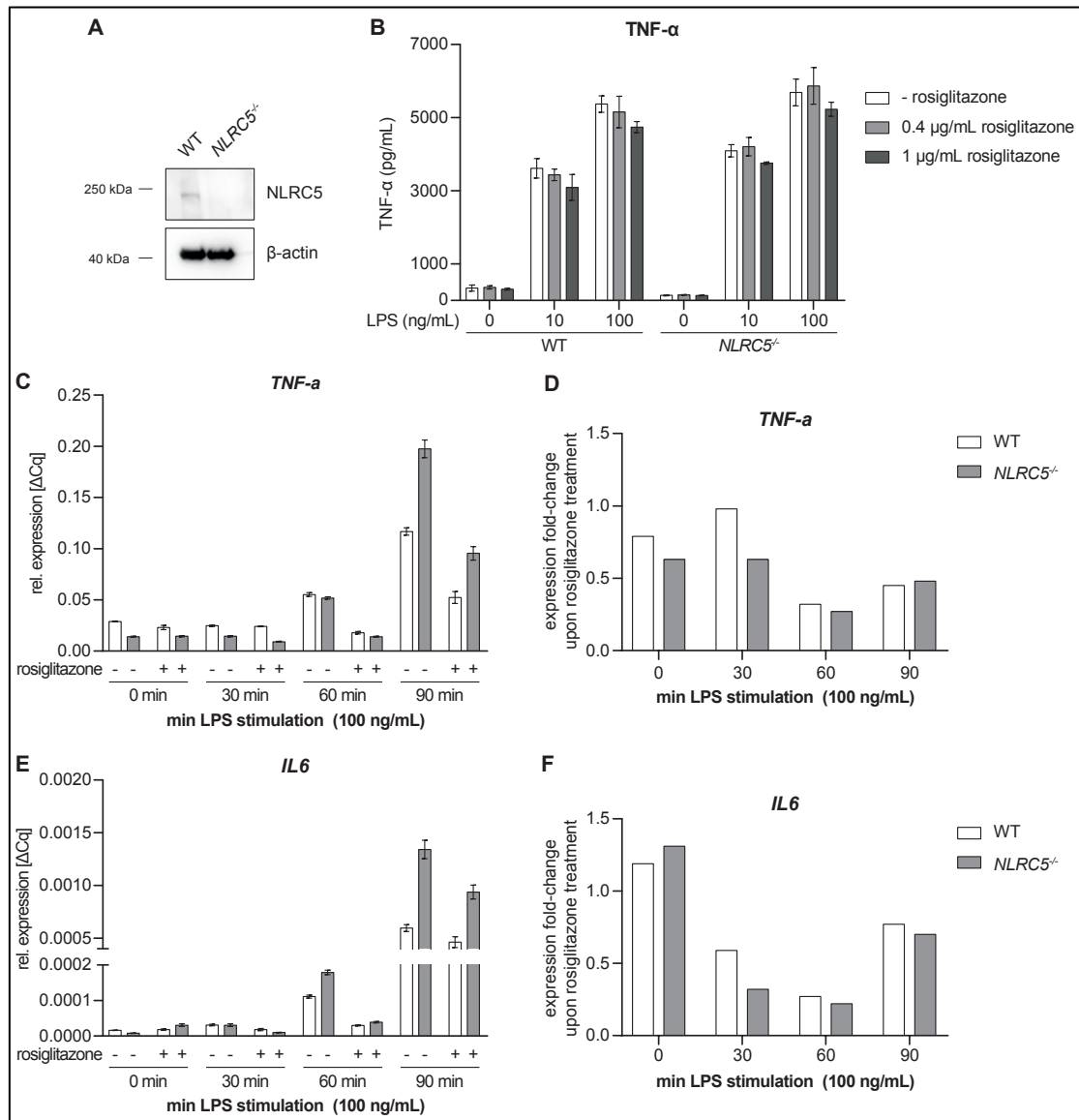


Figure 18: ***NLRC5* deficiency in THP-1 macrophage like cells increases pro-inflammatory cytokine production and reduces PPAR γ 's anti-inflammatory properties in LPS-induced inflammation.** THP-1 WT and *NLRC5*^{-/-} cells were differentiated using 100 nM PMA for 24 h. **(A)** Immunoblot of protein lysates from differentiated THP-1 WT and *NLRC5*^{-/-} cells. Blot was probed for NLRC5 and β -actin as loading control. **(B)** TNF- α secretion of differentiated THP-1 WT and *NLRC5*^{-/-} cells stimulated with rosiglitazone and LPS in the indicated concentrations for 6 h. TNF- α secretion was measured by ELISA. **(C - F)** Differentiated THP-1 WT and *NLRC5*^{-/-} cells were stimulated with 0.4 μ g/ml rosiglitazone for 6 h and treated with 100 ng/ml LPS for the indicated time. **(C, E)** TNF- α (C) and IL6 (E) mRNA levels were determined by qRT-PCR. Data show mean \pm S.D. of technical duplicates. **(D, F)** Expression fold-change of TNF- α (D) and IL6 (F) mRNA levels upon rosiglitazone treatment, normalized to control cells not treated with rosiglitazone. Data is shown as $2^{-\Delta\Delta C_t}$. Data were generated and analysed by Theresa Auer in the context of a Bachelor's Thesis supervised by Sarah Bauer.

To further consolidate these findings, the effects of PPAR γ activation and *NLRC5* deficiency on p38 MAPK phosphorylation, and thus activation, were investigated. p38 MAPK is acting downstream of TLR4 and together with other MAPK enables the expression of pro-inflammatory cytokines and type I IFNs via activating protein 1 (AP-1) (Kawai & Akira, 2006). Thus, p38 activation is a suitable readout in the context of LPS-induced inflammation. THP-1 WT and *NLRC5*^{-/-} cells were treated with 0.4 μ g/ml rosiglitazone for 24 h before being stimulated with 100 ng/ml LPS for the indicated time (Figure 19). LPS stimulation readily increased p38 phosphorylation after 15 minutes of LPS stimulation. Phosphorylated p38 (p-p38) levels increased until 30 to 60 minutes of LPS stimulation, and then slowly subsided (Figure 19 A). In THP-1 WT cells, rosiglitazone treatment reduced levels of p-p38 for up to 60 minutes of LPS stimulation (Figure 19 A, left). This was also seen upon normalizing p-p38 band intensity to total p38 band intensity (Figure 19 B). In THP-1 *NLRC5*^{-/-} cells, PPAR γ activation showed no reducing effect on p-p38 levels. In contrast, rosiglitazone treatment enhanced p-38 phosphorylation (Figure 19 A right, C).

In summary, NLRC5 supports PPAR γ in reducing LPS-induced pro-inflammatory responses in THP-1 macrophage-like cells.

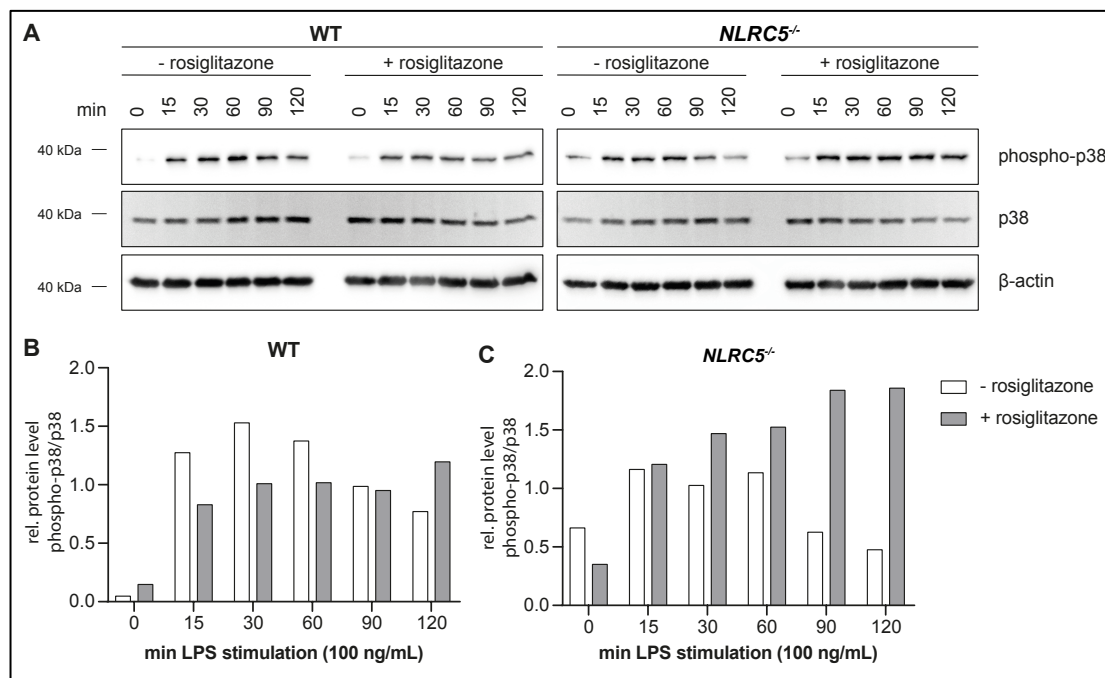


Figure 19: ***NLRC5* deficiency in THP-1 macrophage like cells reduces PPAR γ 's anti-inflammatory properties on p38 activation in LPS-induced inflammation.** Differentiated THP-1 WT and *NLRC5*^{-/-} cells were stimulated with 0.4 μ g/ml rosiglitazone for 24 h, followed by stimulation with 100 ng/ml LPS for the indicated time. (A) Immunoblot probed for p38, phosphorylated p38 and β -actin as loading control. (B, C) Quantification of phosphorylated p38 band intensity normalized to p38 band intensity for THP-1 WT (B) and *NLRC5*^{-/-} (C) cells. Data is representative of 2 independent experiments. Data were generated and analysed by Theresa Auer in the context of a Bachelor's Thesis supervised by Sarah Bauer.

NLRC5 deficiency in murine bone marrow-derived macrophages increases pro-inflammatory responses and reduces PPAR γ 's anti-inflammatory properties in LPS-induced inflammation

To corroborate the results obtained in THP-1 macrophage like cells in primary cells, we used BMDMs from WT and *Nlrc5*^{ΔExon4-7} (in the following referred to as *Nlrc5*^{-/-}) animals. BMDMs were treated with 0.4 $\mu\text{g/ml}$ rosiglitazone overnight, followed by stimulation with 50 ng LPS for 6 h. Tnf- α secretion was measured by ELISA. LPS stimulation highly induced Tnf- α secretion in both WT and *Nlrc5*^{-/-} cells (Figure 20 A). As seen for the THP-1 macrophage-like cells, *Nlrc5* KO cells showed higher Tnf- α levels compared to WT cells, again indicating an anti-inflammatory effect of NLRC5 in the context of LPS-induced inflammation. PPAR γ activation by pre-treatment of BMDMs with rosiglitazone markedly reduced Tnf- α secretion. This effect was obvious in both WT and *Nlrc5* KO cells (Figure 20 A). However, alike what was observed for *NLRC5*^{-/-} THP-1 cells, in *Nlrc5*^{-/-} BMDMs the reducing effect of rosiglitazone was less stringent as in the WT BMDMs (Figure 20 B, 63% reduction of Tnf- α production in WT vs. 48% reduction in KO BMDMs). Identical to the experimental setup used for THP-1 macrophage-like cells, *Nlrc5*^{-/-} and WT BMDMs were stimulated with 0.4 $\mu\text{g/ml}$ rosiglitazone overnight, treated with 50 ng/ml LPS for the indicated time and p38 phosphorylation was investigated (Figure 20 C – E). For both genotypes, p-p38 levels increased until 60 minutes of LPS stimulation and then subsided. For WT cells, rosiglitazone treatment highly reduced p-p38 levels for all timepoints investigated (Figure 20 C left, D), whereas this effect in the *Nlrc5*^{-/-} cells was only visible for the early timepoint of LPS stimulation. For 90 and 120 minutes of LPS stimulation, no more difference was observed between rosiglitazone treated and untreated KO cells (Figure 20 C right, E). Thus, also in primary murine macrophages, NLRC5 acts together with PPAR γ activation in dampening LPS-induced inflammation.

All taken together, these findings obtained in THP-1 macrophage-like cells as well as primary macrophages point towards a synergistic effect of NLRC5 and PPAR γ , not only in PPAR γ target gene induction as seen in the HeLa Flp-In cell lines (Figure 16), but also in the context of LPS-induced inflammation. This might indicate that besides a direct effect on adipocytes, NLRC5 might also regulate pro-inflammatory macrophages in the AT and thus eventually influence obesity-associated low-grade inflammation.

The role of NLRC5 in obesity – Results

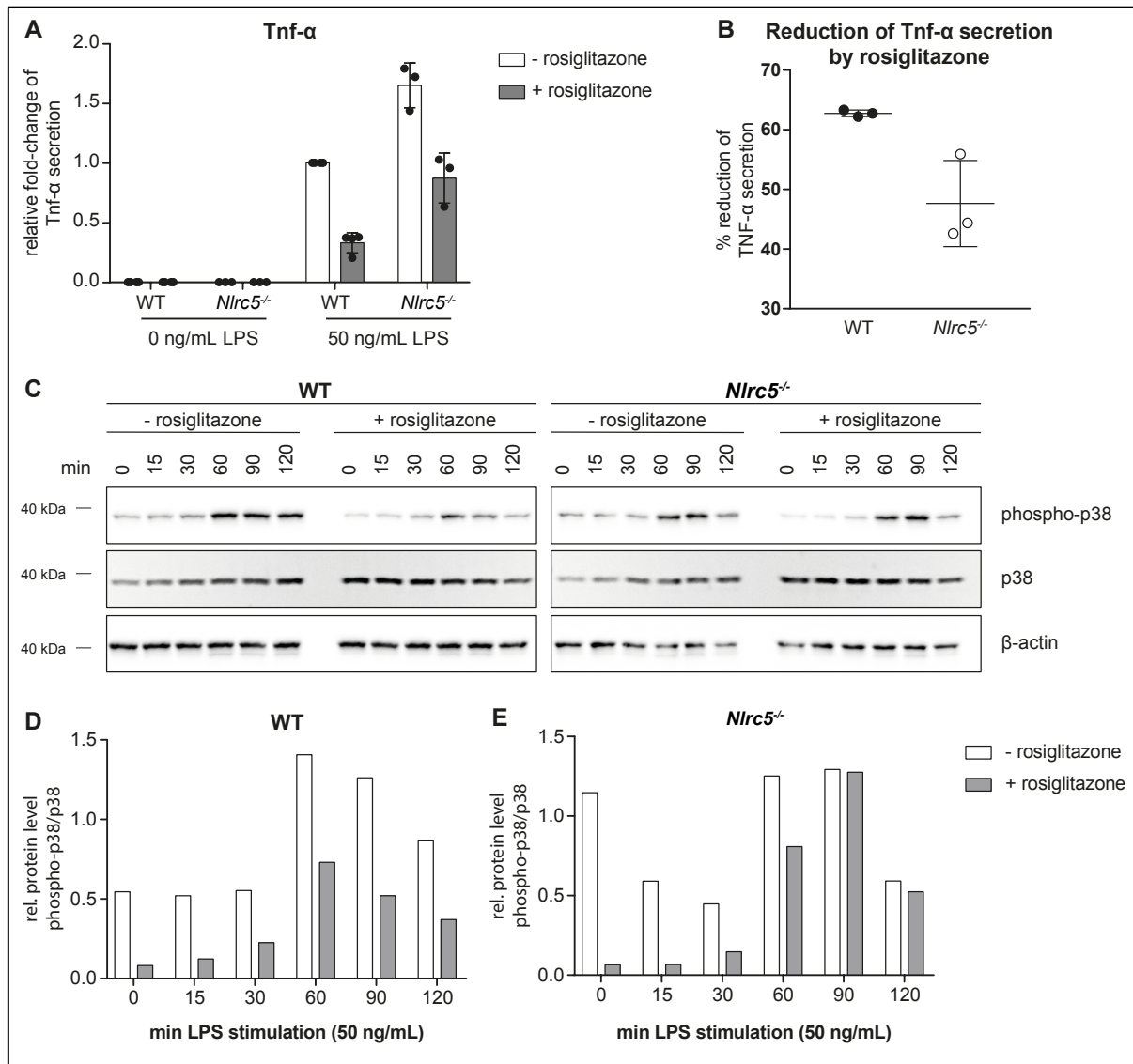


Figure 20: ***NLRC5* deficiency in murine bone marrow-derived macrophages increases pro-inflammatory responses and reduces PPAR γ 's anti-inflammatory properties in LPS-induced inflammation.** Bone marrow-derived macrophages (BMDMs) from WT and *Nlrc5*^{-/-} animals were treated with 50 ng/ml LPS for 6 h (A, B) or the indicated time (C – E). If indicated, BMDMs were treated overnight with 0.4 μ g/ml rosiglitazone prior to LPS treatment. (A) Tnf- α secretion of WT and *Nlrc5*^{-/-} BMDMs normalized on the Tnf- α secretion of WT BMDMs + 50 ng/ml LPS - rosiglitazone. (B) % reduction of Tnf- α secretion by rosiglitazone treatment in WT and *Nlrc5*^{-/-} BMDMs. (C) Immunoblot probed for p38, phosphorylated p38 and β -actin as loading control. (D, E) Quantification of phosphorylated p38 band intensity normalized to p38 band intensity for WT (D) and *Nlrc5*^{-/-} (E) BMDMs. (A, B) Data show mean \pm S.D. of three independent experiments conducted in biological duplicates with n = 4 (WT) or 3 (*Nlrc5*^{-/-}) animals. (C - E) Data is representative of 2 independent experiments using 2 (WT) or 3 (*Nlrc5*^{-/-}) animals in total.

Investigation of the molecular mechanisms underlying PPAR γ target gene regulation by NLRC5

NLRC5 reduces PPAR γ 's transcriptional activity in luciferase reporter gene assays

NLRC5, itself a known transcriptional regulator (Meissner et al., 2010), co-regulates PPAR γ target genes (Figure 16) and contributes to PPAR γ 's anti-inflammatory function in macrophages (Figure 18, Figure 19, Figure 20). As we additionally show here that NLRC5 and PPAR γ directly interact (Figure 15), these data open the intriguing possibility that NLRC5 and PPAR γ act together, as a transcriptional complex, and bind to the promoters of PPAR γ target genes, thereby synergistically regulating their transcription. Thus, we attempted to gain mechanistical insights into how NLRC5-mediated the synergistic co-regulation of PPAR γ targets. PPAR γ is bound to the promoters of its target genes by a consensus AGGTCA sequence repeated once and separated by one nucleotide, the so-called DR-1 or PPRE (A et al., 1997), thereby mediating its transcriptional activity. To investigate if PPRE activity was influenced by NLRC5, reporter gene assays were conducted using HEK293T cells transfected with a PPRE-containing luciferase reporter construct (PPRE X3 TK Luc (Forman et al., 1995)). Functionality of the reporter construct was verified by increased luciferase activity upon treatment of cells with rosiglitazone (Figure 21 A). In contrast to the data obtained before, transfection of increasing amounts of NLRC5 decreased PPRE-mediated luciferase activity in both, rosiglitazone treated and untreated cells (Figure 21 A).

For DNA binding, PPAR γ requires heterodimerization with the nuclear RXR (Lehrke & Lazar, 2005; Miyata et al., 1994). We hypothesized HEK293T cells to have too little endogenous RXR expression to guarantee sufficient PPAR γ DNA binding and thus co-transfected the indicated amounts of an RXR expression plasmid alongside NLRC5. Combined RXR and NLRC5 expression however did not enhance luciferase activity compared to cells transfected with NLRC5 only (Figure 21 B).

CCAAT/enhancer-binding protein α (C/EBP α) besides PPAR γ is considered the most important factor in adipogenesis, and PPAR γ and C/EBP α mutually induce each other's expression in late stage adipogenesis to keep adipocytes in a differentiated state (Rosen et al., 2002; Rosen & MacDougald, 2006; Tontonoz, Hu, & Spiegelman, 1994; Wang et al., 1995). Thus, we tested, whether C/EBP α expression was the missing factor eventually contributing to increased PPRE activity by NLRC5. However, as observed for co-expression of RXR and NLRC5,

also combined C/EBP α and NLRC5 expression did not enhance luciferase activity compared to cells transfected with NLRC5 only (Figure 21 C).

As we were not able to recapitulate the enhancing effect of NLRC5 on PPRE activity in HEK293T cells that was expected based on the previous results generated with HeLa cells, we set out for a closer investigation of the PPRE luciferase reporter plasmid used. The PPRE 3X TK Luc reporter plasmid contains three copies of the PPRE of the acyl-CoA oxidase gene (Forman et al., 1995). Given the close homology of PPRES throughout the PPAR family, the PPRE of the acyl-CoA oxidase gene is bound by and mediates PPAR γ transcriptional activity (Figure 21 A – C). However, the acyl-CoA oxidase PPRES originally has been described to be targeted by PPAR α (Demoz et al., 1994; Tugwood et al., 1992). Thus, we hypothesized NLRC5 to confer a certain level of specificity when regulating PPAR γ transcriptional activity which might be conferred by different PPRES. As we previously showed that NLRC5, in synergy with PPAR γ , induces the transcription of *FABP4* (Figure 16) we decided to generate a new luciferase reporter construct, containing the PPRES of the murine *Fabp4* for the following two reasons. First, we wanted to stay as close to the murine system as possible, given the pronounced adiposity phenotype for female *Nlrc5* ^{Δ Exon4-7} mice on HFD. And second, upon screening of the murine *Fabp4* promoter sequence, consensus sequence modules were detected (data not shown) resembling the S, X and Y box consensus sequences of MHC class I genes and other known NLRC5 targets (Ludigs et al., 2015). Interestingly, some of these sequence modules clustered around the PPRES. Thus, a new luciferase reporter construct was cloned (mFabp4 PPRES), containing a 2,300 bp fragment of the murine *Fabp4* promoter, including the PPRES and most of the consensus sequence modules. Functionality of the mFabp4 PPRES reporter construct was tested by transfection of the indicated amounts alongside 2 ng of PPAR γ 1 into HEK293T cells and treatment with rosiglitazone (Figure 21 D). Luciferase activity was considerably lower compared to the PPRES X3 TK Luc reporter construct, probably because the new construct contained only one PPRES copy, but increased upon rosiglitazone treatment at reporter concentrations of 75 ng and more, verifying reporter construct functionality. Thus, the mFabp4 PPRES reporter construct was co-transfected with 2 ng PPAR γ 1 and the indicated amounts of NLRC5 into HEK293T cells (Figure 21 E). Still, NLRC5 expression dose-dependently decreased luciferase activity in rosiglitazone treated cells. No change in luciferase activity was observed for non-stimulated cells (Figure 21 E). Taken together, NLRC5 overexpression reduced PPAR γ 's transcriptional activity as measured by reporter gene assays.

The role of NLRC5 in obesity – Results

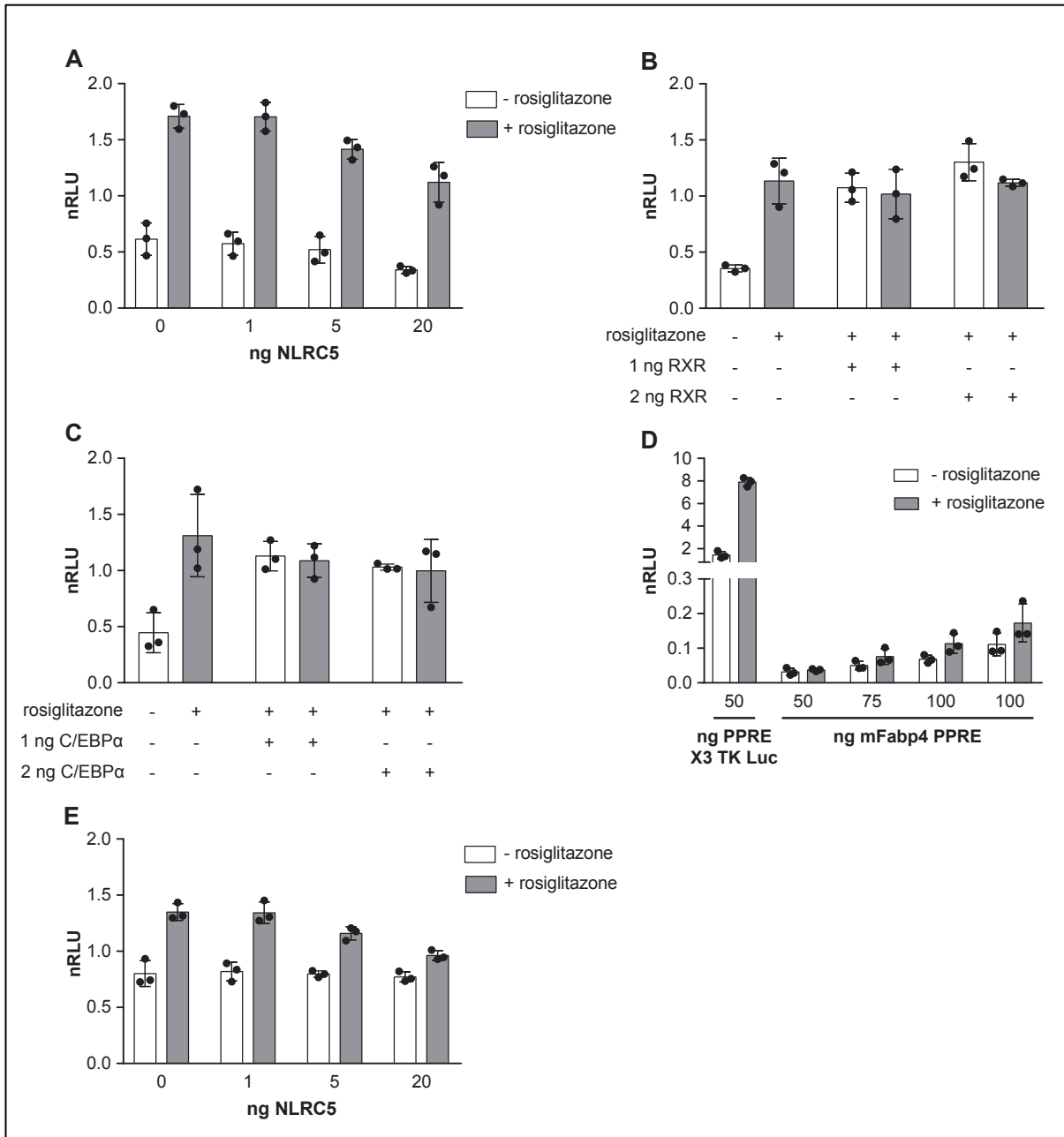


Figure 21: **NLRC5 reduces PPAR γ 's transcriptional activity in reporter gene assays.** Reporter gene assays in HEK293T cells overexpressing 50 ng PPRE 3X TK Luc (A-D) or 100 ng mFabp4 PPRE Luc (D, E) reporter gene constructs if not indicated otherwise and **(A)** the indicated amount of myc-NLRC5; **(B, C)** 2 ng myc-NLRC5 and the indicated amounts of RXR (B) or C/EBP α (C) or **(D, E)** the indicated amounts of myc-NLRC5 and 2 ng PPAR γ . Data show mean \pm S.D. of three independent experiments each conducted in technical triplicates.

Analysis of the NLRC5:DNA interaction at the *FABP4* promoter by ChIP

Luciferase reporter gene assays are useful to study gene expression, however they are also prone to generating artefacts. In addition, it has been shown that some NLRs are able to artifactually inhibit luciferase activity by post-transcriptional modifications (Ling et al., 2012), an effect that has also been observed by members of our lab (personal conversation). Also, reporter gene assays are prone to titration effects, such as overexpression of transcriptional co-factors possibly leading to reduced instead of increased promoter activation because an excess of co-factor scavenges the transcriptional complex and thus inhibits promoter activation (T. A. Kufer, personal conversation). Thus, to directly assess binding of NLRC5 to the promoter of PPAR γ targets, chromatin-immunoprecipitation (ChIP) studies were conducted using HeLa Flp-In GFP-NLRC5 cells. Two different protocols of GFP-NLRC5 pulldown were conducted, using antibody-coupled protein G beads (Figure 22) or a commercially available GFP-Trap agarose resin (Figure 23), respectively. If indicated, cells were treated with 1 $\mu\text{g/ml}$ doxycycline and 0.4 $\mu\text{g/ml}$ rosiglitazone overnight prior to crosslinking, cell harvest and lysis. Chromatin was sheared using ultrasound, yielding DNA fragments of 500 bp and smaller (Figure 22 A, Figure 23 A). After pulldown, immunoprecipitated DNA was analysed by ChIP qRT-PCR, amplifying the promoter region of the indicated genes. For *HLA-B*, *FABP4* and *HLA-DRA* the promoter regions containing the docking sites for NLRC5, PPAR γ and CIITA, respectively, were amplified. For glyceraldehyde-3-phosphate dehydrogenase (*GAPDH*), a 180 bp fragment containing the TATA box and the TSS was amplified. Data is presented as % Input, reflecting the amount of DNA pulled down by the indicated antibody in respect to the amount of DNA used per reaction.

First, pulldown was performed using an anti-GFP or anti-RNA polymerase II (RNA Pol II) antibody bound to protein G beads. Beads bound to a species-matched isotype control antibody were used to control for unspecific DNA binding (Figure 22 B – E). Detection of highly increased RNA Pol II binding to the promoter of the house keeping gene *GAPDH* verified successful pulldown and assay functionality (Figure 22 B). NLRC5 is known to associate with the promoters of MHC class I genes (Meissner et al., 2010; Neerinx et al., 2012). Thus, to control for successful pulldown of GFP-NLRC5-bound chromatin, immunoprecipitated DNA was analysed for the abundance of *HLA-B* promoter fragments (Figure 22 C). Induction of *HLA-B* by doxycycline-mediated expression of NLRC5 was verified by binding of the RNA Pol II to the *HLA-B* promoter (Figure 22 C, white and black bars) which was determined by IP of RNA

Pol II using a specific antibody. For GFP-NLRC5, only marginal binding over isotype control at the *HLA-B* promoter was detected (Figure 22 C, compare light to dark grey bars) and % Input levels were generally low. To answer the question of potential NLRC5 binding to the *FABP4* promoter, chromatin co-immunoprecipitating with GFP-NLRC5 was analysed for the abundance of the PPRE-containing *FABP4* promoter region (Figure 22 D). Enhanced binding over isotype control was observed for uninduced HeLa GFP-NLRC5 cells and, to a higher extend, for cells treated with doxycycline and rosiglitazone, matching the data on enhanced *FABP4* transcription mediated by low, leaky levels of NLRC5 and the synergistic induction of high *FABP4* levels by NLRC5 and PPAR γ activation (Figure 16 C, D). However, no binding of GFP-NLRC5 to the *FABP4* promoter was seen for induced cells not treated with rosiglitazone nor was RNA Pol II binding to the *FABP4* promoter observed for induced and rosiglitazone treated cells, contrasting the data on *FABP4* induction by NLRC5 and PPAR γ (Figure 16 C, D). The general small amount of DNA that was co-immunoprecipitated questioned the robustness of the data, especially as NLRC5 presented with similar binding pattern and % Input levels at the promoter of *HLA-DRA* (Figure 22 E), which as an MHC class II gene is not regulated by NLRC5 (Meissner et al., 2010; Neerincx et al., 2012). This is also reflected by RNA Pol II not binding to the *HLA-DRA* promoter over isotype control (Figure 22 E, white and black bars).

The role of NLRC5 in obesity – Results

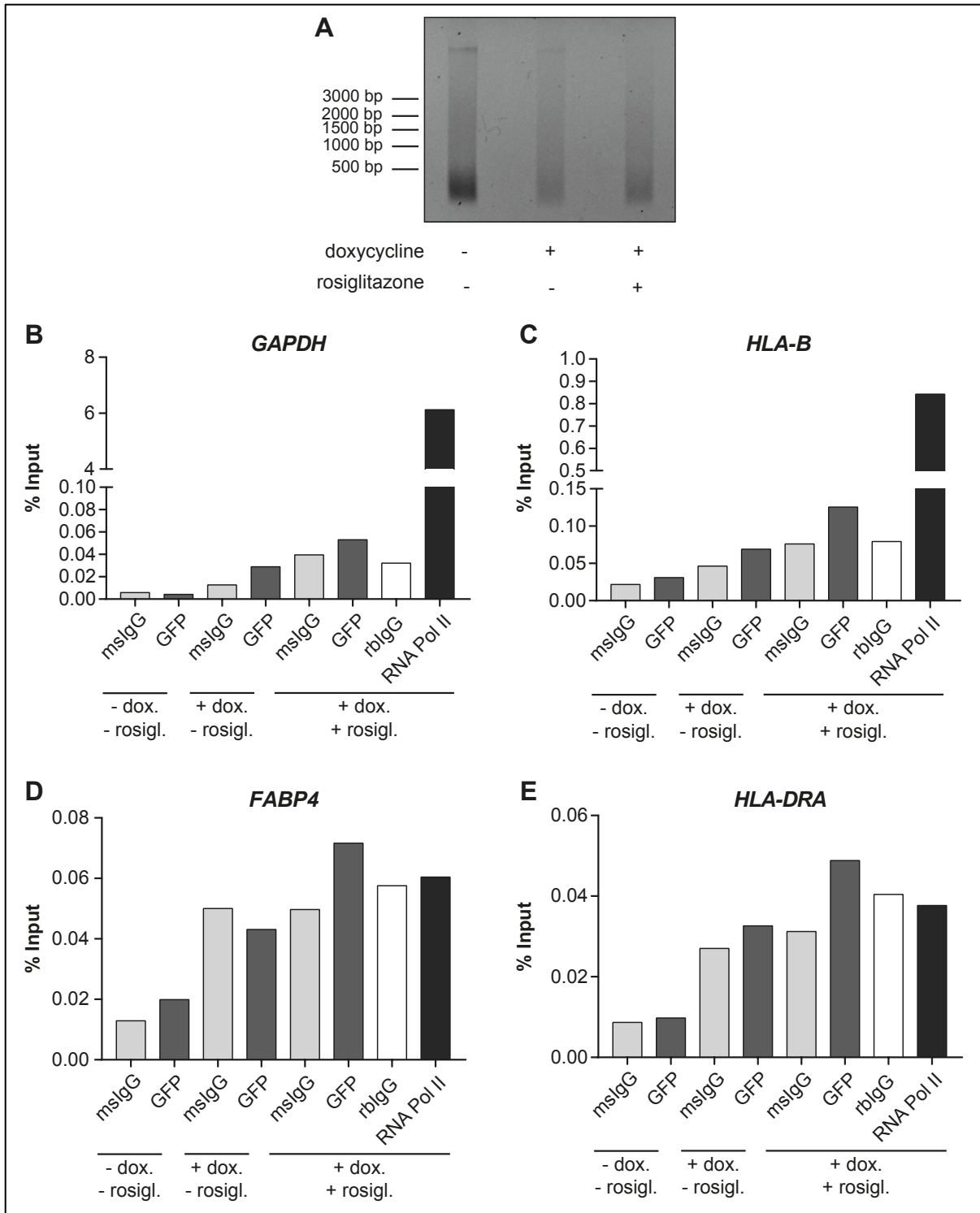


Figure 22: **Analysis of NLRC5:DNA interaction at the *FABP4* promoter by ChIP assays using GFP antibody-coupled beads.** HeLa GFP-NLRC5 cells were treated with 1 $\mu\text{g/ml}$ doxycycline and 0.4 $\mu\text{g/ml}$ rosiglitazone overnight, where indicated. Cells were lysed, chromatin was sheared by ultrasound and chromatin immunoprecipitation (ChIP) was performed (**A**) Sheared chromatin of HeLa GFP-NLRC5 cells treated as indicated. (**B – E**) Immunoprecipitated chromatin was analysed by qRT-PCR for the abundance of promoter sequences of the indicated genes. Data is presented as % Input, reflecting the amount of DNA pulled down by the indicated antibody in respect to the amount of DNA used per reaction.

The low levels of *HLA-B* detected in the GFP-NLRC5-precipitated DNA indicated experimental problems with the pulldown of GFP-NLRC5 and bound DNA, hampering drawing conclusions on potential NLRC5 binding to the *FABP4* promoter. Thus, we improved GFP-NLRC5 pulldown by using a commercially available GFP-Trap agarose resin, which in previous experiments proved to be highly efficient in pulling down GFP-tagged NLRC5 (Figure 15 A, B). Sheared chromatin (Figure 23 A) was incubated with GFP-Trap agarose or the corresponding control resin and precipitated DNA was analysed for the abundance of *HLA-B* (Figure 23 B) and *FABP4* (Figure 23 C) promoter fragments. Independent of treatment, an approximate two-fold increased binding over control of NLRC5 to the *HLA-B* promoter was detected (Figure 23 B), matching the data on robust and low threshold MHC class I induction by NLRC5 (Figure 16 A, B). Generally, more DNA was immunoprecipitated compared to pulldown with GFP antibody-coupled protein G beads (Figure 22 C), proving GFP-Trap agarose resin to be more efficient for GFP-NLRC5 pulldown in CHIP assays. Analysing co-immunoprecipitated chromatin for the abundance of *FABP4* promoter fragments revealed no enrichment of NLRC5 over control at the *FABP4* promoter for untreated cells or cells treated with either doxycycline or rosiglitazone alone (Figure 23 C), contrasting the data generated by pulldown of GFP-NLRC5 with protein G beads (Figure 22 C). For HeLa GFP-NLRC5 cells induced by doxycycline and stimulated with rosiglitazone, slightly enhanced binding of NLRC5 over control was detected (Figure 23 C), in turn reflecting what has been observed for the pulldown using GFP antibody-coupled protein G beads (Figure 22 C). However, it must be noted that binding of the control beads to the *FABP4* promoter was lower compared to the other pulldown conditions, questioning the enhanced binding of NLRC5 to be a real effect of NLRC5 induction in synergy with PPAR γ activation or rather an artefact caused by reduced binding of the control beads to the *FABP4* promoter for reasons that remain to be determined.

In summary, binding of NLRC5 to the *FABP4* promoter over control was observed for some experimental conditions (Figure 22 D; Figure 23 C), reflecting the induction of *FABP4* by NLRC5, alone or in synergy with PPAR γ . However, given the low amounts of DNA pulled down with GFP-NLRC5 and the varying results for the experimental conditions, these data must be interpreted cautiously. Thus, the hypothesis of NLRC5 and PPAR γ together as one transcriptional complex binding to the promoters of PPAR γ target genes involved in adipogenesis and inflammation, thereby synergistically regulating their transcription, needs validation by independent means.

The role of NLRC5 in obesity – Results

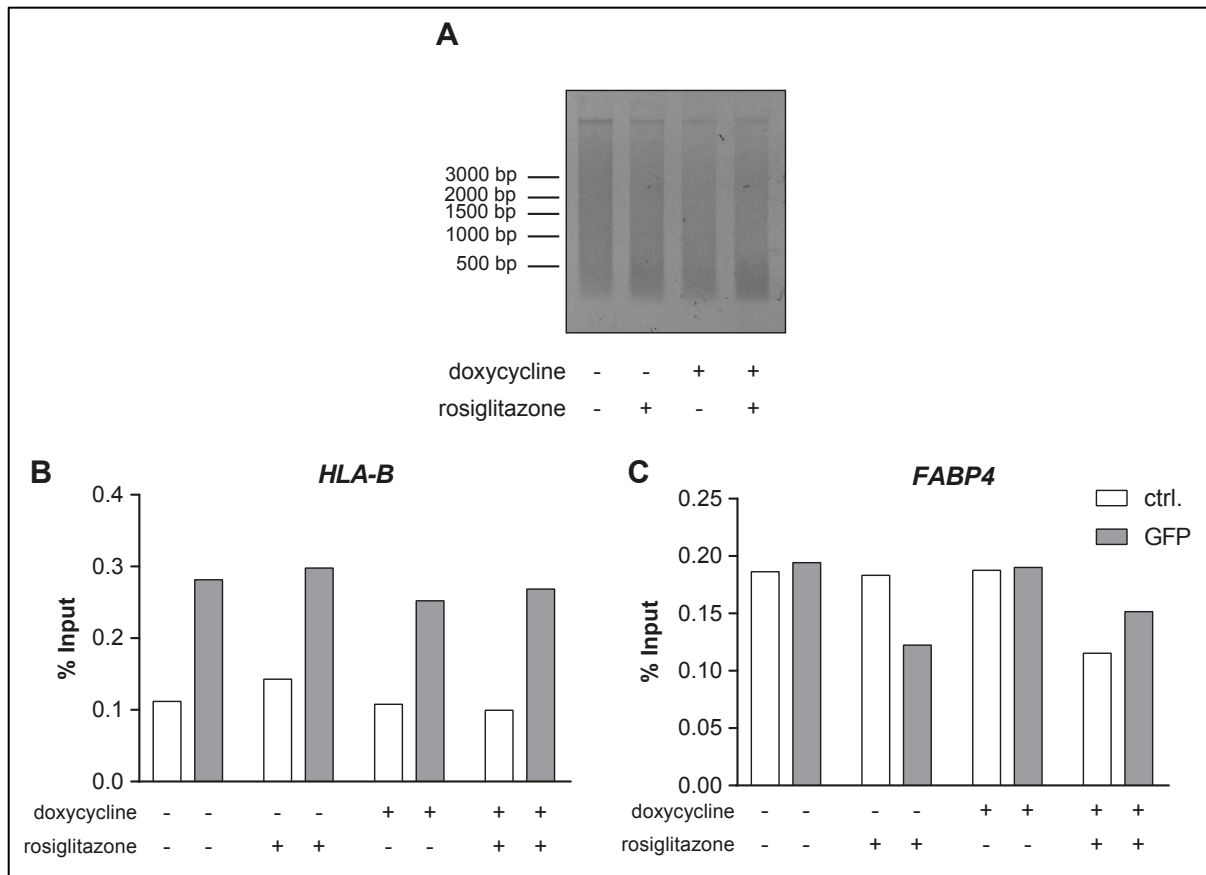


Figure 23: **Analysis of NLRC5:DNA interaction at the *FABP4* promoter by ChIP assays using GFP-Trap agarose resin.** HeLa GFP-NLRC5 cells were treated with 1 $\mu\text{g/ml}$ doxycycline and 0.4 $\mu\text{g/ml}$ rosiglitazone overnight, where indicated. Cells were lysed, chromatin was sheared by ultrasound and chromatin immunoprecipitation (ChIP) was performed using GFP-trap agarose beads. **(A)** Sheared chromatin of HeLa GFP-NLRC5 cells treated as indicated. **(B, C)** Immunoprecipitated chromatin was analysed by qRT-PCR for the abundance of promoter sequences of the indicated genes. Data is presented as % Input, reflecting the amount of DNA pulled down by the indicated antibody in respect to the amount of DNA used per reaction.

Influence of HFD and obesity on NLR expression in mouse and men

NLR expression in mouse adipose tissue and liver

NLR proteins, most prominently NOD1 and NLRP3, have been shown to play essential roles in the chronic state of sterile, low-grade inflammation accompanying the state of obesity and its associating morbidities (Bauer et al., 2023b). To investigate the influence of HFD feeding on NLR expression, the mRNA levels of a range of NLR proteins and accessory signalling molecules were determined by qRT-PCR in epididymal AT (Figure 24) and liver (Figure 25) of female WT mice fed a control (ctrl.) or HFD for 11 weeks (Figure 3). mRNA levels of *Nlrc5*, *Nod1*, *Nod2*, *Nlrp3*, *Nlrp6* and *Nlrp12*, as well as *Ripk2* and *Asc*, the downstream kinase of Nod1 and Nod2 and the adaptor molecule of Nlrp3, Nlrp6 and Nlrp12, respectively, were determined. These proteins have already been described to be involved in or associated with adiposity and

its associated morbidities (Bauer et al., 2023b). In addition, to put their expression in the context of the whole NLR family, the expression of *Nlrp1b*, *Nlr1*, *Nlrc3* and *Nlrp10* was investigated, which so far have not been implicated in metabolic processes.

NLRP1B belongs to the inflammasome forming NLR proteins, and is activated by the cleavage of the N-terminus, resulting in its proteasomal degradation and liberation of the CARD-containing C-terminal fragment which downstream induces Caspase-1 activation (Chui et al., 2019; Robinson et al., 2020; Sandstrom et al., 2019). Recently, human but not murine NLRP1B was identified as direct sensor for double stranded (ds) viral RNA (Bauernfried et al., 2021). NLRX1 recognizes viral RNA and has been implicated in the regulation of type I IFN responses (Snaka & Fasel, 2020). Targeted to the mitochondria (Arnoult et al., 2009; Moore et al., 2008), NLRX1 maintains mitochondrial homeostasis (Chu, Wu, & Raju, 2019; Jaworska et al., 2014; Stokman et al., 2017) by regulating autophagy, mitophagy and production of mitochondrial reactive oxygen species (ROS) (Huang et al., 2018; Lei et al., 2012; Zhang et al., 2019). NLRC3 is primarily known as negative regulator of innate immune signalling and has been shown to inhibit NF- κ B-mediated inflammation, type I IFN responses and inflammasome formation (Sun et al., 2022). NLRP10, the smallest NLR family member, has been implicated in enhancement of NF- κ B-mediated pro-inflammatory signalling upon bacterial infection (Lautz et al., 2012; Mirza et al., 2019) and was recently identified to form an inflammasome upon sensing of mitochondrial damage (Prochnicki et al., 2023).

Nlrc5 and *Nod1* presented with a non-significant increase in expression upon HFD feeding which was more pronounced in the AT (Figure 24 A, B; Figure 25 A, B). *Nod2* in the AT also presented with a non-significantly increased expression (Figure 24 C), while in the liver *Nod2* levels were unchanged (Figure 25 C). The *Nod1* and *Nod2* associated kinase *Ripk2* presented with a faint decrease in expression in AT (Figure 24 D) and stable expression levels in the liver comparing control and HFD fed animals (Figure 25 D). Expression of *Nlrp3* and its adaptor molecule *Asc* did not differ in the AT of the two intervention groups (Figure 24 E, F) whereas mRNA levels of both proteins were increased in the liver, reaching high statistical significance for *Asc* (Figure 25 E, F). *Nlrp6* and *Nlrp12*, also inflammasome forming NLRs, presented with a non-significant reduction in expression in the AT (Figure 24 G, H). For *Nlrp12*, this reduced expression was also observed in the liver (Figure 25 H), where *Nlrp6* presented with unchanged expression levels (Figure 25 G). It must be noted that *Nlrp6* and *Nlrp12* were only very low expressed in the AT, which must be considered upon data interpretation. *Nlr1*

expression did not change upon HFD feeding in both organs (Figure 24 I; Figure 25 I). *Nlrp1b* and *Nlrc3* were only expressed in liver tissue, both presenting with faintly increased expression in the HFD group (Figure 25 J, K). Notably, the only NLR presenting with significant alterations in expression by HFD was *Nlrp10*, whose expression was highly increased in both, epididymal AT and liver (Figure 24 J; Figure 25 L).

In summary, the expression of many of the investigated NLRs and accessory proteins were influenced by HFD (Figure 24 K; Figure 25 M). However, expression changes for most NLRs were marginal and did not reach statistical significance, with exception of *Asc* and *Nlrp10*, which were increased significantly in liver or both tissues investigated, respectively.

The role of NLRC5 in obesity – Results

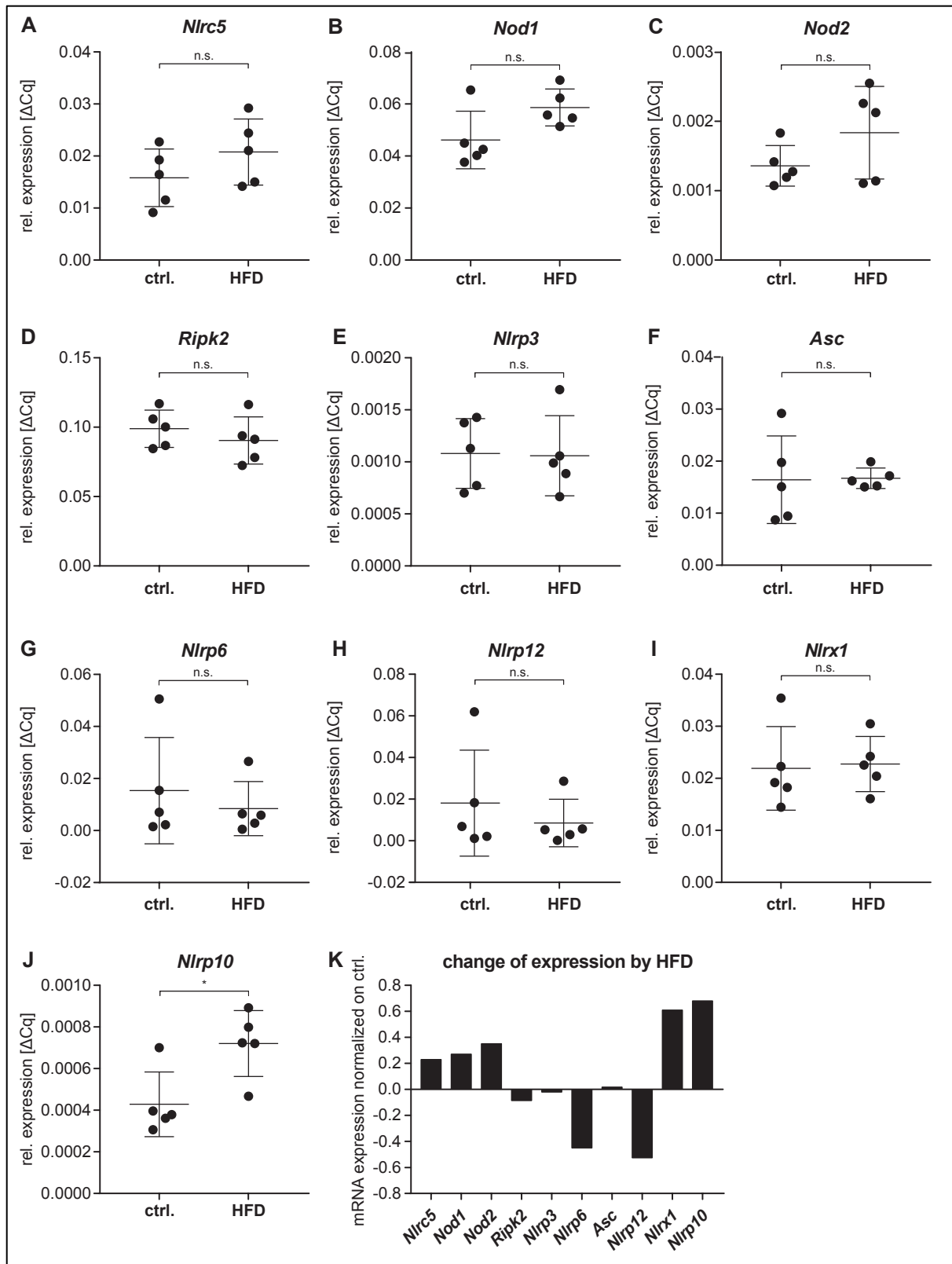


Figure 24: NLR expression in mouse adipose tissue. (A – J) mRNA expression of the indicated NLR or adjacent signalling molecule in the epididymal adipose tissue of female WT mice after 11 week of control (ctrl.) or high-fat diet (HFD). n = 5 animals per group. 4 animals from the study described in Figure 3 and one animal from a pilot experiment using the same experimental setup were used. Data show mean ± S.D. (K) Change of mRNA expression by HFD. Data show $\left(\frac{\text{mean mRNA expression of HFD group}}{\text{mean mRNA expression of ctrl. group}}\right) - 1$. n.s. = non-significant, *p ≤ 0.05 unpaired t-test.

The role of NLRC5 in obesity – Results

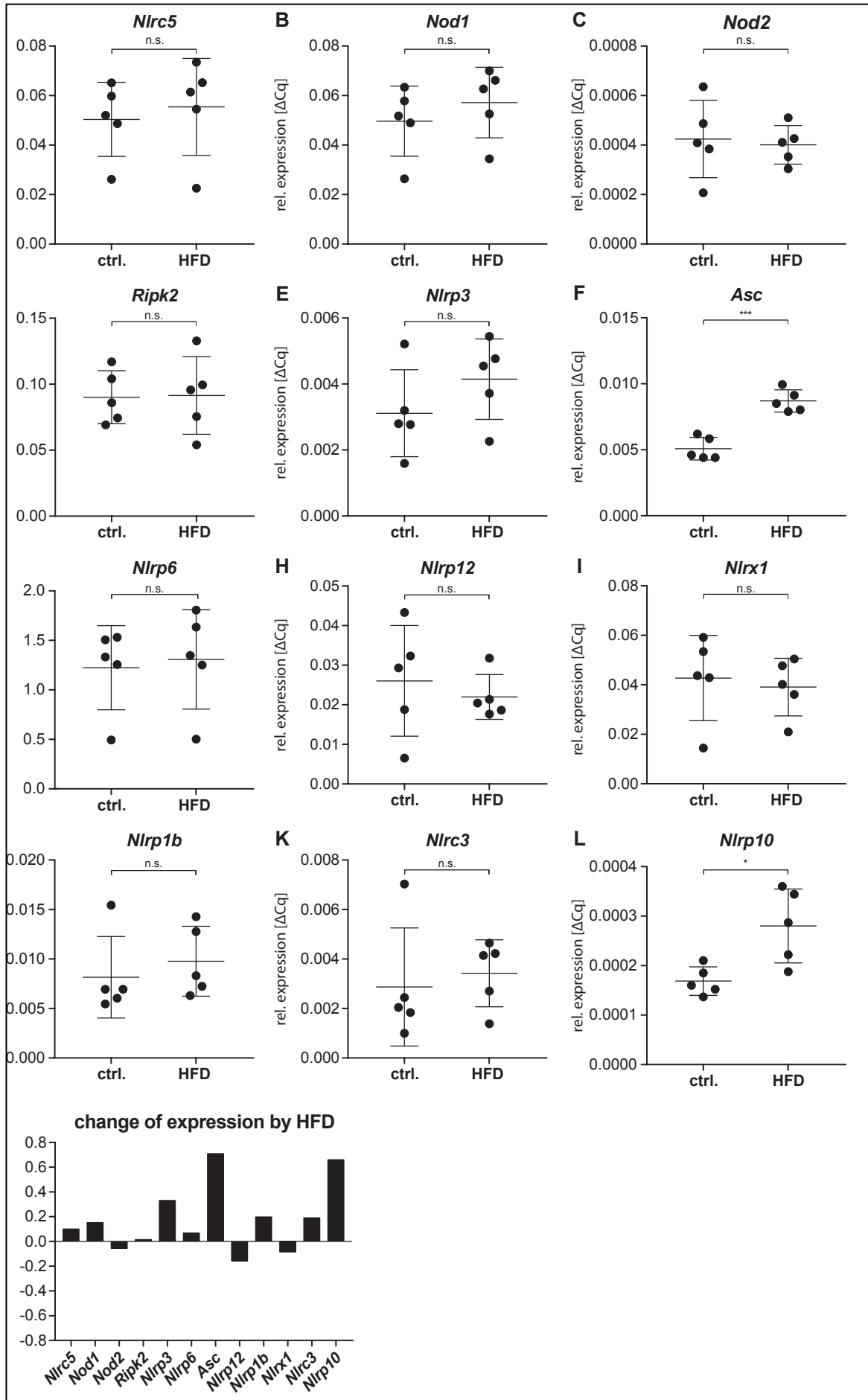


Figure 25: **NLR expression in mouse liver tissue. (A – L)** mRNA expression of the indicated NLR or adjacent signalling molecule in the liver of female WT mice after 11 week of control (ctrl.) or high-fat diet (HFD). n = 5 animals per group. 4 animals from the study described in Figure 3 and one animal from a pilot experiment using the same experimental setup were used. Data show mean \pm S.D. **(M)** Change of mRNA expression by HFD. Data show $\left(\frac{\text{mean mRNA expression of HFD group}}{\text{mean mRNA expression of ctrl.group}}\right) - 1$. n.s. = non-significant, *p \leq 0.05, ***p \leq 0.0005 unpaired t-test.

Expression of *NLRC5*, *NOD1* and *NOD2* in obese human individuals

To consolidate the NLR expression data generated in mice, expression of some NLRs was determined in obese patients with BMI ranging from 30.3 to 62.9 kg/m², using cDNA obtained from full blood RNA, which was kindly provided by the group of Stephan Bischoff (University of Hohenheim, Stuttgart). Due to limited sample availability, only the mRNA levels of *NLRC5*, *NOD1* and *NOD2* were determined. *NLRC5* was chosen to potentially be able to transfer the data on more pronounced adiposity for *Nlrc5* ^{Δ Exon4-7} animals to the human setting, whereas *NOD1* and *NOD2* were selected based on the already existing data on their regulation in obese individuals (Lappas, 2014; Shiny et al., 2013; Zhou et al., 2015), serving as reassurance of assay functionality. Given the highly increased expression of *Nlrp10* upon HFD feeding in mice (Figure 24, Figure 25), additional detection of *NLRP10* was attempted, however failed due to too low expression in the whole blood samples.

NLRC5 expression correlated negatively with BMI (Figure 26 A, dashed red line). This negative correlation, however, was mainly driven by two samples presenting with extraordinary high *NLRC5* expression in comparison the other samples (Figure 26 A, red dots). The laboratory data of these patients revealed increased alanine aminotransferase (ALT) levels, indicative of liver damage possibly caused by viral infection. Given that viral infections are known to drive *NLRC5* expression (Kuenzel et al., 2010), these two samples were excluded from analysis, resulting in no more correlation of *NLRC5* expression with BMI (Figure 26 A, solid black line). For *NOD1*, a negative correlation with BMI was found (Figure 26 B). Also *NOD2* expression correlated negatively with BMI (Figure 26 C), although it must be noted that *NOD2* levels in the full blood samples were very low, which must be considered upon data interpretation.

Taken together, *NOD1* negatively correlates with BMI in full blood samples of obese patients. The same might held true for *NLRC5* and *NOD2*, whereby here the limitations listed above must be considered upon data interpretation.

The role of NLRC5 in obesity – Results

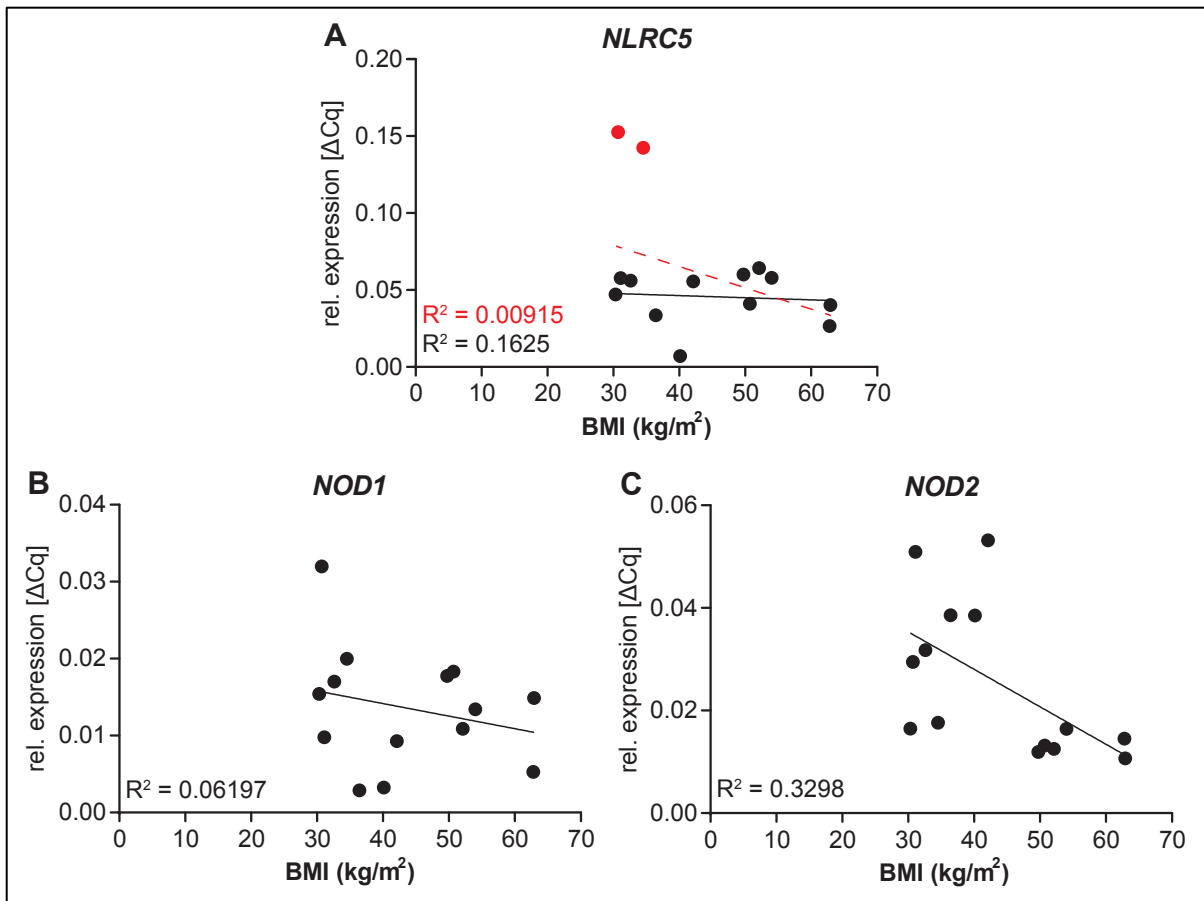


Figure 26: *NLRC5*, *NOD1* and *NOD2* expression in obese human individuals. (A – C) Expression of *NLRC5* (A), *NOD1* (B) and *NOD2* (C) obtained from full blood RNA samples of obese human individuals. Data show mRNA expression in correlation to body mass index (BMI). n = 14.

Discussion

NLRC5 initially has been identified as the master regulator of MHC class I genes (Meissner et al., 2010; Neerincx et al., 2014; Neerincx et al., 2012). While MHC class I regulation is undoubtedly a key function, NLRC5 was additionally shown to be involved in the negative regulation of NF- κ B-mediated pro-inflammatory responses (Benko et al., 2010; Cui et al., 2010; Li et al., 2014; Tong et al., 2012) and modulation of antiviral type I IFN responses (Cui et al., 2010; Kuenzel et al., 2010; Neerincx et al., 2010; Tong et al., 2012; Wu et al., 2017). In the recent years, NLRC5 has also been implicated in metabolic traits (Cao-Lei et al., 2019; Charlesworth et al., 2009; Hosseinzadeh et al., 2019; Lin et al., 2018; Meeks et al., 2017). However, so far, no confirmation of these singular observations is available nor have functional mechanisms been proposed or experimentally proven. Thus, we set out to investigate the effect of NLRC5 in obesity *in vivo*, using two different *Nlrc5* deficient mouse lines, and *in vitro*, using the 3T3-L1 preadipocyte cell line with modified *Nlrc5* expression, and embarked to unravel the molecular mechanisms behind NLRC5's effect on diet-induced adiposity.

The effect of *Nlrc5* deficiency on diet-induced obesity, microbiome composition and *in vitro* adipocyte differentiation

Nlrc5 ^{Δ Exon4-7} mice presented with highly increased body and adipose tissue weight gain and significantly bigger adipocytes. Interestingly, another study also reported a trend towards increased weight gain in *Nlrc5* deficient animals on HFD, however without mechanistically elaborating on this finding (Ma & Xie, 2017). In the human setting, two independent epigenome-wide associations studies identified the *NLRC5* locus to be differentially methylated in normal weight versus obese individuals, but with conflicting results. Meeks et al. positively and Cao-Lei et al. negatively associated methylation of the *NLRC5* locus with obesity (Cao-Lei et al., 2019; Meeks et al., 2017), BMI and waist circumference (Meeks et al., 2017). In most cases, DNA methylation mediates gene repression (Moore, Le, & Fan, 2013). Thus, our results are in line with the work of Meeks et al. finding associations of lower accessibility of the *NLRC5* locus with obesity (Meeks et al., 2017). Matching these data, we found *NLRC5* expression in whole blood samples from obese patients to be negatively correlated with BMI. It should be noted, however, that this correlation was mainly driven by

two samples presenting with comparably high *NLRC5* expression, potentially driven by viral infection, complicating data interpretation.

In contrast to the more pronounced adiposity of *Nlrc5*^{ΔExon4-7} mice, serum triglycerides were significantly reduced compared to WT mice on HFD. SNPs in *NLRC5* have been associated with alterations in lipid metabolism (Charlesworth et al., 2009; Hosseinzadeh et al., 2019; Lin et al., 2018). Charlesworth et al. showed that SNPs in *NLRC5* significantly correlated with HDL cholesterol levels (Charlesworth et al., 2009). In line, Hosseinzadeh et al. correlated SNPs in *NLRC5* with HDL cholesterol, total cholesterol and triglyceride levels (Hosseinzadeh et al., 2019) and one SNP in *NLRC5* (rs2178950) has been associated with low-density lipoprotein (LDL) and total cholesterol dyslipidaemia (Lin et al., 2018). Together with our observations on reduced serum triglyceride levels of *Nlrc5*^{ΔExon4-7} compared to WT mice, these data point towards an influence of *NLRC5* on lipid metabolism, the nature of which remains to be determined in more detail in further studies.

In this work, we identify a strong adiposity phenotype for female *Nlrc5*^{ΔExon4-7} mice. We did also include male *Nlrc5*^{ΔExon4-7} mice in the feeding study, but the results were inconclusive compared to the strong phenotype in female mice (data not shown). Strikingly, female mice have been shown to be fairly resistant to diet-induced obesity, a protection that is conferred by the female sex hormone oestrogen (Dakin et al., 2015; Pettersson et al., 2012; Stubbins et al., 2012; Yasrebi et al., 2017). Alike PPAR γ , the oestrogen receptors (ER) belong to the family of NRs and share their common domain architecture (Fuentes & Silveyra, 2019). *NLRC5* was shown to interact with the LBD of PPAR γ (Luan et al., 2019). As the LBD of NRs contains some conserved structural features (Huang, Chandra, & Rastinejad, 2010; Wurtz et al., 1996) this opens up the possibility that *NLRC5* also interacts with ERs and modulates their signalling, thereby mediating the strong effect of diet-induced obesity on female compared to male mice. Investigation of the underlying mechanisms mediating the sex-specificity of *Nlrc5* deficiency in the obesity context should be subject to future research.

For other NLRs, effects on gut microbiota composition have been reported, that in the case of NLRP12 were associated with weight gain (Truax et al., 2018). Faecal microbiome composition analysis by 16S rRNA sequencing of *Nlrc5*^{ΔExon4-7} mice on HFD revealed 10 bacterial taxa to be significantly altered in abundance and seven of those being associated with our dietary intervention. Of those, most (*Ruminococcaceae*, *Oscillibacter*, *Lactobacillus*, *Erysipelatoclostridium* and *Clostridiales* Family XIII) have been described to be altered in

abundance by HFD or in the obesity context before (Bailen et al., 2020; Daniel et al., 2014; He et al., 2022; Jo et al., 2021), reflecting our result. Only for *Lachnospiraceae* NK4A136, our data is contradicting the finding of reduced relative abundance upon HFD feeding, as described by others (Bisanz et al., 2019; Li et al., 2020). The reasons for these conflicting findings remain to be determined. Interestingly, two of the three bacterial groups that were differentially affected by diet:genotype interactions in a broader sense are associated with metabolic traits. *Lachnospiraceae* NK4A136 has been shown to be increased in abundance in rats with T2DM (Cui et al., 2019). And the relative abundance of *Marvinbryantia* was increased in rats upon high fructose intake (Wang et al., 2020) and in rabbits after HFD feeding (Guo et al., 2022). The identified alterations in relative abundance were only small and based on compositional data, which does not allow conclusion to be drawn on absolute changes of specific bacteria (Gloor et al., 2016). Still, these microbial changes could contribute to the phenotype of *Nlrc5*^{ΔExon4-7} animals.

In contrast to female *Nlrc5*^{ΔExon4-7} mice, male and female *Nlrc5*^{ΔExon4} mice did not present with increased adiposity compared to WT mice on HFD, even though the HFD feeding duration was increased with 20 compared to 11 weeks. The possible reasons for this discrepancy are manifold. Both *Nlrc5* deficient mouse lines were generated via the Cre/LoxP system in C57BL/6N background. While in *Nlrc5*^{ΔExon4-7} mice the NACHT domain and parts of the LRR domain are deleted, *Nlrc5*^{ΔExon4} mice only lack the NACHT domain. Both the ATPase activity of the NACHT and the presence of the LRR domain of NLRC5 have been shown to be essential for NLRC5's transcriptional activity (Neerincx et al., 2012). Thus, no functional *Nlrc5* constructs should be present in either of the two *Nlrc5* deficient mouse lines, rendering it unlikely that the differences observed between *Nlrc5*^{ΔExon4-7} and *Nlrc5*^{ΔExon4} mice result from different targeting strategies for *Nlrc5* deletion. A more likely cause for the different reactions of the two *Nlrc5* deficient mouse lines on HFD feeding are differences in microbiome composition, which was only investigated for the *Nlrc5*^{ΔExon4-7} mice. The microbiome of laboratory mice is known to influence experimental outcome and reproducibility and to be influenced by many factors, including housing, diet and stress factors like handling or noise (Laukens et al., 2016). The two feeding studies were conducted in different animal facilities by different people. Although both animal facilities have SPF status, this only guarantees the absence of certain pathogens, but does not allow any conclusions to be drawn on the microbiome composition of the housed animals. *Nlrc5*^{ΔExon4-7} mice were kept in open cages

whereas *Nlrc5*^{ΔExon4} animals were housed in individually ventilated cages. On top, *Nlrc5*^{ΔExon4-7} and *Nlrc5*^{ΔExon4} mice received a different HFD with slightly varying nutrient composition. *Nlrc5*^{ΔExon4-7} mice received a diet containing 54 kcal% fat, 29 kcal% carbohydrates and 17 kcal% protein, whereas *Nlrc5*^{ΔExon4} mice received a diet higher in fat (60 kcal%) and protein (20 kcal%) and lower in carbohydrates (20 kcal%). On top, dietary intervention for *Nlrc5*^{ΔExon4-7} mice was started simultaneously for all animals, while *Nlrc5*^{ΔExon4} mice were started on HFD as and when the mice became available. Thus, *Nlrc5*^{ΔExon4-7} and *Nlrc5*^{ΔExon4} mice almost certainly presented with different microbiome compositions. As we show the gut microbiome composition to be altered by both, *Nlrc5* deficiency and HFD feeding, the effect of *Nlrc5* deficiency on diet-induced obesity might be influenced by the microbiome composition, relying on the presence and/or absence of certain bacterial species. Further studies will be needed to address this question.

Due to the pronounced effect of NLRC5 on AT and adipocytes, we set out to investigate the effects of *Nlrc5* deficiency on adipocyte differentiation using the 3T3-L1 preadipocyte cell line. 3T3-L1 differentiation to mature adipocytes was successfully established. *Nlrc5* modified 3T3-L1 clones presented with reduced differentiation compared to WT cells, however this was also true for the non-modified EV control clone. 3T3-L1 cells are known to lose their differentiation behaviour with high passage number (Wolins et al., 2006), although a precise maximal passage number has not yet been determined. Generation of new, passage-matched CRISPR/Cas9 cell pools did not reveal any differences in differentiation between *Nlrc5* modified, EV and WT pool cells, indicating senescence due to heavy passaging of the *Nlrc5* modified 3T3-L1 cell clones to be the reason for the reduced differentiation behaviour observed. In addition, as Ppar γ and Fabp4 protein levels were reduced in all cell pools, independent of the presence of a *Nlrc5* targeting gRNA, lentiviral transduction independent of DNA modification might artifactually reduce the expression of adipocyte differentiation markers. The absence of an effect of *Nlrc5* modification on *in vitro* adipocyte differentiation in this study does not necessarily imply that NLRC5 does not influence adipogenesis. Modification of the *Nlrc5* locus by CRISPR/Cas9 technology was verified by T7 endonuclease assays and Sanger Sequencing, however, could not be verified on protein level, as no suitable antibody targeting murine *Nlrc5* was available. Introduction of insertions or deletions (INDELS) by CRISPR/Cas9-induced DNA double strand breaks and subsequent DNA repair by non-homologous end joining (NHEJ) can result in alternative transcriptional start codon usage or

exon skipping, generating truncated proteins with potentially retained functionality (Tuladhar et al., 2019). This, however, in our case is highly unlikely, as we targeted exon 2 or 3 which encode for the transcriptionally active DD domain of *Nlrc5* (Neerinx et al., 2014; Yao & Qian, 2013). More likely, *Nlrc5* modification in only up to 50% of the newly generated CRISPR/Cas9 pool cells is not sufficient to perceivably influence 3T3-L1 differentiation behaviour. Thus, the effect of *Nlrc5* deficiency on adipocyte differentiation awaits further investigation. Future studies should focus on using adipocyte cell lines not prone to senescence or even primary preadipocytes from WT and *Nlrc5* deficient animals. Additionally, adipocyte cell lines with shorter differentiation duration like the murine bone marrow-derived OP9 stromal cell line (Wolins et al., 2006) could be used, allowing transient gene silencing as means for investigating the effect of NLRC5 on adipocyte differentiation.

NLRC5 interacts with PPAR γ and synergistically regulates PPAR γ target genes involved in metabolism and inflammation

Understanding the molecular details behind a phenotypic effect is pivotal for the development of preventive or therapeutic interventions. Thus, we set out to explore the mechanism behind the pronounced effect of NLRC5 on diet-induced adiposity observed in *Nlrc5* ^{Δ Exon4-7} mice.

In agreement with published work (Luan et al., 2019) we show that the master regulator of adipogenesis, PPAR γ , interacts with the NACHT domain of NLRC5. We further characterize this interaction by providing evidence that only PPAR γ isoform 1, but not isoform 2, is binding to NLRC5. PPAR γ 2 differs from PPAR γ 1 only by possessing 28 additional N-terminal amino acids (Elbrecht et al., 1996; Janani & Ranjitha Kumari, 2015). Hence, it was unexpected that only the shorter PPAR γ isoform interacts with NLRC5, especially taking into consideration that the binding site for NLRC5 has been mapped to the C-terminal LBD of PPAR γ (Luan et al., 2019). PPAR γ ligand-binding has been shown to be regulated via intra-domain communications between the N-terminal domain and the LBD, and modifications of the PPAR γ N-terminus result in altered ligand-binding affinity (Shao et al., 1998). Thus, differences in the isoforms' N-termini could explain the differential binding of NLRC5. We also observed the co-immunoprecipitation of CIITA, but not NOD1, with PPAR γ 1. CIITA, like NLRC5, functions as a transcriptional activator, is considered the master regulator of MHC class II genes (Steimle et al., 1993) and phylogenetically is NLRC5's next closest relative, especially concerning the

NACHT domain (Benko et al., 2010). The fact that PPAR γ 1 did not associate with NOD1, which is NLRC5's next closest phylogenetic relative in the NACHT domain after CIITA (Benko et al., 2010), highlights the high specificity of the PPAR γ 1:NLRC5 interaction. CIITA has been shown before to interact with PPAR γ in a human lung fibroblast cell line (Xu, Farmer, & Smith, 2007). Interestingly, this study provided evidence for PPAR γ aiding CIITA in the transcriptional suppression of collagen synthesis by being recruited to CIITA sitting at the promoter of collagen genes. In addition, the authors showed transcriptional enhancement of CIITA by ectopical PPAR γ expression (Xu, Farmer, & Smith, 2007). This illustrates that NLR proteins can act in synergy with PPAR γ and thus opens up the possibility of a functional implication of the NLRC5:PPAR γ interaction, potentially involving a positive feedback loop, with PPAR γ upregulating *NLRC5* expression. In fact, Luan et al. showed PPAR γ to bind to the *NLRC5* promoter and to facilitate *NLRC5* transcription (Luan et al., 2019).

The main transcriptional targets of NLRC5 known so far are MHC class I and associated genes (Biswas et al., 2012; Ludigs et al., 2015; Meissner et al., 2010; Meissner et al., 2012b). As NLRC5 is devoid of a *bona fide* DBD, its association with chromatin at the MHC I promoter is mediated indirectly via the MHC enhanceosome complex (Neerincx et al., 2012), a multiprotein DNA binding complex binding to conserved S/X/Y motifs in MHC class I gene promoters (Ludigs et al., 2015; Meissner et al., 2010; Neerincx et al., 2012). We show here that NLRC5 is also involved in the regulation of the PPAR γ target *FABP4*. *FABP4* is an intracellular lipid chaperone responsible for lipid storage, lipolysis, and metabolism (Amiri et al., 2018; Chmurzynska, 2006; Hotamisligil & Bernlohr, 2015; Lee, Lui, & Lam, 2021). For *FABP4* induction, NLRC5 nuclear localization was needed and NLRC5 isoform 3 failed to mediate *FABP4* transcription, similar as observed earlier for NLRC5-mediated MHC class I gene expression (Meissner et al., 2012a; Neerincx et al., 2012), rendering it likely that nuclear shuttling of NLRC5 is a prerequisite for the transcriptional activation of PPAR γ targets. Interestingly, there is independent evidence that NLRC5 is a potent transcriptional regulator beyond MHC class I genes (Dang et al., 2021; Luan et al., 2019). In accordance with our data, Luan et al. showed reduced *FABP4* and *CD36* mRNA levels upon KD of *NLRC5* in human aortic smooth muscle cells and upregulation of PPRE activity by NLRC5 in a HEK293T cell-based PPRE reporter gene assay (Luan et al., 2019). We were not able to reproduce this enhancing effect of NLRC5 on PPRE activity in HEK293T cells but witnessed a dose-dependent decrease in luciferase activity for both PPRE reporter constructs used. The reason for this discrepancy

remains to be determined. As reporter gene assays are highly artificial systems prone to artefacts (Ling et al., 2012), they eventually lie within subtle differences in the experimental set-up and reporter constructs used. The reporter construct used by Luan et al. was not specified (Luan et al., 2019), impairing the investigation of potential differences to the reporter construct used by us. It has been shown that the NLR proteins NLRX1 and NLRC3 are able to reduce luciferase activity independent of the controlling transcription factor response element by means of post-transcriptional modifications, presumably targeting luciferase mRNA translation or protein stability (Ling et al., 2012). Additionally, it was observed that titration of co-factors can lead to decreased reporter gene activity due to scavenging of transcriptional complexes, impeding DNA binding and promoter activation (T. A. Kufer, personal communication). These facts question the suitability of luciferase reporter gene assays as tool for investigating the effects of NLRs on promoter activation in general and the specificity of the NLRC5-mediated decreasing effect on PPRE-mediated luciferase activity observed by us in specific.

Apart from regulation of PPAR γ targets and transcriptional activity discussed above (Luan et al., 2019), NLRC5 has recently also been shown to regulate the transcription of BTN genes via an atypical S/X/Y module (Dang et al., 2021), thereby proving NLRC5 to be implicated in transcriptional regulation far beyond MHC class I genes. Both studies provide evidence for NLRC5-mediated regulation of non-MHC class I genes. NLRC5 via PPAR γ activation alleviated vascular remodelling and neointima formation (Luan et al., 2019) and NLRC5-regulated *BTN3A* gene expression was proposed to aid in anti-mycobacterial immunity (Dang et al., 2021). Thus, it is likely that the synergistic regulation of PPAR γ targets by PPAR γ and NLRC5 observed by us is functionally connected to the obesity-phenotype we observed in *Nlrc5* ^{Δ Exon4-7} animals. Together with the interaction data, these results suggest the scenario of PPAR γ and NLRC5 functioning as a transcriptional complex, binding to the promoters of PPAR γ target genes via PPAR γ :PPRE interaction, resulting in synergistic regulation of transcription. CHIP assays performed to investigate this possibility however yielded inconclusive results. Detection of NLRC5 binding to the promoter of *HLA-B*, a known NLRC5 target (Meissner et al., 2010; Neerincx et al., 2012) and thus serving as positive control, was weak. Coherently, no consistent binding of NLRC5 to the *FABP4* promoter at site of the PPRE was observed over control. As mentioned above, NLRC5 associates with the promoters of its target genes indirectly (Neerincx et al., 2012), complicating NLRC5-bound chromatin pulldown as direct protein:DNA

interaction is missing. Also in the case of *FABP4*, indirect promoter binding via PPAR γ would be expected. Additionally, high-molecular weight proteins like NLRC5 are prone to degradation upon chromatin sonication (Pchelintsev, Adams, & Nelson, 2016), likewise hampering NLRC5 pulldown. Thus, to answer the question of NLRC5 binding to the promoter of PPAR γ target genes, thereby synergistically regulating their transcription, further refinement of the CHIP conditions is needed to allow for more efficient NLRC5 pulldown.

NLRC5 confers its specificity towards MHC class I genes and its transcriptional activity via its N-terminal DD, albeit this domain presents with comparably low activation potential (Neerincx et al., 2014). In this study we show that silencing of *Sin3A*, a most recently identified interactor of the NLRC5 DD (Kienes, 2021), enhances NLRC5-regulated *FABP4* transcription. *Sin3A* is primarily known as a transcriptional repressor by providing a scaffold for transcriptional complex formation, most prominently the Sin3-HDAC1/2 complex. *Sin3A* has no intrinsic DNA binding activity and thus needs the interaction with transcription factors, direct or via a third adaptor molecule, to be able to associate with the DNA (Silverstein & Ekwall, 2005). Murine *Sin3A* has been shown to be recruited to the PPAR γ promoter by TGF- β 1 stimulation in the scenario of cardiac pressure overload, leading to PPAR γ repression (Gong et al., 2016). Interestingly, *Sin3A* has also been shown to interact and thus help with the recruitment of HDACs to the two co-repressor complexes NCoR and SMRT (Heinzel et al., 1997; Laherty et al., 1997; Nagy et al., 1997; Wen et al., 2000), both known to associate with and mediate the transcriptional repression of type II nuclear hormone receptors, like PPAR γ , in unliganded state (Yu et al., 2005) (reviewed in (Feige & Auwerx, 2007)). Upon ligand binding, the co-repressor complex is released and co-activators are recruited (Lehrke & Lazar, 2005; McKenna & O'Malley, 2002).

Thus, a possible working hypothesis would be a “double” negative transcriptional regulation of PPAR γ targets in the absence of ligands: Once by the binding of the long-known transcriptional co-repressor/Sin3A/HDAC complexes and once by *Sin3A* (via NLRC5's DD) binding to and mediating additional HDAC recruitment to the NLRC5:PPAR γ complex sitting at the *FABP4* promoter (Figure 27 A). While the classical co-repressor complexes are exchanged for co-activators upon ligand-binding, the *Sin3A*/NLRC5 complex remains associated with PPAR γ , thereby fine-tuning PPAR γ target gene transcription (Figure 27 B). This role of *Sin3A* in refining transcription would explain the moderate effect of *Sin3A* KD (Figure 27 C) on *FABP4* transcription. In line with this working hypothesis, *Sin3A* has been shown to fine-tune the

transcriptional response of the thyroid hormone (TH) receptor, also a type II nuclear hormone receptor, via interaction with a newly identified protein interacting with the DBD of the TH receptor (Mathur, Tucker, & Samuels, 2001).

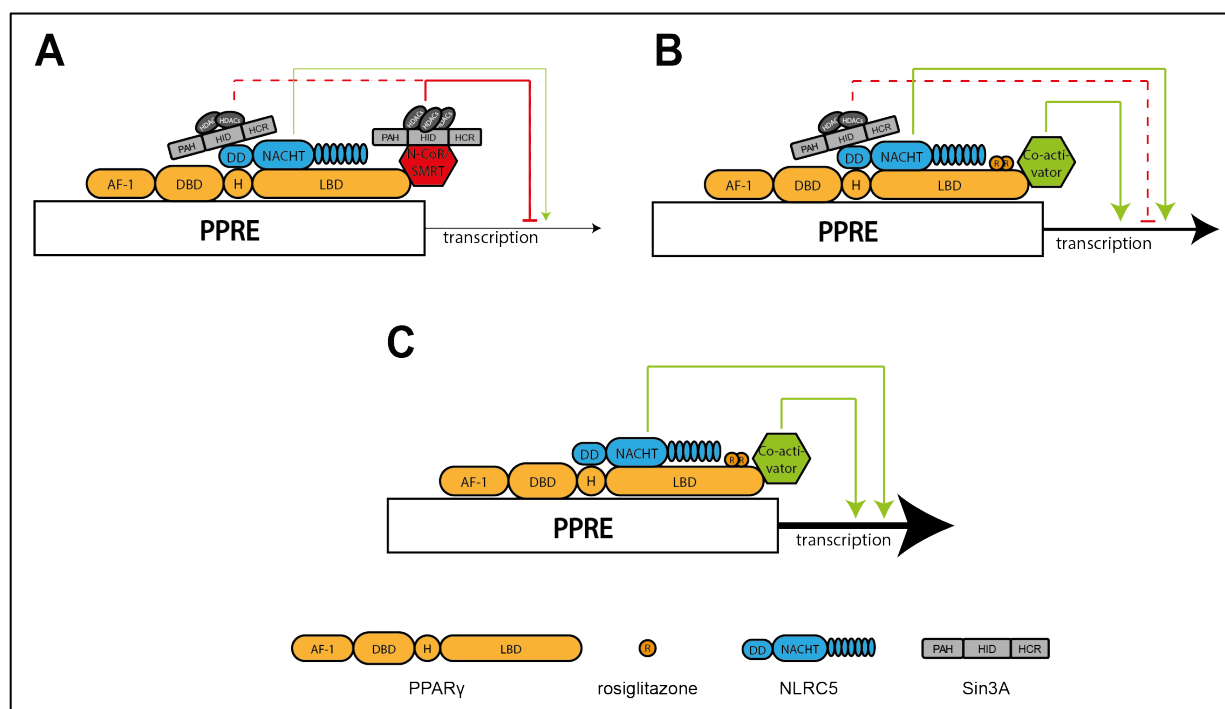


Figure 27: **Proposed working model of NLRC5-mediated regulation of PPAR γ target genes.** (A) NLRC5 interacts with the PPAR γ ligand-binding domain (LBD) and thus associates with the PPAR response element (PPRE) in the *FABP4* promoter. Simultaneously, Sin3A interacts with the death domain (DD) of NLRC5 and, in the absence of the PPAR γ ligand rosiglitazone (R), also with the co-repressor complexes NCoR and SMRT, which restrain PPAR γ -mediated transcription. Sin3A recruits histone-deacetylases (HDACs), thereby repressing transcription of *FABP4*, while NLRC5 even in the absence of a ligand mediates a certain level of *FABP4* transcription. (B) In the presence of a ligand, the co-repressor complex is exchanged for a co-activator complex and *FABP4* transcription is initiated by PPAR γ and NLRC5 in synergy, with NLRC5-bound Sin3A fine-tuning transcription. (C) Upon *Sin3A* KD, this fine-tuning effect is lost and *FABP4* transcription is further increased.

How exactly the synergistic regulation of *FABP4* by NLRC5, PPAR γ and eventually Sin3A is connected to the obesity-like phenotype of *Nlrc5*^{Exon4-7} animals on HFD remains to be clarified. Interestingly, it has been shown that *Fabp4* deficient mice are protected against the development of diet-induced IR and impaired glucose tolerance albeit the development of more severe obesity, and that adipocytes of *Fabp4*^{-/-} animals present with reduced lipolysis efficiency (Hotamisligil et al., 1996). In line, genetically obese mice (*ob/ob* mice) presented with significantly reduced blood glucose levels and insulin sensitivity upon genetic disruption of *Fabp4*, which was accompanied by higher body weight and reduced plasma triglyceride and cholesterol levels (Uysal et al., 2000). A more recent study demonstrated that RNA interference (RNAi)-mediated germline KD of *Fabp4* increased body weight and fat mass in diet-induced obesity in mice but did not affect plasma glucose and lipid homeostasis or insulin

sensitivity (Yang et al., 2011). These data match our working model in which *NLRC5* deficiency would lead to highly reduced *FABP4* transcription, culminating in increased body weight gain, adipose tissues and adipocyte size, eventually due to defective adipocyte lipolysis (Figure 28), but improvements in serum cholesterol and triglyceride levels in the *Nlrc5*^{ΔExon4-7} animals. As *CD36* was also upregulated in GFP-NLRC5 compared to GFP expressing HeLa cells it is likely that also other PPAR γ targets involved in metabolism are co-regulated by NLRC5, their dysfunctional regulation by *NLRC5* deficiency possibly contributing to the here-described role of NLRC5 in HFD-induced obesity.

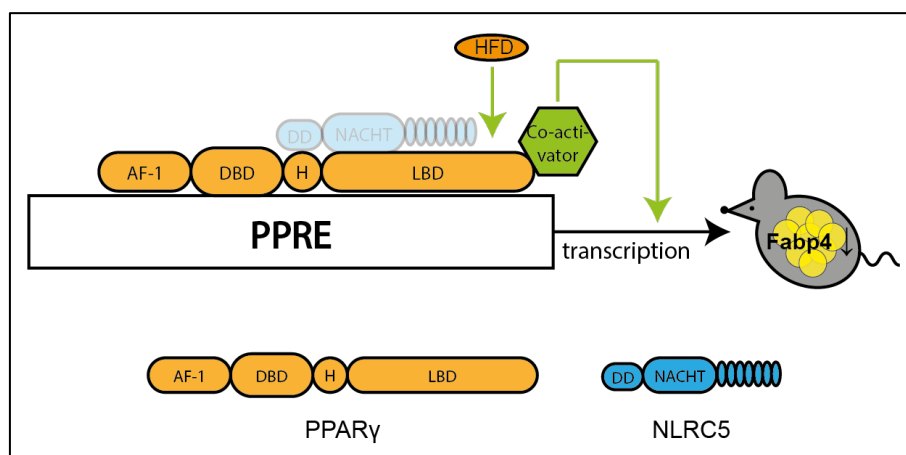


Figure 28: **Proposed molecular mechanism behind NLRC5's effect on diet-induced adiposity.** *In vivo*, high-fat diet (HFD)-feeding leads to PPAR γ activation and *Fabp4* transcription, which is reduced upon *Nlrc5* KO. The resulting decrease in *Fabp4* leads to higher body weight and more adipose tissue compared to WT animals.

Obesity is accompanied by a chronic state of sterile, low-grade inflammation which is known to at least contribute if not cause obesity-associated morbidities (Hotamisligil, 2006). PRRs in general and NLRs in specific in the recent years have been implicated in this metabolic inflammation (Bauer et al., 2023b). The role of NLRC5 in inflammation is controversially discussed. NLRC5 has been shown to inhibit NF- κ B signalling and pro-inflammatory cytokine secretion *in vitro* in HEK293T cell-based reporter gene assays and murine RAW264.7 macrophages (Benko et al., 2010; Cui et al., 2010; Li et al., 2014). *In vivo*, *Nlrc5* KO was shown to lead to enhanced NF- κ B activation, pro-inflammatory cytokine secretion and accelerated cardiac fibrosis upon HFD feeding (Ma & Xie, 2017; Tong et al., 2012). In contrast, *Nlrc5* deficiency reduced diabetic kidney injury by NF- κ B suppression (Luan et al., 2018). For some *Nlrc5* KO mouse models, no differences in NF- κ B activation and downstream signalling were found (Kumar et al., 2011; Robbins et al., 2012; Yao et al., 2012). In humans, DNA methylation of *NLRC5* has been positively associated with circulating TNF- α levels and inversely correlated with the risk of coronary heart disease (Aslibekyan et al., 2018). Our results on increased

TNF- α secretion of *NLRC5* deficient THP-1 macrophage-like cells and *Nlrc5* KO BMDMs is in accordance with most of published data, which describe an anti-inflammatory role of NLRC5 (Aslibekyan et al., 2018; Benko et al., 2010; Cui et al., 2010; Li et al., 2014; Ma & Xie, 2017; Tong et al., 2012) and together, these data suggest a protective role of NLRC5 in the context of obesity-associated low-grade inflammation. It must be noted that we could not confirm this in our *Nlrc5*^{ΔExon4-7} mice, as these, in contrast to the findings of Ma and Xi (Ma & Xie, 2017), did not present with differences in *Tnf- α* and *Tgf- β* mRNA levels in liver and epididymal AT upon HFD feeding compared to WT animals. This discrepancy might be explained as we examined different tissues (liver and AT vs. heart) and by differences in the study design, as we used females and 11 weeks of intervention compared to male animals and 15 weeks of HFD (Ma & Xie, 2017). Interestingly, deficiency in *NLRC5* not only enhanced pro-inflammatory responses in THP-1 macrophage-like cells and BMDMs, but also reduced their responsiveness to PPAR γ activation as seen by lower reduction of TNF- α secretion and p38 activation upon PPAR γ stimulation. This indicates synergistic action between NLRC5 and PPAR γ also in the context of LPS-induced inflammation. Given the fact that obesity-associated low-grade inflammation has been shown to be driven in major parts by adipose tissue macrophages (Olefsky & Glass, 2010), it is tempting to speculate that NLRC5 might play an important role in obesity-associated low-grade inflammation, with lowered or absent *NLRC5* expression not only driving adipose tissue accumulation but also obesity-associated inflammation.

Different mechanisms behind PPAR γ 's anti-inflammatory properties have been proposed, ranging from degradation (Hou, Moreau, & Chadee, 2012) or nuclear translocation impairment of the NF- κ B subunit p65 (Zhang et al., 2016) to interaction of PPAR γ with and thus trapping of NF- κ B (Chung et al., 2000). How exactly PPAR γ confers its anti-inflammatory properties, however, is not clear. Given the interaction between NLRC5 and PPAR γ , it might be possible that NLRC5 aides PPAR γ in NF- κ B trapping and inhibition of DNA binding. In addition, PPAR γ ligands have been shown to trigger PPAR γ SUMOylation, allowing for DNA-independent interaction with and thus stabilization of NCoR/SMRT co-repressor complexes at the promoters of pro-inflammatory genes, preventing their transcription (Pascual et al., 2005). NLRC5 might aid PPAR γ in blocking the recruitment of ubiquitin-conjugating enzymes and subsequent proteasomal degradation of the co-repressor complex (Pascual et al., 2005) by interaction with PPAR γ .

In summary, NLRC5 co-regulates PPAR γ targets involved in metabolism and modulates PPAR γ 's anti-inflammatory properties. Dysfunctional regulation of these processes by *NLRC5* deficiency possibly contributes to the here-described role of NLRC5 in protecting against HFD-induced obesity and potentially obesity-associated low-grade inflammation.

Other NLRs and their expression in relation to HFD

NLR proteins in the recent years have been identified as important players in adiposity, essentially contributing to obesity-associated morbidities (Bauer et al., 2023b). Upon investigation of the influence of an 11-week HFD feeding on the expression of several NLR family members and accessory signalling molecules in liver and AT of female WT mice, we found *Asc* and *Nlrp10* to be significantly upregulated in liver or both tissues, respectively. In line with our data, *Asc* has been shown to be upregulated in the liver of WT mice by HFD feeding before (Yang, Lee, & Lee, 2016). Coherently with its increased expression by HFD, ASC was shown to contribute essentially to obesity-associated NAFLD, with *Asc* deficient animals presenting with reduced liver steatosis (Sokolova et al., 2019; Vandanmagsar et al., 2011) and increased hepatic insulin sensitivity upon HFD feeding (Sokolova et al., 2019). NLRP10 is highly expressed in the skin (Lautz et al., 2012), but also hepatic *NLRP10* expression has been reported, although the data vary. Wang et al. reported weak expression of *NLRP10* in the liver and in the hepatic cell line HepG2 (Wang et al., 2004). In contrast, Lech et al. showed *NLRP10* to be highly expressed in human liver samples relative to its expression in the spleen, with considerably weaker *Nlrp10* expression for murine liver samples (Lech et al., 2010). No data on adipose tissue expression of *NLRP10* is available so far and neither are data on a role of NLRP10 in obesity and its associated morbidities. Recently, NLRP10 was identified as inflammasome forming NLR, sensing mitochondrial damage (Prochnicki et al., 2023). Given that excessive nutrient intake leads to mitochondrial dysfunction and ROS production (Bournat & Brown, 2010; Furukawa et al., 2004; Traba & Sack, 2017), this opens up the intriguing possibility that NLRP10 is functioning as sensor of nutrient-induced mitochondrial dysfunction. As it has been shown that the NLRP10 inflammasome in intestinal epithelial cells is dispensable at steady-state but confers protective effects in dextran sodium sulphate (DSS)-induced colitis (Zheng et al., 2023), *Nlrp10* upregulation might serve to alleviate HFD-induced inflammation. These data highlight NLRP10 as promising candidate to further investigate the role of NLR proteins in obesity.

In contrast to published data, we did not observe significant upregulation of *Nlrp3* (Finucane et al., 2015; Jager et al., 2007; Nagareddy et al., 2014; Sokolova et al., 2019; Vandanmagsar et al., 2011; Yin et al., 2014) and *Nod1* (Sharma et al., 2022) by HFD, although a non-significant increase of *Nlrp3* and *Nod1* expression was observed in liver and AT, respectively. Reasons for these discrepancies remain elusive, but eventually lie within differences in HFD composition and feeding duration. In the human setting, *NOD1* negatively correlated with BMI in obese patients, contrasting published data on increased *NOD1* expression in the AT of MetS patients and women with gestational diabetes (Lappas, 2014; Zhou et al., 2015). *NOD2* also negatively correlated with BMI, which would be in line with the reported protective effect of *NOD2* in obesity and associated morbidities (Carlos et al., 2020; Cavallari et al., 2020a; Cavallari et al., 2017; Cavallari et al., 2020b; Denou et al., 2015). It has to be noted, however, that *NOD2* expression in whole blood samples was very low, necessitating careful data interpretation. In general, the low sample number as well as the lack of normal weight individuals to determine steady-state NLR expression limit data validity. Thus, the effect of HFD and obesity on NLR expression awaits further clarification, but also highlights NLRP10 as promising new starting point to further unravel the roles of NLRs in obesity.

In summary, in this work we show female *Nlrc5*^{ΔExon4-7}, but not *Nlrc5*^{ΔExon4} mice, to present with strongly enhanced HFD-induced adiposity compared to WT animals. While the effect of *Nlrc5* deficiency on *in vitro* adipogenesis remains elusive, we show NLRC5 to interact with the master regulator of adipogenesis PPAR γ and further describe a synergistic regulation of the PPAR γ target FABP4 by PPAR γ activation and NLRC5 expression. Additionally, our data demonstrate a contribution of NLRC5 to PPAR γ 's anti-inflammatory properties in LPS-induced inflammation. NLRC5's co-regulation of PPAR γ targets might be mediated by forming a transcriptional complex with PPAR γ and Sin3A, although we were not able to clearly prove an association of NLRC5 with the promoter regions of PPAR γ targets. Lastly, this work revealed that *Nlrp10* expression is induced by HFD. This highlights NLRP10 as an interesting candidate to further investigate the role of NLR proteins in obesity.

References

- A, I. J., Jeannin, E., Wahli, W., & Desvergne, B. (1997). Polarity and specific sequence requirements of peroxisome proliferator-activated receptor (PPAR)/retinoid X receptor heterodimer binding to DNA. A functional analysis of the malic enzyme gene PPAR response element. *J Biol Chem*, *272*(32), 20108-20117. <https://doi.org/10.1074/jbc.272.32.20108>
- Abele, J., & Khayam-Bashi, H. (1979). Aqueous primary standard for use in measuring cholesterol by the cholesterol oxidase method. *Clin Chem*, *25*(1), 132-135. <https://www.ncbi.nlm.nih.gov/pubmed/761351>
- Agarwal, A. K., & Garg, A. (2002). A novel heterozygous mutation in peroxisome proliferator-activated receptor-gamma gene in a patient with familial partial lipodystrophy. *J Clin Endocrinol Metab*, *87*(1), 408-411. <https://doi.org/10.1210/jcem.87.1.8290>
- Agostini, M., Schoenmakers, E., Mitchell, C., Szatmari, I., Savage, D., Smith, A., Rajanayagam, O., Semple, R., Luan, J., Bath, L., Zalin, A., Labib, M., Kumar, S., Simpson, H., Blom, D., Marais, D., Schwabe, J., Barroso, I., Trembath, R., . . . Chatterjee, K. (2006). Non-DNA binding, dominant-negative, human PPARgamma mutations cause lipodystrophic insulin resistance. *Cell Metab*, *4*(4), 303-311. <https://doi.org/10.1016/j.cmet.2006.09.003>
- Akiyama, T. E., Baumann, C. T., Sakai, S., Hager, G. L., & Gonzalez, F. J. (2002). Selective intranuclear redistribution of PPAR isoforms by RXR alpha. *Mol Endocrinol*, *16*(4), 707-721. <https://doi.org/10.1210/mend.16.4.0797>
- Allen, I. C., Wilson, J. E., Schneider, M., Lich, J. D., Roberts, R. A., Arthur, J. C., Woodford, R. M., Davis, B. K., Uronis, J. M., Herfarth, H. H., Jobin, C., Rogers, A. B., & Ting, J. P. (2012). NLRP12 suppresses colon inflammation and tumorigenesis through the negative regulation of noncanonical NF-kappaB signaling. *Immunity*, *36*(5), 742-754. <https://doi.org/10.1016/j.immuni.2012.03.012>
- Almeida-Oliveira, F., Leandro, J. G. B., Ausina, P., Sola-Penna, M., & Majerowicz, D. (2017). Reference genes for quantitative PCR in the adipose tissue of mice with metabolic disease. *Biomed Pharmacother*, *88*, 948-955. <https://doi.org/10.1016/j.biopha.2017.01.091>
- Altshuler, D., Hirschhorn, J. N., Klannemark, M., Lindgren, C. M., Vohl, M. C., Nemesh, J., Lane, C. R., Schaffner, S. F., Bolk, S., Brewer, C., Tuomi, T., Gaudet, D., Hudson, T. J., Daly, M., Groop, L., & Lander, E. S. (2000). The common PPARgamma Pro12Ala polymorphism is associated with decreased risk of type 2 diabetes. *Nat Genet*, *26*(1), 76-80. <https://doi.org/10.1038/79216>
- Amiri, M., Yousefnia, S., Seyed Forootan, F., Peymani, M., Ghaedi, K., & Nasr Esfahani, M. H. (2018). Diverse roles of fatty acid binding proteins (FABPs) in development and pathogenesis of cancers. *Gene*, *676*, 171-183. <https://doi.org/10.1016/j.gene.2018.07.035>
- Arnold, C., Kienes, I., Sowa, A. S., & Kufer, T. A. (2018). NOD-like receptors. *eLS. John Wiley & Sons, Ltd: Chichester*. <https://doi.org/10.1002/9780470015902.a0026236>
- Arnoult, D., Soares, F., Tattoli, I., Castanier, C., Philpott, D. J., & Girardin, S. E. (2009). An N-terminal addressing sequence targets NLRX1 to the mitochondrial matrix. *J Cell Sci*, *122*(Pt 17), 3161-3168. <https://doi.org/10.1242/jcs.051193>

- Aslibekyan, S., Agha, G., Colicino, E., Do, A. N., Lahti, J., Ligthart, S., Marioni, R. E., Marzi, C., Mendelson, M. M., Tanaka, T., Wielscher, M., Absher, D. M., Ferrucci, L., Franco, O. H., Gieger, C., Grallert, H., Hernandez, D., Huan, T., Iurato, S., . . . Arnett, D. K. (2018). Association of Methylation Signals With Incident Coronary Heart Disease in an Epigenome-Wide Assessment of Circulating Tumor Necrosis Factor alpha. *JAMA Cardiol*, 3(6), 463-472. <https://doi.org/10.1001/jamacardio.2018.0510>
- Auboeuf, D., Rieusset, J., Fajas, L., Vallier, P., Frering, V., Riou, J. P., Staels, B., Auwerx, J., Laville, M., & Vidal, H. (1997). Tissue distribution and quantification of the expression of mRNAs of peroxisome proliferator-activated receptors and liver X receptor-alpha in humans: no alteration in adipose tissue of obese and NIDDM patients. *Diabetes*, 46(8), 1319-1327. <https://doi.org/10.2337/diab.46.8.1319>
- Bailen, M., Bressa, C., Martinez-Lopez, S., Gonzalez-Soltero, R., Montalvo Lominchar, M. G., San Juan, C., & Larrosa, M. (2020). Microbiota Features Associated With a High-Fat/Low-Fiber Diet in Healthy Adults. *Front Nutr*, 7, 583608. <https://doi.org/10.3389/fnut.2020.583608>
- Bando, S., Fukuda, D., Soeki, T., Nishimoto, S., Uematsu, E., Matsuura, T., Ise, T., Tobiume, T., Yamaguchi, K., Yagi, S., Iwase, T., Yamada, H., Wakatsuki, T., Shimabukuro, M., & Sata, M. (2015). Expression of NLRP3 in subcutaneous adipose tissue is associated with coronary atherosclerosis. *Atherosclerosis*, 242(2), 407-414. <https://doi.org/10.1016/j.atherosclerosis.2015.07.043>
- Barak, Y., Nelson, M. C., Ong, E. S., Jones, Y. Z., Ruiz-Lozano, P., Chien, K. R., Koder, A., & Evans, R. M. (1999). PPAR gamma is required for placental, cardiac, and adipose tissue development. *Mol Cell*, 4(4), 585-595. [https://doi.org/10.1016/s1097-2765\(00\)80209-9](https://doi.org/10.1016/s1097-2765(00)80209-9)
- Barroso, I., Gurnell, M., Crowley, V. E., Agostini, M., Schwabe, J. W., Soos, M. A., Maslen, G. L., Williams, T. D., Lewis, H., Schafer, A. J., Chatterjee, V. K., & O'Rahilly, S. (1999). Dominant negative mutations in human PPARgamma associated with severe insulin resistance, diabetes mellitus and hypertension. *Nature*, 402(6764), 880-883. <https://doi.org/10.1038/47254>
- Bauer, D. E., Canver, M. C., & Orkin, S. H. (2015). Generation of genomic deletions in mammalian cell lines via CRISPR/Cas9. *J Vis Exp*(95), e52118. <https://doi.org/10.3791/52118>
- Bauer, S., Aeissen, V., Bubeck, A. M., Kienes, I., Ellwanger, K., Scheurenbrand, M., Rexhepi, F., Ramanathan, S., Rosenstiel, P., Fricke, W. F., & Kufer, T. A. (2023a). NLRC5 affects diet-induced adiposity in female mice and co-regulates peroxisome proliferator-activated receptor PPARgamma target genes. *iScience*, 26(4), 106313. <https://doi.org/10.1016/j.isci.2023.106313>
- Bauer, S., Hezinger, L., Rexhepi, F., Ramanathan, S., & Kufer, T. A. (2023b). NOD-like Receptors-Emerging Links to Obesity and Associated Morbidities. *Int J Mol Sci*, 24(10). <https://doi.org/10.3390/ijms24108595>
- Bauernfried, S., Scherr, M. J., Pichlmair, A., Duderstadt, K. E., & Hornung, V. (2021). Human NLRP1 is a sensor for double-stranded RNA. *Science*, 371(6528). <https://doi.org/10.1126/science.abd0811>
- Beamer, B. A., Negri, C., Yen, C. J., Gavrilova, O., Rumberger, J. M., Durcan, M. J., Yarnall, D. P., Hawkins, A. L., Griffin, C. A., Burns, D. K., Roth, J., Reitman, M., & Shuldiner, A. R. (1997). Chromosomal localization and partial genomic structure of the human peroxisome proliferator activated receptor-gamma (hPPAR gamma) gene. *Biochem Biophys Res Commun*, 233(3), 756-759. <https://doi.org/10.1006/bbrc.1997.6540>

- Benko, S., Magalhaes, J. G., Philpott, D. J., & Girardin, S. E. (2010). NLRC5 limits the activation of inflammatory pathways. *J Immunol*, *185*(3), 1681-1691. <https://doi.org/10.4049/jimmunol.0903900>
- Bisanz, J. E., Upadhyay, V., Turnbaugh, J. A., Ly, K., & Turnbaugh, P. J. (2019). Meta-Analysis Reveals Reproducible Gut Microbiome Alterations in Response to a High-Fat Diet. *Cell Host Microbe*, *26*(2), 265-272 e264. <https://doi.org/10.1016/j.chom.2019.06.013>
- Biswas, A., Meissner, T. B., Kawai, T., & Kobayashi, K. S. (2012). Cutting edge: impaired MHC class I expression in mice deficient for Nlr5/class I transactivator. *J Immunol*, *189*(2), 516-520. <https://doi.org/10.4049/jimmunol.1200064>
- Bolyen, E., Rideout, J. R., Dillon, M. R., Bokulich, N. A., Abnet, C. C., Al-Ghalith, G. A., Alexander, H., Alm, E. J., Arumugam, M., Asnicar, F., Bai, Y., Bisanz, J. E., Bittinger, K., Brejnrod, A., Brislawn, C. J., Brown, C. T., Callahan, B. J., Caraballo-Rodriguez, A. M., Chase, J., . . . Caporaso, J. G. (2019). Reproducible, interactive, scalable and extensible microbiome data science using QIIME 2. *Nat Biotechnol*, *37*(8), 852-857. <https://doi.org/10.1038/s41587-019-0209-9>
- Bouhrel, M. A., Derudas, B., Rigamonti, E., Dievart, R., Brozek, J., Haulon, S., Zawadzki, C., Jude, B., Torpier, G., Marx, N., Staels, B., & Chinetti-Gbaguidi, G. (2007). PPARgamma activation primes human monocytes into alternative M2 macrophages with anti-inflammatory properties. *Cell Metab*, *6*(2), 137-143. <https://doi.org/10.1016/j.cmet.2007.06.010>
- Bournat, J. C., & Brown, C. W. (2010). Mitochondrial dysfunction in obesity. *Curr Opin Endocrinol Diabetes Obes*, *17*(5), 446-452. <https://doi.org/10.1097/MED.0b013e32833c3026>
- Brown, G. D., Willment, J. A., & Whitehead, L. (2018). C-type lectins in immunity and homeostasis. *Nat Rev Immunol*, *18*(6), 374-389. <https://doi.org/10.1038/s41577-018-0004-8>
- Callahan, B. J., McMurdie, P. J., Rosen, M. J., Han, A. W., Johnson, A. J., & Holmes, S. P. (2016). DADA2: High-resolution sample inference from Illumina amplicon data. *Nat Methods*, *13*(7), 581-583. <https://doi.org/10.1038/nmeth.3869>
- Cani, P. D., Amar, J., Iglesias, M. A., Poggi, M., Knauf, C., Bastelica, D., Neyrinck, A. M., Fava, F., Tuohy, K. M., Chabo, C., Waget, A., Delmee, E., Cousin, B., Sulpice, T., Chamontin, B., Ferrieres, J., Tanti, J. F., Gibson, G. R., Casteilla, L., . . . Burcelin, R. (2007). Metabolic endotoxemia initiates obesity and insulin resistance. *Diabetes*, *56*(7), 1761-1772. <https://doi.org/10.2337/db06-1491>
- Cani, P. D., Bibiloni, R., Knauf, C., Waget, A., Neyrinck, A. M., Delzenne, N. M., & Burcelin, R. (2008). Changes in gut microbiota control metabolic endotoxemia-induced inflammation in high-fat diet-induced obesity and diabetes in mice. *Diabetes*, *57*(6), 1470-1481. <https://doi.org/10.2337/db07-1403>
- Cao-Lei, L., Elgbeili, G., Szyf, M., Laplante, D. P., & King, S. (2019). Differential genome-wide DNA methylation patterns in childhood obesity. *BMC Res Notes*, *12*(1), 174. <https://doi.org/10.1186/s13104-019-4189-0>
- Carlos, D., Perez, M. M., Leite, J. A., Rocha, F. A., Martins, L. M. S., Pereira, C. A., Fraga-Silva, T. F. C., Pucci, T. A., Ramos, S. G., Camara, N. O. S., Bonato, V. L. D., Tostes, R. C., & Silva, J. S. (2020). NOD2 Deficiency Promotes Intestinal CD4+ T Lymphocyte Imbalance, Metainflammation, and Aggravates Type 2 Diabetes in Murine Model. *Front Immunol*, *11*, 1265. <https://doi.org/10.3389/fimmu.2020.01265>
- Carty, M., Kearney, J., Shanahan, K. A., Hams, E., Sugisawa, R., Connolly, D., Doran, C. G., Munoz-Wolf, N., Gurtler, C., Fitzgerald, K. A., Lavelle, E. C., Fallon, P. G., & Bowie, A. G.

- (2019). Cell Survival and Cytokine Release after Inflammasome Activation Is Regulated by the Toll-IL-1R Protein SARM. *Immunity*, 50(6), 1412-1424 e1416. <https://doi.org/10.1016/j.immuni.2019.04.005>
- Caruso, R., Warner, N., Inohara, N., & Nunez, G. (2014). NOD1 and NOD2: signaling, host defense, and inflammatory disease. *Immunity*, 41(6), 898-908. <https://doi.org/10.1016/j.immuni.2014.12.010>
- Cavallari, J. F., Barra, N. G., Foley, K. P., Lee, A., Duggan, B. M., Henriksbo, B. D., Anhe, F. F., Ashkar, A. A., & Schertzer, J. D. (2020a). Postbiotics for NOD2 require nonhematopoietic RIPK2 to improve blood glucose and metabolic inflammation in mice. *Am J Physiol Endocrinol Metab*, 318(4), E579-E585. <https://doi.org/10.1152/ajpendo.00033.2020>
- Cavallari, J. F., Fullerton, M. D., Duggan, B. M., Foley, K. P., Denou, E., Smith, B. K., Desjardins, E. M., Henriksbo, B. D., Kim, K. J., Tuinema, B. R., Stearns, J. C., Prescott, D., Rosenstiel, P., Coombes, B. K., Steinberg, G. R., & Schertzer, J. D. (2017). Muramyl Dipeptide-Based Postbiotics Mitigate Obesity-Induced Insulin Resistance via IRF4. *Cell Metab*, 25(5), 1063-1074 e1063. <https://doi.org/10.1016/j.cmet.2017.03.021>
- Cavallari, J. F., Pokrajac, N. T., Zlitni, S., Foley, K. P., Henriksbo, B. D., & Schertzer, J. D. (2020b). NOD2 in hepatocytes engages a liver-gut axis to protect against steatosis, fibrosis, and gut dysbiosis during fatty liver disease in mice. *Am J Physiol Endocrinol Metab*, 319(2), E305-E314. <https://doi.org/10.1152/ajpendo.00181.2020>
- Chamaillard, M., Hashimoto, M., Horie, Y., Masumoto, J., Qiu, S., Saab, L., Ogura, Y., Kawasaki, A., Fukase, K., Kusumoto, S., Valvano, M. A., Foster, S. J., Mak, T. W., Nunez, G., & Inohara, N. (2003). An essential role for NOD1 in host recognition of bacterial peptidoglycan containing diaminopimelic acid. *Nat Immunol*, 4(7), 702-707. <https://doi.org/10.1038/ni945>
- Chan, K. L., Tam, T. H., Boroumand, P., Prescott, D., Costford, S. R., Escalante, N. K., Fine, N., Tu, Y., Robertson, S. J., Prabakaran, D., Liu, Z., Bilan, P. J., Salter, M. W., Glogauer, M., Girardin, S. E., Philpott, D. J., & Klip, A. (2017). Circulating NOD1 Activators and Hematopoietic NOD1 Contribute to Metabolic Inflammation and Insulin Resistance. *Cell Rep*, 18(10), 2415-2426. <https://doi.org/10.1016/j.celrep.2017.02.027>
- Chandra, V., Huang, P., Hamuro, Y., Raghuram, S., Wang, Y., Burris, T. P., & Rastinejad, F. (2008). Structure of the intact PPAR-gamma-RXR- nuclear receptor complex on DNA. *Nature*, 456(7220), 350-356. <https://doi.org/10.1038/nature07413>
- Charlesworth, J. C., Peralta, J. M., Drigalenko, E., Goring, H. H., Almasy, L., Dyer, T. D., & Blangero, J. (2009). Toward the identification of causal genes in complex diseases: a gene-centric joint test of significance combining genomic and transcriptomic data. *BMC Proc*, 3 Suppl 7, S92. <https://doi.org/10.1186/1753-6561-3-s7-s92>
- Chelbi, S. T., & Guarda, G. (2016). NLRC5, a promising new entry in tumor immunology. *J Immunother Cancer*, 4, 39. <https://doi.org/10.1186/s40425-016-0143-z>
- Chen, S. T., Chen, L., Lin, D. S., Chen, S. Y., Tsao, Y. P., Guo, H., Li, F. J., Tseng, W. T., Tam, J. W., Chao, C. W., Brickey, W. J., Dzhagalov, I., Song, M. J., Kang, H. R., Jung, J. U., & Ting, J. P. (2019). NLRP12 Regulates Anti-viral RIG-I Activation via Interaction with TRIM25. *Cell Host Microbe*, 25(4), 602-616 e607. <https://doi.org/10.1016/j.chom.2019.02.013>
- Chmurzynska, A. (2006). The multigene family of fatty acid-binding proteins (FABPs): function, structure and polymorphism. *J Appl Genet*, 47(1), 39-48. <https://doi.org/10.1007/BF03194597>

- Cho, S. W., Kim, S., Kim, Y., Kweon, J., Kim, H. S., Bae, S., & Kim, J. S. (2014). Analysis of off-target effects of CRISPR/Cas-derived RNA-guided endonucleases and nickases. *Genome Res*, 24(1), 132-141. <https://doi.org/10.1101/gr.162339.113>
- Chu, X., Wu, S., & Raju, R. (2019). NLRX1 Regulation Following Acute Mitochondrial Injury. *Front Immunol*, 10, 2431. <https://doi.org/10.3389/fimmu.2019.02431>
- Chui, A. J., Okondo, M. C., Rao, S. D., Gai, K., Griswold, A. R., Johnson, D. C., Ball, D. P., Taabazuing, C. Y., Orth, E. L., Vittimberga, B. A., & Bachovchin, D. A. (2019). N-terminal degradation activates the NLRP1B inflammasome. *Science*, 364(6435), 82-85. <https://doi.org/10.1126/science.aau1208>
- Chung, S. W., Kang, B. Y., Kim, S. H., Pak, Y. K., Cho, D., Trinchieri, G., & Kim, T. S. (2000). Oxidized low density lipoprotein inhibits interleukin-12 production in lipopolysaccharide-activated mouse macrophages via direct interactions between peroxisome proliferator-activated receptor-gamma and nuclear factor-kappa B. *J Biol Chem*, 275(42), 32681-32687. <https://doi.org/10.1074/jbc.M002577200>
- Cinti, S., Mitchell, G., Barbatelli, G., Murano, I., Ceresi, E., Faloia, E., Wang, S., Fortier, M., Greenberg, A. S., & Obin, M. S. (2005). Adipocyte death defines macrophage localization and function in adipose tissue of obese mice and humans. *J Lipid Res*, 46(11), 2347-2355. <https://doi.org/10.1194/jlr.M500294-JLR200>
- Cui, H. X., Zhang, L. S., Luo, Y., Yuan, K., Huang, Z. Y., & Guo, Y. (2019). A Purified Anthraquinone-Glycoside Preparation From Rhubarb Ameliorates Type 2 Diabetes Mellitus by Modulating the Gut Microbiota and Reducing Inflammation. *Front Microbiol*, 10, 1423. <https://doi.org/10.3389/fmicb.2019.01423>
- Cui, J., Zhu, L., Xia, X., Wang, H. Y., Legras, X., Hong, J., Ji, J., Shen, P., Zheng, S., Chen, Z. J., & Wang, R. F. (2010). NLRC5 negatively regulates the NF-kappaB and type I interferon signaling pathways. *Cell*, 141(3), 483-496. <https://doi.org/10.1016/j.cell.2010.03.040>
- Dakin, R. S., Walker, B. R., Seckl, J. R., Hadoke, P. W., & Drake, A. J. (2015). Estrogens protect male mice from obesity complications and influence glucocorticoid metabolism. *Int J Obes (Lond)*, 39(10), 1539-1547. <https://doi.org/10.1038/ijo.2015.102>
- Dang, A. T., Strietz, J., Zenobi, A., Khameneh, H. J., Brandl, S. M., Lozza, L., Conradt, G., Kaufmann, S. H. E., Reith, W., Kwee, I., Minguet, S., Chelbi, S. T., & Guarda, G. (2021). NLRC5 promotes transcription of BTN3A1-3 genes and Vgamma9Vdelta2 T cell-mediated killing. *iScience*, 24(1), 101900. <https://doi.org/10.1016/j.isci.2020.101900>
- Daniel, H., Gholami, A. M., Berry, D., Desmarchelier, C., Hahne, H., Loh, G., Mondot, S., Lepage, P., Rothballer, M., Walker, A., Bohm, C., Wenning, M., Wagner, M., Blaut, M., Schmitt-Kopplin, P., Kuster, B., Haller, D., & Clavel, T. (2014). High-fat diet alters gut microbiota physiology in mice. *ISME J*, 8(2), 295-308. <https://doi.org/10.1038/ismej.2013.155>
- Davis, B. K., Roberts, R. A., Huang, M. T., Willingham, S. B., Conti, B. J., Brickey, W. J., Barker, B. R., Kwan, M., Taxman, D. J., Accavitti-Loper, M. A., Duncan, J. A., & Ting, J. P. (2011). Cutting edge: NLRC5-dependent activation of the inflammasome. *J Immunol*, 186(3), 1333-1337. <https://doi.org/10.4049/jimmunol.1003111>
- Demoz, A., Vaagenes, H., Aarsaether, N., Hvattum, E., Skorve, J., Gottlicher, M., Lillehaug, J. R., Gibson, G. G., Gustafsson, J. A., Hood, S., & et al. (1994). Coordinate induction of hepatic fatty acyl-CoA oxidase and P4504A1 in rat after activation of the peroxisome proliferator-activated receptor (PPAR) by sulphur-substituted fatty acid analogues. *Xenobiotica*, 24(9), 943-956. <https://doi.org/10.3109/00498259409043292>
- Denou, E., Lolmede, K., Garidou, L., Pomie, C., Chabo, C., Lau, T. C., Fullerton, M. D., Nigro, G., Zakaroff-Girard, A., Luche, E., Garret, C., Serino, M., Amar, J., Courtney, M., Cavallari, J.

- F., Henriksbo, B. D., Barra, N. G., Foley, K. P., McPhee, J. B., . . . Schertzer, J. D. (2015). Defective NOD2 peptidoglycan sensing promotes diet-induced inflammation, dysbiosis, and insulin resistance. *EMBO Mol Med*, *7*(3), 259-274. <https://doi.org/10.15252/emmm.201404169>
- Downs, I., Vijayan, S., Sidiq, T., & Kobayashi, K. S. (2016). CITA/NLRC5: A critical transcriptional regulator of MHC class I gene expression. *Biofactors*, *42*(4), 349-357. <https://doi.org/10.1002/biof.1285>
- Duewell, P., Kono, H., Rayner, K. J., Sirois, C. M., Vladimer, G., Bauernfeind, F. G., Abela, G. S., Franchi, L., Nunez, G., Schnurr, M., Espevik, T., Lien, E., Fitzgerald, K. A., Rock, K. L., Moore, K. J., Wright, S. D., Hornung, V., & Latz, E. (2010). NLRP3 inflammasomes are required for atherogenesis and activated by cholesterol crystals. *Nature*, *464*(7293), 1357-1361. <https://doi.org/10.1038/nature08938>
- Eckel, R. H., Grundy, S. M., & Zimmet, P. Z. (2005). The metabolic syndrome. *Lancet*, *365*(9468), 1415-1428. [https://doi.org/10.1016/S0140-6736\(05\)66378-7](https://doi.org/10.1016/S0140-6736(05)66378-7)
- El Maassarani, M., Barbarin, A., Fromont, G., Kaissi, O., Lebbe, M., Vannier, B., Moussa, A., & Seite, P. (2016). Integrated and Functional Genomics Analysis Validates the Relevance of the Nuclear Variant ErbB380kDa in Prostate Cancer Progression. *PLoS One*, *11*(5), e0155950. <https://doi.org/10.1371/journal.pone.0155950>
- Elbrecht, A., Chen, Y., Cullinan, C. A., Hayes, N., Leibowitz, M., Moller, D. E., & Berger, J. (1996). Molecular cloning, expression and characterization of human peroxisome proliferator activated receptors gamma 1 and gamma 2. *Biochem Biophys Res Commun*, *224*(2), 431-437. <https://doi.org/10.1006/bbrc.1996.1044>
- Ellwanger, K., Briese, S., Arnold, C., Kienes, I., Heim, V., Nachbur, U., & Kufer, T. A. (2019). XIAP controls RIPK2 signaling by preventing its deposition in speck-like structures. *Life Sci Alliance*, *2*(4). <https://doi.org/10.26508/lsa.201900346>
- Engler, C., Kandzia, R., & Marillonnet, S. (2008). A one pot, one step, precision cloning method with high throughput capability. *PLoS One*, *3*(11), e3647. <https://doi.org/10.1371/journal.pone.0003647>
- Erridge, C., Attina, T., Spickett, C. M., & Webb, D. J. (2007). A high-fat meal induces low-grade endotoxemia: evidence of a novel mechanism of postprandial inflammation. In *Am J Clin Nutr* (Vol. 86, pp. 1286-1292). <http://dx.doi.org/http://ajcn.nutrition.org/content/86/5/1286.full.pdf>
- Esser, N., L'Homme, L., De Roover, A., Kohnen, L., Scheen, A. J., Moutschen, M., Piette, J., Legrand-Poels, S., & Paquot, N. (2013). Obesity phenotype is related to NLRP3 inflammasome activity and immunological profile of visceral adipose tissue. *Diabetologia*, *56*(11), 2487-2497. <https://doi.org/10.1007/s00125-013-3023-9>
- Evans, R. M., & Mangelsdorf, D. J. (2014). Nuclear Receptors, RXR, and the Big Bang. *Cell*, *157*(1), 255-266. <https://doi.org/10.1016/j.cell.2014.03.012>
- Fajas, L., Auboeuf, D., Raspe, E., Schoonjans, K., Lefebvre, A. M., Saladin, R., Najib, J., Laville, M., Fruchart, J. C., Deeb, S., Vidal-Puig, A., Flier, J., Briggs, M. R., Staels, B., Vidal, H., & Auwerx, J. (1997). The organization, promoter analysis, and expression of the human PPARgamma gene. *J Biol Chem*, *272*(30), 18779-18789. <https://doi.org/10.1074/jbc.272.30.18779>
- Fajas, L., Fruchart, J. C., & Auwerx, J. (1998). PPARgamma3 mRNA: a distinct PPARgamma mRNA subtype transcribed from an independent promoter. *FEBS Lett*, *438*(1-2), 55-60. [https://doi.org/10.1016/s0014-5793\(98\)01273-3](https://doi.org/10.1016/s0014-5793(98)01273-3)

- Feige, J. N., & Auwerx, J. (2007). Transcriptional coregulators in the control of energy homeostasis. *Trends Cell Biol*, *17*(6), 292-301. <https://doi.org/10.1016/j.tcb.2007.04.001>
- Finucane, O. M., Lyons, C. L., Murphy, A. M., Reynolds, C. M., Klinger, R., Healy, N. P., Cooke, A. A., Coll, R. C., McAllan, L., Nilaweera, K. N., O'Reilly, M. E., Tierney, A. C., Morine, M. J., Alcalá-Díaz, J. F., Lopez-Miranda, J., O'Connor, D. P., O'Neill, L. A., McGillicuddy, F. C., & Roche, H. M. (2015). Monounsaturated fatty acid-enriched high-fat diets impede adipose NLRP3 inflammasome-mediated IL-1 β secretion and insulin resistance despite obesity. *Diabetes*, *64*(6), 2116-2128. <https://doi.org/10.2337/db14-1098>
- Fitzgerald, K. A., & Kagan, J. C. (2020). Toll-like Receptors and the Control of Immunity. *Cell*, *180*(6), 1044-1066. <https://doi.org/10.1016/j.cell.2020.02.041>
- Forman, B. M., Tontonoz, P., Chen, J., Brun, R. P., Spiegelman, B. M., & Evans, R. M. (1995). 15-Deoxy- Δ 12, 14-prostaglandin J2 is a ligand for the adipocyte determination factor PPAR γ . *Cell*, *83*(5), 803-812. [https://doi.org/10.1016/0092-8674\(95\)90193-0](https://doi.org/10.1016/0092-8674(95)90193-0)
- Freedman, B. D., Lee, E. J., Park, Y., & Jameson, J. L. (2005). A dominant negative peroxisome proliferator-activated receptor- γ knock-in mouse exhibits features of the metabolic syndrome. *J Biol Chem*, *280*(17), 17118-17125. <https://doi.org/10.1074/jbc.M407539200>
- Fu, J., Zhao, B., Ni, C., Ni, H., Xu, L., He, Q., Xu, M., Xu, C., Luo, G., Zhu, J., Tao, J., & Yao, M. (2021). Rosiglitazone Alleviates Mechanical Allodynia of Rats with Bone Cancer Pain through the Activation of PPAR- γ to Inhibit the NF- κ B/NLRP3 Inflammatory Axis in Spinal Cord Neurons. *PPAR Res*, *2021*, 6086265. <https://doi.org/10.1155/2021/6086265>
- Fuentes, N., & Silveyra, P. (2019). Estrogen receptor signaling mechanisms. *Adv Protein Chem Struct Biol*, *116*, 135-170. <https://doi.org/10.1016/bs.apcsb.2019.01.001>
- Furukawa, S., Fujita, T., Shimabukuro, M., Iwaki, M., Yamada, Y., Nakajima, Y., Nakayama, O., Makishima, M., Matsuda, M., & Shimomura, I. (2004). Increased oxidative stress in obesity and its impact on metabolic syndrome. *J Clin Invest*, *114*(12), 1752-1761. <https://doi.org/10.1172/jci21625>
- Galarraga, M., Campion, J., Munoz-Barrutia, A., Boque, N., Moreno, H., Martinez, J. A., Milagro, F., & Ortiz-de-Solorzano, C. (2012). Adiposoft: automated software for the analysis of white adipose tissue cellularity in histological sections. *J Lipid Res*, *53*(12), 2791-2796. <https://doi.org/10.1194/jlr.D023788>
- Girardin, S. E., Boneca, I. G., Carneiro, L. A., Antignac, A., Jehanno, M., Viala, J., Tedin, K., Taha, M. K., Labigne, A., Zahringer, U., Coyle, A. J., DiStefano, P. S., Bertin, J., Sansonetti, P. J., & Philpott, D. J. (2003a). Nod1 detects a unique muropeptide from gram-negative bacterial peptidoglycan. *Science*, *300*(5625), 1584-1587. <https://doi.org/10.1126/science.1084677>
- Girardin, S. E., Boneca, I. G., Viala, J., Chamaillard, M., Labigne, A., Thomas, G., Philpott, D. J., & Sansonetti, P. J. (2003b). Nod2 is a general sensor of peptidoglycan through muramyl dipeptide (MDP) detection. *J Biol Chem*, *278*(11), 8869-8872. <https://doi.org/10.1074/jbc.C200651200>
- Glastonbury, C. A., Pulit, S. L., Honecker, J., Censin, J. C., Laber, S., Yaghootkar, H., Rahmioglu, N., Pastel, E., Kos, K., Pitt, A., Hudson, M., Nellaker, C., Beer, N. L., Hauner, H., Becker, C. M., Zondervan, K. T., Frayling, T. M., Claussnitzer, M., & Lindgren, C. M. (2020). Machine Learning based histology phenotyping to investigate the epidemiologic and

- genetic basis of adipocyte morphology and cardiometabolic traits. *PLoS Comput Biol*, 16(8), e1008044. <https://doi.org/10.1371/journal.pcbi.1008044>
- Gloor, G. B., Wu, J. R., Pawlowsky-Glahn, V., & Egozcue, J. J. (2016). It's all relative: analyzing microbiome data as compositions. *Ann Epidemiol*, 26(5), 322-329. <https://doi.org/10.1016/j.annepidem.2016.03.003>
- Gong, K., Chen, M., Li, R., He, Y., Zhu, H., Yao, D., Oparil, S., & Zhang, Z. (2016). Smad3-mSin3A-HDAC1 Complex is Required for TGF-beta1-Induced Transcriptional Inhibition of PPARgamma in Mouse Cardiac Fibroblasts. *Cell Physiol Biochem*, 40(5), 908-920. <https://doi.org/10.1159/000453149>
- Green, H., & Meuth, M. (1974). An established pre-adipose cell line and its differentiation in culture. *Cell*, 3(2), 127-133. [https://doi.org/10.1016/0092-8674\(74\)90116-0](https://doi.org/10.1016/0092-8674(74)90116-0)
- Grygiel-Gorniak, B. (2014). Peroxisome proliferator-activated receptors and their ligands: nutritional and clinical implications--a review. *Nutr J*, 13, 17. <https://doi.org/10.1186/1475-2891-13-17>
- Guo, Z., Ali, Q., Abaidullah, M., Gao, Z., Diao, X., Liu, B., Wang, Z., Zhu, X., Cui, Y., Li, D., & Shi, Y. (2022). High fat diet-induced hyperlipidemia and tissue steatosis in rabbits through modulating ileal microbiota. *Appl Microbiol Biotechnol*, 106(21), 7187-7207. <https://doi.org/10.1007/s00253-022-12203-7>
- Gustin, A., Kirchmeyer, M., Koncina, E., Felten, P., Losciuto, S., Heurtaux, T., Tardivel, A., Heuschling, P., & Dostert, C. (2015). NLRP3 Inflammasome Is Expressed and Functional in Mouse Brain Microglia but Not in Astrocytes. *PLoS One*, 10(6), e0130624. <https://doi.org/10.1371/journal.pone.0130624>
- Gutte, P. G., Jurt, S., Grutter, M. G., & Zerbe, O. (2014). Unusual structural features revealed by the solution NMR structure of the NLRC5 caspase recruitment domain. *Biochemistry*, 53(19), 3106-3117. <https://doi.org/10.1021/bi500177x>
- Halberg, N., Khan, T., Trujillo, M. E., Wernstedt-Asterholm, I., Attie, A. D., Sherwani, S., Wang, Z. V., Landskroner-Eiger, S., Dineen, S., Magalang, U. J., Brekken, R. A., & Scherer, P. E. (2009). Hypoxia-inducible factor 1alpha induces fibrosis and insulin resistance in white adipose tissue. *Mol Cell Biol*, 29(16), 4467-4483. <https://doi.org/10.1128/MCB.00192-09>
- Hayashi, F., Smith, K. D., Ozinsky, A., Hawn, T. R., Yi, E. C., Goodlett, D. R., Eng, J. K., Akira, S., Underhill, D. M., & Aderem, A. (2001). The innate immune response to bacterial flagellin is mediated by Toll-like receptor 5. *Nature*, 410(6832), 1099-1103. <https://doi.org/10.1038/35074106>
- He, T. C., Chan, T. A., Vogelstein, B., & Kinzler, K. W. (1999). PPARdelta is an APC-regulated target of nonsteroidal anti-inflammatory drugs. *Cell*, 99(3), 335-345. [https://doi.org/10.1016/s0092-8674\(00\)81664-5](https://doi.org/10.1016/s0092-8674(00)81664-5)
- He, W., Barak, Y., Hevener, A., Olson, P., Liao, D., Le, J., Nelson, M., Ong, E., Olefsky, J. M., & Evans, R. M. (2003). Adipose-specific peroxisome proliferator-activated receptor gamma knockout causes insulin resistance in fat and liver but not in muscle. *Proc Natl Acad Sci U S A*, 100(26), 15712-15717. <https://doi.org/10.1073/pnas.2536828100>
- He, X., Zhang, M., Li, S. T., Li, X., Huang, Q., Zhang, K., Zheng, X., Xu, X. T., Zhao, D. G., & Ma, Y. Y. (2022). Alteration of gut microbiota in high-fat diet-induced obese mice using carnosic acid from rosemary. *Food Sci Nutr*, 10(7), 2325-2332. <https://doi.org/10.1002/fsn3.2841>
- Hegele, R. A., Cao, H., Frankowski, C., Mathews, S. T., & Leff, T. (2002). PPARG F388L, a transactivation-deficient mutant, in familial partial lipodystrophy. *Diabetes*, 51(12), 3586-3590. <https://doi.org/10.2337/diabetes.51.12.3586>

- Heinzel, T., Lavinsky, R. M., Mullen, T. M., Soderstrom, M., Laherty, C. D., Torchia, J., Yang, W. M., Brard, G., Ngo, S. D., Davie, J. R., Seto, E., Eisenman, R. N., Rose, D. W., Glass, C. K., & Rosenfeld, M. G. (1997). A complex containing N-CoR, mSin3 and histone deacetylase mediates transcriptional repression. *Nature*, *387*(6628), 43-48. <https://doi.org/10.1038/387043a0>
- Helsen, C., & Claessens, F. (2014). Looking at nuclear receptors from a new angle. *Mol Cell Endocrinol*, *382*(1), 97-106. <https://doi.org/10.1016/j.mce.2013.09.009>
- Henao-Mejia, J., Elinav, E., Jin, C., Hao, L., Mehal, W. Z., Strowig, T., Thaiss, C. A., Kau, A. L., Eisenbarth, S. C., Jurczak, M. J., Camporez, J. P., Shulman, G. I., Gordon, J. I., Hoffman, H. M., & Flavell, R. A. (2012). Inflammasome-mediated dysbiosis regulates progression of NAFLD and obesity. *Nature*, *482*(7384), 179-185. <https://doi.org/10.1038/nature10809>
- Hofer, P., Boeszoermenyi, A., Jaeger, D., Feiler, U., Arthanari, H., Mayer, N., Zehender, F., Rechberger, G., Oberer, M., Zimmermann, R., Lass, A., Haemmerle, G., Breinbauer, R., Zechner, R., & Preiss-Landl, K. (2015). Fatty Acid-binding Proteins Interact with Comparative Gene Identification-58 Linking Lipolysis with Lipid Ligand Shuttling. *J Biol Chem*, *290*(30), 18438-18453. <https://doi.org/10.1074/jbc.M114.628958>
- Hoffart, E., Ghebreghiorgis, L., Nussler, A. K., Thasler, W. E., Weiss, T. S., Schwab, M., & Burk, O. (2012). Effects of atorvastatin metabolites on induction of drug-metabolizing enzymes and membrane transporters through human pregnane X receptor. *Br J Pharmacol*, *165*(5), 1595-1608. <https://doi.org/10.1111/j.1476-5381.2011.01665.x>
- Hong, G., Davis, B., Khatoon, N., Baker, S. F., & Brown, J. (2003). PPAR gamma-dependent anti-inflammatory action of rosiglitazone in human monocytes: suppression of TNF alpha secretion is not mediated by PTEN regulation. *Biochem Biophys Res Commun*, *303*(3), 782-787. [https://doi.org/10.1016/s0006-291x\(03\)00418-2](https://doi.org/10.1016/s0006-291x(03)00418-2)
- Hosseinzadeh, N., Mehrabi, Y., Daneshpour, M. S., Zayeri, F., Guity, K., & Azizi, F. (2019). Identifying new associated pleiotropic SNPs with lipids by simultaneous test of multiple longitudinal traits: An Iranian family-based study. *Gene*, *692*, 156-169. <https://doi.org/10.1016/j.gene.2019.01.007>
- Hotamisligil, G. S. (2006). Inflammation and metabolic disorders. *Nature*, *444*(7121), 860-867. <https://doi.org/10.1038/nature05485>
- Hotamisligil, G. S., & Bernlohr, D. A. (2015). Metabolic functions of FABPs--mechanisms and therapeutic implications. *Nat Rev Endocrinol*, *11*(10), 592-605. <https://doi.org/10.1038/nrendo.2015.122>
- Hotamisligil, G. S., Johnson, R. S., Distel, R. J., Ellis, R., Papaioannou, V. E., & Spiegelman, B. M. (1996). Uncoupling of obesity from insulin resistance through a targeted mutation in aP2, the adipocyte fatty acid binding protein. *Science*, *274*(5291), 1377-1379. <https://doi.org/10.1126/science.274.5291.1377>
- Hotamisligil, G. S., Shargill, N. S., & Spiegelman, B. M. (1993). Adipose expression of tumor necrosis factor-alpha: direct role in obesity-linked insulin resistance. *Science*, *259*(5091), 87-91. <https://doi.org/10.1126/science.7678183>
- Hou, Y., Moreau, F., & Chadee, K. (2012). PPARgamma is an E3 ligase that induces the degradation of NFkappaB/p65. *Nat Commun*, *3*, 1300. <https://doi.org/10.1038/ncomms2270>
- Hsu, P. D., Scott, D. A., Weinstein, J. A., Ran, F. A., Konermann, S., Agarwala, V., Li, Y., Fine, E. J., Wu, X., Shalem, O., Cradick, T. J., Marraffini, L. A., Bao, G., & Zhang, F. (2013). DNA targeting specificity of RNA-guided Cas9 nucleases. *Nat Biotechnol*, *31*(9), 827-832. <https://doi.org/10.1038/nbt.2647>

- Huang, J. H., Liu, C. Y., Wu, S. Y., Chen, W. Y., Chang, T. H., Kan, H. W., Hsieh, S. T., Ting, J. P., & Wu-Hsieh, B. A. (2018). NLRX1 Facilitates Histoplasma capsulatum-Induced LC3-Associated Phagocytosis for Cytokine Production in Macrophages. *Front Immunol*, *9*, 2761. <https://doi.org/10.3389/fimmu.2018.02761>
- Huang, P., Chandra, V., & Rastinejad, F. (2010). Structural overview of the nuclear receptor superfamily: insights into physiology and therapeutics. *Annu Rev Physiol*, *72*, 247-272. <https://doi.org/10.1146/annurev-physiol-021909-135917>
- Imai, T., Takakuwa, R., Marchand, S., Dentz, E., Bornert, J. M., Messaddeq, N., Wendling, O., Mark, M., Desvergne, B., Wahli, W., Chambon, P., & Metzger, D. (2004). Peroxisome proliferator-activated receptor gamma is required in mature white and brown adipocytes for their survival in the mouse. *Proc Natl Acad Sci U S A*, *101*(13), 4543-4547. <https://doi.org/10.1073/pnas.0400356101>
- Jager, J., Gremeaux, T., Cormont, M., Le Marchand-Brustel, Y., & Tanti, J. F. (2007). Interleukin-1beta-induced insulin resistance in adipocytes through down-regulation of insulin receptor substrate-1 expression. *Endocrinology*, *148*(1), 241-251. <https://doi.org/10.1210/en.2006-0692>
- Janani, C., & Ranjitha Kumari, B. D. (2015). PPAR gamma gene--a review. *Diabetes Metab Syndr*, *9*(1), 46-50. <https://doi.org/10.1016/j.dsx.2014.09.015>
- Janeway, C. A., Jr. (1989). Approaching the asymptote? Evolution and revolution in immunology. *Cold Spring Harb Symp Quant Biol*, *54 Pt 1*, 1-13. <https://doi.org/10.1101/sqb.1989.054.01.003>
- Janeway, C. A., Jr., & Medzhitov, R. (2002). Innate immune recognition. *Annu Rev Immunol*, *20*, 197-216. <https://doi.org/10.1146/annurev.immunol.20.083001.084359>
- Jaworska, J., Coulombe, F., Downey, J., Tzelepis, F., Shalaby, K., Tattoli, I., Berube, J., Rousseau, S., Martin, J. G., Girardin, S. E., McCullers, J. A., & Divangahi, M. (2014). NLRX1 prevents mitochondrial induced apoptosis and enhances macrophage antiviral immunity by interacting with influenza virus PB1-F2 protein. *Proc Natl Acad Sci U S A*, *111*(20), E2110-2119. <https://doi.org/10.1073/pnas.1322118111>
- Jenkins-Kruchten, A. E., Bennaars-Eiden, A., Ross, J. R., Shen, W. J., Kraemer, F. B., & Bernlohr, D. A. (2003). Fatty acid-binding protein-hormone-sensitive lipase interaction. Fatty acid dependence on binding. *J Biol Chem*, *278*(48), 47636-47643. <https://doi.org/10.1074/jbc.M307680200>
- Ji, H., Wang, H., Zhang, F., Li, X., Xiang, L., & Aiguo, S. (2010). PPARgamma agonist pioglitazone inhibits microglia inflammation by blocking p38 mitogen-activated protein kinase signaling pathways. *Inflamm Res*, *59*(11), 921-929. <https://doi.org/10.1007/s00011-010-0203-7>
- Jiang, C., Ting, A. T., & Seed, B. (1998). PPAR-gamma agonists inhibit production of monocyte inflammatory cytokines. *Nature*, *391*(6662), 82-86. <https://doi.org/10.1038/34184>
- Jo, E. K., Kim, J. K., Shin, D. M., & Sasakawa, C. (2016). Molecular mechanisms regulating NLRP3 inflammasome activation. *Cell Mol Immunol*, *13*(2), 148-159. <https://doi.org/10.1038/cmi.2015.95>
- Jo, J. K., Seo, S. H., Park, S. E., Kim, H. W., Kim, E. J., Kim, J. S., Pyo, J. Y., Cho, K. M., Kwon, S. J., Park, D. H., & Son, H. S. (2021). Gut Microbiome and Metabolome Profiles Associated with High-Fat Diet in Mice. *Metabolites*, *11*(8). <https://doi.org/10.3390/metabo11080482>
- Johnson, B. A., Wilson, E. M., Li, Y., Moller, D. E., Smith, R. G., & Zhou, G. (2000). Ligand-induced stabilization of PPARgamma monitored by NMR spectroscopy: implications

- for nuclear receptor activation. *J Mol Biol*, 298(2), 187-194.
<https://doi.org/10.1006/jmbi.2000.3636>
- Kawai, T., & Akira, S. (2006). TLR signaling. *Cell Death Differ*, 13(5), 816-825.
<https://doi.org/10.1038/sj.cdd.4401850>
- Kawasaki, T., Kawai, T., & Akira, S. (2011). Recognition of nucleic acids by pattern-recognition receptors and its relevance in autoimmunity. *Immunol Rev*, 243(1), 61-73.
<https://doi.org/10.1111/j.1600-065X.2011.01048.x>
- Khan, T., Muise, E. S., Iyengar, P., Wang, Z. V., Chandalia, M., Abate, N., Zhang, B. B., Bonaldo, P., Chua, S., & Scherer, P. E. (2009). Metabolic dysregulation and adipose tissue fibrosis: role of collagen VI. *Mol Cell Biol*, 29(6), 1575-1591.
<https://doi.org/10.1128/MCB.01300-08>
- Kienes, I. (2021). *Characterization of the role of the NLR proteins NLRC5 and NLRP11 in the immune response* [University of Hohenheim]. Stuttgart. <http://opus.uni-hohenheim.de/volltexte/2022/1996/>
- Kienes, I., Bauer, S., Gottschild, C., Mirza, N., Pfannstiel, J., Schroder, M., & Kufer, T. A. (2021). DDX3X Links NLRP11 to the Regulation of Type I Interferon Responses and NLRP3 Inflammasome Activation. *Front Immunol*, 12, 653883.
<https://doi.org/10.3389/fimmu.2021.653883>
- Kim, Y. K., Shin, J. S., & Nahm, M. H. (2016). NOD-Like Receptors in Infection, Immunity, and Diseases. *Yonsei Med J*, 57(1), 5-14. <https://doi.org/10.3349/ymj.2016.57.1.5>
- Kliwer, S. A., Lenhard, J. M., Willson, T. M., Patel, I., Morris, D. C., & Lehmann, J. M. (1995). A prostaglandin J2 metabolite binds peroxisome proliferator-activated receptor gamma and promotes adipocyte differentiation. *Cell*, 83(5), 813-819.
[https://doi.org/10.1016/0092-8674\(95\)90194-9](https://doi.org/10.1016/0092-8674(95)90194-9)
- Kobayashi, K. S., & van den Elsen, P. J. (2012). NLRC5: a key regulator of MHC class I-dependent immune responses. *Nat Rev Immunol*, 12(12), 813-820.
<https://doi.org/10.1038/nri3339>
- Kong, X., Fang, M., Fang, F., Li, P., & Xu, Y. (2009). PPARgamma enhances IFNgamma-mediated transcription and rescues the TGFbeta antagonism by stimulating CIITA in vascular smooth muscle cells. *J Mol Cell Cardiol*, 46(5), 748-757.
<https://doi.org/10.1016/j.yjmcc.2009.01.011>
- Kraus, N. A., Ehebauer, F., Zapp, B., Rudolphi, B., Kraus, B. J., & Kraus, D. (2016). Quantitative assessment of adipocyte differentiation in cell culture. *Adipocyte*, 5(4), 351-358.
<https://doi.org/10.1080/21623945.2016.1240137>
- Kroker, A. J., & Bruning, J. B. (2015). Review of the Structural and Dynamic Mechanisms of PPARgamma Partial Agonism. *PPAR Res*, 2015, 816856.
<https://doi.org/10.1155/2015/816856>
- Kuenzel, S., Till, A., Winkler, M., Hasler, R., Lipinski, S., Jung, S., Grotzinger, J., Fickenscher, H., Schreiber, S., & Rosenstiel, P. (2010). The nucleotide-binding oligomerization domain-like receptor NLRC5 is involved in IFN-dependent antiviral immune responses. *J Immunol*, 184(4), 1990-2000. <https://doi.org/10.4049/jimmunol.0900557>
- Kufer, T. A., Kremmer, E., Adam, A. C., Philpott, D. J., & Sansonetti, P. J. (2008). The pattern-recognition molecule Nod1 is localized at the plasma membrane at sites of bacterial interaction. *Cell Microbiol*, 10(2), 477-486. <https://doi.org/10.1111/j.1462-5822.2007.01062.x>
- Kumar, H., Pandey, S., Zou, J., Kumagai, Y., Takahashi, K., Akira, S., & Kawai, T. (2011). NLRC5 deficiency does not influence cytokine induction by virus and bacteria infections. *J Immunol*, 186(2), 994-1000. <https://doi.org/10.4049/jimmunol.1002094>

- Kumar, V., & McNerney, M. E. (2005). A new self: MHC-class-I-independent natural-killer-cell self-tolerance. *Nat Rev Immunol*, 5(5), 363-374. <https://doi.org/10.1038/nri1603>
- Laherty, C. D., Yang, W. M., Sun, J. M., Davie, J. R., Seto, E., & Eisenman, R. N. (1997). Histone deacetylases associated with the mSin3 corepressor mediate mad transcriptional repression. *Cell*, 89(3), 349-356. [https://doi.org/10.1016/s0092-8674\(00\)80215-9](https://doi.org/10.1016/s0092-8674(00)80215-9)
- Lappas, M. (2014). NOD1 expression is increased in the adipose tissue of women with gestational diabetes. *J Endocrinol*, 222(1), 99-112. <https://doi.org/10.1530/JOE-14-0179>
- Laukens, D., Brinkman, B. M., Raes, J., De Vos, M., & Vandenabeele, P. (2016). Heterogeneity of the gut microbiome in mice: guidelines for optimizing experimental design. *FEMS Microbiol Rev*, 40(1), 117-132. <https://doi.org/10.1093/femsre/fuv036>
- Lautz, K., Damm, A., Menning, M., Wenger, J., Adam, A. C., Zigrino, P., Kremmer, E., & Kufer, T. A. (2012). NLRP10 enhances Shigella-induced pro-inflammatory responses. *Cell Microbiol*, 14(10), 1568-1583. <https://doi.org/10.1111/j.1462-5822.2012.01822.x>
- Lech, M., Avila-Ferrufino, A., Skuginna, V., Susanti, H. E., & Anders, H. J. (2010). Quantitative expression of RIG-like helicase, NOD-like receptor and inflammasome-related mRNAs in humans and mice. *Int Immunol*, 22(9), 717-728. <https://doi.org/10.1093/intimm/dxq058>
- Lee, C. H., Lui, D. T. W., & Lam, K. S. L. (2021). Adipocyte Fatty Acid-Binding Protein, Cardiovascular Diseases and Mortality. *Front Immunol*, 12, 589206. <https://doi.org/10.3389/fimmu.2021.589206>
- Lehrke, M., & Lazar, M. A. (2005). The many faces of PPARgamma. *Cell*, 123(6), 993-999. <https://doi.org/10.1016/j.cell.2005.11.026>
- Lei, Y., Wen, H., Yu, Y., Taxman, D. J., Zhang, L., Widman, D. G., Swanson, K. V., Wen, K. W., Damania, B., Moore, C. B., Giguere, P. M., Siderovski, D. P., Hiscott, J., Razani, B., Semenkovich, C. F., Chen, X., & Ting, J. P. (2012). The mitochondrial proteins NLRX1 and TUFM form a complex that regulates type I interferon and autophagy. *Immunity*, 36(6), 933-946. <https://doi.org/10.1016/j.immuni.2012.03.025>
- Leone, P., Shin, E. C., Perosa, F., Vacca, A., Dammacco, F., & Racanelli, V. (2013). MHC class I antigen processing and presenting machinery: organization, function, and defects in tumor cells. *J Natl Cancer Inst*, 105(16), 1172-1187. <https://doi.org/10.1093/jnci/djt184>
- Li, H., Liu, F., Lu, J., Shi, J., Guan, J., Yan, F., Li, B., & Huo, G. (2020). Probiotic Mixture of Lactobacillus plantarum Strains Improves Lipid Metabolism and Gut Microbiota Structure in High Fat Diet-Fed Mice. *Front Microbiol*, 11, 512. <https://doi.org/10.3389/fmicb.2020.00512>
- Li, J., Liu, Y., Rhee, H. S., Ghosh, S. K., Bai, L., Pugh, B. F., & Gilmour, D. S. (2013). Kinetic competition between elongation rate and binding of NELF controls promoter-proximal pausing. *Mol Cell*, 50(5), 711-722. <https://doi.org/10.1016/j.molcel.2013.05.016>
- Li, L., Xu, T., Huang, C., Peng, Y., & Li, J. (2014). NLRC5 mediates cytokine secretion in RAW264.7 macrophages and modulated by the JAK2/STAT3 pathway. *Inflammation*, 37(3), 835-847. <https://doi.org/10.1007/s10753-013-9804-y>
- Lich, J. D., Williams, K. L., Moore, C. B., Arthur, J. C., Davis, B. K., Taxman, D. J., & Ting, J. P. (2007). Monarch-1 suppresses non-canonical NF-kappaB activation and p52-dependent chemokine expression in monocytes. *J Immunol*, 178(3), 1256-1260. <https://doi.org/10.4049/jimmunol.178.3.1256>

- Lin, X., Peng, C., Greenbaum, J., Li, Z. F., Wu, K. H., Ao, Z. X., Zhang, T., Shen, J., & Deng, H. W. (2018). Identifying potentially common genes between dyslipidemia and osteoporosis using novel analytical approaches. *Mol Genet Genomics*, 293(3), 711-723. <https://doi.org/10.1007/s00438-017-1414-1>
- Lindhorst, A., Raulien, N., Wieghofer, P., Eilers, J., Rossi, F. M. V., Bechmann, I., & Gericke, M. (2021). Adipocyte death triggers a pro-inflammatory response and induces metabolic activation of resident macrophages. *Cell Death Dis*, 12(6), 579. <https://doi.org/10.1038/s41419-021-03872-9>
- Ling, A., Soares, F., Croitoru, D. O., Tattoli, I., Carneiro, L. A., Boniotto, M., Benko, S., Philpott, D. J., & Girardin, S. E. (2012). Post-transcriptional inhibition of luciferase reporter assays by the Nod-like receptor proteins NLRX1 and NLRC3. *J Biol Chem*, 287(34), 28705-28716. <https://doi.org/10.1074/jbc.M111.333146>
- Luan, P., Jian, W., Xu, X., Kou, W., Yu, Q., Hu, H., Li, D., Wang, W., Feinberg, M. W., Zhuang, J., Xu, Y., & Peng, W. (2019). NLRC5 inhibits neointima formation following vascular injury and directly interacts with PPARgamma. *Nat Commun*, 10(1), 2882. <https://doi.org/10.1038/s41467-019-10784-y>
- Luan, P., Zhuang, J., Zou, J., Li, H., Shuai, P., Xu, X., Zhao, Y., Kou, W., Ji, S., Peng, A., Xu, Y., Su, Q., Jian, W., & Peng, W. (2018). NLRC5 deficiency ameliorates diabetic nephropathy through alleviating inflammation. *FASEB J*, 32(2), 1070-1084. <https://doi.org/10.1096/fj.201700511RR>
- Luck, H., Tsai, S., Chung, J., Clemente-Casares, X., Ghazarian, M., Revelo, X. S., Lei, H., Luk, C. T., Shi, S. Y., Surendra, A., Copeland, J. K., Ahn, J., Prescott, D., Rasmussen, B. A., Chng, M. H., Engleman, E. G., Girardin, S. E., Lam, T. K., Croitoru, K., . . . Winer, D. A. (2015). Regulation of obesity-related insulin resistance with gut anti-inflammatory agents. *Cell Metab*, 21(4), 527-542. <https://doi.org/10.1016/j.cmet.2015.03.001>
- Ludigs, K., Seguin-Estevez, Q., Lemeille, S., Ferrero, I., Rota, G., Chelbi, S., Mattmann, C., MacDonald, H. R., Reith, W., & Guarda, G. (2015). NLRC5 exclusively transactivates MHC class I and related genes through a distinctive SXY module. *PLoS Genet*, 11(3), e1005088. <https://doi.org/10.1371/journal.pgen.1005088>
- Ma, H. L., Zhao, X. F., Chen, G. Z., Fang, R. H., & Zhang, F. R. (2016). Silencing NLRC5 inhibits extracellular matrix expression in keloid fibroblasts via inhibition of transforming growth factor-beta1/Smad signaling pathway. *Biomed Pharmacother*, 83, 1016-1021. <https://doi.org/10.1016/j.biopha.2016.08.012>
- Ma, S. R., & Xie, X. W. (2017). NLRC5 deficiency promotes myocardial damage induced by high fat diet in mice through activating TLR4/NF-kappaB. *Biomed Pharmacother*, 91, 755-766. <https://doi.org/10.1016/j.biopha.2017.03.062>
- MacDougald, O. A., & Lane, M. D. (1995). Transcriptional regulation of gene expression during adipocyte differentiation. *Annu Rev Biochem*, 64, 345-373. <https://doi.org/10.1146/annurev.bi.64.070195.002021>
- Mansen, A., Guardiola-Diaz, H., Rafter, J., Branting, C., & Gustafsson, J. A. (1996). Expression of the peroxisome proliferator-activated receptor (PPAR) in the mouse colonic mucosa. *Biochem Biophys Res Commun*, 222(3), 844-851. <https://doi.org/10.1006/bbrc.1996.0832>
- Marx, N., Bourcier, T., Sukhova, G. K., Libby, P., & Plutzky, J. (1999). PPARgamma activation in human endothelial cells increases plasminogen activator inhibitor type-1 expression: PPARgamma as a potential mediator in vascular disease. *Arterioscler Thromb Vasc Biol*, 19(3), 546-551. <https://doi.org/10.1161/01.atv.19.3.546>

- Matarese, V., & Bernlohr, D. A. (1988). Purification of murine adipocyte lipid-binding protein. Characterization as a fatty acid- and retinoic acid-binding protein. *J Biol Chem*, 263(28), 14544-14551. <https://www.ncbi.nlm.nih.gov/pubmed/2844775>
- Mathur, M., Tucker, P. W., & Samuels, H. H. (2001). PSF is a novel corepressor that mediates its effect through Sin3A and the DNA binding domain of nuclear hormone receptors. *Mol Cell Biol*, 21(7), 2298-2311. <https://doi.org/10.1128/MCB.21.7.2298-2311.2001>
- Matzinger, P. (2002). The danger model: a renewed sense of self. *Science*, 296(5566), 301-305. <https://doi.org/10.1126/science.1071059>
- McKenna, N. J., & O'Malley, B. W. (2002). Combinatorial control of gene expression by nuclear receptors and coregulators. *Cell*, 108(4), 465-474. [https://doi.org/10.1016/s0092-8674\(02\)00641-4](https://doi.org/10.1016/s0092-8674(02)00641-4)
- Medrikova, D., Jilkova, Z. M., Bardova, K., Janovska, P., Rossmeisl, M., & Kopecky, J. (2012). Sex differences during the course of diet-induced obesity in mice: adipose tissue expandability and glycemic control. *Int J Obes (Lond)*, 36(2), 262-272. <https://doi.org/10.1038/ijo.2011.87>
- Meeks, K. A. C., Henneman, P., Venema, A., Burr, T., Galbete, C., Danquah, I., Schulze, M. B., Mockenhaupt, F. P., Owusu-Dabo, E., Rotimi, C. N., Addo, J., Smeeth, L., Bahendeka, S., Spranger, J., Mannens, M., Zafarmand, M. H., Agyemang, C., & Adeyemo, A. (2017). An epigenome-wide association study in whole blood of measures of adiposity among Ghanaians: the RODAM study. *Clin Epigenetics*, 9, 103. <https://doi.org/10.1186/s13148-017-0403-x>
- Meissner, T. B., Li, A., Biswas, A., Lee, K. H., Liu, Y. J., Bayir, E., Iliopoulos, D., van den Elsen, P. J., & Kobayashi, K. S. (2010). NLR family member NLRC5 is a transcriptional regulator of MHC class I genes. *Proc Natl Acad Sci U S A*, 107(31), 13794-13799. <https://doi.org/10.1073/pnas.1008684107>
- Meissner, T. B., Li, A., Liu, Y. J., Gagnon, E., & Kobayashi, K. S. (2012a). The nucleotide-binding domain of NLRC5 is critical for nuclear import and transactivation activity. *Biochem Biophys Res Commun*, 418(4), 786-791. <https://doi.org/10.1016/j.bbrc.2012.01.104>
- Meissner, T. B., Liu, Y. J., Lee, K. H., Li, A., Biswas, A., van Eggermond, M. C., van den Elsen, P. J., & Kobayashi, K. S. (2012b). NLRC5 cooperates with the RFX transcription factor complex to induce MHC class I gene expression. *J Immunol*, 188(10), 4951-4958. <https://doi.org/10.4049/jimmunol.1103160>
- Meng, Q., Cai, C., Sun, T., Wang, Q., Xie, W., Wang, R., & Cui, J. (2015). Reversible ubiquitination shapes NLRC5 function and modulates NF-kappaB activation switch. *J Cell Biol*, 211(5), 1025-1040. <https://doi.org/10.1083/jcb.201505091>
- Meng, Q. Q., Feng, Z. C., Zhang, X. L., Hu, L. Q., Wang, M., Zhang, H. F., & Li, S. M. (2019). PPAR-gamma Activation Exerts an Anti-inflammatory Effect by Suppressing the NLRP3 Inflammasome in Spinal Cord-Derived Neurons. *Mediators Inflamm*, 2019, 6386729. <https://doi.org/10.1155/2019/6386729>
- Mirza, N., Sowa, A. S., Lautz, K., & Kufer, T. A. (2019). NLRP10 Affects the Stability of Abin-1 To Control Inflammatory Responses. *J Immunol*, 202(1), 218-227. <https://doi.org/10.4049/jimmunol.1800334>
- Miyata, K. S., McCaw, S. E., Marcus, S. L., Rachubinski, R. A., & Capone, J. P. (1994). The peroxisome proliferator-activated receptor interacts with the retinoid X receptor in vivo. *Gene*, 148(2), 327-330. [https://doi.org/10.1016/0378-1119\(94\)90707-2](https://doi.org/10.1016/0378-1119(94)90707-2)
- Moore, C. B., Bergstralh, D. T., Duncan, J. A., Lei, Y., Morrison, T. E., Zimmermann, A. G., Accavitti-Loper, M. A., Madden, V. J., Sun, L., Ye, Z., Lich, J. D., Heise, M. T., Chen, Z., &

- Ting, J. P. (2008). NLRX1 is a regulator of mitochondrial antiviral immunity. *Nature*, 451(7178), 573-577. <https://doi.org/10.1038/nature06501>
- Moore, L. D., Le, T., & Fan, G. (2013). DNA methylation and its basic function. *Neuropsychopharmacology*, 38(1), 23-38. <https://doi.org/10.1038/npp.2012.112>
- Motta, V., Soares, F., Sun, T., & Philpott, D. J. (2015). NOD-like receptors: versatile cytosolic sentinels. *Physiol Rev*, 95(1), 149-178. <https://doi.org/10.1152/physrev.00009.2014>
- Motyan, J. A., Bagossi, P., Benko, S., & Tozser, J. (2013). A molecular model of the full-length human NOD-like receptor family CARD domain containing 5 (NLRC5) protein. *BMC Bioinformatics*, 14, 275. <https://doi.org/10.1186/1471-2105-14-275>
- Munoz-Planillo, R., Kuffa, P., Martinez-Colon, G., Smith, B. L., Rajendiran, T. M., & Nunez, G. (2013). K(+) efflux is the common trigger of NLRP3 inflammasome activation by bacterial toxins and particulate matter. *Immunity*, 38(6), 1142-1153. <https://doi.org/10.1016/j.immuni.2013.05.016>
- Murano, I., Barbatelli, G., Parisani, V., Latini, C., Muzzonigro, G., Castellucci, M., & Cinti, S. (2008). Dead adipocytes, detected as crown-like structures, are prevalent in visceral fat depots of genetically obese mice. *J Lipid Res*, 49(7), 1562-1568. <https://doi.org/10.1194/jlr.M800019-JLR200>
- Nagareddy, P. R., Kraakman, M., Masters, S. L., Stirzaker, R. A., Gorman, D. J., Grant, R. W., Dragoljevic, D., Hong, E. S., Abdel-Latif, A., Smyth, S. S., Choi, S. H., Korner, J., Bornfeldt, K. E., Fisher, E. A., Dixit, V. D., Tall, A. R., Goldberg, I. J., & Murphy, A. J. (2014). Adipose tissue macrophages promote myelopoiesis and monocyte in obesity. *Cell Metab*, 19(5), 821-835. <https://doi.org/10.1016/j.cmet.2014.03.029>
- Nagy, L., Kao, H. Y., Chakravarti, D., Lin, R. J., Hassig, C. A., Ayer, D. E., Schreiber, S. L., & Evans, R. M. (1997). Nuclear receptor repression mediated by a complex containing SMRT, mSin3A, and histone deacetylase. *Cell*, 89(3), 373-380. [https://doi.org/10.1016/s0092-8674\(00\)80218-4](https://doi.org/10.1016/s0092-8674(00)80218-4)
- Nakachi, Y., Yagi, K., Nikaido, I., Bono, H., Tonouchi, M., Schonbach, C., & Okazaki, Y. (2008). Identification of novel PPARgamma target genes by integrated analysis of ChIP-on-chip and microarray expression data during adipocyte differentiation. *Biochem Biophys Res Commun*, 372(2), 362-366. <https://doi.org/10.1016/j.bbrc.2008.05.037>
- Nechaev, S., Fargo, D. C., dos Santos, G., Liu, L., Gao, Y., & Adelman, K. (2010). Global analysis of short RNAs reveals widespread promoter-proximal stalling and arrest of Pol II in Drosophila. *Science*, 327(5963), 335-338. <https://doi.org/10.1126/science.1181421>
- Neerincx, A., Jakobshagen, K., Utermohlen, O., Buning, H., Steimle, V., & Kufer, T. A. (2014). The N-terminal domain of NLRC5 confers transcriptional activity for MHC class I and II gene expression. *J Immunol*, 193(6), 3090-3100. <https://doi.org/10.4049/jimmunol.1401065>
- Neerincx, A., Lautz, K., Menning, M., Kremmer, E., Zigrino, P., Hosel, M., Buning, H., Schwarzenbacher, R., & Kufer, T. A. (2010). A role for the human nucleotide-binding domain, leucine-rich repeat-containing family member NLRC5 in antiviral responses. *J Biol Chem*, 285(34), 26223-26232. <https://doi.org/10.1074/jbc.M110.109736>
- Neerincx, A., Rodriguez, G. M., Steimle, V., & Kufer, T. A. (2012). NLRC5 controls basal MHC class I gene expression in an MHC enhanceosome-dependent manner. *J Immunol*, 188(10), 4940-4950. <https://doi.org/10.4049/jimmunol.1103136>
- Ng, M., Fleming, T., Robinson, M., Thomson, B., Graetz, N., Margono, C., Mullany, E. C., Biryukov, S., Abbafati, C., Abera, S. F., Abraham, J. P., Abu-Rmeileh, N. M., Achoki, T., AlBuhairan, F. S., Alemu, Z. A., Alfonso, R., Ali, M. K., Ali, R., Guzman, N. A., . . . Gakidou, E. (2014). Global, regional, and national prevalence of overweight and

- obesity in children and adults during 1980-2013: a systematic analysis for the Global Burden of Disease Study 2013. *Lancet*, 384(9945), 766-781.
[https://doi.org/10.1016/S0140-6736\(14\)60460-8](https://doi.org/10.1016/S0140-6736(14)60460-8)
- Novikoff, A. B., Novikoff, P. M., Rosen, O. M., & Rubin, C. S. (1980). Organelle relationships in cultured 3T3-L1 preadipocytes. *J Cell Biol*, 87(1), 180-196.
<https://doi.org/10.1083/jcb.87.1.180>
- Odegaard, J. I., Ricardo-Gonzalez, R. R., Goforth, M. H., Morel, C. R., Subramanian, V., Mukundan, L., Red Eagle, A., Vats, D., Brombacher, F., Ferrante, A. W., & Chawla, A. (2007). Macrophage-specific PPARgamma controls alternative activation and improves insulin resistance. *Nature*, 447(7148), 1116-1120.
<https://doi.org/10.1038/nature05894>
- Olefsky, J. M., & Glass, C. K. (2010). Macrophages, inflammation, and insulin resistance. *Annu Rev Physiol*, 72, 219-246. <https://doi.org/10.1146/annurev-physiol-021909-135846>
- Pascual, G., Fong, A. L., Ogawa, S., Gamliel, A., Li, A. C., Perissi, V., Rose, D. W., Willson, T. M., Rosenfeld, M. G., & Glass, C. K. (2005). A SUMOylation-dependent pathway mediates transrepression of inflammatory response genes by PPAR-gamma. *Nature*, 437(7059), 759-763. <https://doi.org/10.1038/nature03988>
- Pchelintsev, N. A., Adams, P. D., & Nelson, D. M. (2016). Critical Parameters for Efficient Sonication and Improved Chromatin Immunoprecipitation of High Molecular Weight Proteins. *PLoS One*, 11(1), e0148023. <https://doi.org/10.1371/journal.pone.0148023>
- Peng, Y. Y., He, Y. H., Chen, C., Xu, T., Li, L., Ni, M. M., Meng, X. M., Huang, C., & Li, J. (2016). NLRC5 regulates cell proliferation, migration and invasion in hepatocellular carcinoma by targeting the Wnt/beta-catenin signaling pathway. *Cancer Lett*, 376(1), 10-21.
<https://doi.org/10.1016/j.canlet.2016.03.006>
- Petrilli, V., Papin, S., Dostert, C., Mayor, A., Martinon, F., & Tschopp, J. (2007). Activation of the NALP3 inflammasome is triggered by low intracellular potassium concentration. *Cell Death Differ*, 14(9), 1583-1589. <https://doi.org/10.1038/sj.cdd.4402195>
- Pettersson, U. S., Walden, T. B., Carlsson, P. O., Jansson, L., & Phillipson, M. (2012). Female mice are protected against high-fat diet induced metabolic syndrome and increase the regulatory T cell population in adipose tissue. *PLoS One*, 7(9), e46057.
<https://doi.org/10.1371/journal.pone.0046057>
- Poltorak, A., He, X., Smirnova, I., Liu, M. Y., Van Huffel, C., Du, X., Birdwell, D., Alejos, E., Silva, M., Galanos, C., Freudenberg, M., Ricciardi-Castagnoli, P., Layton, B., & Beutler, B. (1998). Defective LPS signaling in C3H/HeJ and C57BL/10ScCr mice: mutations in Tlr4 gene. *Science*, 282(5396), 2085-2088. <https://doi.org/10.1126/science.282.5396.2085>
- Prochnicki, T., Vasconcelos, M. B., Robinson, K. S., Mangan, M. S. J., De Graaf, D., Shkarina, K., Lovotti, M., Standke, L., Kaiser, R., Stahl, R., Duthie, F. G., Rothe, M., Antonova, K., Jenster, L. M., Lau, Z. H., Rosing, S., Mirza, N., Gottschild, C., Wachten, D., . . . Latz, E. (2023). Mitochondrial damage activates the NLRP10 inflammasome. *Nat Immunol*, 24(4), 595-603. <https://doi.org/10.1038/s41590-023-01451-y>
- Quast, C., Pruesse, E., Yilmaz, P., Gerken, J., Schweer, T., Yarza, P., Peplies, J., & Glockner, F. O. (2013). The SILVA ribosomal RNA gene database project: improved data processing and web-based tools. *Nucleic Acids Res*, 41(Database issue), D590-596.
<https://doi.org/10.1093/nar/gks1219>
- Rehwinkel, J., & Gack, M. U. (2020). RIG-I-like receptors: their regulation and roles in RNA sensing. *Nat Rev Immunol*, 20(9), 537-551. <https://doi.org/10.1038/s41577-020-0288-3>

- Ricote, M., Huang, J., Fajas, L., Li, A., Welch, J., Najib, J., Witztum, J. L., Auwerx, J., Palinski, W., & Glass, C. K. (1998). Expression of the peroxisome proliferator-activated receptor gamma (PPARgamma) in human atherosclerosis and regulation in macrophages by colony stimulating factors and oxidized low density lipoprotein. *Proc Natl Acad Sci U S A*, 95(13), 7614-7619. <https://doi.org/10.1073/pnas.95.13.7614>
- Robbins, G. R., Truax, A. D., Davis, B. K., Zhang, L., Brickey, W. J., & Ting, J. P. (2012). Regulation of class I major histocompatibility complex (MHC) by nucleotide-binding domain, leucine-rich repeat-containing (NLR) proteins. *J Biol Chem*, 287(29), 24294-24303. <https://doi.org/10.1074/jbc.M112.364604>
- Robinson, K. S., Teo, D. E. T., Tan, K. S., Toh, G. A., Ong, H. H., Lim, C. K., Lay, K., Au, B. V., Lew, T. S., Chu, J. J. H., Chow, V. T. K., Wang, Y., Zhong, F. L., & Reversade, B. (2020). Enteroviral 3C protease activates the human NLRP1 inflammasome in airway epithelia. *Science*, 370(6521). <https://doi.org/10.1126/science.aay2002>
- Rodriguez, G. M., Bobbala, D., Serrano, D., Mayhue, M., Champagne, A., Saucier, C., Steimle, V., Kufer, T. A., Menendez, A., Ramanathan, S., & Ilangumaran, S. (2016). NLRC5 elicits antitumor immunity by enhancing processing and presentation of tumor antigens to CD8(+) T lymphocytes. *Oncoimmunology*, 5(6), e1151593. <https://doi.org/10.1080/2162402X.2016.1151593>
- Rodriguez-Nunez, I., Caluag, T., Kirby, K., Rudick, C. N., Dziarski, R., & Gupta, D. (2017). Nod2 and Nod2-regulated microbiota protect BALB/c mice from diet-induced obesity and metabolic dysfunction. *Sci Rep*, 7(1), 548. <https://doi.org/10.1038/s41598-017-00484-2>
- Rosen, E. D., Hsu, C. H., Wang, X., Sakai, S., Freeman, M. W., Gonzalez, F. J., & Spiegelman, B. M. (2002). C/EBPalpha induces adipogenesis through PPARgamma: a unified pathway. *Genes Dev*, 16(1), 22-26. <https://doi.org/10.1101/gad.948702>
- Rosen, E. D., & MacDougald, O. A. (2006). Adipocyte differentiation from the inside out. *Nat Rev Mol Cell Biol*, 7(12), 885-896. <https://doi.org/10.1038/nrm2066>
- Rosen, E. D., Sarraf, P., Troy, A. E., Bradwin, G., Moore, K., Milstone, D. S., Spiegelman, B. M., & Mortensen, R. M. (1999). PPAR gamma is required for the differentiation of adipose tissue in vivo and in vitro. *Mol Cell*, 4(4), 611-617. [https://doi.org/10.1016/s1097-2765\(00\)80211-7](https://doi.org/10.1016/s1097-2765(00)80211-7)
- Ruiz-Ojeda, F. J., Ruperez, A. I., Gomez-Llorente, C., Gil, A., & Aguilera, C. M. (2016). Cell Models and Their Application for Studying Adipogenic Differentiation in Relation to Obesity: A Review. *Int J Mol Sci*, 17(7). <https://doi.org/10.3390/ijms17071040>
- Sandstrom, A., Mitchell, P. S., Goers, L., Mu, E. W., Lesser, C. F., & Vance, R. E. (2019). Functional degradation: A mechanism of NLRP1 inflammasome activation by diverse pathogen enzymes. *Science*, 364(6435). <https://doi.org/10.1126/science.aau1330>
- Sanjana, N. E., Shalem, O., & Zhang, F. (2014). Improved vectors and genome-wide libraries for CRISPR screening. *Nat Methods*, 11(8), 783-784. <https://doi.org/10.1038/nmeth.3047>
- Savage, D. B., Tan, G. D., Acerini, C. L., Jebb, S. A., Agostini, M., Gurnell, M., Williams, R. L., Umpleby, A. M., Thomas, E. L., Bell, J. D., Dixon, A. K., Dunne, F., Boiani, R., Cinti, S., Vidal-Puig, A., Karpe, F., Chatterjee, V. K., & O'Rahilly, S. (2003). Human metabolic syndrome resulting from dominant-negative mutations in the nuclear receptor peroxisome proliferator-activated receptor-gamma. *Diabetes*, 52(4), 910-917. <https://doi.org/10.2337/diabetes.52.4.910>
- Schertzer, J. D., & Klip, A. (2011). Give a NOD to insulin resistance. *Am J Physiol Endocrinol Metab*, 301(4), E585-586. <https://doi.org/10.1152/ajpendo.00362.2011>

- Schertzer, J. D., Tamrakar, A. K., Magalhaes, J. G., Pereira, S., Bilan, P. J., Fullerton, M. D., Liu, Z., Steinberg, G. R., Giacca, A., Philpott, D. J., & Klip, A. (2011). NOD1 activators link innate immunity to insulin resistance. *Diabetes*, *60*(9), 2206-2215. <https://doi.org/10.2337/db11-0004>
- Schroeder, F., Petrescu, A. D., Huang, H., Atshaves, B. P., McIntosh, A. L., Martin, G. G., Hostetler, H. A., Vespa, A., Landrock, D., Landrock, K. K., Payne, H. R., & Kier, A. B. (2008). Role of fatty acid binding proteins and long chain fatty acids in modulating nuclear receptors and gene transcription. *Lipids*, *43*(1), 1-17. <https://doi.org/10.1007/s11745-007-3111-z>
- Seimandi, M., Lemaire, G., Pillon, A., Perrin, A., Carlavan, I., Voegel, J. J., Vignon, F., Nicolas, J. C., & Balaguer, P. (2005). Differential responses of PPARalpha, PPARdelta, and PPARgamma reporter cell lines to selective PPAR synthetic ligands. *Anal Biochem*, *344*(1), 8-15. <https://doi.org/10.1016/j.ab.2005.06.010>
- Serena, C., Keiran, N., Ceperuelo-Mallafre, V., Ejarque, M., Fradera, R., Roche, K., Nunez-Roa, C., Vendrell, J., & Fernandez-Veledo, S. (2016). Obesity and Type 2 Diabetes Alters the Immune Properties of Human Adipose Derived Stem Cells. *Stem Cells*, *34*(10), 2559-2573. <https://doi.org/10.1002/stem.2429>
- Shalem, O., Sanjana, N. E., Hartenian, E., Shi, X., Scott, D. A., Mikkelsen, T., Heckl, D., Ebert, B. L., Root, D. E., Doench, J. G., & Zhang, F. (2014). Genome-scale CRISPR-Cas9 knockout screening in human cells. *Science*, *343*(6166), 84-87. <https://doi.org/10.1126/science.1247005>
- Shao, D., Rangwala, S. M., Bailey, S. T., Krakow, S. L., Reginato, M. J., & Lazar, M. A. (1998). Interdomain communication regulating ligand binding by PPAR-gamma. *Nature*, *396*(6709), 377-380. <https://doi.org/10.1038/24634>
- Sharma, A., Singh, S., Mishra, A., Rai, A. K., Ahmad, I., Ahmad, S., Gulzar, F., Schertzer, J. D., Shrivastava, A., & Tamrakar, A. K. (2022). Insulin resistance corresponds with a progressive increase in NOD1 in high fat diet-fed mice. *Endocrine*, *76*(2), 282-293. <https://doi.org/10.1007/s12020-022-02995-z>
- Shi, H., Kokoeva, M. V., Inouye, K., Tzameli, I., Yin, H., & Flier, J. S. (2006). TLR4 links innate immunity and fatty acid-induced insulin resistance. *J Clin Invest*, *116*(11), 3015-3025. <https://doi.org/10.1172/JCI28898>
- Shimada, K., Porritt, R. A., Markman, J. L., O'Rourke, J. G., Wakita, D., Noval Rivas, M., Ogawa, C., Kozhaya, L., Martins, G. A., Unutmaz, D., Baloh, R. H., Crother, T. R., Chen, S., & Arditi, M. (2018). T-Cell-Intrinsic Receptor Interacting Protein 2 Regulates Pathogenic T Helper 17 Cell Differentiation. *Immunity*, *49*(5), 873-885 e877. <https://doi.org/10.1016/j.immuni.2018.08.022>
- Shiny, A., Regin, B., Balachandar, V., Gokulakrishnan, K., Mohan, V., Babu, S., & Balasubramanyam, M. (2013). Convergence of innate immunity and insulin resistance as evidenced by increased nucleotide oligomerization domain (NOD) expression and signaling in monocytes from patients with type 2 diabetes. *Cytokine*, *64*(2), 564-570. <https://doi.org/10.1016/j.cyto.2013.08.003>
- Shoelson, S. E., Lee, J., & Yuan, M. (2003). Inflammation and the IKK beta/I kappa B/NF-kappa B axis in obesity- and diet-induced insulin resistance. *Int J Obes Relat Metab Disord*, *27 Suppl 3*, S49-52. <https://doi.org/10.1038/sj.ijo.0802501>
- Shukla, A., Cloutier, M., Appiya Santharam, M., Ramanathan, S., & Ilangumaran, S. (2021). The MHC Class-I Transactivator NLRC5: Implications to Cancer Immunology and Potential Applications to Cancer Immunotherapy. *Int J Mol Sci*, *22*(4). <https://doi.org/10.3390/ijms22041964>

- Silverstein, R. A., & Ekwall, K. (2005). Sin3: a flexible regulator of global gene expression and genome stability. *Curr Genet*, 47(1), 1-17. <https://doi.org/10.1007/s00294-004-0541-5>
- Singh, K., Sripada, L., Lipatova, A., Roy, M., Prajapati, P., Gohel, D., Bhatelia, K., Chumakov, P. M., & Singh, R. (2018). NLRX1 resides in mitochondrial RNA granules and regulates mitochondrial RNA processing and bioenergetic adaptation. *Biochim Biophys Acta Mol Cell Res*, 1865(9), 1260-1276. <https://doi.org/10.1016/j.bbamcr.2018.06.008>
- Snaka, T., & Fasel, N. (2020). Behind the Scenes: Nod-Like Receptor X1 Controls Inflammation and Metabolism. *Front Cell Infect Microbiol*, 10, 609812. <https://doi.org/10.3389/fcimb.2020.609812>
- Sokolova, M., Sjaastad, I., Louwe, M. C., Alfsnes, K., Aronsen, J. M., Zhang, L., Haugstad, S. B., Bendiksen, B. A., Ogaard, J., Bliksoen, M., Lien, E., Berge, R. K., Aukrust, P., Ranheim, T., & Yndestad, A. (2019). NLRP3 Inflammasome Promotes Myocardial Remodeling During Diet-Induced Obesity. *Front Immunol*, 10, 1621. <https://doi.org/10.3389/fimmu.2019.01621>
- Staehli, F., Ludigs, K., Heinz, L. X., Seguin-Estevez, Q., Ferrero, I., Braun, M., Schroder, K., Rebsamen, M., Tardivel, A., Mattmann, C., MacDonald, H. R., Romero, P., Reith, W., Guarda, G., & Tschopp, J. (2012). NLRC5 deficiency selectively impairs MHC class I-dependent lymphocyte killing by cytotoxic T cells. *J Immunol*, 188(8), 3820-3828. <https://doi.org/10.4049/jimmunol.1102671>
- Steimle, V., Otten, L. A., Zufferey, M., & Mach, B. (1993). Complementation cloning of an MHC class II transactivator mutated in hereditary MHC class II deficiency (or bare lymphocyte syndrome). *Cell*, 75(1), 135-146. <https://www.ncbi.nlm.nih.gov/pubmed/8402893>
- Stemmer, M., Thumberger, T., Del Sol Keyer, M., Wittbrodt, J., & Mateo, J. L. (2015). CCTop: An Intuitive, Flexible and Reliable CRISPR/Cas9 Target Prediction Tool. *PLoS One*, 10(4), e0124633. <https://doi.org/10.1371/journal.pone.0124633>
- Stewart, S. A., Dykxhoorn, D. M., Palliser, D., Mizuno, H., Yu, E. Y., An, D. S., Sabatini, D. M., Chen, I. S., Hahn, W. C., Sharp, P. A., Weinberg, R. A., & Novina, C. D. (2003). Lentivirus-delivered stable gene silencing by RNAi in primary cells. *RNA*, 9(4), 493-501. <https://doi.org/10.1261/rna.2192803>
- Stienstra, R., van Diepen, J. A., Tack, C. J., Zaki, M. H., van de Veerdonk, F. L., Perera, D., Neale, G. A., Hooiveld, G. J., Hijmans, A., Vroegrijk, I., van den Berg, S., Romijn, J., Rensen, P. C., Joosten, L. A., Netea, M. G., & Kanneganti, T. D. (2011). Inflammasome is a central player in the induction of obesity and insulin resistance. *Proc Natl Acad Sci U S A*, 108(37), 15324-15329. <https://doi.org/10.1073/pnas.1100255108>
- Stokman, G., Kors, L., Bakker, P. J., Rampanelli, E., Claessen, N., Teske, G. J. D., Butter, L., van Andel, H., van den Bergh Weerman, M. A., Larsen, P. W. B., Dessing, M. C., Zuurbier, C. J., Girardin, S. E., Florquin, S., & Leemans, J. C. (2017). NLRX1 dampens oxidative stress and apoptosis in tissue injury via control of mitochondrial activity. *J Exp Med*, 214(8), 2405-2420. <https://doi.org/10.1084/jem.20161031>
- Stubbins, R. E., Holcomb, V. B., Hong, J., & Nunez, N. P. (2012). Estrogen modulates abdominal adiposity and protects female mice from obesity and impaired glucose tolerance. *Eur J Nutr*, 51(7), 861-870. <https://doi.org/10.1007/s00394-011-0266-4>
- Sun, D., Xu, J., Zhang, W., Song, C., Gao, C., He, Y., & Shang, Y. (2022). Negative regulator NLRC3: Its potential role and regulatory mechanism in immune response and immune-related diseases. *Front Immunol*, 13, 1012459. <https://doi.org/10.3389/fimmu.2022.1012459>

- Sun, K., Tordjman, J., Clement, K., & Scherer, P. E. (2013). Fibrosis and adipose tissue dysfunction. *Cell Metab*, 18(4), 470-477. <https://doi.org/10.1016/j.cmet.2013.06.016>
- Sun, T., Ferrero, R. L., Girardin, S. E., Gommerman, J. L., & Philpott, D. J. (2019). NLRC5 deficiency has a moderate impact on immunodominant CD8(+) T-cell responses during rotavirus infection of adult mice. *Immunol Cell Biol*, 97(6), 552-562. <https://doi.org/10.1111/imcb.12244>
- Tachibana, K., Kobayashi, Y., Tanaka, T., Tagami, M., Sugiyama, A., Katayama, T., Ueda, C., Yamasaki, D., Ishimoto, K., Sumitomo, M., Uchiyama, Y., Kohro, T., Sakai, J., Hamakubo, T., Kodama, T., & Doi, T. (2005). Gene expression profiling of potential peroxisome proliferator-activated receptor (PPAR) target genes in human hepatoblastoma cell lines inducibly expressing different PPAR isoforms. *Nucl Recept*, 3, 3. <https://doi.org/10.1186/1478-1336-3-3>
- Tanaka, T., Takeno, T., Watanabe, Y., Uchiyama, Y., Murakami, T., Yamashita, H., Suzuki, A., Aoi, R., Iwanari, H., Jiang, S. Y., Naito, M., Tachibana, K., Doi, T., Shulman, A. I., Mangelsdorf, D. J., Reiter, R., Auwerx, J., Hamakubo, T., & Kodama, T. (2002). The generation of monoclonal antibodies against human peroxisome proliferator-activated receptors (PPARs). *J Atheroscler Thromb*, 9(5), 233-242. <https://doi.org/10.5551/jat.9.233>
- Tang, Q. Q., & Lane, M. D. (2012). Adipogenesis: from stem cell to adipocyte. *Annu Rev Biochem*, 81, 715-736. <https://doi.org/10.1146/annurev-biochem-052110-115718>
- Tattoli, I., Travassos, L. H., Carneiro, L. A., Magalhaes, J. G., & Girardin, S. E. (2007). The Nodosome: Nod1 and Nod2 control bacterial infections and inflammation. *Semin Immunopathol*, 29(3), 289-301. <https://doi.org/10.1007/s00281-007-0083-2>
- Ting, J. P., Lovering, R. C., Alnemri, E. S., Bertin, J., Boss, J. M., Davis, B. K., Flavell, R. A., Girardin, S. E., Godzik, A., Harton, J. A., Hoffman, H. M., Hugot, J. P., Inohara, N., Mackenzie, A., Maltais, L. J., Nunez, G., Ogura, Y., Otten, L. A., Philpott, D., . . . Ward, P. A. (2008). The NLR gene family: a standard nomenclature. *Immunity*, 28(3), 285-287. <https://doi.org/10.1016/j.immuni.2008.02.005>
- Tong, Y., Cui, J., Li, Q., Zou, J., Wang, H. Y., & Wang, R. F. (2012). Enhanced TLR-induced NF-kappaB signaling and type I interferon responses in NLRC5 deficient mice. *Cell Res*, 22(5), 822-835. <https://doi.org/10.1038/cr.2012.53>
- Tontonoz, P., Graves, R. A., Budavari, A. I., Erdjument-Bromage, H., Lui, M., Hu, E., Tempst, P., & Spiegelman, B. M. (1994). Adipocyte-specific transcription factor ARF6 is a heterodimeric complex of two nuclear hormone receptors, PPAR gamma and RXR alpha. *Nucleic Acids Res*, 22(25), 5628-5634. <https://doi.org/10.1093/nar/22.25.5628>
- Tontonoz, P., Hu, E., & Spiegelman, B. M. (1994). Stimulation of adipogenesis in fibroblasts by PPAR gamma 2, a lipid-activated transcription factor. *Cell*, 79(7), 1147-1156. [https://doi.org/10.1016/0092-8674\(94\)90006-x](https://doi.org/10.1016/0092-8674(94)90006-x)
- Tourneur, E., Ben Mkaddem, S., Chassin, C., Bens, M., Goujon, J. M., Charles, N., Pellefigues, C., Aloulou, M., Hertig, A., Monteiro, R. C., Girardin, S. E., Philpott, D. J., Rondeau, E., Elbim, C., Werts, C., & Vandewalle, A. (2013). Cyclosporine A impairs nucleotide binding oligomerization domain (Nod1)-mediated innate antibacterial renal defenses in mice and human transplant recipients. *PLoS Pathog*, 9(1), e1003152. <https://doi.org/10.1371/journal.ppat.1003152>
- Traba, J., & Sack, M. N. (2017). The role of caloric load and mitochondrial homeostasis in the regulation of the NLRP3 inflammasome. *Cell Mol Life Sci*, 74(10), 1777-1791. <https://doi.org/10.1007/s00018-016-2431-7>

- Triantafilou, K., Kar, S., van Kuppeveld, F. J., & Triantafilou, M. (2013). Rhinovirus-induced calcium flux triggers NLRP3 and NLRC5 activation in bronchial cells. *Am J Respir Cell Mol Biol*, 49(6), 923-934. <https://doi.org/10.1165/rcmb.2013-0032OC>
- Truax, A. D., Chen, L., Tam, J. W., Cheng, N., Guo, H., Koblansky, A. A., Chou, W. C., Wilson, J. E., Brickey, W. J., Petrucelli, A., Liu, R., Cooper, D. E., Koenigsnecht, M. J., Young, V. B., Netea, M. G., Stienstra, R., Sartor, R. B., Montgomery, S. A., Coleman, R. A., & Ting, J. P. (2018). The Inhibitory Innate Immune Sensor NLRP12 Maintains a Threshold against Obesity by Regulating Gut Microbiota Homeostasis. *Cell Host Microbe*, 24(3), 364-378 e366. <https://doi.org/10.1016/j.chom.2018.08.009>
- Tugwood, J. D., Issemann, I., Anderson, R. G., Bundell, K. R., McPheat, W. L., & Green, S. (1992). The mouse peroxisome proliferator activated receptor recognizes a response element in the 5' flanking sequence of the rat acyl CoA oxidase gene. *EMBO J*, 11(2), 433-439. <https://doi.org/10.1002/j.1460-2075.1992.tb05072.x>
- Tuladhar, R., Yeu, Y., Tyler Piazza, J., Tan, Z., Rene Clemenceau, J., Wu, X., Barrett, Q., Herbert, J., Mathews, D. H., Kim, J., Hyun Hwang, T., & Lum, L. (2019). CRISPR-Cas9-based mutagenesis frequently provokes on-target mRNA misregulation. *Nat Commun*, 10(1), 4056. <https://doi.org/10.1038/s41467-019-12028-5>
- Umemoto, T., & Fujiki, Y. (2012). Ligand-dependent nucleo-cytoplasmic shuttling of peroxisome proliferator-activated receptors, PPARalpha and PPARgamma. *Genes Cells*, 17(7), 576-596. <https://doi.org/10.1111/j.1365-2443.2012.01607.x>
- Uysal, K. T., Scheja, L., Wiesbrock, S. M., Bonner-Weir, S., & Hotamisligil, G. S. (2000). Improved glucose and lipid metabolism in genetically obese mice lacking aP2. *Endocrinology*, 141(9), 3388-3396. <https://doi.org/10.1210/endo.141.9.7637>
- van den Elsen, P. J., Gobin, S. J., van Eggermond, M. C., & Peijnenburg, A. (1998a). Regulation of MHC class I and II gene transcription: differences and similarities. *Immunogenetics*, 48(3), 208-221. <https://doi.org/10.1007/s002510050425>
- van den Elsen, P. J., Peijnenburg, A., van Eggermond, M. C., & Gobin, S. J. (1998b). Shared regulatory elements in the promoters of MHC class I and class II genes. *Immunol Today*, 19(7), 308-312. [https://doi.org/10.1016/s0167-5699\(98\)01287-0](https://doi.org/10.1016/s0167-5699(98)01287-0)
- Vandanmagsar, B., Youm, Y. H., Ravussin, A., Galgani, J. E., Stadler, K., Mynatt, R. L., Ravussin, E., Stephens, J. M., & Dixit, V. D. (2011). The NLRP3 inflammasome instigates obesity-induced inflammation and insulin resistance. *Nat Med*, 17(2), 179-188. <https://doi.org/10.1038/nm.2279>
- Vara, D., Morell, C., Rodriguez-Henche, N., & Diaz-Laviada, I. (2013). Involvement of PPARgamma in the antitumoral action of cannabinoids on hepatocellular carcinoma. *Cell Death Dis*, 4, e618. <https://doi.org/10.1038/cddis.2013.141>
- Vidal-Puig, A., Jimenez-Linan, M., Lowell, B. B., Hamann, A., Hu, E., Spiegelman, B., Flier, J. S., & Moller, D. E. (1996). Regulation of PPAR gamma gene expression by nutrition and obesity in rodents. *J Clin Invest*, 97(11), 2553-2561. <https://doi.org/10.1172/JCI118703>
- Vidal-Puig, A. J., Considine, R. V., Jimenez-Linan, M., Werman, A., Pories, W. J., Caro, J. F., & Flier, J. S. (1997). Peroxisome proliferator-activated receptor gene expression in human tissues. Effects of obesity, weight loss, and regulation by insulin and glucocorticoids. *J Clin Invest*, 99(10), 2416-2422. <https://doi.org/10.1172/JCI119424>
- Vilaysane, A., Chun, J., Seamone, M. E., Wang, W., Chin, R., Hirota, S., Li, Y., Clark, S. A., Tschopp, J., Trpkov, K., Hemmelgarn, B. R., Beck, P. L., & Muruve, D. A. (2010). The NLRP3 inflammasome promotes renal inflammation and contributes to CKD. *J Am Soc Nephrol*, 21(10), 1732-1744. <https://doi.org/10.1681/ASN.2010020143>

- Vladimer, G. I., Marty-Roix, R., Ghosh, S., Weng, D., & Lien, E. (2013). Inflammasomes and host defenses against bacterial infections. *Curr Opin Microbiol*, *16*(1), 23-31. <https://doi.org/10.1016/j.mib.2012.11.008>
- Wang, C., Shi, J., Xu, J., Fu, Q., Ding, Y., Yang, J., Liu, B., Gao, Q., Qin, J., & Liang, C. (2022). NLRC3 High Expression Represents a Novel Predictor for Positive Overall Survival Correlated With CCL5 and CXCL9 in HCC Patients. *Front Oncol*, *12*, 815326. <https://doi.org/10.3389/fonc.2022.815326>
- Wang, F., Mullican, S. E., DiSpirito, J. R., Peed, L. C., & Lazar, M. A. (2013). Lipoatrophy and severe metabolic disturbance in mice with fat-specific deletion of PPARgamma. *Proc Natl Acad Sci U S A*, *110*(46), 18656-18661. <https://doi.org/10.1073/pnas.1314863110>
- Wang, L., Manji, G. A., Grenier, J. M., Al-Garawi, A., Merriam, S., Lora, J. M., Geddes, B. J., Briskin, M., DiStefano, P. S., & Bertin, J. (2002). PYPAF7, a novel PYRIN-containing Apaf1-like protein that regulates activation of NF-kappa B and caspase-1-dependent cytokine processing. *J Biol Chem*, *277*(33), 29874-29880. <https://doi.org/10.1074/jbc.M203915200>
- Wang, N. D., Finegold, M. J., Bradley, A., Ou, C. N., Abdelsayed, S. V., Wilde, M. D., Taylor, L. R., Wilson, D. R., & Darlington, G. J. (1995). Impaired energy homeostasis in C/EBP alpha knockout mice. *Science*, *269*(5227), 1108-1112. <https://doi.org/10.1126/science.7652557>
- Wang, Y., Hasegawa, M., Imamura, R., Kinoshita, T., Kondo, C., Konaka, K., & Suda, T. (2004). PYNOD, a novel Apaf-1/CED4-like protein is an inhibitor of ASC and caspase-1. *Int Immunol*, *16*(6), 777-786. <https://doi.org/10.1093/intimm/dxh081>
- Wang, Y., Qi, W., Song, G., Pang, S., Peng, Z., Li, Y., & Wang, P. (2020). High-Fructose Diet Increases Inflammatory Cytokines and Alters Gut Microbiota Composition in Rats. *Mediators Inflamm*, *2020*, 6672636. <https://doi.org/10.1155/2020/6672636>
- Weisberg, S. P., McCann, D., Desai, M., Rosenbaum, M., Leibel, R. L., & Ferrante, A. W., Jr. (2003). Obesity is associated with macrophage accumulation in adipose tissue. *J Clin Invest*, *112*(12), 1796-1808. <https://doi.org/10.1172/JCI19246>
- Wellen, K. E., & Hotamisligil, G. S. (2005). Inflammation, stress, and diabetes. *J Clin Invest*, *115*(5), 1111-1119. <https://doi.org/10.1172/JCI25102>
- Wen, H., Gris, D., Lei, Y., Jha, S., Zhang, L., Huang, M. T., Brickey, W. J., & Ting, J. P. (2011). Fatty acid-induced NLRP3-ASC inflammasome activation interferes with insulin signaling. *Nat Immunol*, *12*(5), 408-415. <https://doi.org/10.1038/ni.2022>
- Wen, Y. D., Perissi, V., Staszewski, L. M., Yang, W. M., Krones, A., Glass, C. K., Rosenfeld, M. G., & Seto, E. (2000). The histone deacetylase-3 complex contains nuclear receptor corepressors. *Proc Natl Acad Sci U S A*, *97*(13), 7202-7207. <https://doi.org/10.1073/pnas.97.13.7202>
- Williams, K. L., Lich, J. D., Duncan, J. A., Reed, W., Rallabhandi, P., Moore, C., Kurtz, S., Coffield, V. M., Accavitti-Loper, M. A., Su, L., Vogel, S. N., Braunstein, M., & Ting, J. P. (2005). The CATERPILLER protein monarch-1 is an antagonist of toll-like receptor-, tumor necrosis factor alpha-, and Mycobacterium tuberculosis-induced pro-inflammatory signals. *J Biol Chem*, *280*(48), 39914-39924. <https://doi.org/10.1074/jbc.M502820200>
- Wolins, N. E., Quaynor, B. K., Skinner, J. R., Tzekov, A., Park, C., Choi, K., & Bickel, P. E. (2006). OP9 mouse stromal cells rapidly differentiate into adipocytes: characterization of a useful new model of adipogenesis. *J Lipid Res*, *47*(2), 450-460. <https://doi.org/10.1194/jlr.D500037-JLR200>

- Wree, A., McGeough, M. D., Pena, C. A., Schlattjan, M., Li, H., Inzaugarat, M. E., Messer, K., Canbay, A., Hoffman, H. M., & Feldstein, A. E. (2014). NLRP3 inflammasome activation is required for fibrosis development in NAFLD. *J Mol Med (Berl)*, *92*(10), 1069-1082. <https://doi.org/10.1007/s00109-014-1170-1>
- Wu, X. M., Hu, Y. W., Xue, N. N., Ren, S. S., Chen, S. N., Nie, P., & Chang, M. X. (2017). Role of zebrafish NLRC5 in antiviral response and transcriptional regulation of MHC related genes. *Dev Comp Immunol*, *68*, 58-68. <https://doi.org/10.1016/j.dci.2016.11.018>
- Wurtz, J. M., Bourguet, W., Renaud, J. P., Vivat, V., Chambon, P., Moras, D., & Gronemeyer, H. (1996). A canonical structure for the ligand-binding domain of nuclear receptors. *Nat Struct Biol*, *3*(1), 87-94. <https://doi.org/10.1038/nsb0196-87>
- Xu, Y., Farmer, S. R., & Smith, B. D. (2007). Peroxisome proliferator-activated receptor gamma interacts with CIITA x RFX5 complex to repress type I collagen gene expression. *J Biol Chem*, *282*(36), 26046-26056. <https://doi.org/10.1074/jbc.M703652200>
- Yang, G., Lee, H. E., & Lee, J. Y. (2016). A pharmacological inhibitor of NLRP3 inflammasome prevents non-alcoholic fatty liver disease in a mouse model induced by high fat diet. *Sci Rep*, *6*, 24399. <https://doi.org/10.1038/srep24399>
- Yang, R., Castriota, G., Chen, Y., Cleary, M. A., Ellsworth, K., Shin, M. K., Tran, J. L., Vogt, T. F., Wu, M., Xu, S., Yang, X., Zhang, B. B., Berger, J. P., & Qureshi, S. A. (2011). RNAi-mediated germline knockdown of FABP4 increases body weight but does not improve the deranged nutrient metabolism of diet-induced obese mice. *Int J Obes (Lond)*, *35*(2), 217-225. <https://doi.org/10.1038/ijo.2010.128>
- Yao, Y., & Qian, Y. (2013). Expression regulation and function of NLRC5. *Protein Cell*, *4*(3), 168-175. <https://doi.org/10.1007/s13238-012-2109-3>
- Yao, Y., Wang, Y., Chen, F., Huang, Y., Zhu, S., Leng, Q., Wang, H., Shi, Y., & Qian, Y. (2012). NLRC5 regulates MHC class I antigen presentation in host defense against intracellular pathogens. *Cell Res*, *22*(5), 836-847. <https://doi.org/10.1038/cr.2012.56>
- Yasrebi, A., Rivera, J. A., Krumm, E. A., Yang, J. A., & Roepke, T. A. (2017). Activation of Estrogen Response Element-Independent ERalpha Signaling Protects Female Mice From Diet-Induced Obesity. *Endocrinology*, *158*(2), 319-334. <https://doi.org/10.1210/en.2016-1535>
- Yin, Z., Deng, T., Peterson, L. E., Yu, R., Lin, J., Hamilton, D. J., Reardon, P. R., Sherman, V., Winnier, G. E., Zhan, M., Lyon, C. J., Wong, S. T., & Hsueh, W. A. (2014). Transcriptome analysis of human adipocytes implicates the NOD-like receptor pathway in obesity-induced adipose inflammation. *Mol Cell Endocrinol*, *394*(1-2), 80-87. <https://doi.org/10.1016/j.mce.2014.06.018>
- Youm, Y. H., Adijiang, A., Vandanmagsar, B., Burk, D., Ravussin, A., & Dixit, V. D. (2011). Elimination of the NLRP3-ASC inflammasome protects against chronic obesity-induced pancreatic damage. *Endocrinology*, *152*(11), 4039-4045. <https://doi.org/10.1210/en.2011-1326>
- Yu, C., Markan, K., Temple, K. A., Deplewski, D., Brady, M. J., & Cohen, R. N. (2005). The nuclear receptor corepressors NCoR and SMRT decrease peroxisome proliferator-activated receptor gamma transcriptional activity and repress 3T3-L1 adipogenesis. *J Biol Chem*, *280*(14), 13600-13605. <https://doi.org/10.1074/jbc.M409468200>
- Yu, Q., Ju, P., Kou, W., Zhai, M., Zeng, Y., Maimaitiaili, N., Shi, Y., Xu, X., Zhao, Y., Jian, W., Feinberg, M. W., Xu, Y., Zhuang, J., & Peng, W. (2023). Macrophage-Specific NLRC5 Protects From Cardiac Remodeling Through Interaction With HSPA8. *JACC Basic Transl Sci*, *8*(5), 479-496. <https://doi.org/10.1016/j.jacbts.2022.10.001>

- Zaki, M. H., Man, S. M., Vogel, P., Lamkanfi, M., & Kanneganti, T. D. (2014). Salmonella exploits NLRP12-dependent innate immune signaling to suppress host defenses during infection. *Proc Natl Acad Sci U S A*, *111*(1), 385-390.
<https://doi.org/10.1073/pnas.1317643111>
- Zaki, M. H., Vogel, P., Malireddi, R. K., Body-Malapel, M., Anand, P. K., Bertin, J., Green, D. R., Lamkanfi, M., & Kanneganti, T. D. (2011). The NOD-like receptor NLRP12 attenuates colon inflammation and tumorigenesis. *Cancer Cell*, *20*(5), 649-660.
<https://doi.org/10.1016/j.ccr.2011.10.022>
- Zebisch, K., Voigt, V., Wabitsch, M., & Brandsch, M. (2012). Protocol for effective differentiation of 3T3-L1 cells to adipocytes. *Anal Biochem*, *425*(1), 88-90.
<https://doi.org/10.1016/j.ab.2012.03.005>
- Zhang, J., Zhang, Y., Xiao, F., Liu, Y., Wang, J., Gao, H., Rong, S., Yao, Y., Li, J., & Xu, G. (2016). The peroxisome proliferator-activated receptor gamma agonist pioglitazone prevents NF-kappaB activation in cisplatin nephrotoxicity through the reduction of p65 acetylation via the AMPK-SIRT1/p300 pathway. *Biochem Pharmacol*, *101*, 100-111.
<https://doi.org/10.1016/j.bcp.2015.11.027>
- Zhang, Y., Yao, Y., Qiu, X., Wang, G., Hu, Z., Chen, S., Wu, Z., Yuan, N., Gao, H., Wang, J., Song, H., Girardin, S. E., & Qian, Y. (2019). Listeria hijacks host mitophagy through a novel mitophagy receptor to evade killing. *Nat Immunol*, *20*(4), 433-446.
<https://doi.org/10.1038/s41590-019-0324-2>
- Zheng, D., Mohapatra, G., Kern, L., He, Y., Shmueli, M. D., Valdes-Mas, R., Kolodziejczyk, A. A., Prochnicki, T., Vasconcelos, M. B., Schorr, L., Hertel, F., Lee, Y. S., Rufino, M. C., Ceddaha, E., Shimshy, S., Hodgetts, R. J., Dori-Bachash, M., Kleimeyer, C., Goldenberg, K., . . . Elinav, E. (2023). Epithelial Nlrp10 inflammasome mediates protection against intestinal autoinflammation. *Nat Immunol*, *24*(4), 585-594.
<https://doi.org/10.1038/s41590-023-01450-z>
- Zhou, Y. J., Liu, C., Li, C. L., Song, Y. L., Tang, Y. S., Zhou, H., Li, A., Li, Y., Weng, Y., & Zheng, F. P. (2015). Increased NOD1, but not NOD2, activity in subcutaneous adipose tissue from patients with metabolic syndrome. *Obesity (Silver Spring)*, *23*(7), 1394-1400.
<https://doi.org/10.1002/oby.21113>
- Zhu, Y., Qi, C., Korenberg, J. R., Chen, X. N., Noya, D., Rao, M. S., & Reddy, J. K. (1995). Structural organization of mouse peroxisome proliferator-activated receptor gamma (mPPAR gamma) gene: alternative promoter use and different splicing yield two mPPAR gamma isoforms. *Proc Natl Acad Sci U S A*, *92*(17), 7921-7925.
<https://doi.org/10.1073/pnas.92.17.7921>

Supplement

Suppl. Table 1: Diet composition of ssniff® low-fat control (E15000) and high-fat diet (E15186) according to supplier. N/S = not specified.

	Low-fat control diet	High-fat diet
Energy	MJ/kg	MJ/kg
Gross energy	18.0	24.2
Metabolizable energy (calculated with the Atwater factors)	15.0	20.8
Crude Nutrient	%	%
Dry matter	95.2	96.3
Crude protein	20.8	20.8
Crude fat	4.2	30.1
Crude fibre	5.0	5.0
Crude ash	5.6	5.6
N free extracts	59.4	34.6
Starch	46.8	16.3
Sugar/dextrins	10.8	17.8
Minerals	%	%
Calcium	0.90	0.92
Phosphorus	0.63	0.62
Sodium	0.19	0.19
Magnesium	0.21	0.21
Potassium	0.97	0.97
Fatty acids	%	%
C 4:0	N/S	0.12
C 6:0	N/S	0.11
C 8:0	-	0.50
C 10:0	-	0.45
C 12:0	-	2.81
C 14:0	0.02	1.77
C 16:0	0.45	8.57
C 16:1	0.02	0.34
C 17:0	N/S	0.13
C 18:0	0.19	2.63
C 18:1	1.07	8.83
C 18:2	2.12	1.60
C 18:3	0.26	0.12
C 20:0	0.02	0.07
C 20:1	-	0.01
C 20:4	N/S	0.02
C 20:5	-	N/S
C 22:6	-	N/S
Cholesterol	mg/kg	mg/kg
	N/S	171
Amino acids	%	%
Lysine	1.71	1.71
Methionine	0.73	0.73
Met+Cys	0.82	1.02

The role of NLRC5 in obesity – Supplement

	Low-fat control diet	High-fat diet
Threonine	0.93	0.93
Amino acids	%	%
Tryptophan	0.27	0.27
Arginine	0.76	0.76
Histidine	0.66	0.66
Valine	1.42	1.42
Isoleucine	1.09	1.09
Leucine	2.05	2.05
Phenylalanine	1.11	1.11
Phe+Tyr	2.22	2.22
Glycine	0.43	0.43
Glutamic acid	4.69	4.69
Aspartic acid	1.55	1.55
Proline	2.39	2.39
Alanine	0.68	0.68
Serine	1.24	1.24
Vitamins	per kg	per kg
Vitamin A	15,000 IU	15,000 IU
Vitamin D ₃	1,5000 IU	1,5000 IU
Vitamin E	150 mg	150 mg
Vitamin K (as menadione)	20 mg	20 mg
Vitamin C	30 mg	30 mg
Thiamin (B ₁)	16 mg	16 mg
Riboflavin (B ₂)	16 mg	16 mg
Pyridoxin (B ₆)	18 mg	18 mg
Cobalamin (B ₁₂)	30 µg	30 µg
Nicotinic acid	49 mg	49 mg
Pantothenic acid	56 mg	56 mg
Folic acid	19 mg	19 mg
Biotin	310 µg	310 µg
Choline-Chloride	1,040 mg	1,040 mg
Inositol	80 mg	80 mg
Trace elements	per kg	per kg
Iron	166 mg	166 mg
Manganese	98 mg	98 mg
Zinc	65 mg	65 mg
Copper	14 mg	14 mg
Iodine	1.2 mg	1.2 mg
Selenium	0.14 mg	0.14 mg
Cobalt	0.15 mg	0.15 mg

Suppl. Table 2: Diet composition of Research Diets Inc. high-fat diet (D12492) according to supplier.

Product Data

D12492



Description

Rodent Diet with 60% kcal% fat.

Used in Research

Obesity
Diabetes

Packaging

Product is packed in 12.5 kg box.
Each box is identified with the product name, description, lot number and expiration date.

Lead Time

IN-STOCK. Ready for next day shipment.

Gamma-Irradiation

Yes. Add 10 days to delivery time.

Form

Pellet, Powder, Liquid

Shelf Life

Most diets require storage in a cool dry environment. Stored correctly they should last 3-6 months. Because of the high fat content is best if kept frozen.

Control Diets

D12450B

Formula

Product #	D12492	
	gm%	kcal%
Protein	26.2	20
Carbohydrate	26.3	20
Fat	34.9	60
Total	5.24	100
	kcal/gm	
	5.24	
Ingredient	gm	kcal
Casein, 80 Mesh	200	800
L-Cystine	3	12
Corn Starch	0	0
Maltodextrin 10	125	500
Sucrose	68.8	275.2
Cellulose, BW200	50	0
Soybean Oil	25	225
Lard*	245	2205
Mineral Mix, S10026	10	0
DiCalcium Phosphate	13	0
Calcium Carbonate	5.5	0
Potassium Citrate, 1 H2O	16.5	0
Vitamin Mix, V10001	10	40
Choline Bitartrate	2	0
FD&C Blue Dye #1	0.05	0
Total	773.85	4057

Formulated by E. A. Ulman, Ph.D., Research Diets, Inc., 8/26/98 and 3/11/99.

*Typical analysis of cholesterol in lard = 0.95 mg/gram.
Cholesterol (mg)/4057 kcal = 232.8
Cholesterol (mg)/kg = 300.8



Research Diets, Inc.
20 Jules Lane
New Brunswick, NJ 08901
Tel: 732.247.2390
Fax: 732.247.2340
info@researchdiets.com

Copyright © 2006 Research Diets, Inc. All rights reserved. D12492

Eidesstattliche Erklärung

Eidesstattliche Versicherung über die eigenständig erbrachte Leistung gemäß § 18 Absatz 3 Satz 5 der Promotionsordnung der Universität Hohenheim für die Fakultäten Agrar-, Natur- sowie Wirtschafts- und Sozialwissenschaften

1. Bei der eingereichten Dissertation zum Thema

The role of NLRC5 in obesity

handelt es sich um meine eigenständig erbrachte Leistung.

2. Ich habe nur die angegebenen Quellen und Hilfsmittel benutzt und mich keiner unzulässigen Hilfe Dritter bedient. Insbesondere habe ich wörtlich oder sinngemäß aus anderen Werken übernommene Inhalte als solche kenntlich gemacht.

3. Ich habe nicht die Hilfe einer kommerziellen Promotionsvermittlung oder -beratung in Anspruch genommen.

4. Die Bedeutung der eidesstattlichen Versicherung und der strafrechtlichen Folgen einer unrichtigen oder unvollständigen eidesstattlichen Versicherung sind mir bekannt.

Die Richtigkeit der vorstehenden Erklärung bestätige ich. Ich versichere an Eides Statt, dass ich nach bestem Wissen die reine Wahrheit erklärt und nichts verschwiegen habe.

Stuttgart, 03.08.23
Ort, Datum

S. Bauer
Sarah Bauer

Danksagung

Mein Dank gilt zuallererst meinem Doktorvater, Prof. Dr. Thomas Kufer, für die Möglichkeit, meine Doktorarbeit in seiner Arbeitsgruppe durchzuführen. Thomas, vielen Dank für die sehr gute Betreuung, moralische Unterstützung und Geduld, gerade in schwierigen Phasen der Promotion, für Dein fachliches Engagement und dafür, dass Du mir den Einstieg in die akademische Welt ermöglicht und mir vielfältige Einblicke in diese ermöglicht hast.

Mein Dank gilt ebenso Prof. Dr. W. Florian Fricke und Prof. Dr. Dr. Sascha Venturelli für die Übernahme der Rolle des Zweit- und Drittgutachters, für die fachliche Unterstützung sowie die immer konstruktiven fachlichen Diskussionen.

Des Weiteren möchte ich mich bei all denen bedanken, die ich durch Zusammenarbeiten im Rahmen meiner Promotion kennen lernen durfte. Mirjam Gerstner, Dr. Christine Feld und Prof. Dr. Jörn Lausen von der Universität Stuttgart danke ich für Ihre tatkräftige Unterstützung in Sachen CHIP. Dr. Alena M. Bubeck und Mona Scheurenbrand gilt mein herzlicher Dank für die fachliche Hilfe und Kooperation in Sachen Mikrobiomanalyse. Und Prof. Sheela Ramanathan, Prof. Subburaj Ilangumaran und vor allem Fjolla Rexhepi bin ich zutiefst dankbar für Ihre großartige Betreuung in- und außerhalb des Labors während meines Forschungsaufenthaltes an der Université de Sherbrooke.

Ein riesiges Dankeschön geht an alle Mitglieder der AG Kufer, auch an die Ehemaligen (Ioannis, Kornelia, Nora, Heidi und Clarissa). Vielen Dank für die großartigen Jahre, in denen ich lernen durfte, was Teamgeist und Zusammenhalt bedeuten. Vielen Dank für Eure Unterstützung und Hilfsbereitschaft. Petra, vielen Dank für die sehr gute Organisation in- und außerhalb des Labors, ohne die wir alle aufgeschmissen wären. Ganz besonders möchte ich mich von Herzen bei Yvonne bedanken, die über die Jahre viel mehr für mich geworden ist als „nur“ eine Arbeitskollegin. Danke für Deine Freundschaft, Deinen Humor und Deine Ratschläge, die für mich mehr als einmal wegweisend waren!

„Einen sicheren Freund erkennt man in unsicherer Sache.“ (Marcus Tullius Cicero). Wenig fühlt sich wohl unsicherer an als eine Promotion und in diesem Sinne möchte ich mich ganz herzlich

The role of NLRC5 in obesity – Danksagung

bei meinen engsten Freunden bedanken. Maraike, Susi und Hannes – Danke, dass Ihr immer für mich da seid und mir mit Rat, Tat und Eurer ehrlichen Meinung durch schwierige Zeiten geholfen habt.

„Dankbarkeit und Liebe sind Geschwister.“ (Christian Morgenstern). In diesem Sinne gilt mein größter Dank meiner Familie, die mich bei jedem meiner Schritte immer unterstützt und mich maßgeblich zu dem Menschen gemacht hat, der ich heute bin. Zu wissen, dass ihr immer für mich da seid, gibt mir Kraft und bedeutet mir unsagbar viel.

Publications

Parts of this thesis have been published in the following articles:

Bauer, S., Aeissen, V., Bubeck, A. M., Kienes, I., Ellwanger, K., Scheurenbrand, M., Rexhepi, F., Ramanathan, S., Rosenstiel, Philip, Fricke, W. F., & Kufer, T. A. (2023). NLRC5 affects diet-induced adiposity in female mice and co-regulates peroxisome proliferator-activated receptor PPAR γ target genes. *iScience*, **26**(4).

Bauer, S., Hezinger, L., Rexhepi, F., Ramanathan, S., & Kufer, T. A. (2023). NOD-like Receptors—Emerging Links to Obesity and Associated Morbidities. *International Journal of Molecular Sciences*, **24**(10), 8595.

Curriculum Vitae

Name Sarah Katharina Bauer
Address Körschstraße 41
70599 Stuttgart, Germany
E-Mail S_Bauer@uni-hohenheim.de
Date of birth March 19th 1995, Karlsruhe

Education and academic career

since 02/2021 **PhD thesis**
The role of NLRC5 in obesity
Prof. Thomas A. Kufer, Institute of
Clinical Nutrition, Department of Immunology, University
of Hohenheim

10/2018 – 01/2021 **Master of Science Molecular Nutritional Science**
(Final grade 1,0)
University of Hohenheim

10/2015 – 09/2018 **Bachelor of Science Nutritional Management and
Dietetics** (Final grade 1,6)
University of Hohenheim
Bachelor's Thesis
*Übersicht über die Rolle und Funktion der Integrierten
Stress Antwort bei Infektion mit invasiven bakteriellen
Erregern*
Prof. Thomas A. Kufer, Institute of
Clinical Nutrition, Department of Immunology, University
of Hohenheim

10/2013 – 09/2015 **Studies in History and Mathematics for the teaching
Profession** (without graduation)
University of Heidelberg

2005 – 2013 **Abitur** (Final grade 1,0)
Markgrafengymnasium Karlsruhe

Publications

Bauer, S., Aeissen, V., Bubeck, A. M., Kienes, I., Ellwanger, K., Scheurenbrand, M., Rexhepi, F., Ramanathan, S., Rosenstiel, Philip, Fricke, W. F., & Kufer, T. A. (2023). NLRC5 affects diet-induced adiposity in female mice and co-regulates peroxisome proliferator-activated receptor PPAR γ target genes. *iScience*, **26**(4).

Bauer, S., Hezinger, L., Rexhepi, F., Ramanathan, S., & Kufer, T. A. (2023). NOD-like Receptors—Emerging Links to Obesity and Associated Morbidities. *International Journal of Molecular Sciences*, **24**(10), 8595.

Hezinger, L., **Bauer, S.**, Ellwanger, K., Piotrowsky, A., Biber, F., Venturelli, S., & Kufer, T. A. (2023). NOD1 cooperates with HAX-1 to promote cell migration in a RIPK2 and NF- κ B independent manner. *The FEBS Journal*.

Jiménez-Aspee, F., Pospiech, J., **Bauer, S.**, Sus, N., Kufer, T. A., & Frank, J. (2023). Prumnopitys Andina Fruit Extract Activates Liver X Receptors after In Vitro Digestion. *Molecular Nutrition & Food Research*, **67**(1), 2200377.

Kienes, I., **Bauer, S.**, Gottschild, C., Mirza, N., Pfannstiel, J., Schröder, M., & Kufer, T. A. (2021). DDX3X links NLRP11 to the regulation of type I interferon responses and NLRP3 inflammasome activation. *Frontiers in Immunology*, **12**, 653883.

Mirza, N., **Bauer, S.**, & Kufer, T. A. (2019). Angeborene Immunität und Adipositas – Die Rolle der Nod-like Rezeptoren (NLR). *Aktuelle Ernährungsmedizin*, **44**(04), 248-260.

Conferences and Poster Presentations

- | | |
|----------------|---|
| 09/2023 | Scheduled participation and Poster presentation at the first joint conference of the Société Française d'Immunologie (SFI) and the Deutsche Gesellschaft für Immunologie (DGfI), Strasbourg, France |
| 01/2023 | Participation at the Keystone eSymposia Integrating Metabolism and Immunity |
| 06/2018 | Participation at the Ernährung 2018, Kassel, Germany |

Scholarships

07/2022 – 08/2022	DAAD – Exchange Scholarship in collaboration with Prof. Sheela Ramanathan, University of Sherbrooke, Canada
05/2021	Landesgraduiertenförderung of the Ministry of Science, Research and Arts in Baden-Württemberg

Further Qualifications

Course in **Basics of Laboratory Animal Science** according to FELASA Category B Guidelines
Experience working in biosafety level S2
Experience in teaching (lectures, seminars, practical courses)
Sound knowledge in the use of MS Office and Adobe Illustrator

Languages

German	Mother tongue
English	Full working proficiency (level C1)
Spanish	Limited working proficiency (level B1)
French	Elementary proficiency (level B1)

Secondary activities

10/2018 – 03/2020	Student assistant, University of Hohenheim, Institute of Nutritional Medicine, Department of Immunology
since 06/2013	Barista, MoccaSin Coffee, Karlsruhe, with additional responsibilities in allergen-management, product development and accounting

References

Prof. Dr. rer. nat. Thomas A. Kufer	Institute of Clinical Nutrition, Department of Immunology, University of Hohenheim Tel: +49 711 459 24850
-------------------------------------	--

Stuttgart, 03.08.23
Place, Date

S. Bauer
Sarah Bauer